SLAC-R-707

A Measurement of B0 Anti-B0 Oscillations Using Fully-Reconstructed Hadronic B Decays at BaBar

Benjamin Paul Brau

Stanford Linear Accelerator Center
Stanford University
Stanford, CA 94309

SLAC-Report-707

Prepared for the Department of Energy
under contract number DE-AC03-76SF00515

Printed in the United States of America. Available from the National Technical Information Service, U.S. Department of Commerce, 5285 Port Royal Road, Springfield, VA 22161.

Ph.D. Thesis, Massachusetts Institute of Technology, Cambridge, MA 02139

A Measurement of B0 Anti-B0 Oscillations Using Fully-Reconstructed Hadronic B Decays at BaBar

by

Benjamin Paul Brau

B.A. Physics
Reed College, 1993

Submitted to the Department of Physics
in partial fulfillment of the requirements for the degree of

Doctor of Philosophy in Physics

at the

MASSACHUSETTS INSTITUTE OF TECHNOLOGY

June 2002

Author .....
Department of Physics
May 3, 2002

Certified by .....
Richard K. Yamamoto
Professor
Thesis Supervisor

Accepted by .....
Thomas J. Greytak
Associate Department Head for Education

A Measurement of B0 Anti-B0 Oscillations Using Fully-Reconstructed Hadronic B Decays at BaBar

by

Benjamin Paul Brau

Submitted to the Department of Physics
on May 3, 2002, in partial fulfillment of the
requirements for the degree of
Doctor of Philosophy in Physics

Abstract

Flavor oscillations of neutral B mesons have been studied with e^+e^- annihilation data collected at center of mass energies near the $\Upsilon(4S)$ at the PEP-II asymmetric collider with the *BABAR* detector. One B^0 is fully reconstructed in a hadronic decay to a flavor eigenstate. The flavor of the other B in the event is determined using an inclusive tagging algorithm which exploits the correlations between the flavor of the b quark and the charges of its decay products. By fitting the decay-time distribution of the observed mixed and unmixed final states, the oscillation frequency, Δm_d, is determined to be $0.516 \pm 0.016\,(\text{stat.}) \pm 0.010\,(\text{syst.})\,\text{ps}^{-1}$.

Thesis Supervisor: Richard K. Yamamoto
Title: Professor

Acknowledgments

I am grateful to many without whom I would not have arrived at this moment.

I will first thank my colleagues and collaborators. Particle physics by its nature is inherently a collaborative endeavor, and therefore I think it appropriate to first thank all of my *BABAR* collaborators, and my colleagues who made PEP-II such a success.

From M.I.T., I first thank the L.Q.S. group: I thank my advisor Richard Yamamoto for mentoring me along all the way from general exams to thesis defense, not to mention teaching me a bit of physics. I also thank Ray Cowan, who always could help me figure out the appropriate shell script or TeX command to do just what I needed. I thank them both for reading and providing valuable feedback on my thesis. I'd also like to thank Professors Peter Fisher and Jeffrey Goldstone who were my readers, and I especially appreciate them both for keeping me honest, if not concise. Jim McBride was my study partner during the grueling General Exam phase of my degree, and he really helped me to get through it all. Thanks Jim.

My collaborators from the University of California at San Diego took me under their wing and taught me many things. More importantly, they made me an honorary member of their formidable analysis good-guys collaboration machine. David Macfarlane first involved me in drift chamber calibration studies, and later helped think through some of the difficult problems we encountered in the analysis. Vivek Sharma seduced me with exclusive reconstruction of hadronic B decays. He had me giving an APS talk on a measurement of the branching fractions for $B^0 \to D^*\pi$ and $B^0 \to D^*\rho$ in a matter of weeks. I was hooked. As $\sin(2\beta)$ coordinator, Riccardo Faccini had me doing sanity checks of my sanity checks, and putting up signs in the office to alert the 100+ visitors he had each day that no, I didn't keep up-to-the-second coordinates of Ric's location (but Shahram might). Mister[1] Shahram Rahatlou has been my comrade in `BReco` production exercises and I have both Soeren Prell and Shahram to thank for thea wonderful `FORTRAN` monstrosity, `tFit`. Finally, Gerhard Raven was my physics analysis mentor. From day one, Gerhard was eager to teach

[1] soon to be Doctor

me anything I needed to know, from how to compile the latest release of the code to just what strange character you had to use to get the right symbol in PAW. Along the way we managed to discuss a fair amount of physics too. We collaborated closely on tracking projects and later the Δm_d measurement, and I am in his debt. Thanks Gerhard.

Thanks to Jim Panetta for reading my thesis in its entirety and providing me very useful feedback.

I wish to express my deep thanks to my late grandpa Williams for inspiring my interest in understanding how things work, and my late grandpa Brau, who gave me a leg up in understanding statistics by encouraging me to play poker at an early age. I will always remember them both and dedicate this work to them.

My cats Miesha and Mercury helped along the way with some purring.

My parents have always been supportive of whatever I wanted to do in life, and for that I thank them. Both of them always tried to help me succeed, but also they encouraged me to do what I found interesting. You guys are the best!

My wife Molly has provided me with solid support and unquestioned love. I could never have finished this degree without her, and without Molly I might never have started. She even proof-read this thesis. Thank You Molly for Everything.

Contents

List of Figures

List of Tables

Chapter 1

Introduction

Since flavor oscillations were first observed in the B^0 system by Argus [1] and UA1 [2], they have been studied using a variety of methods. This document describes a precision, time-dependent measurement of the B^0 flavor oscillation (mixing) frequency, Δm_d, using a new technique, with *BABAR* data. In this introduction, I will discuss the relevant theory, describe the experiment, and explain the organization of the rest of this document.

1.1 Weak Interactions of Quarks

In the Standard Model, the weak interactions of quarks are described by the interaction shown in Figure 1-1. The strength of the interaction at the vertex is

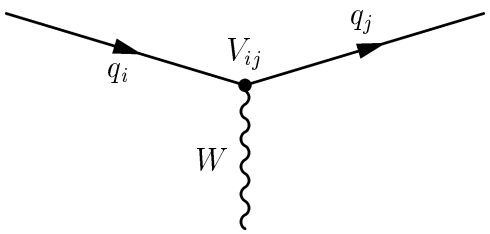

Figure 1-1: Feynman diagram describing weak interactions of quarks

given by gV_{ij}, where g is the universal Fermi weak coupling, and V_{ij} depends on

which quarks are involved. For 3 generations, the V_{ij} can be written as a 3×3 matrix V, referred to as the Cabibbo-Kobayashi-Maskawa (CKM) matrix. We can think of this 3×3 matrix as rotating the quark states from one in which they are Mass eigenstates to one in which they are Weak eigenstates:

$$\begin{pmatrix} d' \\ s' \\ b' \end{pmatrix} = \begin{pmatrix} V_{ud} & V_{us} & V_{ub} \\ V_{cd} & V_{cs} & V_{cb} \\ V_{td} & V_{ts} & V_{tb} \end{pmatrix} \begin{pmatrix} d \\ s \\ b \end{pmatrix} \tag{1.1}$$

The elements of the CKM matrix form a hierarchy. First, the requirement that the matrix be unitary reduces the nine complex parameters to three real ones and one complex phase. Second, in general, elements on the diagonal are close to unity, while off-diagonal elements are smaller the further from the diagonal they are and hence generation-changing interactions are suppressed. Wolfenstein [3] recognized these facts and his parameterization of the matrix makes the hierarchy explicit:

$$V = \begin{pmatrix} 1 - \lambda^2/2 & \lambda & A\lambda^3(\rho - i\eta) \\ -\lambda & 1 - \lambda^2/2 & A\lambda^2 \\ A\lambda^3(1 - \rho + i\eta) & -A\lambda^2 & 1 \end{pmatrix} + O(\lambda^4) \tag{1.2}$$

By requiring the matrix to be unitary, nine relationships among the elements can be obtained. In particular, there are two equations which have all terms approximately the same size. One of those, $V_{ud}V_{ub}^* + V_{cd}V_{cb}^* + V_{td}V_{tb}^* = 0$ is particularly interesting because all terms are of order λ^3. Normalizing the equation by dividing by $V_{cd}V_{cb}^*$ gives

$$\frac{V_{ud}V_{ub}^*}{V_{cd}V_{cb}^*} + \frac{V_{cd}V_{cb}^*}{V_{cd}V_{cb}^*} + \frac{V_{td}V_{tb}^*}{V_{cd}V_{cb}^*} = 0 \tag{1.3}$$

This normalized equation can be represented pictorially as a triangle in the complex plane. Each term in the equation is a complex number and hence has a magnitude and direction (i.e., phase). Each term can therefore be thought of as a vector. By drawing the vectors the terms represent end-to-end in the complex plane, a triangle is formed

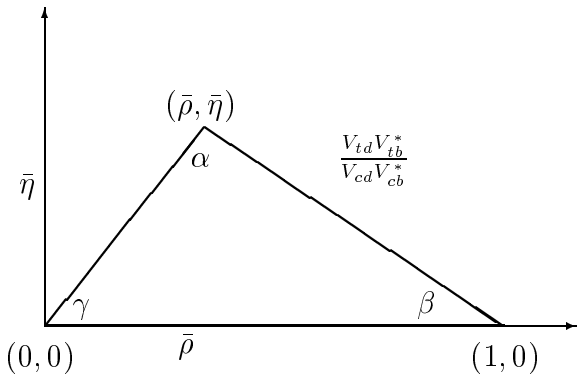

Figure 1-2: The Unitarity Triangle. The side labeled $\frac{V_{td}V_{tb}^*}{V_{cd}V_{cb}^*}$ can be constrained by measuring Δm_d

(see Figure 1-2). What makes this relation especially interesting is that because the terms are all similar in magnitude, the angles of the triangle are non-trivial, i.e., they are not very close to zero or π. If measurements of the sides and angles of the Unitarity Triangle turned out to be inconsistent with each other, this would be a sure sign that there is new physics not accounted for. For example, in some SUSY [4] models, the $B^0\overline{B}^0$ mixing amplitude could be modified by box-diagrams involving intermediate gluinos and squarks [5], and these would change the constraint on the Unitarity Triangle from Δm_d. In other words, making measurements which over-constrain the Unitarity Triangle is a good probe for new physics. As I will discuss, measuring B flavor oscillations helps provide one such constraint.

Flavor oscillations of neutral B mesons are described in the Standard Model by second-order weak interactions (see Figure 1-3). The amplitudes represented by these diagrams are proportional to $(m_q/M_W)^2$ [6], where m_q is the mass of the up-type quark involved. Because of its mass, the top quark contributes the dominant amplitude, and therefore the oscillation frequency is sensitive to the CKM matrix element V_{td}, which is proportional to one side of the CKM matrix. The theoretical prediction for Δm_d,

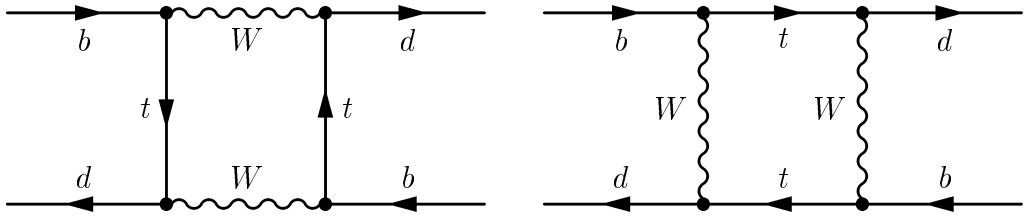

Figure 1-3: Lowest order Feynman diagrams contributing to $B^0\overline{B}^0$ oscillations in the Standard Model

in the limit of large top mass, is given by

$$\Delta m_d = \frac{G_F^2}{6\pi^2}\eta_B m_{B_d} f_{B_d}^2 B_d m_W^2 S(x_t)\,|V_{td}V_{tb}^*| \tag{1.4}$$

where B_d is the bag parameter, $S(x_t)$ and η_B are the Inami-Lim [7] function and its correction factor, f_{B_d} is the decay constant, and x_t is the ratio m_t^2/M_W^2. The determination of $|V_{td}|$ from Δm_d is currently theoretically limited [6]. The two main contributions to the uncertainty are the uncertainty in the decay constant f_{B_d} and the bag parameter B_d, both of which must be determined using lattice QCD.

The length of the side of the Unitarity Triangle can be better constrained by the ratio $\Delta m_d/\Delta m_s$, where many theoretical uncertainties cancel, and the residual uncertainties in the lattice calculations are now believed to be known to a few percent.

This ratio, $\Delta m_d/\Delta m_s$, is related to the length of the side of the Unitarity Triangle which is proportional to $|V_{td}|\,|V_{tb}^*|\,/\,|V_{cd}|\,|V_{cb}^*|$ as follows. The matrix elements V_{tb} and V_{cd} are well known. If we assume unitarity, then from the Wolfenstein parameterization one can see that to order λ^3, both $|V_{cb}|$ and $|V_{ts}|$ are equal to $A\lambda^2$. Thus if we assume that the CKM matrix is unitary, we can conclude that these two matrix elements must be equal. Therefore, the ratio $\Delta m_d/\Delta m_s$ is proportional to $|V_{cb}|\,/\,|V_{td}| = |V_{ts}|\,/\,|V_{td}|$.

Mixing in the B_s system has been established from a measurement of time-integrated mixing probability χ_B, for an admixture of B_d and B_s [8]. The B_s oscillation frequency is expected to be measured soon. Precision knowledge of

both Δm_s and Δm_d, together with improved theoretical calculations, will provide a stringent constraint on the magnitude of one side of the Unitarity Triangle.

Mixing in the $B^0\overline{B}^0$ system is also potentially sensitive to new physics contributions. For one example of such contributions, see [9] in which studies of extra dimensions have examined the compatibility of the value of Δm_d with various models.

1.2 Experimental Method

This section provides a summary of the technique used to measure the $B^0\overline{B}^0$ oscillation frequency, Δm_d at *BABAR* with fully-reconstructed hadronic B decays.

At center of mass energies near the mass of the $\Upsilon(4S)$, e^+e^- collisions produce $B^0\overline{B}^0$ pairs in a coherent $L = 1$ state through the transition shown in Figure 1-4. While this diagram may seem trivial, it illustrates several features unique to time-

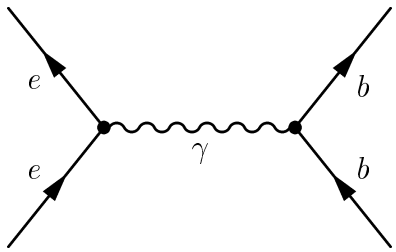

Figure 1-4: Feynman diagram representing $\Upsilon(4S)$ production

dependent measurements at the $\Upsilon(4S)$ and this measurement in particular. First, because the mass of the $\Upsilon(4S)$ is barely more than twice the mass of the B^0 meson, when the $\Upsilon(4S)$ decays to a $B^0\overline{B}^0$ pair, there is no further hadronization. This means that the $B^0\overline{B}^0$ pair evolves *coherently*, i.e., with a single entangled state function. Because the production mechanism is mediated by a photon, the entangled state carries $L = 1$.

At the moment the first B^0 decays, the entangled wavefunction collapses (see Figure 1-5). At that instant, the flavor quantum numbers of the two B mesons are opposite. Specifically, the other (undecayed) B is in an unambiguous flavor eigenstate,

determined by the flavor of the decayed B. As the wavefunction of the second B evolves, its flavor oscillates with a characteristic frequency Δm_d. The details of the quantum mechanics describing the oscillation can be found in Appendix A. The goal of the measurement is to study a large sample of such $B^0\overline{B}^0$ decays and measure the time-dependence of the flavor-correlations of the two B decays.

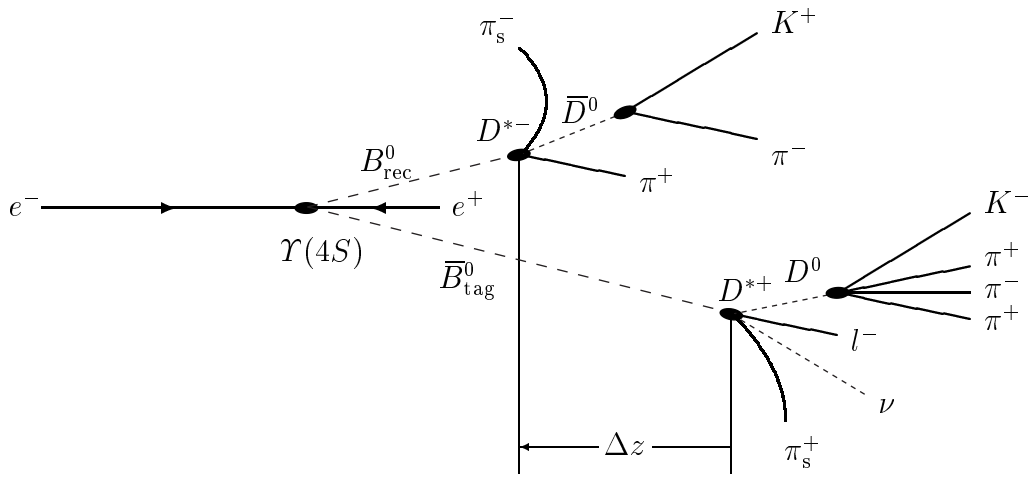

Figure 1-5: Typical $\Upsilon(4S) \to B^0\overline{B}^0$ event at *BABAR*. Here, the $B_{\rm rec}$ decays in the channel $B^0 \to D^{*-}\pi^+$, where the D^{*-} decays to $\overline{D}^0\pi_s^-$, and finally the $\overline{D}^0$ decays to $K^+\pi^-$. The $B_{\rm tag}$ decays in the channel $B \to D^*\ell\nu$, where the D^{*+} decays to $D^0\pi_s^+$, and the D^0 decays to $K^-\pi^+\pi^-\pi^+$. The boosted CMS allows the two decay vertices to be resolved and Δz to be measured.

In the center of momentum system (CMS), the $B^0\overline{B}^0$ pair from $\Upsilon(4S)$ decays drifts approximately 20 microns before they themselves decay. This is not far enough to accurately resolve the difference in the decay positions (times) of the two B mesons. In order to measure the decay-time difference of the two Bs, at *BABAR* the center of mass system is boosted in the laboratory frame in the z direction just enough to allow the decay vertices of the two B mesons to be resolved. The difference in the z positions of the decay vertices of the two B mesons in the laboratory, Δz, is related to their decay time difference, Δt, by

$$\Delta z \simeq \beta\gamma\gamma_B c\tau\Delta t, \tag{1.5}$$

where β and γ are the velocity and Lorentz boost factor of the center of momentum (i.e., $\Upsilon(4S)$) system, and γ_B is the boost factor of the B within the $\Upsilon(4S)$ system. In this analysis, one B is fully reconstructed in a flavor eigenstate, so its flavor is known and its decay vertex is measured well. The flavor of the other B is determined in an inclusive way, using flavor-tagging techniques which exploit correlations between the B flavor and its decay products. In particular, the charge of the primary lepton from semileptonic decays is correlated with the flavor of the B, as is the charge of secondary kaons from $b \to c \to s$ transitions. An inclusive vertexing algorithm is used to determine the tag-side vertex position. The difference in decay times is extracted from the measured decay vertices and momentum of the reconstructed B. Finally, an unbinned maximum-likelihood fit is performed to extract Δm_d as well as the resolution functions and mistag rates from the data themselves.

1.3 Blind Analysis

In order to avoid possible experimenter's bias, the central value of Δm_d was hidden until the systematic uncertainties and consistency checks were completed. The method used to hide the central value was a Gaussian smearing of width 0.100 ps^{-1}, i.e., more than six times larger than the expected statistical error. Many of the systematic studies and variations performed on the data are therefore reported as changes in the value observed with respect to the nominal fit, i.e., $\delta\Delta m_d$.

1.4 Organization

This document is arranged as follows: Chapter 2 describes the *BABAR* detector, the data and Monte Carlo samples used for the analysis, the event selection criteria, and reconstruction of B^0 decays to open charm and charmonium flavor eigenstates. Chapter 3 explains the inclusive techniques used to reconstruct the second B's vertex and flavor. In Chapters 4 and 5, the unbinned maximum likelihood fit and the results of the fit to data are presented. The suite of consistency checks performed

and systematic uncertainties assigned are described in Chapters 6 and 7. Finally, this measurement is put into the context of the current state of knowledge of the CKM description of flavor interactions in Chapter 8. Throughout this document, the convention $\hbar = c = 1$ is used, the symbol B^0 refers to the B_d meson, and unless otherwise stated, charge-conjugated processes are implied.

Chapter 2

The *BABAR* Detector, Dataset, and Event Selection

This chapter briefly describes the *BABAR* detector, the data sample used for the event selection and background characterization studies, and the Monte Carlo samples used. Event selection requirements and reconstruction of candidate composite particles is described. Finally, B meson reconstruction techniques are explained, and the event samples used in the Δm_d measurement are presented.

2.1 The *BABAR* Detector

The *BABAR* detector is an asymmetric 4π steradian solid-angle coverage charged and neutral spectrometer that has been optimized for the asymmetric decays of the $\Upsilon(4S)$ center of mass produced by the PEP-II collider and is described in detail in [10].

Charged particles are detected and their momenta and positions measured by a tracking system which employs a five-layer silicon vertex tracker (SVT) and a 40-layer drift chamber (DCH) embedded in a 1.5 T solenoidal magnetic field. Single hit resolution in the SVT approaches 15 μm for perpindicular tracks. The drift chamber single hit resolution is typically 125 μm. B decay vertices are typically reconstructed with a resolution of 80μm along the boost direction for the fully reconstructed candidate, $B_{\rm rec}$, and 100 to 150 μm for the tagging decay $B_{\rm tag}$.

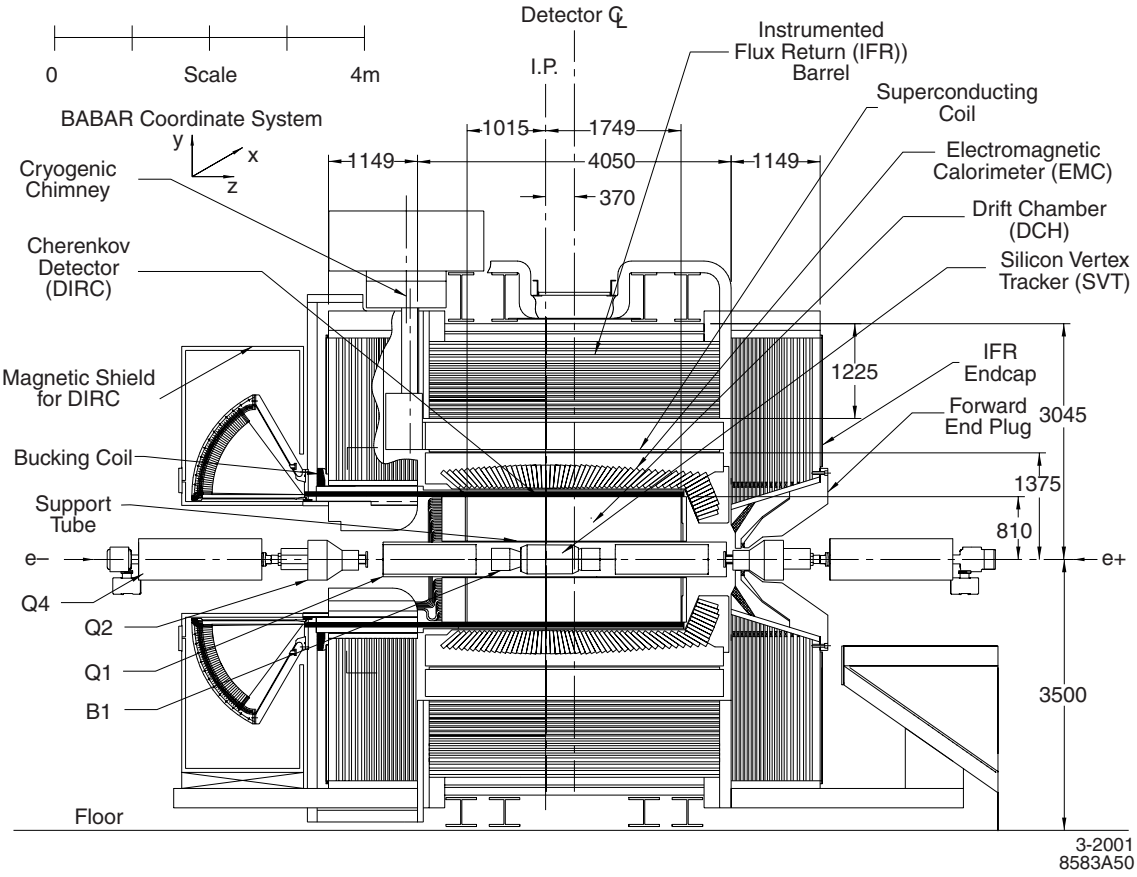

Figure 2-1: The *BABAR* detector

A detector of internally reflected Cherenkov radiation generated in quartz bars (DIRC) is used for charged hadron identification. 2.5 σ separation between kaons and pions is achieved at 4 GeV, with better separation at lower momenta.

A CsI(Tl) electromagnetic calorimeter (EMC) is used to detect photons and neutral hadrons, and for electron identification. Typical energy resolution is $\sigma(E)/E = (2.3\pm0.03\pm0.3)/\sqrt[4]{E} \oplus (1.85\pm0.07\pm0.1)\%$.

The instrumented flux return (IFR) for the magnet contains multiple layers of resistive plate chambers (RPC) sandwiched between layers of iron, and is used to identify muons and neutral hadrons.

2.2 Data Sample

The data sample consists of 30.7 fb^{-1} of electron-positron annihilation data produced at a center of mass energy near the $\Upsilon(4S)$ resonance by the PEP-II asymmetric collider at the Stanford Linear Accelerator Center. PEP-II collides 3.1 GeV positrons in the low-energy ring (LER) with 9 GeV electrons in the high-energy ring (HER), providing a Lorentz boost of $\beta\gamma = 0.55$. The size of the luminous regoin is given in Table 2.1. This data was collected by the *BABAR* detector in two running periods. Run 1 was collected in the period 1999–2000, while Run 2 was collected in the year 2001. A breif shutdown between the two runs was used to perform maintenance on the EMC and DCH, but no significant changes were made. An improved tracking system alignment algorithm was used for Run 2, so a different treatment of the Δt resolution is necessary.

2.3 Monte Carlo Samples

Several Monte Carlo samples are used to verify the analysis procedure and study systematic effects. A high-statistics fast parameterized Monte Carlo is used to check a variety of systematic effects. A full `GEANT-3` based detector simulation is also used. The `GEANT-3` sample is comprised of a "cocktail" of the subset of B^0 decays $B^0 \rightarrow$

Table 2.1: PEP-II parameters

Parameters	Design	Typical
Energy HER/LER (GeV)	9.0/3.1	9.0/3.1
Current HER/LER (A)	0.75/2.15	0.7/1.3
# of bunches	1658	553-829
Bunch spacing (ns)	4.2	6.3-10.5
$\sigma_x(\mu\mathrm{m})$	110	120
$\sigma_y(\mu\mathrm{m})$	3.3	5.6
$\sigma_z(\mathrm{mm})$	9	9
Luminosity ($10^{33}\mathrm{cm}^{-2}\mathrm{s}^{-1}$)	3.0	4.0

$D^{*-}\pi^+$, $B^0 \to D^{*-}\rho^+$, $B^0 \to D^{*-}a_1^+$, $B^0 \to D^-\pi^+$, $B^0 \to D^-\rho^+$, $B^0 \to D^-a_1^+$. The $B^0 \to J/\psi K^{*0}$ was not included in this cocktail, but rather was generated separately for technical reasons. Each decay in the cocktail is included in an amount proportional to its relative branching fraction. This sample consists of 2.9 million events and corresponds to 574 fb^{-1} of on-peak running. Two similar B^+ `GEANT-3` cocktails are used for background characterization.

2.4 Basic Event and Candidate Selection

The events used in this analysis are selected by requiring a minimum of four charged tracks and a total observed energy greater than 5 GeV, and demanding the production vertex of the event be within 0.5 cm of the measured interaction point in the plane transverse to the beam axis.

The sample of B decays used includes seven different two-body B^0 decay topologies that unambiguously determine the flavor of the parent B^0. They include the following decay modes: $B^0 \to D^{*-}\pi^+$, $B^0 \to D^{*-}\rho^+$, $B^0 \to D^{*-}a_1^+$, $B^0 \to D^-\pi^+$, $B^0 \to D^-\rho^+$, $B^0 \to D^-a_1^+$, and $B^0 \to J/\psi K^{*0}$. The daughter particles of the B decays are reconstructed in a variety of final states. Selection of the daughter particles in these decays is described in this section, and B reconstruction is described in Section 2.5.

2.4.1 Selection of Leptons

Electron candidates are required to have a ratio of electromagnetic calorimeter energy to track momentum in the range $0.88 < E/p < 1.3$, a cluster shape consistent with an electromagnetic shower, and DCH dE/dx and DIRC Cherenkov angle consistent with an electron.

Muon candidates must satisfy requirements on the number of interaction lengths of IFR iron penetrated ($N_\lambda > 2.2$), the difference in measured and expected interaction lengths penetrated ($N_\lambda^{\rm exp} - N_\lambda < 1$), the position match between the extrapolated DCH track and the IFR hits, and the average number and spread of IFR hits per layer.

2.4.2 Selection of Light Hadrons

Pairs of photons detected by the EMC are constrained to the known π^0 mass if they are within $\pm$ 20 MeV of the nominal invariant mass and their total energy is greater than 200 MeV.

$K_s^0 \to \pi^+\pi^-$ candidates are required to have an invariant mass between 462 and 534 MeV and a χ^2 probability for the vertex fit greater than 0.1 %. The opening angle between the K_s^0 flight direction and momentum vector is required to be less than 200 miliradians, and the transverse flight distance from the primary event vertex must be greater than 2 mm.

2.4.3 Selection of Charm Mesons and Charmonium

$\overline{D}^0$ candidates are reconstructed in their decays to $K^+\pi^-, K^+\pi^-\pi^0, K^+\pi^+\pi^-\pi^-$, and $K_s^0\pi^+\pi^-$. D^- candidates are selected in decays to $K^+\pi^-\pi^-$ and $K_s^0\pi^-$. Their daughters are required to have a momentum greater than 200 MeV. For $\overline{D}^0 \to K^+\pi^-\pi^0$, the resonant mode $\overline{D}^0 \to K^+\rho^-$ is reconstructed, followed by $\rho^- \to \pi^-\pi^0$, and the $\pi^-\pi^0$ invariant mass is required to be within 150 MeV of the nominal ρ mass, and the angle between the π^- and $\overline{D}^0$ in the ρ rest frame, $\theta^*_{D^0\pi}$ must satisfy $|\cos\theta^*_{D^0\pi}| > 0.4$. Finally, D candidates with a momentum greater than 1.3 GeV in

the $\Upsilon(4S)$ frame, a vertex fit χ^2 probability greater than 0.1 % , and an invariant mass within $\pm$ 3 σ calculated on an event-by-event basis of the nominal value, are subject to a mass-constrained fit for further analysis.

D^{*-} candidates are formed by combining a D^0 and a pion with momentum greater than 70 MeV. The pion is constrained to originate at the nominal beam spot position when the vertex fit is performed. Candidates with $m(D^0\pi) - m(D^0)$ within 3 σ of the nominal value are selected, where $\sigma = 1.1$ MeV for the $D^0 \to K^+\pi^-\pi^0$ mode and 0.8 MeV for the other modes.

$J/\psi \to e^+e^-$ or $\mu^+\mu^-$ candidates are required to have at least one daughter positively identified as an electron or a muon. Electron candidates outside the EMC acceptance must have DCH dE/dx consistent with an electron. The second muon candidate, if in the EMC acceptance, must have E/p consistent with a minimum ionizing particle. J/ψ candidates must have an invariant mass between 2.95 (3.06) and 3.14 GeV for the e^+e^- ($\mu^+\mu^-$) channels.

2.5 Reconstruction and Selection of B^0 Mesons

Candidate B^0s are reconstructed in the flavor eigenstate decay modes $D^{(*)-}\pi^+/\rho^+/a_1^+$ by combining a D^{*-} or D^- candidate with a π^+, ρ^+ ($\rho^+ \to \pi^+\pi^0$), or a_1^+ ($a_1^+ \to \pi^+\pi^-\pi^+$). Similarly, B^0 candidates are reconstructed in the flavor eigenstate decay mode $J/\psi K^{*0}, K^{*0} \to K^-\pi^+$. Typical reconstruction efficiencies vary between 8% and 35 %, depending on the particular final state.

For $B^0 \to D^{*-}\rho^+$, the π^0 from the ρ decay is required to have an energy greater than 300 MeV. For $B^0 \to D^{*-}a_1^+$, the a_1^+ candidate is formed from three charged pions with an invariant mass in the range 1.0 to 1.6 GeV, and requiring the vertex fit to have a χ^2 probability greater than 0.1 %. For many modes with a charged kaon in the final state, acceptable purity is achieved with no particle identification requirements. In less pure modes, where combinitorial background results from mis-identifying the daughter kaon, a minimal requirement on the kaon is sufficient to achieve acceptable signal purity.

Continuum background is rejected by requiring the normalized second Fox-Wolfram [11] moment be less than 0.5. Further suppression is achieved by a mode-dependent requirement on the angle between the thrust axis of the B decay and the thrust axis of the rest of the event in the $\Upsilon(4S)$ frame ($\theta_{\rm thrust}$).

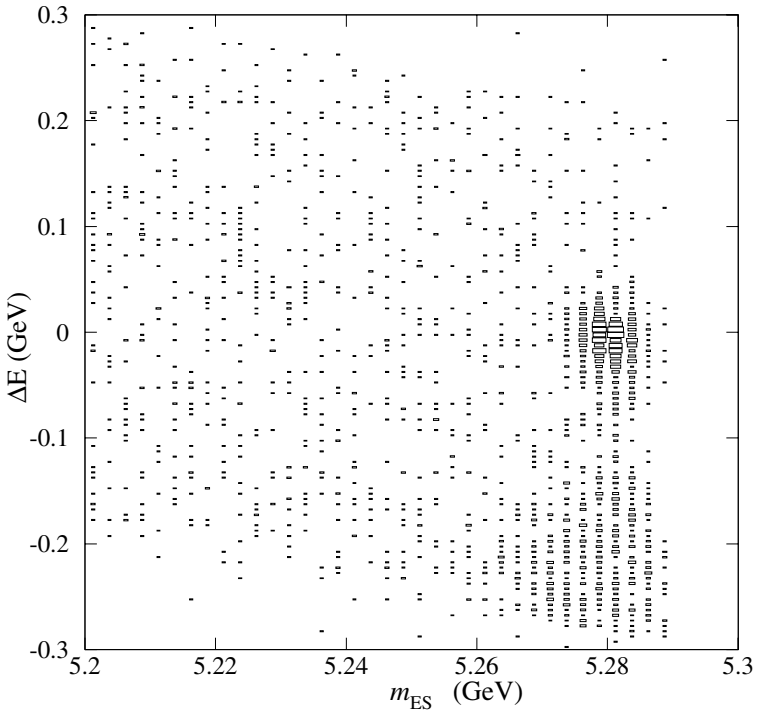

Figure 2-2: Distribution of ΔE versus $m_{\rm ES}$ for the decay $B^0 \to D^{*-}\pi^+$, $D^0 \to K^-\pi^+$. in Run 1 data. Signal is clustered around $m_{\rm ES}$ of 5.28 GeV, ΔE =0. Note the enhancement in the region of the nominal B mass at negative ΔE from higher-multiplicity B decays (e.g., $B^0 \to D^{*-}\rho^+$).

Two kinematic variables are used to identify B candidates. The first of these, ΔE, is defined $\Delta E = E_{\rm rec} - E_{\rm beam}$ where $E_{\rm rec}$ is the energy of the B candidate, and $E_{\rm beam}$ is equal to half of the measured beam energy in the $\Upsilon(4S)$ frame. The resolution in ΔE is dominated by detector effects. The second variable is the energy-substituted B mass, defined $m_{ES} = \sqrt{E_{\rm beam} - \sum p_i}$, where p_i are the momenta of the B daughters. The resolution in this variable is dominated by the spread in the beam energies. The distribution of ΔE versus $m_{\rm ES}$ for the decay $B^0 \to D^{*-}\pi^+$ is shown in Figure 2-2. An

example of an event in which both B decays are reconstructed is shown in Figure 2-3.

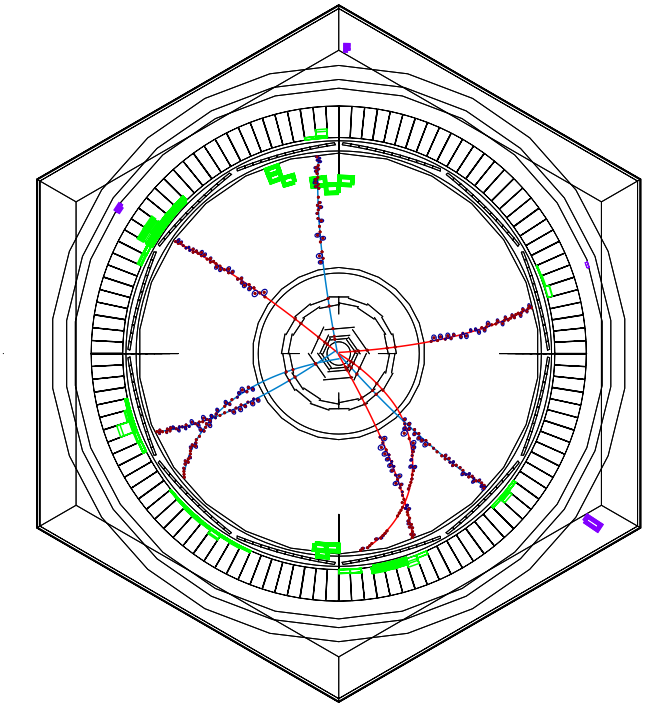

Figure 2-3: A fully reconstructed $\Upsilon(4S)$ decay. The event is shown in a fish-eye projection which magnifies the central portion near the vertex detector relative to the rest of the detector. The two B mesons in the event decay to $B^0 \to D^{*-}\pi^+$, and $\psi(2S)K^0_S$. The two pions from the K^0_S can be seen in the lower left at about the eight o'clock position, and the muons from the $\psi(2S)$ decay are the tracks at twelve o'clock and four o'clock. The high-momentum pion from the $B^0 \to D^{*-}\pi^+$ decay can be seen at about ten o'clock. The low-momentum pion from the $D^* \to D^0\pi$ decay can be seen looping around clockwise towards six o'clock, and the daughters in the $D^0 \to K\pi$ decay are at three and 5 o'clock respectively.

If there are multiple candidates in the region $5.2 < m_{\rm ES} < 5.3$ GeV, $|\Delta E| < 3\sigma_{\Delta E}$, the candidate with the smallest $|\Delta E|$ is retained. The error on ΔE depends on the B decay channel, but typically ranges from 15 to 35 MeV. Fewer than 1 % of events have multiple candidates. Finally, a topological vertex fit of the candidate must converge, and have $|\Delta z| < 3$ mm, and $\sigma_{\Delta z} < 400$ μm. The B^0 sample obtained with these criteria contains 10941 ± 133 signal events in the region $m_{\rm ES} > 5.27$ GeV, with a

purity ranging from 67–95 %, depending on the B^0 decay mode.

The $m_{\rm ES}$ distributions are described by a Gaussian signal component and an Argus [12] function to parameterize the background distribution:

$$B(m_{\rm ES}|E_{\rm beam},\kappa) = \frac{\theta(m_{\rm ES} < E_{\rm beam})}{N} m_{\rm ES}\sqrt{1-(m_{\rm ES}/E_{\rm beam})^2}\exp\left[\kappa(1-(m_{\rm ES}/E_{\rm beam})^2)\right] \quad (2.1)$$

The parameters of the Argus function are the kinematic cutoff (equal to one half of the available center of mass energy), $E_{\rm beam}$, the normalization N, and the shape parameter κ. This function is motivated by assuming that the background is uniformly distributed in phase space. The distributions of $m_{\rm ES}$ for open charm and charmonium modes are shown in Figures 2-4 and 2-5, and for all modes together in Figure B-7, along with fits to the parameterization just described. Appendix B shows distributions for each individual decay chain reconstructed. The yields are summarized in Table 2.2.

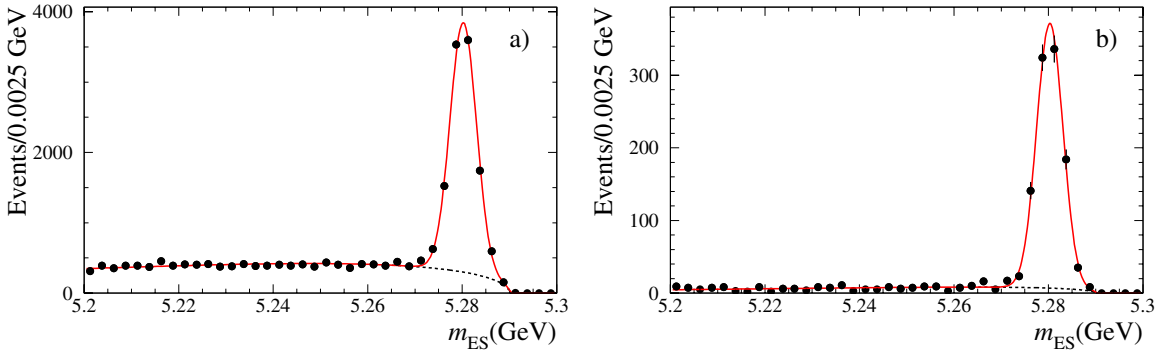

Figure 2-4: Beam-energy substituted mass $m_{\rm ES}$ for the selected B^0 candidates in data for (a) $B \to D^{(*)}h$ and (b) $B \to J/\psi K^{*0}$.

2.6 Background Characterization

The background to the selected hadronic B decays has contributions from continuum (udsc) events and $B\overline{B}$ events. The relative ratios vary depending on the track

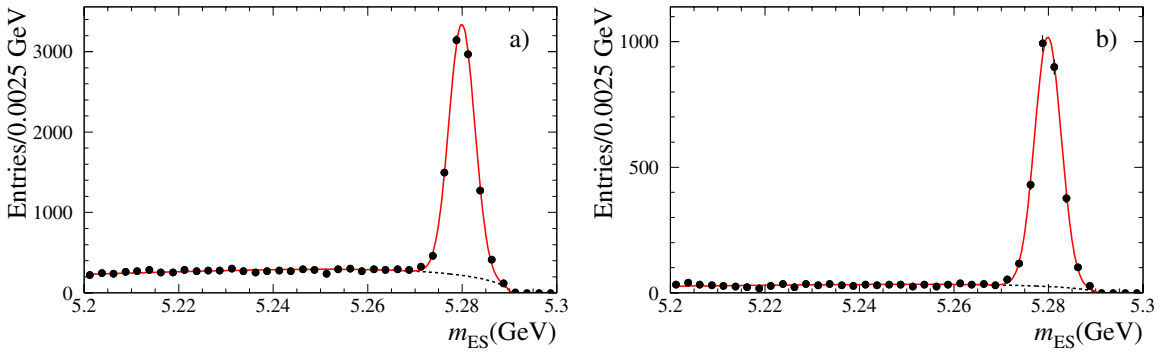

Figure 2-5: Beam-energy substituted mass $m_{\rm ES}$ for the selected B^+ candidates in data for $B \to D^{(*)}h$ (a) and $B \to J/\psi K^{(*)+}$ and $\chi_{c1}K^+$ (b).

multiplicity in the reconstructed decay mode. The fraction of combinatorial (non-peaking) background candidates in the signal sample is determined from a fit to the $m_{\rm ES}$ distribution in which the signal is described by a Gaussian and the background by the Argus shape [12].

A small fraction of the signal peak ($\sim$1.3 $\pm$ 0.8 %) arises from backgrounds which are not well-described by the phase-space motivated Argus background parameterization. They are enhanced near the signal region relative to the Argus shape and are therefore called "peaking backgrounds". A study of generic $B\overline{B}$ Monte Carlo indicates that the source of this kind of background is mis-reconstructed B mesons, where a slow pion from the reconstructed B is swapped with a slow pion from the other B in the event. For example, when reconstructing the decay $B^0 \to D^{*-}\pi^+$, if the true decay was $B^+ \to D^{*0}\pi^+$, the D^{*0} can be mis-reconstructed as a D^{*-} simply by using a low-momentum pion from the other B^+ in the event, if one is present. This type of mis-reconstruction peaks near the nominal B^0 mass, and at ΔE near 0, since the total energy is approximately right (provided the two pions which are confused have similar momenta).

The peaking background from neutral B decays has the same time structure as signal, and is thus considered as such. This hypothesis is checked and described in Section 7.1.10. On the other hand, the peaking background from charged B decays needs to be accounted for explicitly in the fit to the Δt distributions because of its

Table 2.2: Event yields for the B^0 and B^+ samples used in this analysis, before any tagging or tagging vertex requirements. The yields, purity, and signal size for B decays to hadronic final states are obtained from a fit to the $m_{\rm ES}$ distribution described in Section 2.5, after selection on ΔE. Purities are quoted for $m_{\rm ES} > 5.27$ GeV.

Sample	Final state	Signal	Purity (%)
B^0	$D^{*-}\pi^+$	2380 ± 57	92
	$D^{*-}\rho^+$	1438 ± 52	84
	$D^{*-}a_1^+$	1146 ± 45	80
	$D^-\pi^+$	2685 ± 65	83
	$D^-\rho^+$	1421 ± 57	74
	$D^-a_1^+$	845 ± 44	67
	$J/\psi K^{*0}$ $(K^{*0} \to K^+\pi^-)$	1013 ± 36	95
	Total	10941 ± 133	83
B^+	$\overline{D}^0\pi^+$	6850 ± 102	83
	$\overline{D}^{*0}\pi^+$	1708 ± 51	91
	$J/\psi K^+$	1921 ± 46	97
	$\psi(2S)K^+$	292 ± 18	98
	$\chi_{c1}K^+$	195 ± 29	95
	$J/\psi K^{*+}$ $(K^{*+} \to K^+\pi^0)$	384 ± 25	87
	Total	11343 ± 129	86

different Δt dependence. The amount of B^+ peaking background is quantified by using Monte Carlo generated in two cocktails of decay modes most likely to be misreconstructed in our B^0 sample. The Monte Carlo distribution for 20 fb^{-1} equivalent is shown in Figure 2-6. In addition, as a cross-check, the amount of B^+ peaking background is allowed to float in the mixing fit (see Section 7.1.10).

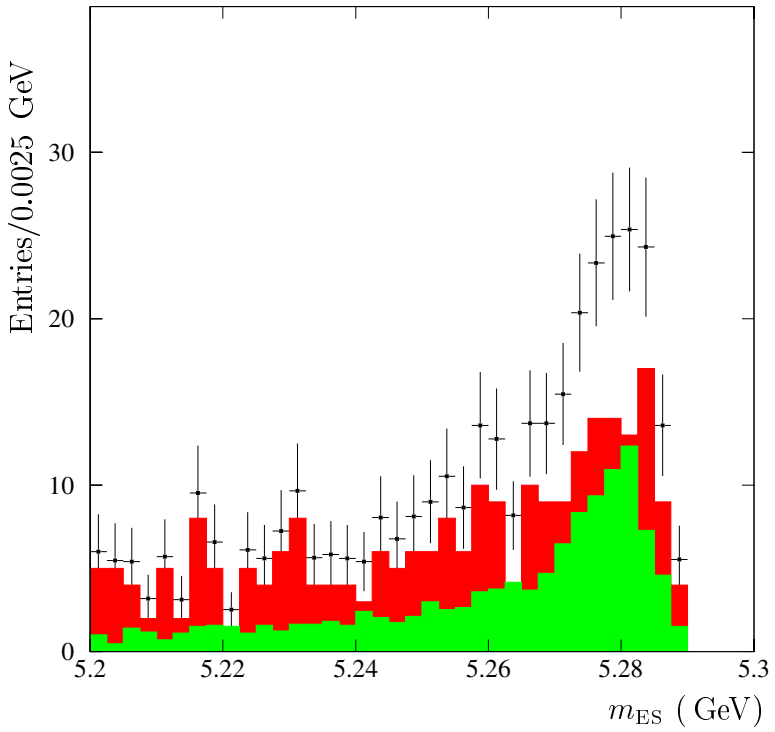

Figure 2-6: Beam-energy substituted mass $m_{\rm ES}$ for B^+ Monte Carlo events reconstructed as the B^0 decay modes used for this analysis, scaled to 20 fb^{-1}. The decays $B^+ \to D^{(*)0}\pi$ are shown in green (lighter), and $B^+ \to D^{(*)0}\rho/a_1/4\pi$ in red (darker). Points with error bars are the sum of the two components.

Chapter 3

Flavor Tagging and Tag-Side Vertexing

This Chapter describes the techniques and algorithms used for tagging and vertexing the other B meson in the event. The techniques described here lay the foundation for the time-dependent B^0 oscillation measurement described in Chapter 4.

3.1 Flavor Tagging

After determining which particles compose the reconstructed $B(B_{\rm rec})$, the remaining particles in the event are analyzed to determine the flavor of the $B_{\rm tag}$. This ensemble is then assigned a flavor tag, either B^0 or $\overline{B}^0$. The flavor-tagging algorithm uses the information carried by primary leptons from semileptonic B decays, charged kaons from $b \to c \to s$ transitions, soft pions from D^* decays, and more generally the charges and momenta of the remaining charged particles in the event. While not as clear a discriminator as charged leptons and kaons, the momentum spectra can provide hints to the tag, and this information is used as input to a neural network based tagging algorithm.

Events are assigned to the `Lepton` category if they contain an identified lepton with a center-of-mass energy greater than 1.0 or 1.1 GeV for electrons and muons, respectively. This requirement selects mostly primary leptons and suppresses lower-

momentum, opposite-sign particles from semileptonic charm decays.

Kaons are identified with a neural network which uses as inputs the likelihood ratios formed from SVT and DCH dE/dx measurements, and the information derived from comparing individual photo-multiplier hits in the DIRC to the expected pattern of Cherenkov light for either kaons or pions. The charges of all identified kaons are summed, and if $\sum Q_K \neq 0$, the event is assigned to the `Kaon` category, and is tagged using the charge of the kaon(s).

The final two categories employ a multivariate analysis using a neural network which is trained to identify primary leptons, kaons, soft pions, and the momentum and charge of the track with the maximum center-of-mass momentum. The details of the implementation of the neural network can be found in [13] and [14]. It uses three neural networks which extract tagging information from the event, and the outputs of these three are combined by a final neural network. Depending on the output of the neural network (see Figure 3-1), events are assigned a tag in two mutually-exclusive categories: `NT1` (more certain tag) or `NT2` (less certain tag). Approximately 30 % of events are not assigned a tag and are excluded from the analysis.

Tag assignments are done in a hierarchical, mutually-exclusive way. Events with a lepton tag and no conflicting kaon tag are assigned to the `Lepton` category. If no `Lepton` tag is assigned, then the event is tagged, if possible, in the `Kaon` category. Otherwise, the two neural network categories are used.

3.1.1 Experimental Consideration: Effect of Mistags

When studying B decays in the laboratory, the experimental procedure used to determine the flavor tag of the second B in the event is imperfect; thus there is a finite probability that the event will be incorrectly tagged. The effect of mistagging events on the mixing asymmetry is explored in this subsection.

Consider a tagging algorithm which correctly tags a B^0 with probability ϵ, and correctly tags a $\overline{B}^0$ with probability $\bar{\epsilon}$. The effect of this algorithm on a sample of events which have true decays to $B\overline{B}$, $N^{\rm t}_{B\overline{B}}$ will be that the observed events have incorrect tag information some of the time. The observed number of correctly tagged

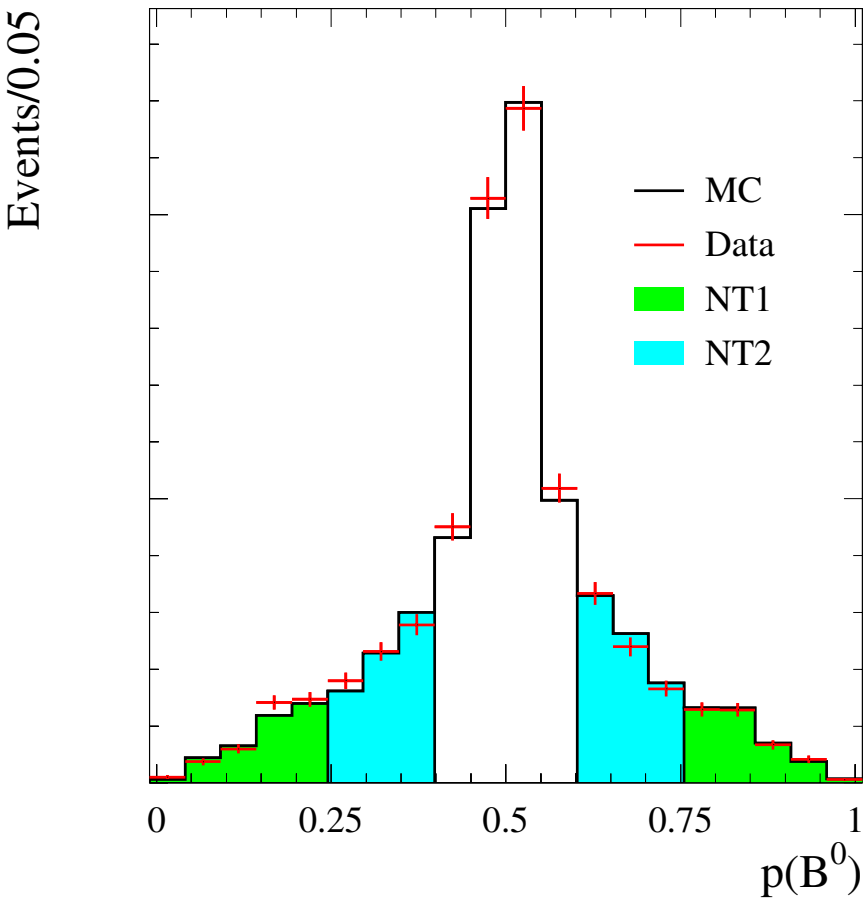

Figure 3-1: Output of neural network based tagging algorithm for events which were not assigned to either the `Lepton` or `Kaon` categories. Events in the unshaded region near 0.5 have ambiguous tag information and were discarded.

events will just be $N_{B\overline{B}} = \epsilon N^{\rm t}_{B\overline{B}}$, and similarly the observed number of incorrectly tagged events will be $N_{\overline{B}\overline{B}} = (1-\epsilon)N^{\rm t}_{B\overline{B}}$. The complete list of possibilities is listed here:

$$\begin{aligned}
N_{B\overline{B}} &= \epsilon N^{\rm t}_{B\overline{B}} \qquad & N_{\overline{B}\overline{B}} &= (1-\epsilon)N^{\rm t}_{B\overline{B}} \\
N_{BB} &= \epsilon N^{\rm t}_{BB} \qquad & N_{\overline{B}B} &= (1-\epsilon)N^{\rm t}_{BB} \\
N_{\overline{B}B} &= \bar{\epsilon} N^{\rm t}_{B\overline{B}} \qquad & N_{\overline{B}\overline{B}} &= (1-\bar{\epsilon})N^{\rm t}_{\overline{B}B} \\
N_{\overline{B}\overline{B}} &= \bar{\epsilon} N^{\rm t}_{\overline{B}\overline{B}} \qquad & N_{B\overline{B}} &= (1-\bar{\epsilon})N^{\rm t}_{\overline{B}\overline{B}}
\end{aligned}$$

The measured asymmetry becomes

$$\begin{aligned}
A_{\rm mix} &= \frac{N_{\rm unmixed} - N_{\rm mixed}}{N_{\rm unmixed} + N_{\rm mixed}} \\
&= \Big[\epsilon N^{\rm t}_{B\overline{B}} + (1-\bar{\epsilon})N^{\rm t}_{\overline{B}\overline{B}} + (1-\epsilon)N^{\rm t}_{BB} + \bar{\epsilon}N^{\rm t}_{B\overline{B}} \\
&\quad -(1-\epsilon)N^{\rm t}_{B\overline{B}} - \epsilon N^{\rm t}_{BB} - (1-\bar{\epsilon})N^{\rm t}_{\overline{B}B} - \bar{\epsilon}N^{\rm t}_{\overline{B}\overline{B}}\Big] \\
&\quad \times \Big[N^{\rm t}_{B\overline{B}} + N^{\rm t}_{\overline{B}B} + N^{\rm t}_{BB} + N^{\rm t}_{\overline{B}\overline{B}}\Big]^{-1} \\
&= \frac{(N^{\rm t}_{B\overline{B}} - N^{\rm t}_{BB})(2\epsilon - 1) + (N^{\rm t}_{\overline{B}B} - N^{\rm t}_{\overline{B}\overline{B}})(2\bar{\epsilon} - 1)}{N^{\rm t}_{B\overline{B}} + N^{\rm t}_{\overline{B}B} + N^{\rm t}_{BB} + N^{\rm t}_{\overline{B}\overline{B}}} \qquad (3.1)
\end{aligned}$$

Since the $N^{\rm t}$ terms are the theoretically true numbers of events, from Equation A.48,

$$\frac{(N^{\rm t}_{B\overline{B}} - N^{\rm t}_{BB})}{N^{\rm t}_{B\overline{B}} + N^{\rm t}_{\overline{B}B} + N^{\rm t}_{BB} + N^{\rm t}_{\overline{B}\overline{B}}} = \frac{(N^{\rm t}_{\overline{B}B} - N^{\rm t}_{\overline{B}\overline{B}})}{N^{\rm t}_{B\overline{B}} + N^{\rm t}_{\overline{B}B} + N^{\rm t}_{BB} + N^{\rm t}_{\overline{B}\overline{B}}} = \frac{\cos(\Delta m_d \Delta t)}{2}$$

Therefore, the observed asymmetry is just

$$A_{\rm mix} = \left[\frac{(2\epsilon - 1)}{2} + \frac{(2\bar{\epsilon} - 1)}{2}\right]\cos(\Delta m_d \Delta t) \qquad (3.2)$$

Now the mistag rate is related to the correct tag rate: $w = 1 - \epsilon$, so

$$A_{\rm mix} = \left[\frac{(1 - 2w)}{2} + \frac{(1 - 2\bar{w})}{2}\right]\cos(\Delta m_d \Delta t) \qquad (3.3)$$

or in terms of dilution $\mathcal{D} = 1 - 2w$,

$$A_{\rm mix} = \left[\frac{\mathcal{D}}{2} + \frac{\bar{\mathcal{D}}}{2}\right] \cos(\Delta m_d \Delta t) \quad (3.4)$$

$$A_{\rm mix} = \langle \mathcal{D} \rangle \cos(\Delta m_d \Delta t) \quad (3.5)$$

The effect of imperfect tagging is that it reduces the amplitude of the observed mixing asymmetry. For this reason, the sample of fully-reconstructed B mesons used to study mixing is also useful to understand tagging performance. These dilutions are extracted from data separately for each tagging category by the likelihood fit as will be described in Chapter 4. The understanding of tagging gleaned from the study of mixing is a critical component in CP violation studies.

3.2 Tag-side Vertexing

The decay time difference, Δt, between the B decays is determined from the measured separation Δz between the reconstructed B meson ($B_{\rm rec}$) and the flavor-tagged B ($B_{\rm tag}$) using the known boost,

$$\Delta z \simeq \beta\gamma\gamma^*_{\rm rec}\Delta t + \gamma\beta^*_{\rm rec}\gamma^*_{\rm rec}\cos\theta^*_{\rm rec}(\tau_B + |\Delta t|), \quad (3.6)$$

where $\theta^*_{\rm rec}$, β^*rec, and $\gamma^*_{\rm rec}$ are the angle between the $B_{\rm rec}$ flight direction and the beam direction, the velocity, and the boost factor of the $B_{\rm rec}$ in the $\Upsilon(4S)$ rest frame. This expression is not exact, and the approximations made are described in detail in [15]. The resolution of the Δt measurement, $\sigma_{\Delta t}$, is dominated by the resolution of the z resolution of the $B_{\rm tag}$ vertex, and is typically 0.75 ps. This vertex is reconstructed using the remaining tracks in the event after removing those used in the $B_{\rm rec}$. To minimize inclusion of tracks from charm decays, an iterative procedure is used to remove tracks with a large χ^2 contribution to the vertex fit until the remaining tracks have a reasonable χ^2 or no tracks remain.

In the likelihood fit, the time resolution function is modeled by the sum of three Gaussians with different means and widths. The widths of the core and tail Gaussians

$\sigma_{1,2} = S_{1,2} \times \sigma_{\Delta t}$ are scaled from the event-by-event measurement error, $\sigma_{\Delta t}$ derived from the vertex fits. The third Gaussian, with a fixed width of $\sigma_3 = 8$ ps, describes outlier events with misreconstructed vertices, and accounts for less than 1 % of all events. A separate core bias, $\delta_{1,i}$, is allowed for each tagging category i to allow for small biases due to including charm decay products in the tag vertex, and a common bias δ_2 is used for the tail component. The tail and outlier fractions and scale factors are assumed to be the same for all decay modes since the precision of the $B_{\rm tag}$ vertex dominates the resolution. This assumption is confirmed in Monte Carlo simulation studies.

Chapter 4

Unbinned Maximum Likelihood Fit

In this Chapter the procedure for fitting the decay-time difference distributions is described. The likelihood functions described in this Chapter are implemented in the maximum likelihood fitting package for time-dependent fitting `tFit` [16], which is a front end to the minimization routine `MINUIT` [17].

4.1 Fit Inputs and Parameters

The quantities measured in each event which are used as input to the fit are the measured $\Delta t = t_{\rm rec} - t_{\rm tag}$ and error, the energy-substituted B mass for the event $m_{\rm ES}$, the flavor tag, and the tagging category (`Lepton`, `Kaon`, `NT1`, `NT2`). The decay time difference Δt is calculated using the average τ_B approximation technique described in Section 3.2 and [15] for the unmixed and mixed samples. The flavor tag is determined using the methods described in Chapter 3.

The fit proceeds in two stages. First, the $m_{\rm ES}$ distributions are fit to extract a per-event signal probability, which is used to weight the signal and background terms of the likelihood function on a per-event basis, as follows. The combinatorial background fraction in the signal sample is determined by fitting the $m_{\rm ES}$ distribution separately for each tagging category i. The $m_{\rm ES}$ distribution is described by a probability density function consisting of a single Gaussian $S_i(m_{\rm ES})$ for the signal, and the Argus function $B_i(m_{\rm ES})$ (Equation. 2.1) for the combinatorial background. In order to maximize the

statistical power of the sample, each event is assigned a probability that it is signal depending on where it lies in the $m_{\rm ES}$ distribution from the results of the fit:

$$p_{i,\rm sig}(m_{\rm ES}) \;=\; \frac{S_i(m_{\rm ES})}{S_i(m_{\rm ES}) + B_i(m_{\rm ES})} \tag{4.1}$$

Events contribute to the signal term or the background term in the Δt likelihood function with probabilities $p_{i,\rm sig}(m_{\rm ES})$ and $1-p_{i,\rm sig}(m_{\rm ES})$ respectively. Because the four tagging categories have different background sources, these fits are done separately by tagging category.

Next, the decay time difference (Δt) distributions fits are performed, and the rest of this Chapter is devoted to describing the likelihood functions used in this fit. The parameters which are simultaneously fit to the Δt distributions are mentioned here for reference, and the total number of free parameters for each type are noted in parenthesis. The parameters of the signal probability density functions are the mixing frequency Δm_d (1), and the B^0 lifetime $\tau_{B^0} = 1/\Gamma_{B^0}$ (1). The parameters describing the goodness-of-tag, by tagging category, are the average tagging dilutions and dilution differences[1] $\mathcal{D}$ and $\Delta\mathcal{D}$ (8). The resolution model is split into components for signal and background, and contains scale factors σ_i (4), biases δ_i (12), and relative fractions F_i (6). Finally, the background time structure is described by empirical lifetime and prompt components and the relative amounts and dilutions of each (13). The B^0 lifetime is fixed to the Particle Data Group (PDG) [8] value in the nominal fit; the total number of floating parameters is 44.

4.2 Physics Δt Distributions

Here the Δt distributions used to describe both signal and background physics sources are described. These distributions are convolved with the detector resolution function described in Section 4.3 to form the final likelihood function used in the fit.

[1] Dilution differences are the differences between the dilutions for events containing a tagged B^0 and $\overline{B}^0$.

4.2.1 Time-Evolution of B^0- $\overline{B}^0$ Mesons

The log likelihood function which describes the time-dependence of $B^0\overline{B}^0$ oscillations is given by

$$\log \mathcal{L} = \sum_{\substack{\text{unmixed} \\ \text{events}}} \log f_+(\Delta t) + \sum_{\substack{\text{mixed} \\ \text{events}}} \log f_-(\Delta t) \tag{4.2}$$

with

$$f_\pm(\Delta t) = \frac{\Gamma_0}{2} \exp(-\Gamma_0 |\Delta t|) \left[1 \pm \mathcal{D} \cos(\Delta m_d \Delta t)\right] \tag{4.3}$$

This is the physics distribution described in Section A, modified by including the effects of mis-identifying the flavor of the tagging B as described in 3.1.1. The effect of such mis-identification, or mistags, is to reduce the overall amplitude of the observed mixing asymmetry. This is modeled in the likelihood function by including a factor describing this tagging dilution $\mathcal{D} = 1 - 2w$. If events were perfectly tagged, the decay time difference (Δt) distributions would be exponential, modulated by $1 \pm \cos(\Delta m_d \Delta t)$, as shown in Figure 4-1. The time-dependent mixing asymmetry $A_{\text{mixing}}(\Delta t)$ between unmixed and mixed events is proportional to the tagging dilution $\mathcal{D}$:

$$A_{\text{mixing}} \equiv \frac{N_{\text{unmix}} - N_{\text{mix}}}{N_{\text{unmix}} + N_{\text{mix}}} = \mathcal{D} \cos(\Delta m_d \Delta t) \tag{4.4}$$

The four tagging categories (`Lepton`, `Kaon`, `NT1`, and `NT2`) have significantly different mistag rates (and the Δt resolution functions could also potentially be different). Averaging over tagging categories with different tagging performance degrades the sensitivity to Δm_d, and could potentially introduce a bias. Therefore, the tagging dilutions of the four tagging categories are fit separately. Possible differences in the tagging dilution for B^0 tagged events ($\mathcal{D}_{B^0}$) and $\overline{B}^0$ tagged events ($\mathcal{D}_{\overline{B}^0}$) are accounted for by fitting for an average dilution $\langle \mathcal{D} \rangle = \frac{1}{2}(\mathcal{D}_{B^0} + \mathcal{D}_{\overline{B}^0})$ and a dilution difference $\Delta\mathcal{D} = \mathcal{D}_{B^0} - \mathcal{D}_{\overline{B}^0}$, where the subscript refers to the true flavor of the

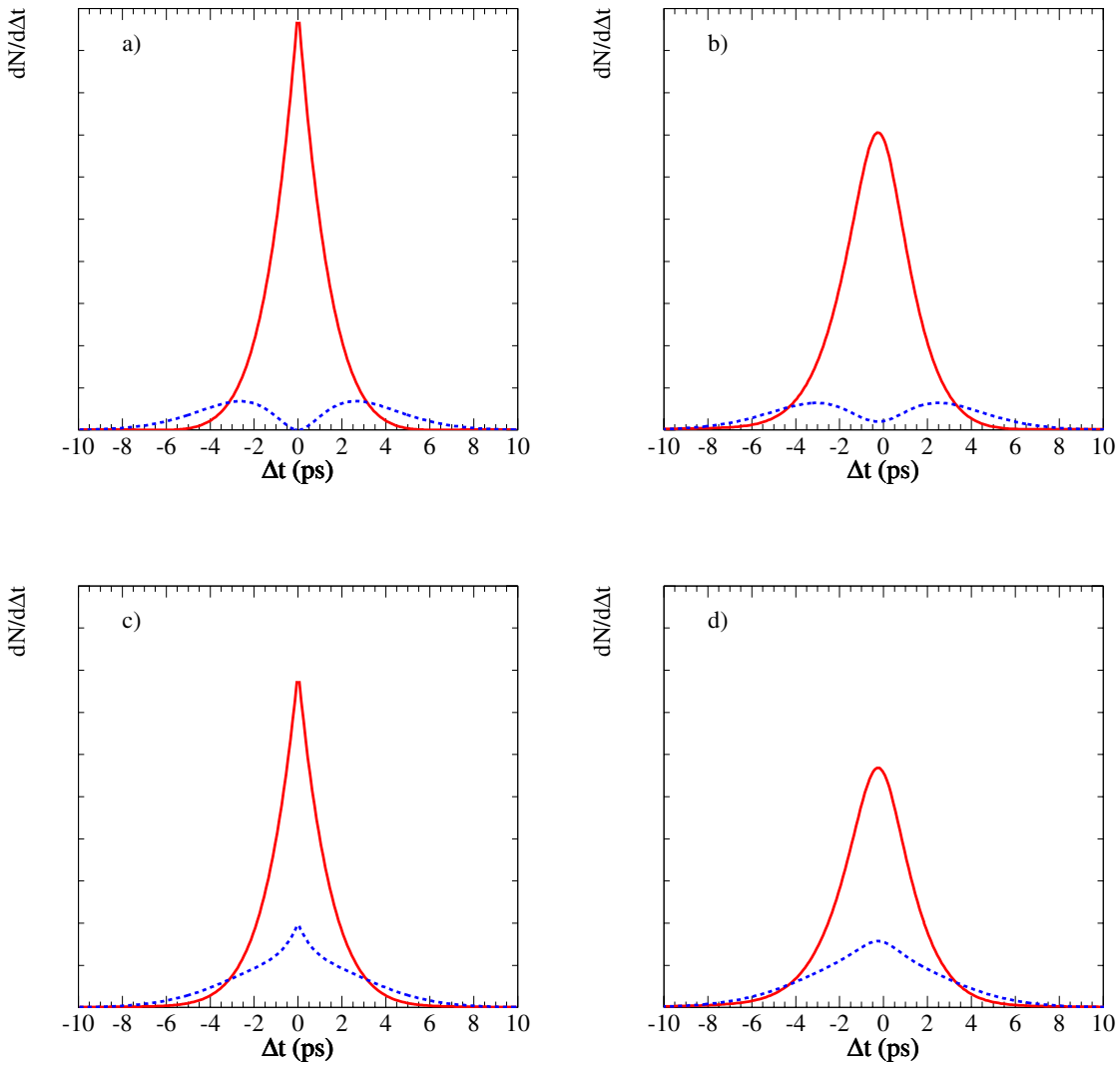

Figure 4-1: Effects of imperfect tagging and detector resolution on the observed Δt distributions. The idealized probabilities of observing events at a given Δt are shown for unmixed (solid) and mixed (dashed) events, for four cases: a) events are perfectly tagged and Δt is perfectly measured, b) events are perfectly tagged, but detector measurement effects are included, c) events are imperfectly tagged but Δt is perfectly measured, and d) events are imperfectly tagged and detector measurement effects are included.

tagging B.

4.2.2 Background Time Structure

Broadly speaking, there are two general kinds of backgrounds in the sample of the selected B^0 candidates. The first background is called combinatorial background (see Section 4.2.2) and it consists of random combinations of charged tracks and neutral showers from both B mesons in $B\overline{B}$ events or from continuum events. This background (by definition) does not peak at the B mass in the $m_{\rm ES}$ distribution. The second background is the so-called peaking background. The peaking background consists of events which tend to peak near the nominal B mass in the $m_{\rm ES}$ distribution. These are misreconstructed events which occur when, for example, a slow pion from the reconstructed B is replaced by a slow pion from the tagging B, causing an enhancement near the nominal B mass. The peaking background from charged B decays is considered explicitly in the likelihood function (see Section 4.2.2), whereas the peaking background from neutral B decays has time-dependent properties very similar to the signal and is treated as such.

Combinatorial Background

Combinatorial backgrounds arise from many different sources and the true time-dependence cannot be derived from first principles. Therefore, the Δt distributions of the backgrounds are approximated with analytical functions and the parameters are measured with control samples (e.g., $m_{\rm ES}$ sideband). In the likelihood fit, the backgrounds are described by separate terms in the likelihood function

$$\begin{aligned}\log\mathcal{L} \;=\; & \sum_{\substack{\text{unmixed}\\ \text{events}}} \log\left(p_{\rm sig} f_{+,\rm sig} + (1-p_{\rm sig}) f_{+,\rm bgd}\right) + \\ & \sum_{\substack{\text{mixed}\\ \text{events}}} \log\left(p_{\rm sig} f_{-,\rm sig} + (1-p_{\rm sig}) f_{-,\rm bgd}\right) \end{aligned} \tag{4.5}$$

An empirical description for the time dependence of the backgrounds in the likelihood fit containing up to three components for each background is used

$$f_{\pm,\mathrm{bgd}} \;=\; \sum_{j=1}^{3} p_j F_{\pm,j}(\Delta t)$$

where p_j is the fraction of the background component j and $F_{\pm,j}(\Delta t)$ contains the time dependence. The three components with different Δt characteristics are listed below:

1. **Zero Lifetime Component:**
   $F_{\pm,1} = (1 \pm \mathcal{D}'_1)$

2. **Non-Zero Lifetime Component (non-mixing):**
   $F_{\pm,2} = (\Gamma_2/2)\ (1 \pm \mathcal{D}'_2)\ \exp(-\Gamma_2|\Delta t|)$

3. **Non-Zero Lifetime Component (mixing):**
   $F_{\pm,3} = (\Gamma_3/2)\ \exp(-\Gamma_3|\Delta t|)\ (1 \pm \mathcal{D}_3 \cos(\Delta m_3 \Delta t))$

The decay times $1/\Gamma_i$ of the backgrounds are not expected to be the exact lifetimes of decaying particles such as B or D mesons. Due to mis-reconstruction, the background lifetimes can be smaller or larger. Based on the same argument, the mixing frequency of the background is not expected to be equal to Δm_d. The dilutions $\mathcal{D}'$ are not dilutions in the sense of mistag rates $\mathcal{D} = 1-2w$. They contain both effects of production asymmetry and incorrect flavor assignment, and are extracted in the fit. In this sense dilutions are also meaningful for non-$B\overline{B}$ events. This rather general approach allows for more fit parameters than may be absolutely necessary to describe the Δt distributions of the backgrounds.

Since the background levels in the signal region are low, the background and signal fit parameters are largely uncorrelated. Therefore, the value of Δm_d extracted in the fit is relatively insensitive to the quality of the fit to the background candidates or the details of the parameterization of their Δt dependence. Note that the goal is to provide an empirical description of the Δt distribution of the background and not to perform a measurement of "physical" parameters of the background candidates.

B^+ Background

The time-dependence of the background from B^+ decays (without detector smearing) can be described by

$$F_{\pm,\text{charged}} = \frac{\Gamma_+}{2}\exp(-\Gamma_+|\Delta t|)(1\pm\mathcal{D}_+) \tag{4.6}$$

where Γ_+ is the B^+ width and the dilution $\mathcal{D}_+$ is different from the dilution for B^0 decays. The B^+ lifetime is fixed to the PDG value [8] and the corresponding tagging dilutions are fixed to values obtained from a study of hadronic B^+ decays [13], which have been cross-checked by doing a combined fit on the B^0 and B^+ samples. In addition, the Δt distribution of this peaking background is checked with Monte Carlo. (See Section 7.1.10).

4.3 Detector Resolution Function

The effects of finite detector resolution in the measurement of Δt are described by an empirical resolution model whose parameters are extracted directly from the data themselves. This requires a modification of the likelihood function. The nominal parameterization used, $\mathcal{R}$, is three Gaussians with different widths and means. This resolution model was chosen based on the observation that in signal Monte Carlo, it has the flexibility to model the Δt residual distributions well. In addition, where appropriate for physics reasons, independent parameters are fit for each of the different tagging categories. Finally, separate resolution function parameters are fit for the signal and the background to minimize correlations between the background parameters and the signal parameters.

$$\begin{aligned}\mathcal{R}_{\text{reso}}(\Delta t, \Delta t_{\text{true}}, \sigma_{\Delta t}|f_{\text{tail}}, f_{\text{outlier}}, \mathcal{S}_{\text{core}}, \delta_{\text{core}}, \mathcal{S}_{\text{tail}}, \delta_{\text{tail}}, \sigma_{\text{outlier}}, \delta_{\text{outlier}}) = \\ (1 - f_{\text{tail}} - f_{\text{outlier}})\frac{\exp -\frac{1}{2}\left(\frac{\Delta t-\delta_{\text{core}}\cdot\sigma_{\Delta t}-\Delta t_{\text{true}}}{\mathcal{S}_{\text{core}}\sigma_{\Delta t}}\right)^2}{\sqrt{2\pi}\mathcal{S}_{\text{core}}\sigma_{\Delta t}} \\ +f_{\text{tail}}\frac{\exp -\frac{1}{2}\left(\frac{\Delta t-\delta_{\text{tail}}\cdot\sigma_{\Delta t}-\Delta t_{\text{true}}}{\mathcal{S}_{\text{tail}}\sigma_{\Delta t}}\right)^2}{\sqrt{2\pi}\mathcal{S}_{\text{tail}}\sigma_{\Delta t}}\end{aligned}$$

$$+f_{\rm outlier}\frac{\exp -\frac{1}{2}\left(\frac{\Delta t-\delta_{\rm outlier}\cdot\sigma_{\Delta t}-\Delta t_{\rm true}}{\sigma_{\rm outlier}}\right)^2}{\sqrt{2\pi}\sigma_{\rm outlier}} \tag{4.7}$$

where $\sigma_{\Delta t}$ is the event-by-event error on Δt computed from the vertex fit.

For most of the events (in data, $f_{\rm core} = 1 - f_{\rm tail} - f_{\rm outlier} \approx 97$ %) the decay time difference Δt is well reconstructed, and well-modeled by the per-event error from the vertex fit. The distribution of $(\Delta t - \Delta t_{\rm true})/\sigma_{\Delta t}$ of those events can be described by a single Gaussian with a width close to unity. The per-event errors are scaled by a global factor $\mathcal{S}_{\rm core}$ to allow for possible deviations from unit width, and this factor is a free parameter in the fit. A possible bias from using tracks from secondary charmed particle decays in the tagging B vertex is modeled by allowing the central value of the resolution $\delta_{\rm core}$ to float.

For a small fraction of the events the Δt error, $\mathcal{S}_{\rm core}\sigma_{\Delta t}$, underestimates the true Δt uncertainty. These events are described by two additional Gaussians in the resolution function: a *tail* Gaussian and an *outlier* Gaussian. The parameterization of the tail Gaussian is identical to the parameterization of the core Gaussian, but the scale factors are fixed at 3. The RMS ($\sigma_{\rm outlier} = 8$ ps) and the mean ($\delta_{\rm outlier} = 0$ ps) of the outlier Gaussian is fixed to be the same for all events and does not use the calculated per-event $\sigma_{\Delta t}$ values.

The fractions of events in the outlier and the tail Gaussians and the means and widths of the core and the tail Gaussian for the signal candidates are free fit parameters. For background candidates, in order to reduce the number of parameters, the fractions of events in the tail Gaussian is fixed to zero. In Section 7.1.9 the small systematic error due to this simplification is discussed.

In general, the mean bias of the $(\Delta t - \Delta t_{\rm true})$ distribution depends on the fraction of tracks from secondary charm decays (and their momenta) in the reconstruction of the tagging B vertex and can be very different in each of the four tagging categories. Therefore, each tagging category is allowed a different $\delta_{\rm core}$. In addition, it was found that the bias is larger for events with larger $\sigma_{\Delta t}$; more details can be found in [18], and in Section 6.11. For this reason, the bias is scaled by the per-event $\sigma_{\Delta t}$ in the

resolution model.

Each of the likelihood functions describing the physics-motivated Δt parameterizations described in Section 4.2 are convolved with the resolution function to take into account the uncertainties in Δt. For example, the parameterization describing the time-evolution of $B^0\overline{B}^0$ oscillations is convolved with the resolution function:

$$F_\pm(\Delta t) \;=\; \int_{-\infty}^{\infty} d(\Delta t')\mathcal{R}(\Delta t - \Delta t')f_\pm(\Delta t') \tag{4.8}$$

For a single Gaussian resolution function with RMS σ,

$$F_\pm(\Delta t) \;=\; \int_{-\infty}^{\infty} d(\Delta t')\frac{1}{\sqrt{2\pi}\sigma}e^{-(\Delta t-\Delta t')^2/2\sigma^2} f_\pm(\Delta t'|\Gamma, \Delta m_d, \mathcal{D}) \tag{4.9}$$

These integrals can be expressed in terms of the complex (complementary) error function erfc(z):

$$\begin{aligned} F_\pm(\Delta t) \;=\; & \frac{\Gamma}{4}\left[e^{-\Gamma\Delta t+(\sigma^2\Gamma^2)/2}\mathrm{erfc}\left(\frac{-\Delta t+\sigma^2\Gamma}{\sqrt{2}\sigma}\right)\right. \\ & \left. \pm\ \mathrm{Re}\left(\mathcal{D}e^{-(\Gamma-i\Delta m_d)\Delta t+\sigma^2(\Gamma-i\Delta m_d)^2}\mathrm{erfc}\left(\frac{-\Delta t+\sigma^2(\Gamma-i\Delta m_d)}{\sqrt{2}\sigma}\right)\right)\right] \end{aligned}$$

The contributions from positive and negative Δt values (with the correct sign of the Δt bias) are added to model the two-sided exponential shape of the Δt distributions:

$$\log\mathcal{F}_\pm(\Delta t) \;=\; \frac{1}{2}(F_\pm(\Delta t - \delta) + F_\pm(-\Delta t + \delta)) \tag{4.10}$$

The equations above do not take into account the possibility to fit in a finite Δt range. The likelihood implementation in `tFit` does include this normalization, and for the measurement described here, only the Δt range from -20 to $+20$ ps is included. Fits in different ranges of Δt are done as a check, and are described in Section 7.1.2.

4.4 Fit Parameters

The fit parameters for the signal events are the $B^0\overline{B}^0$ oscillation frequency Δm_d, the average dilution $\langle \mathcal{D}_i \rangle$ and the dilution difference $\Delta\mathcal{D}_i$ for each of the four tagging categories i and the scale factors, biases and fractions of events in the resolution function terms (double Gaussian resolution + outlier: $\mathcal{S}_{core}$, $4\times\delta_{\mathrm{core},i}$, δ_{tail}, f_{tail} and f_{outlier}). Note that $\mathcal{S}_{\mathrm{tail}}$ is fixed to 3 for both Run 1 and Run 2 (see also [19]).

The background parameters in the nominal fit are the average dilution for each tagging category for the prompt ($\mathcal{D}'_{\tau=0,i}$) and the non-prompt component ($\mathcal{D}'_{\tau>0,i}$), the fraction of events in the prompt component $f_{\tau=0,i}$ and the average lifetime of the non-prompt events $\tau_{\tau>0}$. The background Δt resolution is described by a scale factor $\mathcal{S}_{\mathrm{bkg}}$ and an average bias δ_{bkg} of a single Gaussian resolution function and the fraction of Δt outliers $f_{\mathrm{bkg,\ outlier}}$. No time-dependent mixing term is included in background description of the nominal fit, but the impact of such a term is studied as a source of systematic error (see Section 7.1.8). Due to the high signal purity and the large m_{ES} side band region the correlations between the signal parameters and the background parameters are small. This significantly limits any potential bias in the signal parameters due to an incorrect description of the background.

The remaining non-trivial external input parameters into the fit are the B^0 lifetime (fixed to the PDG [8] average 1.548 ps); the fraction of B^+ peaking background (fixed to 1.3 %), the B^+ lifetime (fixed to the PDG [8] value of 1.653 ps) and B^+ "dilutions" (0.908, 0.764, 0.574 and 0.256 for the `Lepton`, `Kaon`, `NT1` and `NT2` tagging categories, taken from [13].) All external parameters are varied within their uncertainties to obtain the corresponding systematic uncertainties.

Chapter 5

Results

The dilutions, resolution function parameters, and Δm_d are extracted from data by fitting the Δt distributions of the selected B candidates with the likelihood function described in Chapter 4. The results of the nominal fits to data and signal Monte Carlo are described.

5.1 Sample Composition

The yields, efficiencies, and purities in data and signal Monte Carlo by tagging category are shown in Table 5.1. The measurement sensitivity of Δm_d is proportional to the flavor tagging dilutions. Because the mistag rates differ between tagging categories, the overall tagging dilution depends on the population of the signal sample in each tagging category. The tagging efficiencies and signal purities for the individual tagging categories in data and simulated signal events are extracted from fits to the $m_{\rm ES}$ distributions shown in Figs. 5-1 and 5-2 and are listed in Table 5.1. As is described in section 4.1, these fits are used to extract a per-event signal probability which is used to determine how much each event contributes to the signal and background portions of the likelihood function.

Table 5.1: Tagging efficiencies for hadronic B decays in simulated events and in data and signal purities (in the region $m_{\rm ES} > 5.27\,\mathrm{GeV}$) in data separately for the four tagging categories. Note: the signal purity is *not* corrected for possible peaking backgrounds. The Monte Carlo numbers are obtained *after* requiring truth association.

	Efficiency (%)			B candidates			S/(S+B) (%)	
	Monte Carlo	Data		MC	Data			
		Run 1	Run 2		Run 1	Run 2	Run 1	Run 2
All	–	–	–	177262	6149 ± 89	3181 ± 64	83.9 ± 0.5	82.5 ± 0.7
Tagged	69.79 ± 0.11	67.8 ± 0.6	68.7 ± 0.8	123722	4167 ± 73	2186 ± 52	86.3 ± 0.6	84.8 ± 0.8
`Lepton`	13.16 ± 0.08	12.0 ± 0.4	11.3 ± 0.6	23321	738 ± 28	360 ± 20	96.6 ± 0.7	94.9 ± 1.2
`Kaon`	32.56 ± 0.11	33.3 ± 0.6	34.9 ± 0.8	57708	2050 ± 51	1110 ± 37	85.0 ± 0.8	84.0 ± 1.1
`NT1`	8.94 ± 0.07	8.7 ± 0.4	8.3 ± 0.5	15841	533 ± 25	264 ± 17	87.9 ± 1.5	90.7 ± 1.7
`NT2`	15.15 ± 0.09	13.8 ± 0.4	14.1 ± 0.6	26852	846 ± 35	450 ± 26	80.9 ± 1.6	77.0 ± 2.2

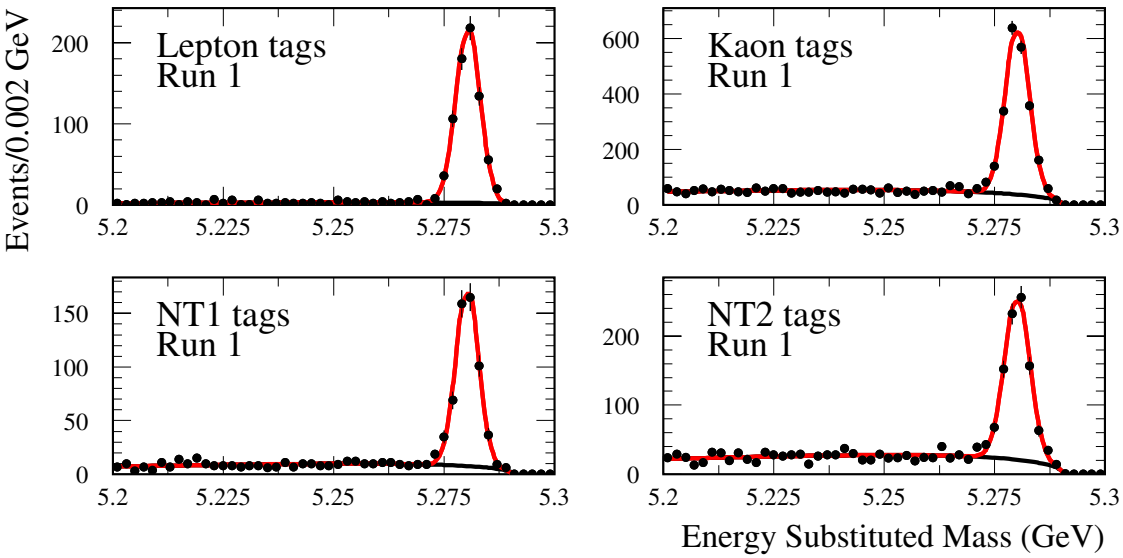

Figure 5-1: Beam-energy substituted mass $m_{\rm ES}$ for the selected B candidates in data separated by tagging category for Run 1. The per-event signal probability is determined from these fits.

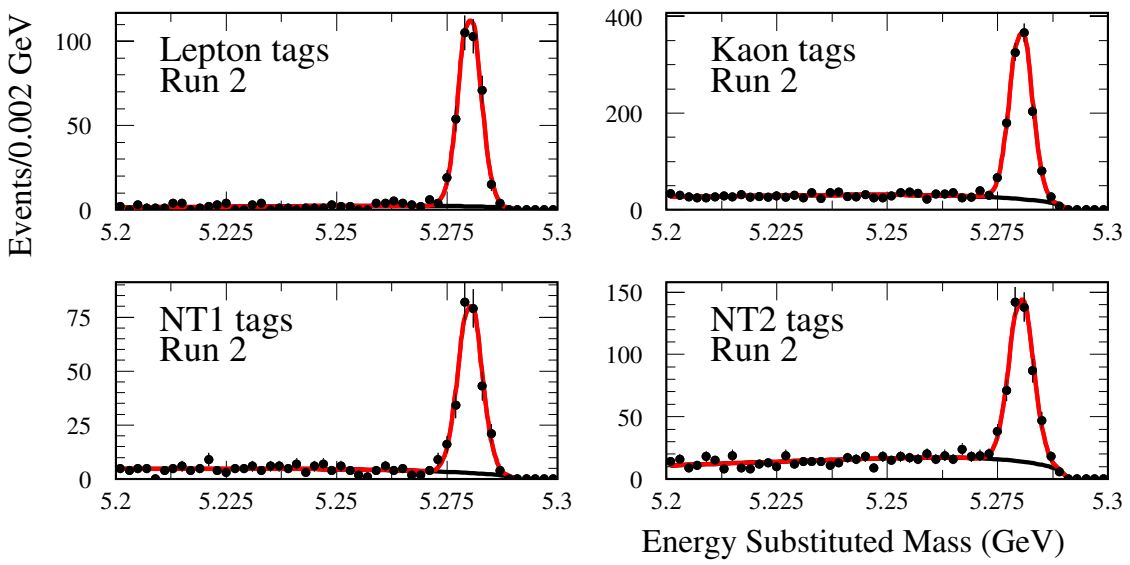

Figure 5-2: Beam-energy substituted mass $m_{\rm ES}$ for the selected B candidates in data separated by tagging category for Run 2. The per-event signal probability is determined from these fits.

5.2 Data Results

In the nominal fit to the Δt distributions of the selected candidates (unmixed and mixed), all four tagging categories are fit simultaneously with 44 floating parameters which describe signal and background properties. The fit parameters are described in Section 4.1 and 4.4. The results of the likelihood fit to the Δt distributions for signal candidates in data and simulated signal events are listed in Table 5.2.

There are two corrections which will be applied to the raw value of Δm_d from the fit, both of which are due to biases in the measurement technique explained in Chapter 7. First, in signal Monte Carlo, the fitted value of the $B^0\overline{B}^0$ oscillation frequency $\Delta m_d = 0.4786 \pm 0.0032$ ps^{-1}, which should be compared to the value used for Monte Carlo generation of 0.472 ps^{-1}. As will be described in Section 7.1.2, Δm_d is corrected by this observed difference. Second, the extrapolation of background parameters from the sideband to the signal region, as described in Section 7.1.10 introduces a second systematic shift of -0.024 ± 0.020 ps^{-1}, which will be corrected for. The total correction applied for both of these effects is -0.0090. The final

Table 5.2: Results from the likelihood fit to the Δt distributions of the hadronic B decays in simulated signal events and in data. In addition to the fit parameter values, the correlation coefficient ρ of the parameter under study with respect to Δm_d is given. For Δm_d, the correlation reported is the *global* correlation. The measured value for Δm_d has not been corrected for potential biases determined from the signal Monte Carlo events or sideband extrapolation. Note that the background parameters for data and signal Monte Carlo should *not* be compared, since the background levels and sources are very different. The value of Δm_d used for event generation in the Monte Carlo sample is 0.4720 ps^{-1}.

Parameter	Fit Value (MC)	ρ	Fit Value (Data)	ρ		
Δm_d (ps^{-1})	0.4786 ± 0.0032	0.52	0.5251 ± 0.016	0.51		
$\mathcal{D}_{\texttt{Lepton}}$	0.853 ± 0.006	0.24	0.842 ± 0.028	0.24		
$\mathcal{D}_{\texttt{Kaon}}$	0.708 ± 0.004	0.31	0.669 ± 0.023	0.30		
$\mathcal{D}_{\texttt{NT1}}$	0.625 ± 0.009	0.12	0.563 ± 0.044	0.11		
$\mathcal{D}_{\texttt{NT2}}$	0.310 ± 0.008	0.08	0.313 ± 0.041	0.11		
$\Delta\mathcal{D}_{\texttt{Lepton}}$	0.005 ± 0.009	-0.01	-0.006 ± 0.045	0.02		
$\Delta\mathcal{D}_{\texttt{Kaon}}$	0.037 ± 0.007	-0.00	0.024 ± 0.033	0.01		
$\Delta\mathcal{D}_{\texttt{NT1}}$	-0.051 ± 0.014	0.00	-0.086 ± 0.068	0.00		
$\Delta\mathcal{D}_{\texttt{NT2}}$	0.070 ± 0.012	0.00	0.100 ± 0.060	-0.00		
$f_{\tau=0,\texttt{Lepton}}$	NA		0.047 ± 0.103	0.01		
$f_{\tau=0,\texttt{Kaon}}$	NA		0.423 ± 0.046	0.01		
$f_{\tau=0,\texttt{NT1}}$	NA		0.329 ± 0.077	0.01		
$f_{\tau=0,\texttt{NT2}}$	NA		0.321 ± 0.078	0.01		
$\tau_{\tau>0}$ (ps)	NA		0.853 ± 0.036	-0.01		
$\mathcal{D}'_{\tau=0,\texttt{Lepton}}$	NA		0.040 ± 2.909	-0.02		
$\mathcal{D}'_{\tau=0,\texttt{Kaon}}$	NA		0.517 ± 0.076	-0.03		
$\mathcal{D}'_{\tau=0,\texttt{NT1}}$	NA		0.669 ± 0.273	-0.01		
$\mathcal{D}'_{\tau=0,\texttt{NT2}}$	NA		-0.046 ± 0.131	-0.00		
$\mathcal{D}'_{\tau>0,\texttt{Lepton}}$	NA		0.338 ± 0.127	0.02		
$\mathcal{D}'_{\tau>0,\texttt{Kaon}}$	NA		0.258 ± 0.056	0.04		
$\mathcal{D}'_{\tau>0,\texttt{NT1}}$	NA		-0.125 ± 0.112	0.01		
$\mathcal{D}'_{\tau>0,\texttt{NT2}}$	NA		0.122 ± 0.031	0.01		
			Run 1	ρ	Run 2	ρ
$\mathcal{S}_{\text{core,sig}}$	1.133 ± 0.019	0.10	1.368 ± 0.089	0.25	1.184 ± 0.113	0.16
$\delta_{\text{core,sig,}\texttt{Lepton}}$	-0.059 ± 0.022	0.04	0.057 ± 0.125	0.08	-0.039 ± 0.156	0.00
$\delta_{\text{core,sig,}\texttt{Kaon}}$	-0.230 ± 0.014	0.03	-0.221 ± 0.081	0.03	-0.253 ± 0.091	0.00
$\delta_{\text{core,sig,}\texttt{NT1}}$	-0.150 ± 0.027	0.02	-0.068 ± 0.152	-0.00	-0.452 ± 0.211	0.00
$\delta_{\text{core,sig,}\texttt{NT2}}$	-0.202 ± 0.020	0.02	-0.461 ± 0.119	0.01	-0.199 ± 0.158	0.03
$f_{\text{tail,sig}}$	0.036 ± 0.008	-0.02	0.014 ± 0.020	0.06	0.015 ± 0.010	0.07
$\mathcal{S}_{\text{tail,sig}}$	3.672 ± 0.283	0.16	NA (fixed at 3)		NA (fixed at 3)	
$\delta_{\text{tail,sig}}$	-2.181 ± 0.430	0.21	-5.025 ± 4.177	0.04	-7.465 ± 2.417	0.06
$f_{\text{outlier,sig}}$	0.004 ± 0.001	-0.08	0.008 ± 0.004	-0.09	0.000 ± 0.014	0.01
$\mathcal{S}_{\text{core,bgd}}$	NA		1.211 ± 0.043	-0.00	1.131 ± 0.046	0.00
$\delta_{\text{core,bgd}}$	NA		-0.135 ± 0.031	-0.00	-0.015 ± 0.038	-0.00
$f_{\text{outlier,bgd}}$	NA		0.022 ± 0.004	-0.01	0.036 ± 0.007	0.02

corrected unblinded value for Δm_d is therefore

$$\Delta m_d \;=\; 0.516 \pm 0.016(\text{stat.})\ \text{ps}^{-1} \tag{5.1}$$

The fitted mistag rates are in good agreement with the values obtained from Monte Carlo truth information, confirming an unbiased measurement of those parameters (see Table 6.3). The fitted signal parameters in data are for the most part compatible with the corresponding values in Monte Carlo.

5.2.1 Goodness of Fit

A goodness-of-fit confidence level that reflects the nature of the unbinned likelihood fit is derived using a fast parameterized (a.k.a. toy) Monte Carlo technique. A large number of samples of signal and background events are generated with toy Monte Carlo using the same probability density functions with the parameters as measured from the selected events in data (for a more detailed description, see Section 7.1.1). The fraction of events with a smaller log likelihood than the one obtained from the fit to the data is interpreted as a goodness-of-fit confidence level. By not binning events in Δt and tagging category and not averaging over $\sigma_{\Delta t}$ this technique takes correctly into account the individual contribution from each event. The distribution of log likelihoods from the fits to 1981 toy Monte Carlo samples is shown in Figure 5-3 and the derived confidence level for the data fit is 44.4 ± 1.1 %.

The Δt distributions of the candidates overlaid with the likelihood fit results are shown in Figs. 5-4 and 5-6 for all candidates and in Figs. 5-5 and 5-7 separated by tagging category for signal Monte Carlo and data, respectively. The Δt distributions for the background candidates in data from the $m_{\rm ES}$ sideband ($m_{\rm ES} < 5.27\,\text{GeV}$) are shown in Figs. 5-8 and 5-9. In Figures 5-10 and 5-11 the mixing asymmetry $A_{\rm mixing}(\Delta t)$ for data and Monte Carlo is shown, and in Figures 5-12 and 5-13 again separately for each tagging category. In all asymmetry distributions the basic cosine dependence is clearly visible.

All fit curves describe the data well. As a crude goodness of fit check, the Poisson

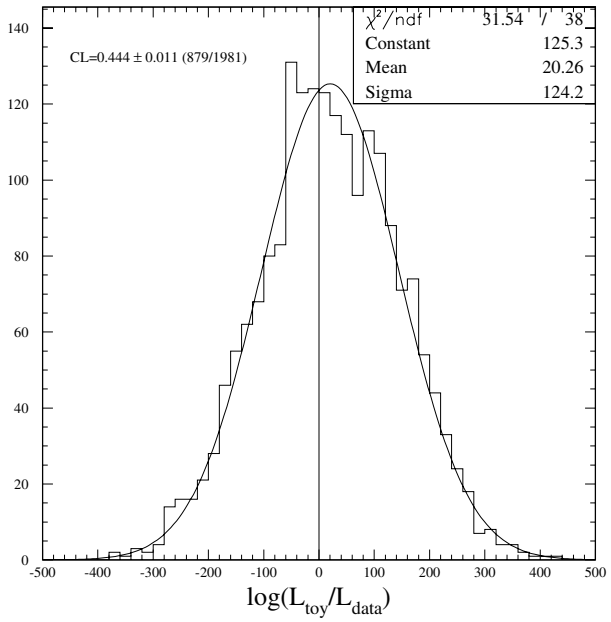

Figure 5-3: Distribution of the log of the likelihood obtained from fits to fast parameterized Monte Carlo samples relative to the one found for the data. The vertical line represents the value found in data. 44.4 % of the toy experiments have likelihoods smaller than the data.

χ^2 (see [8],page 196) is calculated for each bin of the Δt distributions of unmixed and mixed events. The square root of the χ^2 is then signed according to whether the central value of the bin is above or below the fit, and plotted for the signal region ($m_{\rm ES} > 5.27$) in Figure 5-6 and in Figure 5-7. The same distributions for the sideband ($m_{\rm ES} < 5.27$) are shown in Figure 5-8 and Figure 5-9.

5.3 Tagging Performance

The mistag rates $w = (1-D)/2$ and the tagging separation $Q = \epsilon_{\rm tag} D^2$ are calculated from the efficiencies and dilutions listed in Table 5.1 and 5.2 for data and simulated events. The results are listed in Table 5.3. The measured mistag rates in data are on average larger than in signal Monte Carlo. This results in a smaller tagging separation Q for data (27.5 ± 1.7 % and 27.7 ± 1.7 % for Run 1 and Run 2 respectively) compared

to simulated events (30.1 ± 0.2 %). Note that the efficiency used in the computation of Q is relative to the sample of events which have a reconstructed value of Δt, and that the dilutions for both Run 1 and Run 2 are assumed to be the same (see also [13]).

Table 5.3: Mistag rate w and tagging separation Q for hadronic B decays for the four tagging categories in data and simulated signal events.

Tagging Category	Mistag Rate w (%)		Tagging Separation Q (%)		
	Monte Carlo	Data (Run 1 and Run 2)	Monte Carlo	Data Run 1	Data Run 2
`Lepton`	7.0 ± 0.2	8.5 ± 1.5	9.73 ± 0.14	8.4 ± 0.7	7.9 ± 0.7
`Kaon`	15.4 ± 0.2	16.7 ± 1.2	15.58 ± 0.15	14.8 ± 1.1	15.3 ± 1.2
`NT1`	19.3 ± 0.3	21.4 ± 2.3	3.37 ± 0.07	2.9 ± 0.5	2.7 ± 0.5
`NT2`	34.7 ± 0.3	34.0 ± 2.2	1.42 ± 0.05	1.4 ± 0.4	1.4 ± 0.4
All	—	—	30.1 ± 0.2	27.5 ± 1.5	27.3 ± 1.5

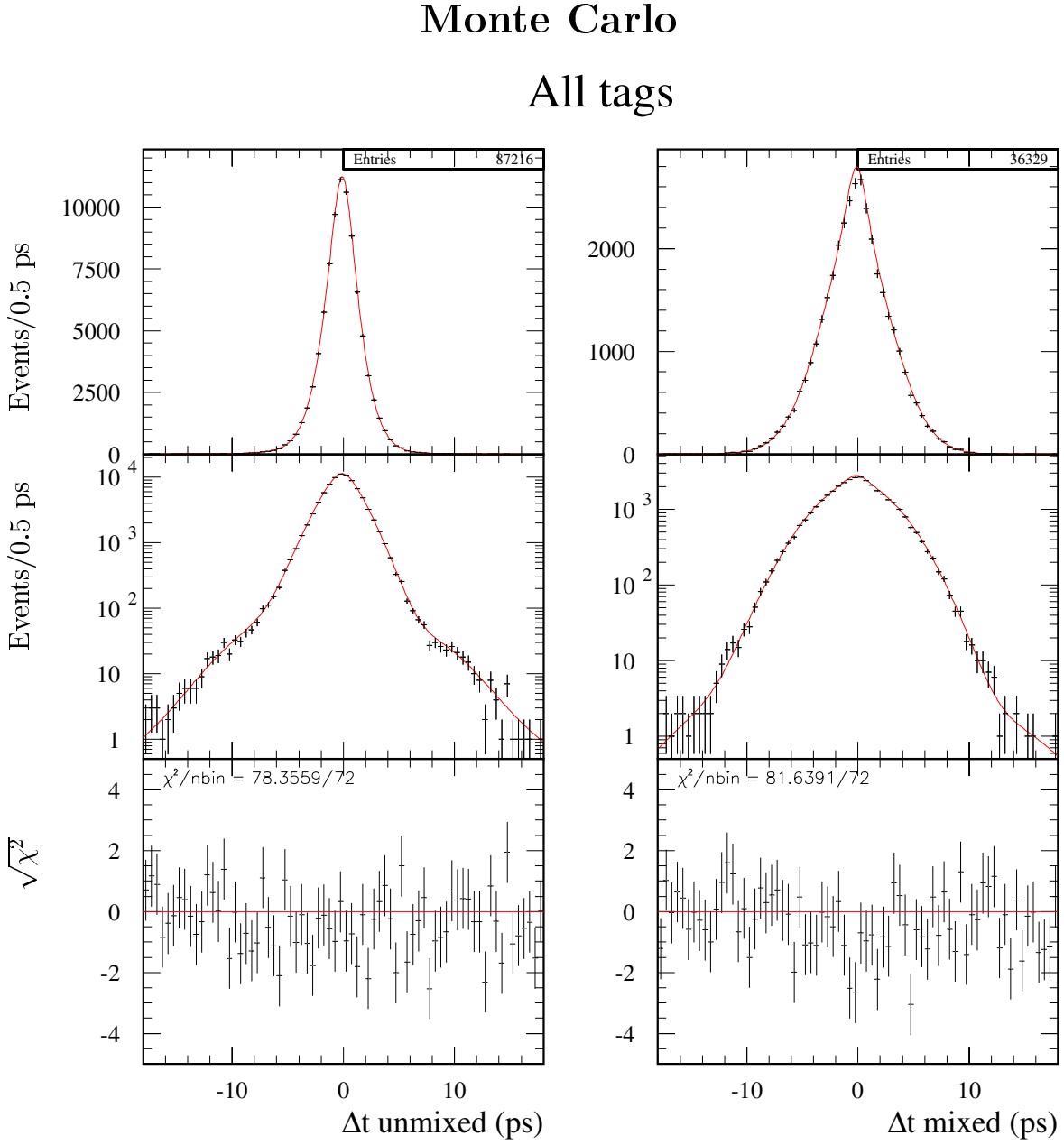

Figure 5-4: Distributions of Δt in signal Monte Carlo for the selected hadronic B decays (after truth association and for $m_{\rm ES} > 5.27\,{\rm GeV}$), separately for unmixed and mixed candidates. The fitted Δt shapes for these candidates are overlaid. In addition, the fit residuals (in the form of signed Poisson χ^2) are shown.

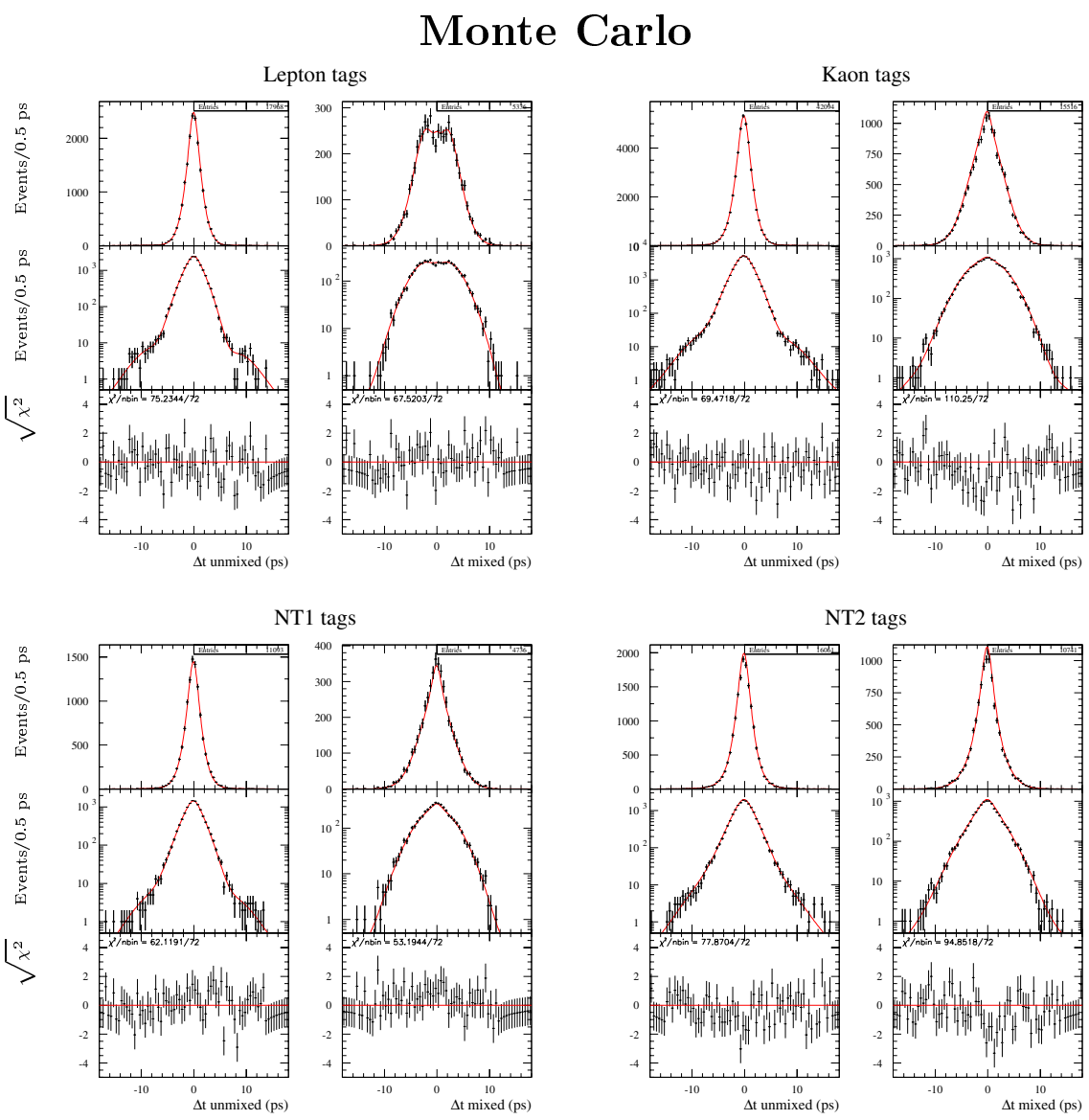

Figure 5-5: Distributions of Δt in signal Monte Carlo for the selected hadronic B decays (after truth association and for $m_{\rm ES} > 5.27\,{\rm GeV}$) separated by tagging category and separately for unmixed and mixed candidates. The fitted Δt shapes for these candidates are overlaid. In addition, the fit residuals (in the form of signed Poisson χ^2) are shown.

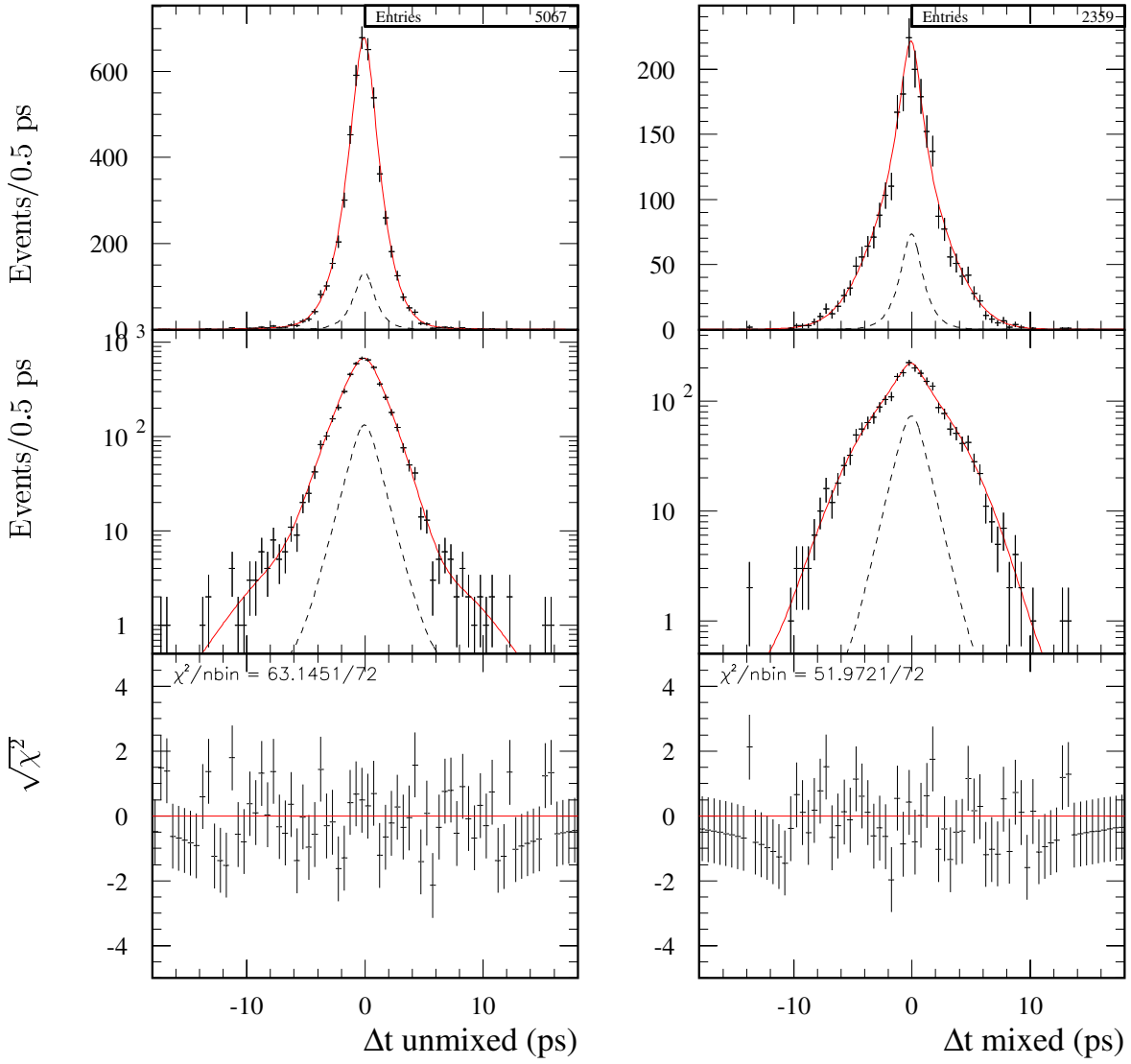

Figure 5-6: Distributions of Δt in data for the selected hadronic B decay candidates in the signal region ($m_{\rm ES} > 5.27$) separately for unmixed and mixed candidates. The fitted Δt shapes for the selected candidates and for the fraction of background candidates are overlaid. In addition, signed Poisson χ^2 distributions from the fits to the Δt distributions are shown.

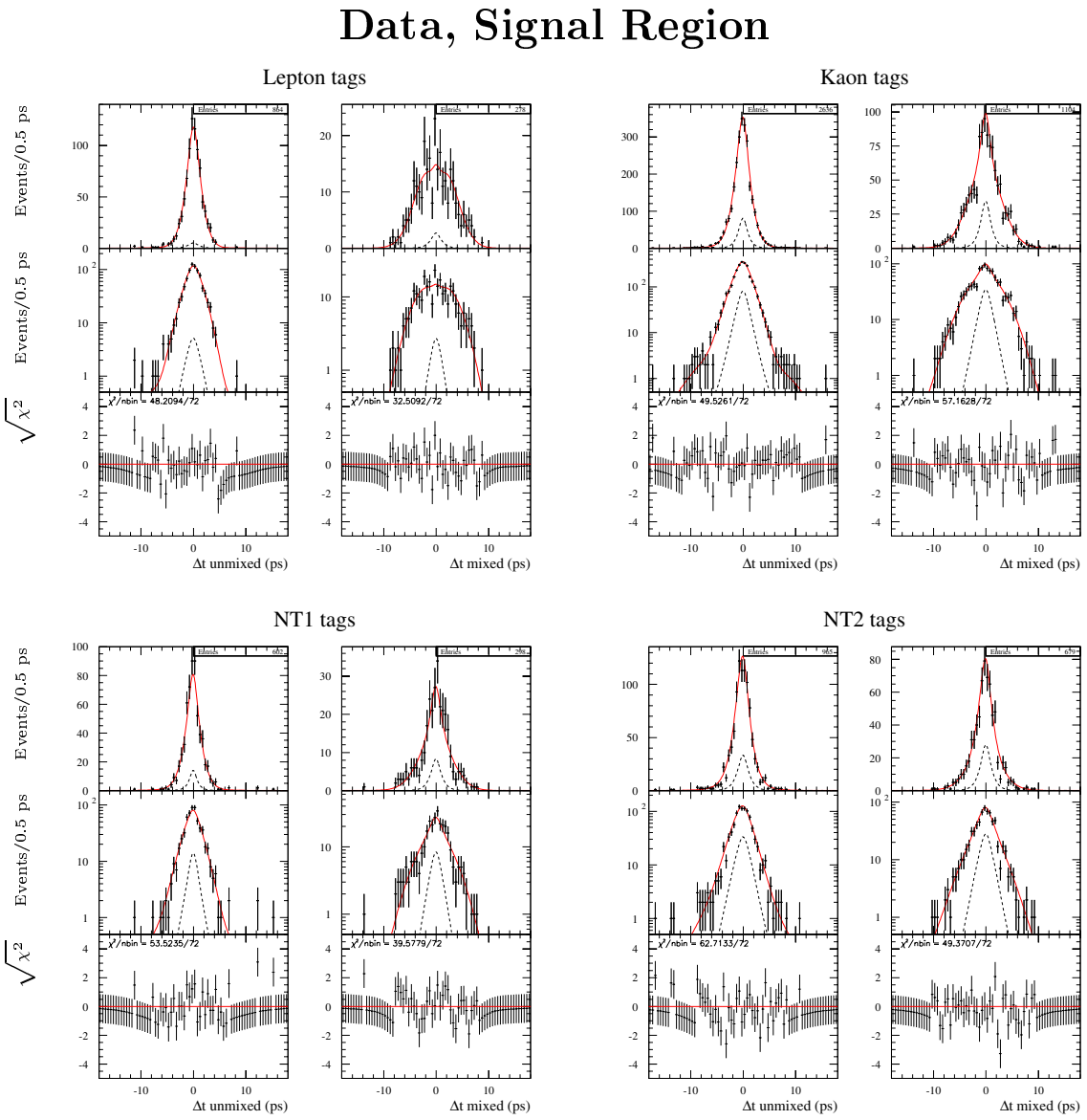

Figure 5-7: Distributions of Δt in data for the selected hadronic B decay candidates in the signal region $m_{\rm ES} > 5.27\,{\rm GeV}$ separated by tagging category and separately for unmixed and mixed candidates. The fitted Δt shapes for the selected candidates and for the fraction of background candidates are overlaid. In addition, signed Poisson χ^2 distributions from the fits to the Δt distributions are shown.

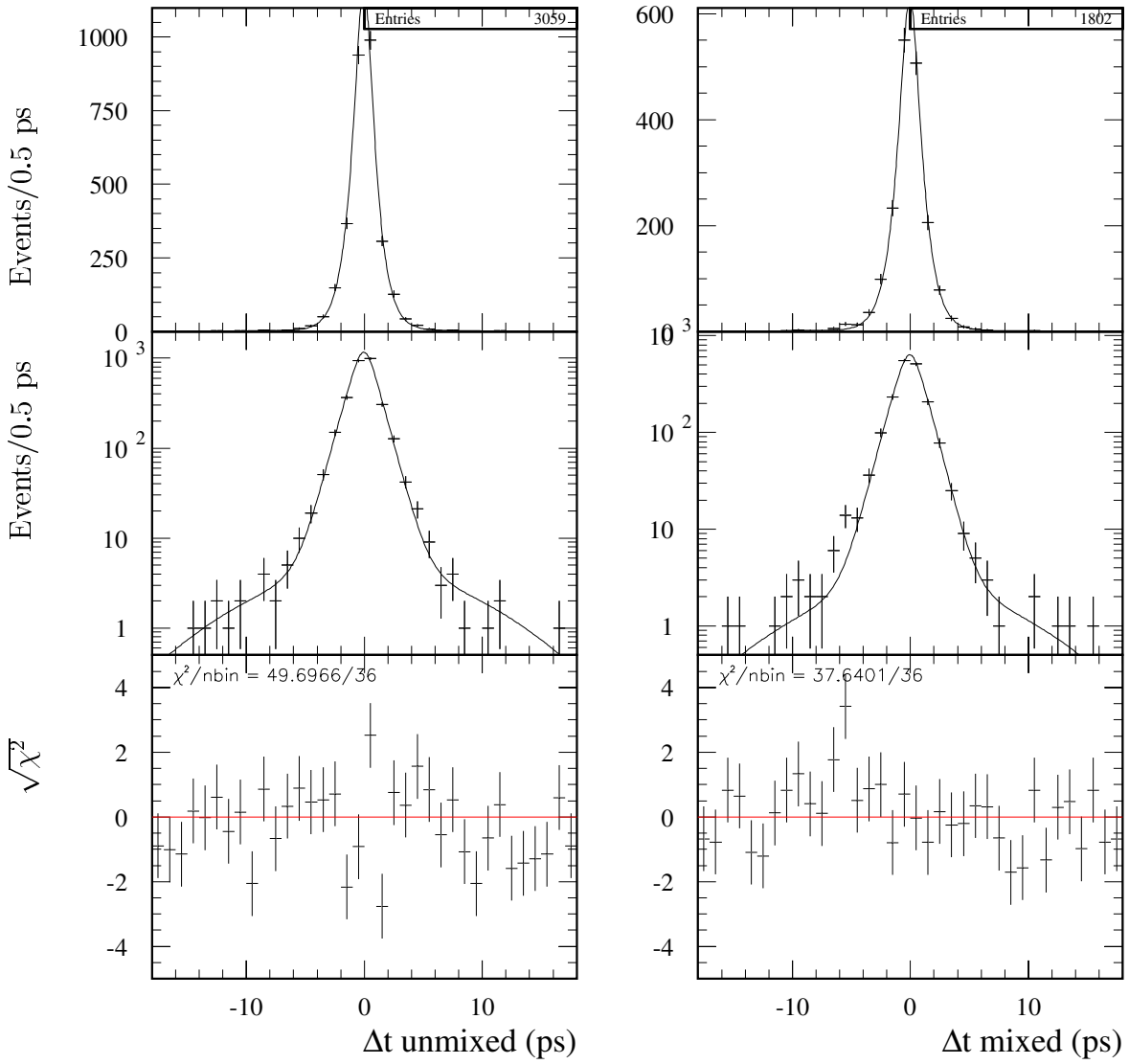

Figure 5-8: Distributions of Δt in data for selected hadronic B decay candidates in the sideband region $m_{\rm ES} < 5.27\,{\rm GeV}$ with tagging information separately for unmixed and mixed candidates. The fitted Δt shapes for these candidates are overlaid. In addition, signed Poisson χ^2 distributions from the fits to the Δt distributions in data are shown.

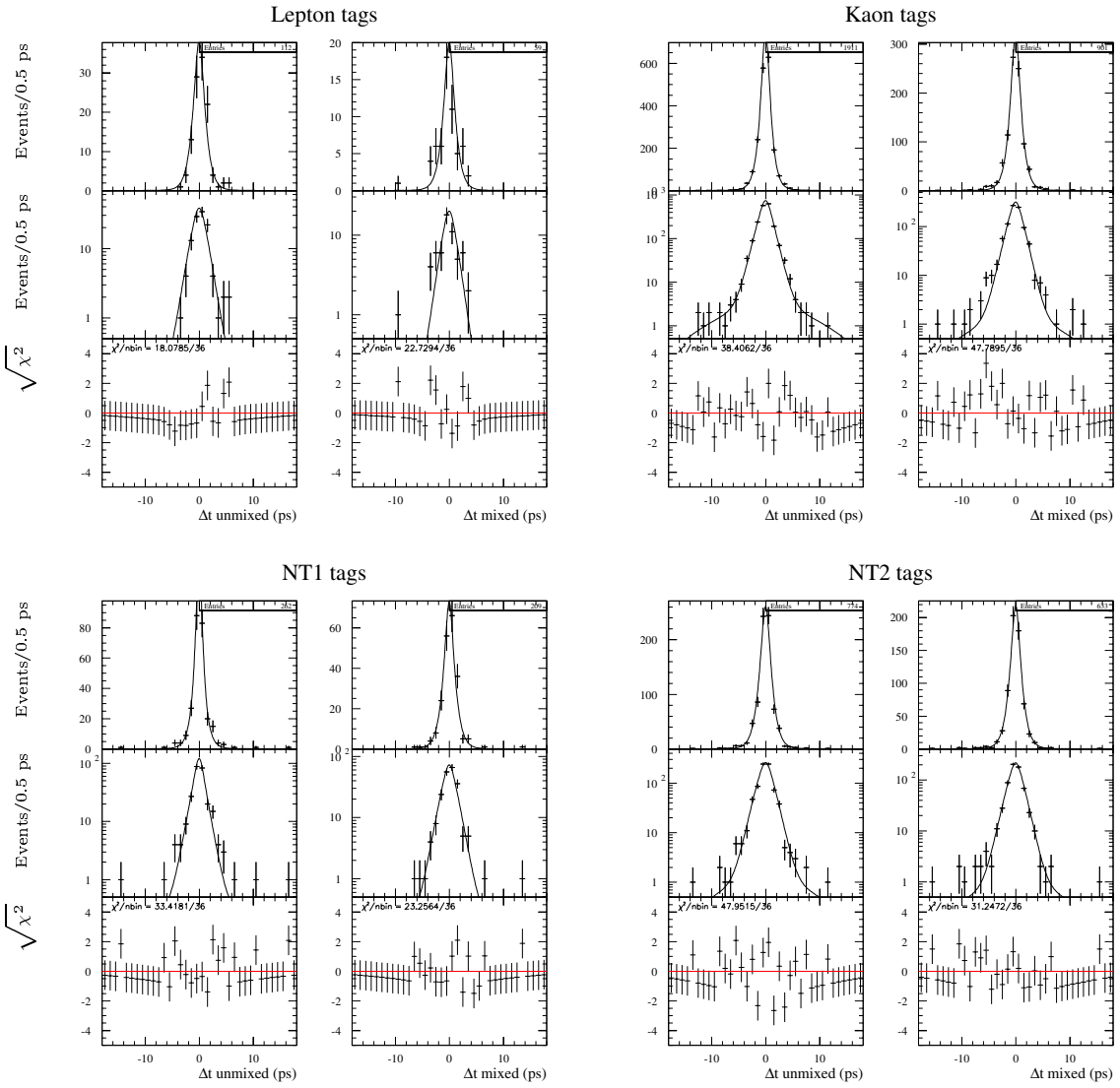

Figure 5-9: Distributions of Δt in data for selected hadronic B decay candidates in the sideband region $m_{\rm ES} < 5.27\,{\rm GeV}$ separated by tagging category and separately for unmixed and mixed candidates. The fitted Δt shapes for those candidates are overlaid.

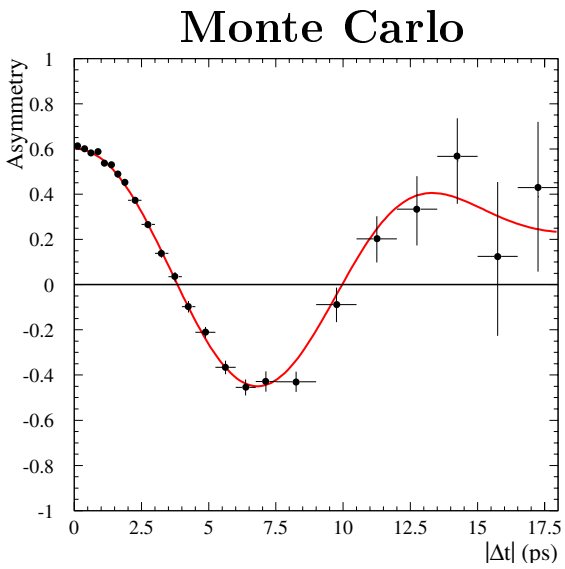

Figure 5-10: Time-dependent asymmetry $A_{\text{mixing}}(|\Delta t|)$ (as defined in Equation 4.4) between unmixed and mixed events in hadronic B decays for signal Monte Carlo. Note that the presence of finite detector resolution distorts the observed asymmetry.

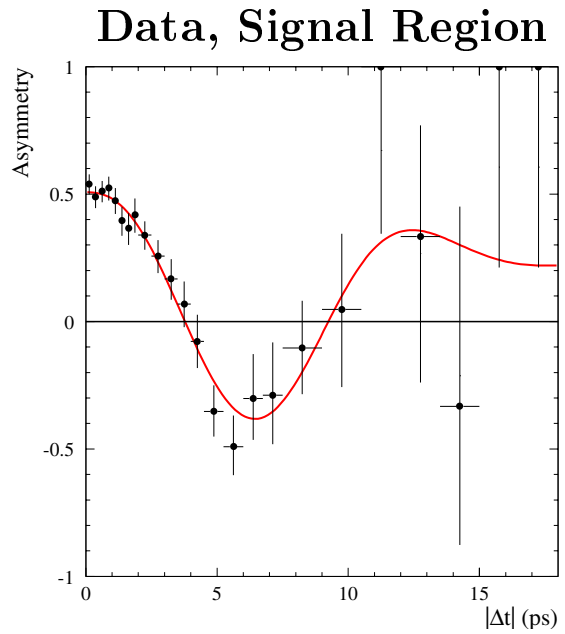

Figure 5-11: Time-dependent asymmetry $A_{\text{mixing}}(|\Delta t|)$ (as defined in Equation 4.4) between unmixed and mixed events in hadronic B decays for data. Note, that the presence of backgrounds in the data sample and the finite resolution change the observed time-dependence of the asymmetry.

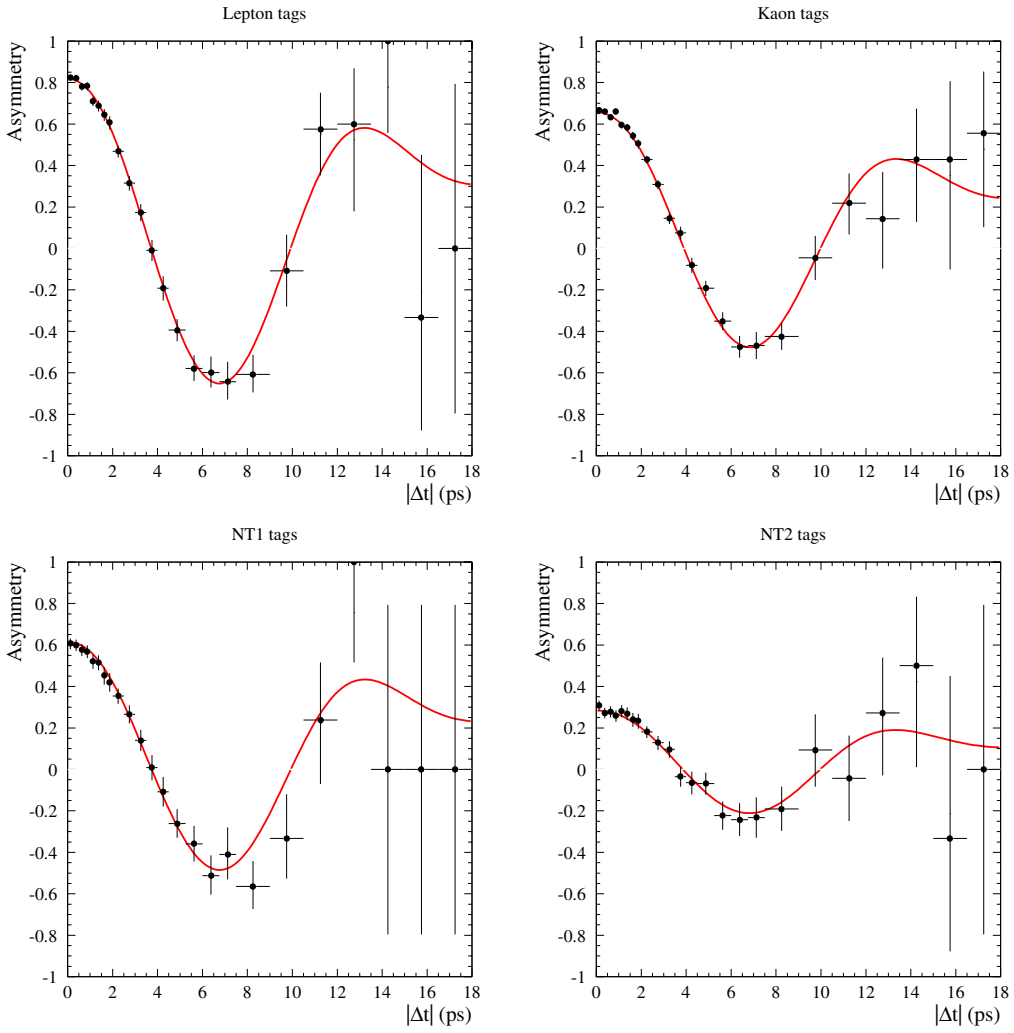

Figure 5-12: Time-dependent asymmetries $A_{\text{mixing}}(|\Delta t|)$ between unmixed and mixed events in hadronic B decays for signal Monte Carlo, by tagging category.

Data, Signal Region

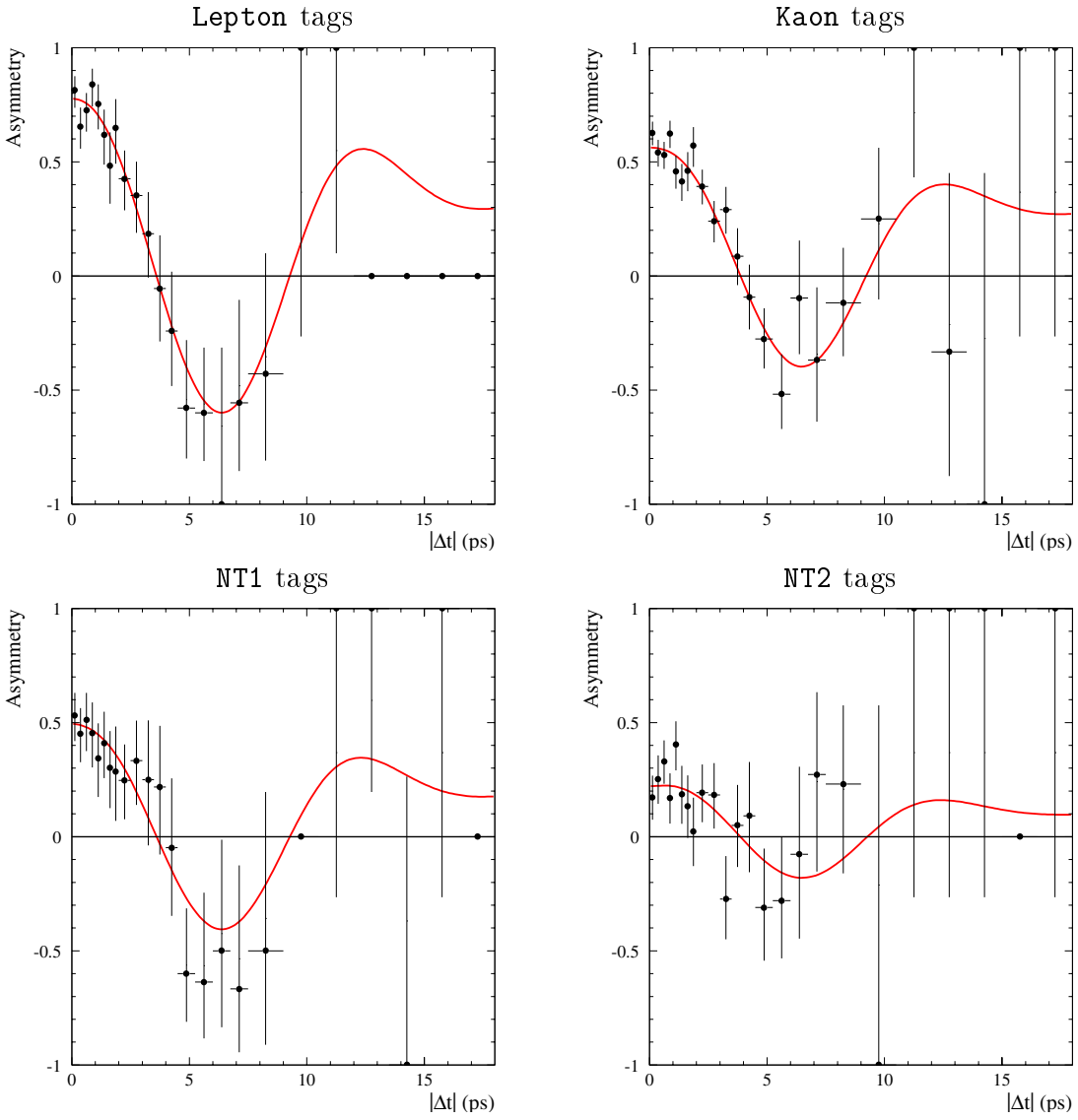

Figure 5-13: Time-dependent asymmetries $A_{\text{mixing}}(|\Delta t|)$ between unmixed and mixed events in hadronic B decays for data, per tagging category.

Chapter 6

Consistency Checks

The measurement has been checked and confirmed to be robust and independent of a variety of factors. These include, among others, splitting the data into sub-samples by key variables, varying parameters of Monte Carlo at the generation level, releasing some of the inputs of the fit (e.g., the B^0 lifetime), fitting to a control sample, and validating the technical implementation of the fit itself. Appropriate systematic errors are assigned for variations which indicate a dependence on the variation. They are described in Chapter 7.

6.1 B^0 Lifetime

When fitting for Δm_d, the B^0 lifetime is fixed to the nominal PDG [8] value, which is 1.548 ± 0.032 ps [8]. The consistency of the signal Δt distributions and this value is confirmed by releasing the B^0 lifetime in the nominal fits.

6.1.1 B^0 Lifetime in Nominal Fit to Data

The B^0 lifetime is measured to be 1.501 ± 0.031 ps, when released in the nominal fit to data. This is 1.0 σ below the PDG [8] value[1] (see Table 6.1). The changes in the tagging dilutions are negligible when compared to their statistical uncertainties, and

[1] This includes the PDG 2000 error of 0.032 ps.

Table 6.1: Variation of Δm_d for the likelihood fit with τ_{B^0} fixed to the PDG [8] value and and as a free fit parameter in data. The error on the quoted difference includes the uncertainty on the PDG [8] value of 0.032 ps.

Variable	τ_{B^0} fixed	τ_{B^0} float	difference
τ_{B^0}	1.548 (fixed)	1.502 ± 0.031	-0.046 ± 0.044 (-1.0 σ)
Δm_d (ps^{-1})	— $\pm$ 0.016	— $\pm$ 0.017	0.008 ± 0.007 (1.3 σ)

Δm_d is shifted by -0.007 ± 0.008 ps^{-1}. This is due to the correlation between Δm_d and τ_{B^0}, and the correlations of both Δm_d and τ_{B^0} and the resolution model.

6.1.2 B^0 Lifetime in Fits to Monte Carlo

The same check is performed on the signal cocktail Monte Carlo sample in several ways. First, the entire sample is fit with the B^0 lifetime floating. Next, in order to check effects which might depend on the sample size, the sample is split into 20 data-sized sub-samples, each of which is fit with the lifetime floating. The results of these checks are summarized in Table 6.2 and Figure 6-1. The measured value for Δm_d,

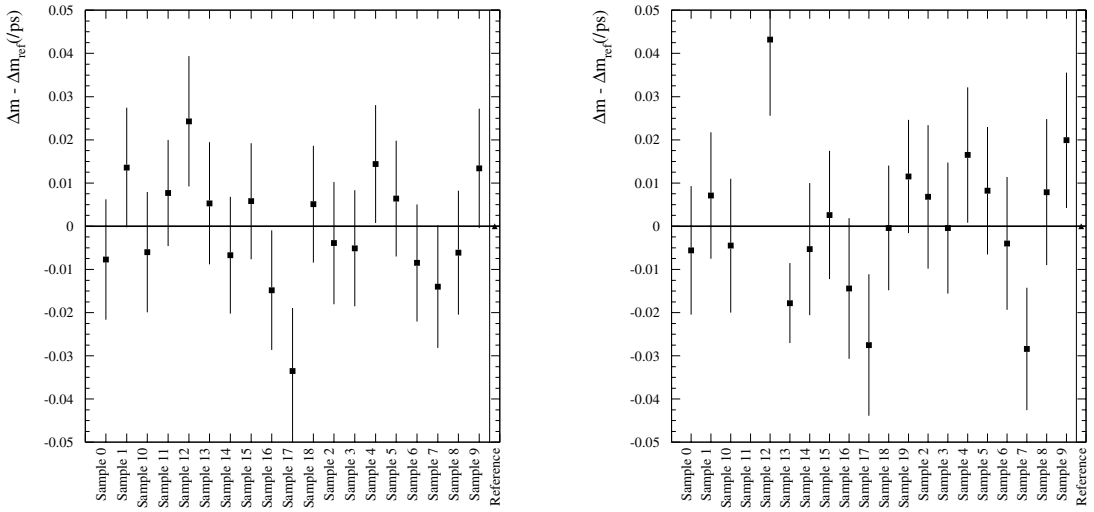

Figure 6-1: Δm_d for likelihood fit with τ_{B^0} fixed to the PDG [8] value (left) and and floating in the fits (right) for cocktail signal Monte Carlo split into 20 samples.

Table 6.2: Δm_d for likelihood fit with τ_{B^0} fixed to the PDG [8] value and as a free fit parameter for cocktail signal Monte Carlo. The error on the difference in Δm_d, $\delta\Delta m_d$ is computed using $\sqrt{|\sigma^2_{i,float} - \sigma^2_{i,fixed}|}$.

Sample	τ_{B^0} fixed to PDG	τ_{B^0} floating		$\delta\Delta m_d$	$n\ \sigma$
	Δm_d	τ_{B^0}	Δm_d		
0	0.4709 ± 0.0143	1.5337 ± 0.0315	0.4730 ± 0.0152	0.0021 ± 0.0052	0.4
1	0.4922 ± 0.0142	1.5867 ± 0.0327	0.4857 ± 0.0150	−0.0065 ± 0.0048	−1.3
2	0.4747 ± 0.0145	1.5015 ± 0.0327	0.4854 ± 0.0169	0.0107 ± 0.0087	1.2
3	0.4735 ± 0.0138	1.5258 ± 0.0318	0.4782 ± 0.0155	0.0047 ± 0.0071	0.7
4	0.4930 ± 0.0140	1.5385 ± 0.0326	0.4951 ± 0.0160	0.0021 ± 0.0077	0.3
5	0.4850 ± 0.0138	1.5384 ± 0.0307	0.4868 ± 0.0151	0.0018 ± 0.0061	0.3
6	0.4701 ± 0.0139	1.5261 ± 0.0333	0.4746 ± 0.0157	0.0045 ± 0.0073	0.6
7	0.4646 ± 0.014535	1.5813 ± 0.0322	0.4502 ± 0.014494	−0.0144 ± 0.0011	13.0
8	0.4725 ± 0.0147	1.4774 ± 0.0339	0.4865 ± 0.0172	0.0140 ± 0.0089	1.6
9	0.4920 ± 0.0142	1.5167 ± 0.0321	0.4985 ± 0.0160	0.0065 ± 0.0074	0.9
10	0.4726 ± 0.0143	1.5402 ± 0.0323	0.4741 ± 0.0158	0.0015 ± 0.0067	0.2
11	0.4863 ± 0.0127	1.1006 ± 0.0318	0.4792 ± 0.0138	−0.0071 ± 0.0054	1.3
12	0.5029 ± 0.0154	1.4777 ± 0.0326	0.5218 ± 0.0179	0.0189 ± 0.0091	2.1
13	0.4839 ± 0.0145	1.5786 ± 0.0316	0.4608 ± 0.0098	−0.0231 ± 0.0107	−2.2
14	0.4719 ± 0.0139	1.5414 ± 0.0321	0.4733 ± 0.0156	0.0014 ± 0.0071	0.2
15	0.4844 ± 0.0138	1.5641 ± 0.0322	0.4812 ± 0.0152	−0.0032 ± 0.0064	−0.5
16	0.4638 ± 0.0142	1.5464 ± 0.0336	0.4642 ± 0.0166	0.0004 ± 0.0086	0.0
17	0.4451 ± 0.0149	1.5188 ± 0.0334	0.4511 ± 0.0167	0.0060 ± 0.0075	0.8
18	0.4837 ± 0.0139	1.5780 ± 0.0318	0.4782 ± 0.0148	−0.0055 ± 0.0051	−1.1
19	0.4938 ± 0.0144	1.5276 ± 0.0304	0.4901 ± 0.0135	−0.0037 ± 0.0050	−1.4
Average	0.4790 ± 0.0032		0.4777 ± 0.0033		
Full sample	0.4786 ± 0.0032				

averaged over the 20 subsamples, is consistent with the result from the full cocktail Monte Carlo sample (Table 6.2), both with and without floating the B^0 lifetime. No sample-size biases are observed. Typical deviation of Δm_d from the nominal fit value in these fits is 0.015 ps^{-1}.

6.2 Fit to Charged B

The complete analysis was performed on the B^+ sample. In the fit to the B^+ sample, Δm_d was fixed to zero. The results are shown in Figure 6-2. No oscillation signal is observed in the charged B data.

6.3 Monte Carlo Fits Using Truth Information

To check for selection biases, the Monte Carlo truth information is used in the fit. Starting from the reconstructed events and requiring that the event be in the signal

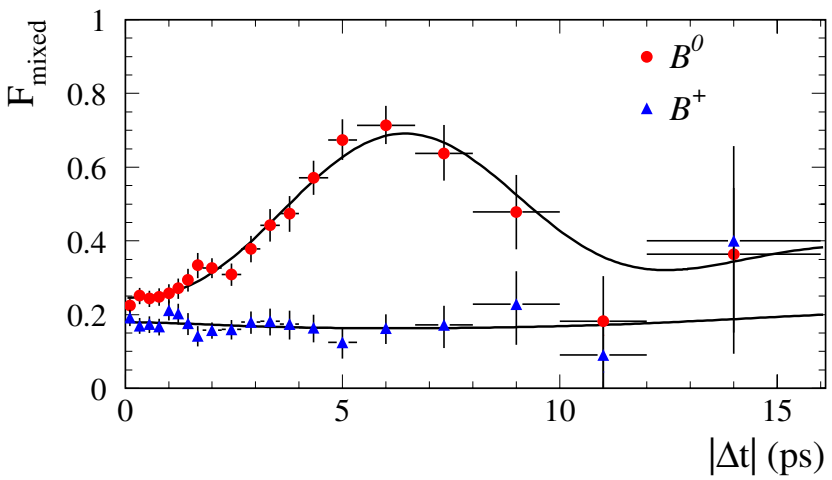

Figure 6-2: Fraction of observed mixed events as a function of $|\Delta t|$ in data. The triangles are the B^+ data sample.

region ($m_{\rm ES} > 5.27\,{\rm GeV}$) and be Monte Carlo truth associated yields 123722 tagged events. The events' reconstructed values of Δt and their flavor tags are replaced with Monte Carlo truth information, and the sample is fit. The deviation[2] of Δm_d from the generated value of 0.472 ps^{-1} is $+0.0008 \pm 0.0012$ ps^{-1} (or $+0.7\ \sigma$). If the B^0 lifetime is also released, the same value of Δm_d is obtained, and a deviation in the B^0 lifetime from the generated value of 1.548 ps is observed to be $+0.010 \pm 0.004$ ps^{-1} (or $+2.2\ \sigma$). The individual tag and reconstructed B generated lifetime distributions are also checked by looking at the true z production and decay positions and B^0 momenta (see Figure 6-3). Next, the reconstructed flavor tag is used in the fit (while keeping the true value of Δt), and therefore the mistag rates (dilutions) are allowed to float in the fit. The results are summarized and compared to Monte Carlo truth in Table 6.3; the observed deviation in Δm_d is observed to be $\delta\Delta m_d = -0.0020 \pm 0.0024$ps^{-1}.

[2]Defined as measured minus generated.

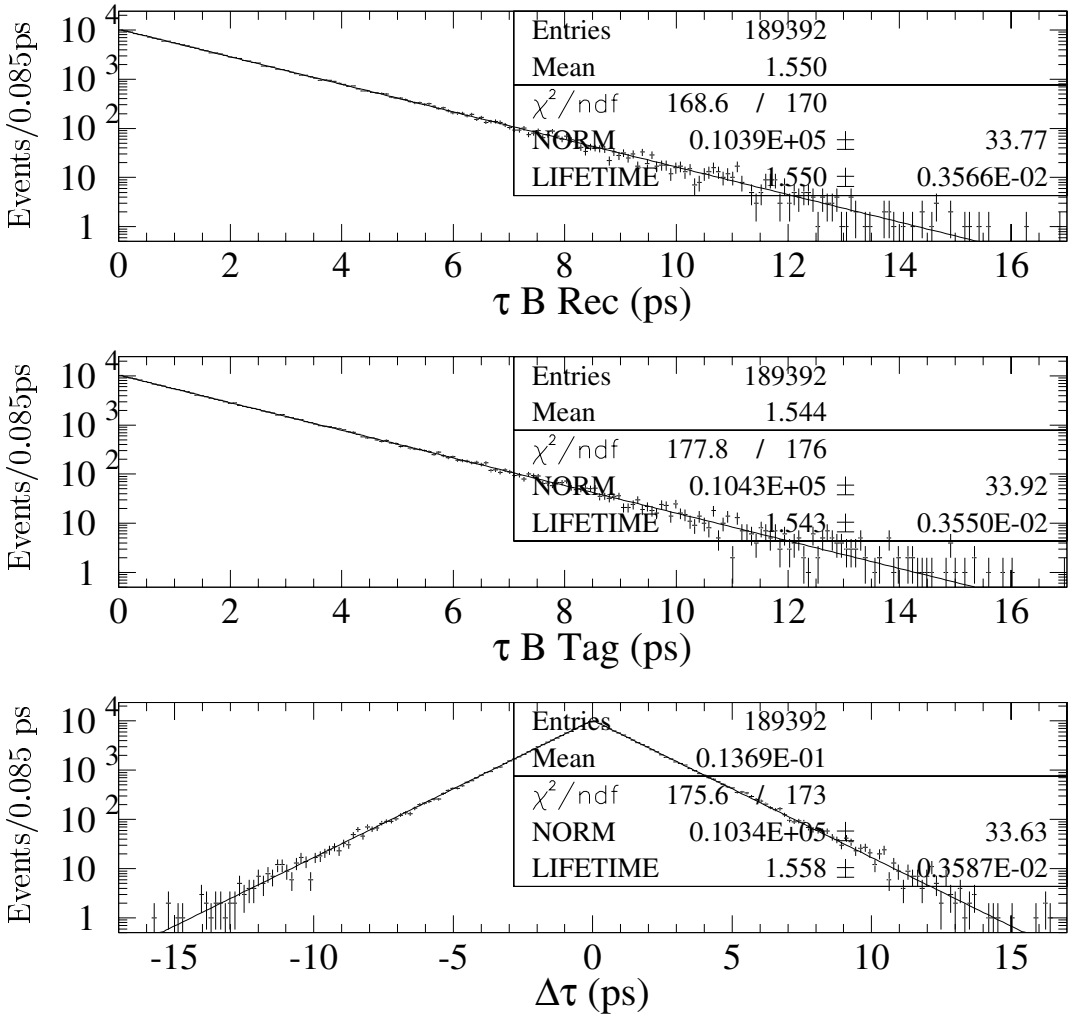

Figure 6-3: Monte Carlo Truth lifetime checks for the reconstructed B(upper), the tagging B (center), and Δt in cocktail Monte Carlo events.

Table 6.3: Values of dilution obtained from a) counting of Monte Carlo truth information; b) the mixing fit using the true Monte Carlo Δt; c) the mixing fit using the reconstructed Δt, with the resolution function fixed to the values obtained from a fit to the Monte Carlo Δt residuals; d) the full mixing fit using the reconstructed Δt; in all cases using events with $m_{\rm ES} > 5.27\,{\rm GeV}$, $\sigma_{\Delta t} < 1.4$ps and with a successful Monte Carlo truth association.

Variable	Counting using Monte Carlo truth	Fit to true Δt distribution	Fit with fixed Δt resolution function	Full fit
$\mathcal{D}_{\texttt{Lepton}}$	0.859 ± 0.003	0.847 ± 0.005	0.852 ± 0.006	0.853 ± 0.006
$\mathcal{D}_{\texttt{Kaon}}$	0.692 ± 0.003	0.698 ± 0.004	0.707 ± 0.004	0.708 ± 0.004
$\mathcal{D}_{\texttt{NT1}}$	0.614 ± 0.006	0.614 ± 0.008	0.624 ± 0.009	0.625 ± 0.009
$\mathcal{D}_{\texttt{NT2}}$	0.306 ± 0.006	0.307 ± 0.007	0.310 ± 0.008	0.310 ± 0.008
$\Delta\mathcal{D}_{\texttt{Lepton}}$	0.007 ± 0.007	0.009 ± 0.009	0.005 ± 0.009	0.005 ± 0.009
$\Delta\mathcal{D}_{\texttt{Kaon}}$	0.031 ± 0.006	0.039 ± 0.007	0.037 ± 0.007	0.037 ± 0.007
$\Delta\mathcal{D}_{\texttt{NT1}}$	-0.036 ± 0.013	-0.050 ± 0.014	-0.051 ± 0.014	-0.051 ± 0.014
$\Delta\mathcal{D}_{\texttt{NT2}}$	0.071 ± 0.012	0.067 ± 0.012	0.070 ± 0.012	0.070 ± 0.012

6.4 Monte Carlo Characterization by Counting

The signal cocktail is checked to confirm that it contains the correct fraction of mixed events (χ_d), split into several different categories. The results of these checks, categorized by the decay mode reconstructed for the $B_{\rm rec}$, are shown in Table 6.4, and categorized by the tagging category are shown in Table 6.5. The sample tagged by leptons has a χ_d which is significantly higher than expected (resulting by itself in an increase in the apparent value of Δm_d). Splitting the `Lepton` tags by whether or not there is also a (confirming) kaon tag, or the species of lepton, it is clear that the largest discrepancy is in the case of lepton tags which also contain a kaon. There is no significant difference between electrons and muons.

The sample is also checked for any difference in reconstruction and tagging efficiencies for B^0 and $\overline{B}^0$, respectively. Following the recipe of Ref. [20] (adopting the same notation), the relative difference in B^0 reconstruction efficiencies is found to be $\nu = 0.0059 \pm 0.0024$ ($+2.5\,\sigma$) and tagging efficiency $\mu = 0.0057 \pm 0.0024$ ($+2.4\,\sigma$), with a tagging efficiency $T = 0.6980 \pm 0.0011$.

Table 6.4: Monte Carlo sample composition split by reconstructed decay mode. The $\chi_d^{\rm true}$ reported is the fraction of mixed events, where (un)mixed is determined using Monte Carlo truth. The values in parentheses are the number of σ that the reported value deviates from the expected value, computed from the input B^0 lifetime and Δm_d to the event generator.

B^0 decay mode	B^0 tag	$\overline{B}^0$ tag	$f(B^0$ tag)	$\chi_d^{\rm true}$
D^- $(K^+\ \pi^+\ \pi^-)\pi^+$	27269	26779	0.505 ± 0.004 (1.21)	0.174 ± 0.002 (−0.21)
D^- $(K^+\ \pi^+\ \pi^-)\ a_1^+$	6596	6420	0.507 ± 0.008 (0.88)	0.173 ± 0.003 (−0.35)
D^- $(K^+\ \pi^+\ \pi^-)\rho^+$	14043	14091	0.499 ± 0.005 (−0.17)	0.178 ± 0.002 (1.65)
D^- $(K_S^0\ \pi^-)\pi^+$	2588	2535	0.505 ± 0.012 (0.42)	0.175 ± 0.005 (0.27)
D^- $(K_S^0\ \pi^-)\rho^+$	1133	1229	0.480 ± 0.017 (−1.17)	0.172 ± 0.008 (−0.28)
D^- $(K_S^0\ \pi^-)\ a_1^+$	704	697	0.502 ± 0.023 (0.11)	0.163 ± 0.010 (−1.07)
D^{*-} $(D^0\ (K^+\ \pi^-)\pi^-)\pi^+$	6672	6473	0.508 ± 0.008 (0.99)	0.176 ± 0.003 (0.58)
D^{*-} $(D^0\ (K^+\ \pi^-)\ \pi^-)a_1^+$	5064	4975	0.504 ± 0.009 (0.51)	0.173 ± 0.004 (−0.19)
D^{*-} $(D^0\ (K^+\ \pi^-\ \pi^+\ \pi^-)\pi^-)a_1^+$	671	648	0.509 ± 0.024 (0.36)	0.170 ± 0.010 (−0.41)
D^{*-} $(D^0\ (K^+\ \pi^-\ \pi^+\ \pi^-)\pi^-)\pi^+$	1055	1066	0.497 ± 0.019 (−0.14)	0.190 ± 0.009 (1.82)
D^{*-} $(D^0\ (K^+\ \pi^-\ \pi^0)\pi^-)\pi^+$	4703	4831	0.493 ± 0.009 (−0.76)	0.173 ± 0.004 (−0.36)
D^{*-} $(D^0\ (K^+\ \pi^-\ \pi^0)\ \pi^-)a_1^+$	3536	3468	0.505 ± 0.010 (0.47)	0.168 ± 0.004 (−1.44)
D^{*-} $(D^0\ (K^+\ \pi^-)\ \pi^-)\rho^+$	3685	3615	0.505 ± 0.010 (0.47)	0.175 ± 0.004 (0.23)
D^{*-} $(D^0\ (K^+\ \pi^-\ \pi^+\ \pi^-)\pi^-)\rho^+$	571	587	0.493 ± 0.025 (−0.27)	0.152 ± 0.011 (−2.09)
D^{*-} $(D^0\ (K^+\ \pi^-\ \pi^0)\ \pi^-)\rho^+$	2734	2772	0.497 ± 0.012 (−0.30)	0.183 ± 0.005 (1.80)
D^{*-} $(D^0\ (K_S^0\ \pi^+\ \pi^-)\pi^-)\pi^+$	1274	1316	0.492 ± 0.017 (−0.48)	0.159 ± 0.007 (−2.14)
D^{*-} $(D^0\ (K_S^0\ \pi^+\ \pi^-)\pi^-)a_1^+$	889	865	0.507 ± 0.021 (0.33)	0.173 ± 0.009 (−0.08)
D^{*-} $(D^0\ (K_S^0\ \pi^+\ \pi^-)\ \pi^-)\rho^+$	725	683	0.515 ± 0.024 (0.63)	0.173 ± 0.010 (−0.07)
J/ψ $(e^+e^-)K^{*0}$ $(K^+\ \pi^-)$	2250	2219	0.503 ± 0.013 (0.27)	0.177 ± 0.006 (0.52)
J/ψ $(\mu^+\mu^-)K^{*0}$ $(K^+\ \pi^-)$	2989	2842	0.513 ± 0.012 (1.09)	0.171 ± 0.005 (−0.69)
All	89151	88111	0.503 ± 0.002 (1.42)	0.174 ± 0.001 (0.21)

6.5 Measuring Δm_d by Counting

The fraction of mixed events, χ_d is given by

$$\chi_d \ = \ \frac{1}{2}\frac{x_d}{1+x_d^2} \tag{6.1}$$

where $x_d = \Delta m_d \cdot \tau_{B^0}$. Therefore, the fraction of mixed events is sensitive to both Δm_d and τ_{B^0}. If the mistag rates and lifetime are known, then Δm_d can be measured in a time-independent way just by counting the fraction of mixed events. Taking the dilutions from the time-dependent fit, the result of measuring Δm_d by counting in data yields a value which is different from the full time-dependent fit by -0.003 ± 0.013 ps^{-1}, where the quoted uncertainty is the difference in quadrature between the error from the counting measurement and the error from the time-dependent fit with Δm_d as the only free parameter. For data the fraction of mixed events is consistent with the fitted value of Δm_d.

Table 6.5: Monte Carlo sample composition split by tagging category. In the top half of the table, Monte Carlo truth is used to determine whether an event is mixed or unmixed. In the bottom half, the reconstructed $B_{\rm rec}$ and the result of the flavor tagging algorithm is used. The value of $\chi_d^{\rm corrected}$ is determined from the observed $\chi_d^{\rm observed}$, and then corrected using the mistag rate determined by comparing the reconstructed flavor tag and Monte Carlo truth. Finally, the column labeled (χ_d pull) is the deviation in units of σ from the expected value.

Truth	Mixed	Unmixed	χ_d (χ_d pull)
`Lepton`	4271	19050	0.183 ± 0.003 (3.60)
e	2295	10119	0.185 ± 0.003 (3.11)
μ	1976	8931	0.181 ± 0.004 (1.94)
`Lepton` *without* `Kaon`	3050	13837	0.181 ± 0.003 (2.23)
`Lepton` *with* `Kaon`	1221	5213	0.190 ± 0.005 (3.22)
`Kaon`	9878	47830	0.171 ± 0.002 (-1.82)
`NT1`	2798	13043	0.177 ± 0.003 (0.86)
`NT2`	4723	22129	0.176 ± 0.002 (0.80)
None	9211	44329	0.172 ± 0.002 (-1.22)
All	30881	146381	0.174 ± 0.001 (0.21)
Reconstructed	Mixed	Unmixed	$\chi_d^{\rm observed}$ $\chi_d^{\rm corrected}$ (χ_d pull)
`Lepton`	5339	17982	0.229 0.184 ± 0.003 (3.04)
e	2833	9581	0.228 0.187 ± 0.005 (2.72)
μ	2506	8401	0.230 0.182 ± 0.005 (1.55)
`Lepton` *without* `Kaon`	4077	12810	0.241 0.181 ± 0.004 (1.67)
`Lepton` *with* `Kaon`	1262	5172	0.196 0.191 ± 0.005 (3.35)
`Kaon`	15560	42148	0.270 0.167 ± 0.003 (-2.31)
`NT1`	4745	11096	0.300 0.174 ± 0.007 (-0.05)
`NT2`	10766	16086	0.401 0.176 ± 0.012 (0.17)
All	62793	114469	0.354 0.171 ± 0.003 (-1.03)

6.6 Measuring Δm_d Using Δt Shapes Only

The normalization of the nominal fit is such that the fraction of mixed events, χ_d, is required to be consistent with the values of τ_{B^0} and Δm_d (see Reference [21] for more details). The shapes of the Δt distributions for mixed and unmixed events provide information about Δm_d, independent of χ_d. The normalization requirement is removed to test the sensitivity of the measurement to imposing this requirement. The results of these fits for several samples are shown in Table 6.6 and Table 6.7.

Table 6.6: Result of likelihood fits on Monte Carlo using only the Δt shapes

Sample	Δm_d
All	0.4786 ± 0.0032
$\overline{B}^0_{\rm rec}$	0.4689 ± 0.0069
$B^0_{\rm rec}$	0.4777 ± 0.0065
$\overline{B}^0_{\rm tag}$	0.4781 ± 0.0045
$B^0_{\rm tag}$	0.4790 ± 0.0046
`Lepton`	0.4875 ± 0.0056
`Kaon`	0.4730 ± 0.0047
`NT1`	0.4691 ± 0.0090
`NT2`	0.4849 ± 0.0145

Table 6.7: Result of likelihood fits on Data using only the Δt shapes

Sample	$\Delta m_{d\rm sample} - \Delta m_{d\rm nominal}$
All	0.003 ± 0.015
$\overline{B}^0_{\rm rec}$	0.012 ± 0.020
$B^0_{\rm rec}$	-0.010 ± 0.021
$\overline{B}^0_{\rm tag}$	0.015 ± 0.021
$B^0_{\rm tag}$	-0.016 ± 0.020
`Lepton`	0.004 ± 0.024
`Kaon`	0.009 ± 0.021
`NT1`	-0.019 ± 0.039
`NT2`	0.189 ± 0.092

6.7 Likelihood Fit Implementation

To check that there are no implementation-specific problems in the likelihood fit, the Δm_d Monte Carlo fit is repeated using two other implementations, `CPExtract` [22] and `RooFitTools/Core` [23]. All three programs are intended to implement the same likelihood functions, and all three use `MINUIT` [17] to perform minimization. The results of all three are identical.

6.8 B^0 Decay Mode

The sample is divided according to which B^0 decay mode was reconstructed; specifically, whether the charm was a (D^{*-} or a D^-), and which light meson was involved ($\pi/\rho/a_1$) in the decay. The $B \to J/\psi K^{*0}$ events are considered separately. The results are listed in Table 6.8. No significant discrepancy is seen among these subsamples.

Table 6.8: Variation of Δm_d for different decay modes in data. The error reported is on the value itself, and *not* on the difference with the reference value.

Mode	$\Delta m_{d\text{mode}} - \Delta m_{d\text{all}}$
$D^*\pi$	-0.029 ± 0.030
$D^*\rho$	0.017 ± 0.039
$D^*a_1^+$	0.066 ± 0.063
$D\pi$	0.022 ± 0.030
$D\rho$	-0.031 ± 0.038
Da_1^+	-0.033 ± 0.041
$D^*\ X$	0.000 ± 0.025
$D\ X$	-0.005 ± 0.023
$J/\psi\, K^{*0}$	0.044 ± 0.035

6.9 Tagging Category

The sample is divided according to which tagging category was used to flavor-tag the events and the full fit is performed. Because some parameters common to all tagging

categories are allowed to float, it is possible that they (and the ones correlated to them) assume different values than the nominal fit. Small differences in tagging dilutions compared to the nominal fit are therefore possible. The results are listed for data in Table 6.9, and for Monte Carlo in Table 6.10. No significant discrepancy is seen among these subsamples.

6.10 B Meson Flavor

The data is divided, according to whether the reconstructed B is a B^0 or a $\overline{B}^0$, and according to whether the tagged B is a B^0 or a $\overline{B}^0$. The results of these four fits is summarized in Table 6.11. No significant discrepancy is seen between these subsamples.

6.11 Resolution Model

To motivate the choice of scaling the bias, as described in Section 4.3, the sample is divided in bins of $\sigma_{\Delta t}$, and for each bin the Monte Carlo residual $(\Delta t - \Delta t_{\rm true})$ distribution is plotted in a range of $\pm$ 5 times the maximum $\sigma_{\Delta t}$ in the bin under consideration. The mean values and RMS deviations obtained from the individual slices are shown as a function of the per-event error (plotted at the center of each bin) in Figure 6-4. From this plot, it is concluded that the resolution model bias should be scaled by the per-event error. An explanation of this behavior can be found in [18], with additional information in [24]. In addition, the per-event $\sigma_{\Delta t}$ is required to be less than 1.4 ps to avoid the region where this scaling no longer holds. Fitting this resolution model on the Monte Carlo residual $\delta\Delta t$ distributions, and constraining the resolution function to those parameters in a fit to the same Monte Carlo sample gives a Δm_d value of 0.4777 ± 0.0029 ps^{-1}.

For the nominal fit to Monte Carlo, where the parameters of the resolution model are floating free in the fit and are determined without the help of the knowledge of the Monte Carlo truth Δt yields the values listed in Table 5.2. The value of Δm_d

Table 6.9: Δm_d and tagging dilutions for fits to different tagging categories. $\delta\Delta m_d$ is the difference between the value of the blinded Δm_d for the specified tagging category and for the total sample.

	Lepton	Kaon	NT1	NT2
$\mathcal{S}_{\mathrm{core,sig}}$ Run 1	1.454 ± 0.164	1.047 ± 0.208	1.089 ± 0.238	1.287 ± 0.190
$\mathcal{S}_{\mathrm{core,sig}}$ Run 2	0.100 ± 1.931	1.120 ± 0.153	0.386 ± 0.357	1.174 ± 0.239
$\delta_{\mathrm{core,sig,Lepton}}$ Run 1	-0.063 ± 0.124			
$\delta_{\mathrm{core,sig,Kaon}}$ Run 1		-0.296 ± 0.114		
$\delta_{\mathrm{core,sig,NT1}}$ Run 1			-0.086 ± 0.149	
$\delta_{\mathrm{core,sig,NT2}}$ Run 1				-0.540 ± 0.119
$\delta_{\mathrm{core,sig,Lepton}}$ Run 2	-0.061 ± 0.151			
$\delta_{\mathrm{core,sig,Kaon}}$ Run 2		-0.203 ± 0.110		
$\delta_{\mathrm{core,sig,NT1}}$ Run 2			-0.358 ± 0.314	
$\delta_{\mathrm{core,sig,NT2}}$ Run 2				-0.193 ± 0.189
$\delta_{\mathrm{tail,sig}}$ Run 1	-2.095 ± 3.665	-0.143 ± 0.418	10.000 ± 4.493	-10.000 ± 2.964
$\delta_{\mathrm{tail,sig}}$ Run 2	-0.364 ± 4.136	-6.087 ± 3.106	-1.211 ± 1.122	-3.525 ± 5.897
$f_{\mathrm{tail,sig}}$ Run 1	0.000 ± 0.071	0.232 ± 0.071	0.004 ± 0.008	0.012 ± 0.009
$f_{\mathrm{tail,sig}}$ Run 2	0.000 ± 0.033	0.029 ± 0.026	0.238 ± 0.131	0.036 ± 0.081
$f_{\mathrm{outlier,sig}}$ Run 1	0.000 ± 0.008	0.003 ± 0.005	0.012 ± 0.011	0.006 ± 0.010
$f_{\mathrm{outlier,sig}}$ Run 2	0.000 ± 0.008	0.007 ± 0.008	0.000 ± 0.006	0.000 ± 0.010
$\mathcal{D}_{\mathrm{Lepton}}$	0.827 ± 0.031			
$\mathcal{D}_{\mathrm{Kaon}}$		0.673 ± 0.026		
$\mathcal{D}_{\mathrm{NT1}}$			0.568 ± 0.047	
$\mathcal{D}_{\mathrm{NT2}}$				0.368 ± 0.053
$\Delta\mathcal{D}_{\mathrm{Lepton}}$	-0.007 ± 0.048			
$\Delta\mathcal{D}_{\mathrm{Kaon}}$		0.019 ± 0.035		
$\Delta\mathcal{D}_{\mathrm{NT1}}$			-0.093 ± 0.071	
$\Delta\mathcal{D}_{\mathrm{NT2}}$				0.105 ± 0.063
$\mathcal{S}_{\mathrm{core,bgd}}$ Run 1	0.598 ± 0.249	1.350 ± 0.048	1.128 ± 0.141	1.142 ± 0.112
$\mathcal{S}_{\mathrm{core,bgd}}$ Run 2	0.840 ± 0.188	1.207 ± 0.053	1.138 ± 0.158	1.236 ± 0.109
$\delta_{\mathrm{core,bgd}}$ Run 1	-0.115 ± 0.180	-0.134 ± 0.039	-0.138 ± 0.095	-0.129 ± 0.059
$\delta_{\mathrm{core,bgd}}$ Run 2	0.420 ± 0.242	-0.043 ± 0.047	0.361 ± 0.137	-0.097 ± 0.076
$f_{\mathrm{outlier,bgd}}$ Run 1	0.012 ± 0.025	0.015 ± 0.005	0.014 ± 0.010	0.024 ± 0.009
$f_{\mathrm{outlier,bgd}}$ Run 2	0.000 ± 0.043	0.019 ± 0.007	0.051 ± 0.027	0.047 ± 0.013
$\tau_{\tau>0}$ (ps)	1.300 ± 0.181	1.275 ± 0.128	0.997 ± 0.142	0.708 ± 0.064
$\mathcal{D}'_{\tau=0,\mathrm{Lepton}}$	0.132 ± 0.470			
$\mathcal{D}'_{\tau=0,\mathrm{Kaon}}$		0.442 ± 0.037		
$\mathcal{D}'_{\tau=0,\mathrm{NT1}}$			0.466 ± 0.224	
$\mathcal{D}'_{\tau=0,\mathrm{NT2}}$				-0.115 ± 0.181
$\mathcal{D}'_{\tau>0,\mathrm{Lepton}}$	0.366 ± 0.108			
$\mathcal{D}'_{\tau>0,\mathrm{Kaon}}$		0.217 ± 0.068		
$\mathcal{D}'_{\tau>0,\mathrm{NT1}}$			-0.117 ± 0.113	
$\mathcal{D}'_{\tau>0,\mathrm{NT2}}$				0.132 ± 0.031
$f_{\tau=0,\mathrm{Lepton}}$	0.163 ± 0.100			
$f_{\tau=0,\mathrm{Kaon}}$		0.673 ± 0.048		
$f_{\tau=0,\mathrm{NT1}}$			0.421 ± 0.127	
$f_{\tau=0,\mathrm{NT2}}$				0.286 ± 0.135
$\delta\Delta m_d$ (ps^{-1})	0.004 ± 0.028	0.002 ± 0.025	-0.022 ± 0.043	0.191 ± 0.106
Weigthed Average:		$+0.003 \pm 0.017$		
χ^2/dof		$3.5/3$		

Table 6.10: Δm_d and tagging dilutions for different tagging categories for Monte Carlo.

	Lepton	Kaon	NT1	NT2
$\mathcal{S}_{\text{core,sig}}$	1.226 ± 0.036	1.098 ± 0.030	1.067 ± 0.063	1.155 ± 0.051
$\delta_{\text{core,sig,Lepton}}$	-0.089 ± 0.021			
$\delta_{\text{core,sig,Kaon}}$		-0.218 ± 0.018		
$\delta_{\text{core,sig,NT1}}$			-0.143 ± 0.033	
$\delta_{\text{core,sig,NT2}}$				-0.185 ± 0.031
$\mathcal{S}_{\text{tail,sig}}$	6.317 ± 1.248	3.257 ± 0.376	3.747 ± 0.524	3.223 ± 0.655
$\delta_{\text{tail,sig}}$	-2.827 ± 1.165	-2.152 ± 0.598	-2.027 ± 1.088	-2.293 ± 1.578
$f_{\text{tail,sig}}$	0.016 ± 0.006	0.042 ± 0.014	0.045 ± 0.022	0.044 ± 0.027
$f_{\text{outlier,sig}}$	0.001 ± 0.001	0.005 ± 0.001	0.002 ± 0.001	0.006 ± 0.001
$\mathcal{D}_{\text{Lepton}}$	0.857 ± 0.006			
$\mathcal{D}_{\text{Kaon}}$		0.705 ± 0.005		
$\mathcal{D}_{\text{NT1}}$			0.621 ± 0.009	
$\mathcal{D}_{\text{NT2}}$				0.311 ± 0.008
$\Delta\mathcal{D}_{\text{Lepton}}$	0.005 ± 0.009			
$\Delta\mathcal{D}_{\text{Kaon}}$		0.037 ± 0.007		
$\Delta\mathcal{D}_{\text{NT1}}$			-0.051 ± 0.014	
$\Delta\mathcal{D}_{\text{NT2}}$				0.070 ± 0.012
Δm_d (ps^{-1})	0.487 ± 0.006	0.473 ± 0.005	0.469 ± 0.009	0.485 ± 0.015

Table 6.11: Variation of Δm_d observed in data depending on the flavor of either the fully reconstructed B^0 or the tagging B^0. The change is reported as the difference between the fit using the subsample and the nominal fit. The reported error is the statistical error of the fit using the subsample.

Category	$\delta\Delta m_d$ (ps^{-1})
B^0 rec	-0.013 ± 0.034
$\overline{B}^0$ rec	0.012 ± 0.033
B^0 tag	-0.018 ± 0.023
$\overline{B}^0$ tag	0.012 ± 0.024

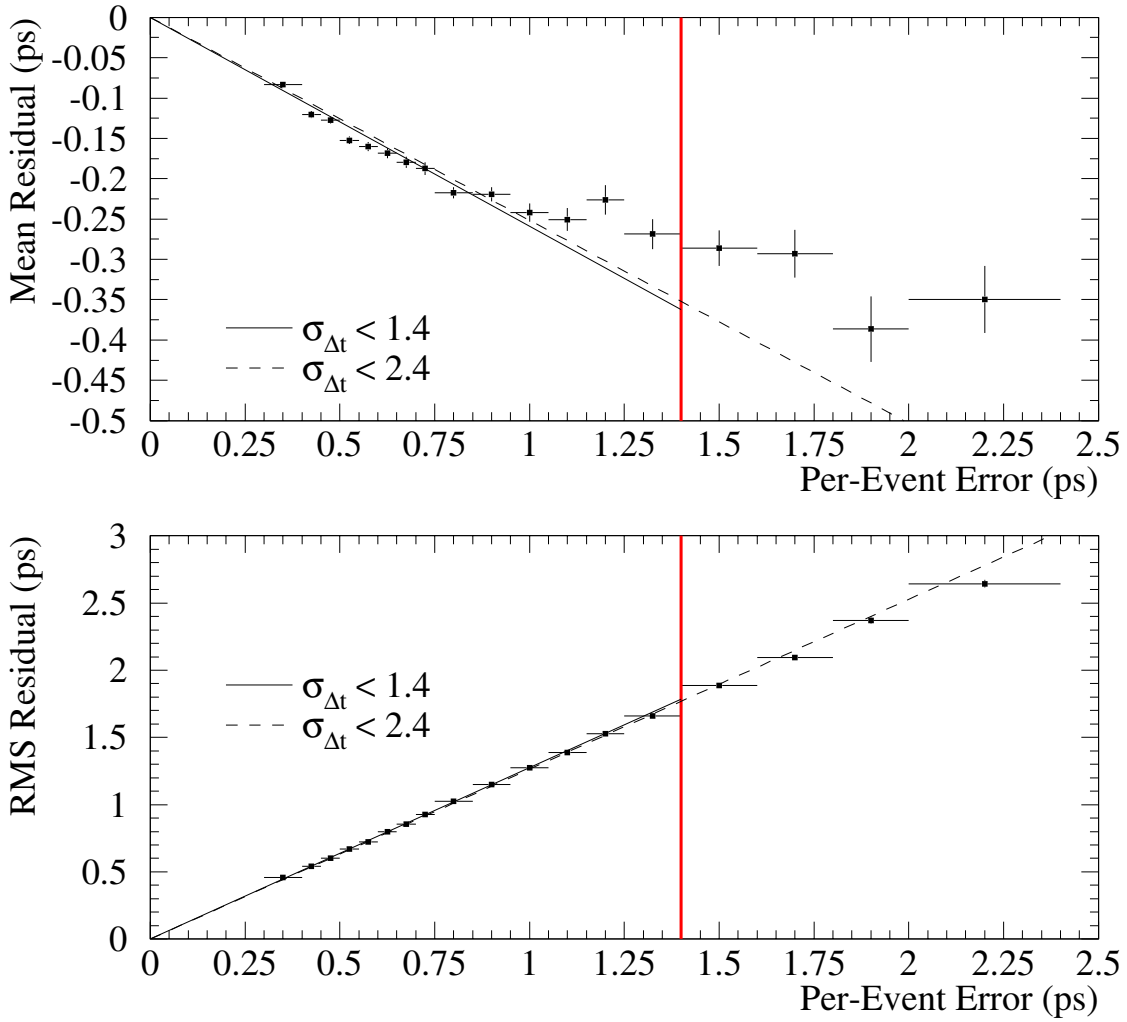

Figure 6-4: Mean and width of the Monte Carlo Δt residual in bins of the per-event error $\sigma_{\Delta t}$. Fits are shown to a line constrained to pass through the origin for $\sigma_{\Delta t} < 1.4$ and $\sigma_{\Delta t} < 2.4$ ps.

Table 6.12: Fitting the Monte Carlo Δt residuals with the nominal resolution model, which scales all biases with the per-event error, and which has individual core biases separately for each tagging category, using only events with a per-event error less than 1.4 ps.

Variable	All	`Lepton`	`Kaon`	`NT1`	`NT2`
$S_{\rm core}$	1.058 ± 0.005	1.036 ± 0.011	1.060 ± 0.007	1.079 ± 0.011	1.054 ± 0.011
$\delta_{\rm core,Lepton}$	-0.088 ± 0.008	-0.101 ± 0.009			
$\delta_{\rm core,Kaon}$	-0.210 ± 0.006		-0.201 ± 0.006		
$\delta_{\rm core,NT1}$	-0.134 ± 0.010			-0.148 ± 0.011	
$\delta_{\rm core,NT2}$	-0.186 ± 0.008				-0.181 ± 0.009
$S_{\rm tail}$	2.310 ± 0.038	2.308 ± 0.110	2.248 ± 0.051	2.659 ± 0.120	2.208 ± 0.073
$\delta_{\rm tail}$	-1.031 ± 0.041	-0.723 ± 0.087	-1.186 ± 0.064	-1.147 ± 0.133	-0.889 ± 0.074
$f_{\rm tail}$	0.106 ± 0.005	0.096 ± 0.012	0.109 ± 0.007	0.082 ± 0.009	0.134 ± 0.013
$f_{\rm outl}$	0.008 ± 0.000	0.006 ± 0.001	0.009 ± 0.001	0.005 ± 0.001	0.011 ± 0.001

is 0.4786 ± 0.0032 ps^{-1}. The main change in the resolution function parameters between the two configurations is the increase in the two scale factors in the nominal fit with respect to the fit on $\delta\Delta t$, and the change in the tail fraction. The fits to the Δt residual distributions are done separately for each tagging category because the Δt resolution can generally depend on the tagging category. Results of these fits are listed in Table 6.12. The Δt resolutions are very similar for the four tagging categories as demonstrated in Figure 6-5 where a global residual fit and fits to individual tagging category residuals are compared; the largest difference occurs in the biases. Therefore the same resolution function parameters are used in the likelihood fit for all tagging categories, but a separate bias is allowed for in each tagging category. The Δt residual distributions overlaid with both the residual and nominal mixing fit results for simulated tagged events are shown in Figure 6-6 for all tagging categories combined.

6.11.1 Resolution vs. $\Delta t_{\rm true}$

To check whether the Δt resolution depends on the actual value of Δt the Monte Carlo sample is split into 10 subsamples, each of which is a different bin in $\Delta t_{\rm true}$, and each containing approximately 1/10th of the events. The results are listed in Table 6.13.

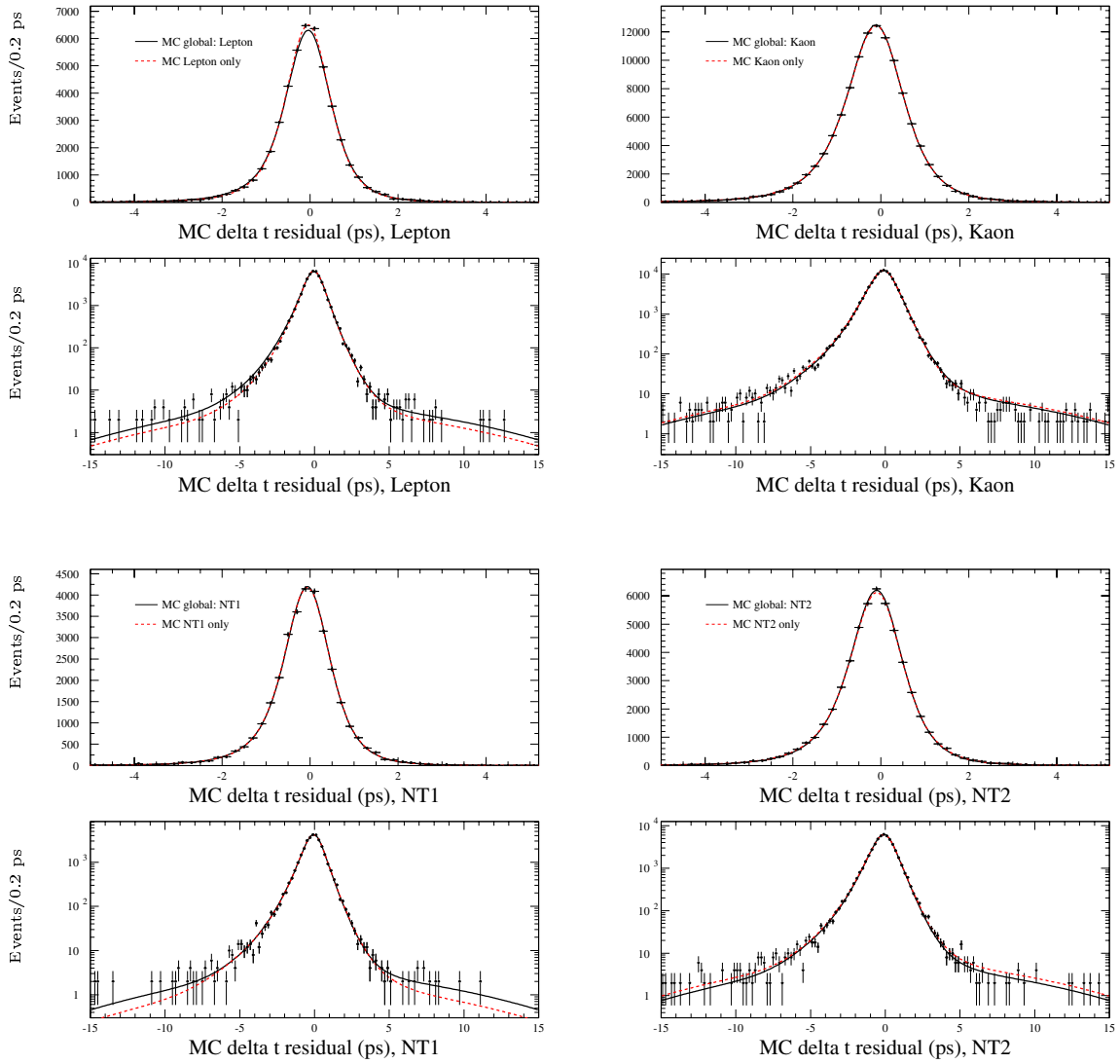

Figure 6-5: Distribution of Δt residuals for each tagging category for selected B candidates in signal Monte Carlo, overlaid with the fitted resolution model. Note that for each tagging category both a linear and log plot are shown. The solid line is the global fit to the residuals (corresponding to the "all" column in Table 6.12), while the dashed line are the fits to the individual tagging categories (i.e., the other columns in Table 6.12). Note that only on the log scale plots a small difference can be seen between these fits.

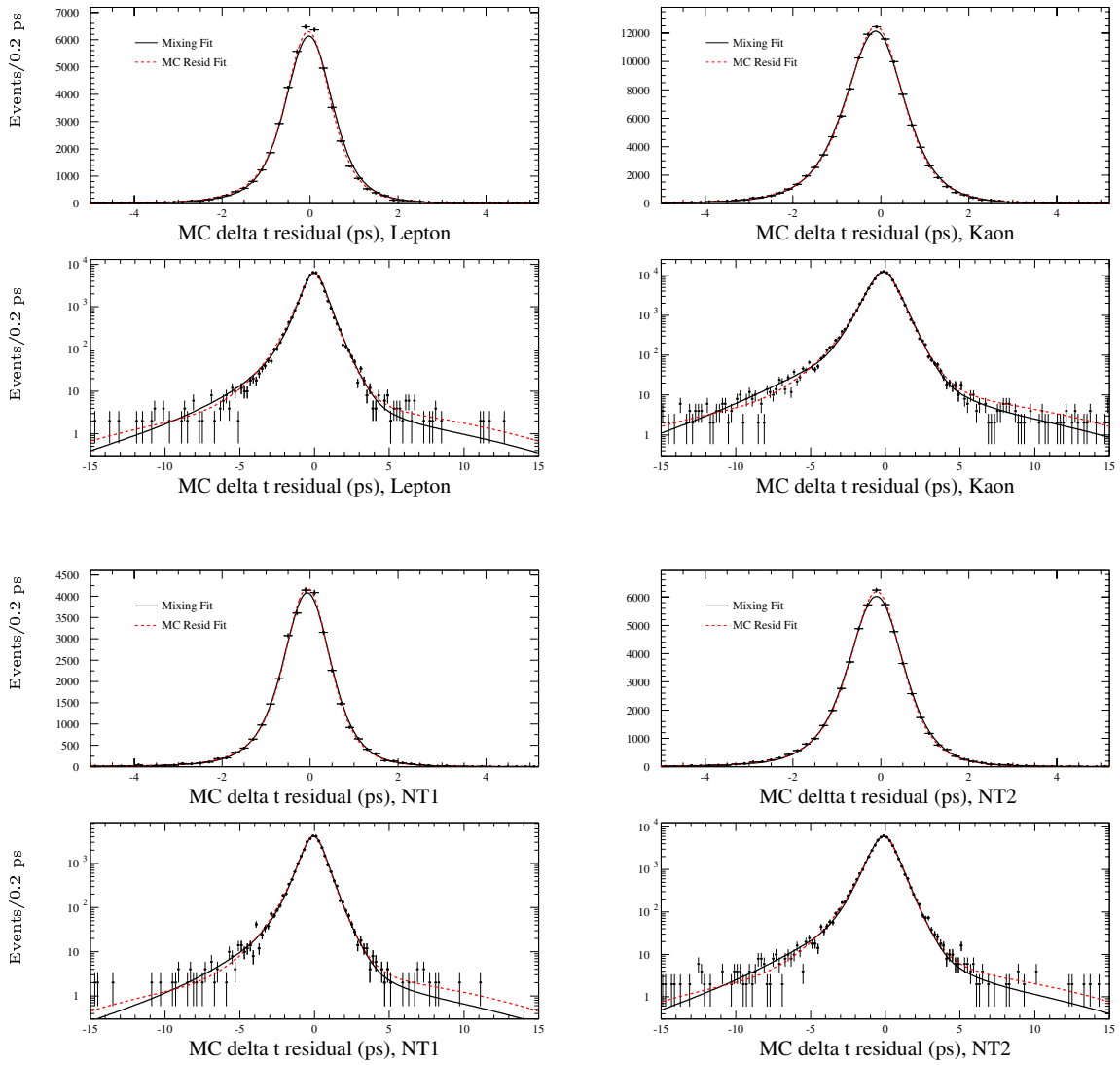

Figure 6-6: Distribution of Δt residuals for selected B candidates in signal Monte Carlo, overlaid with the fitted resolution model. The solid line is the fit to the residuals (corresponding to the "all" column in Table 6.12, and also shown as the solid line in Figure 6-5), while the dashed line is the nominal mixing fit (corresponding to Table 5.2)

Table 6.13: Parameters of fit of the signal resolution model to the Δt residual ($\Delta t_{\rm reco} - \Delta t_{\rm true}$) distributions for simulated hadronic B cocktail events for bins of $\Delta t_{\rm true}$.

$\Delta t_{\rm true}$ interval (ps)	$(-\infty, -2.48]$	$(-2.48, -1.41]$	$(-1.41, -0.79]$	$(-0.79, -0.34]$	$(-0.34 : 0]$
$\mathcal{S}_{\rm core,sig}$	1.052 ± 0.016	1.040 ± 0.013	1.055 ± 0.014	1.051 ± 0.013	1.060 ± 0.017
$\delta_{\rm core,sig,Lepton}$	-0.073 ± 0.026	-0.080 ± 0.025	-0.101 ± 0.026	-0.084 ± 0.026	-0.084 ± 0.028
$\delta_{\rm core,sig,Kaon}$	-0.207 ± 0.018	-0.168 ± 0.017	-0.227 ± 0.017	-0.211 ± 0.017	-0.183 ± 0.019
$\delta_{\rm core,sig,NT1}$	-0.164 ± 0.032	-0.114 ± 0.031	-0.131 ± 0.032	-0.103 ± 0.030	-0.104 ± 0.033
$\delta_{\rm core,sig,NT2}$	-0.171 ± 0.025	-0.200 ± 0.024	-0.207 ± 0.025	-0.207 ± 0.025	-0.196 ± 0.027
$\mathcal{S}_{\rm tail,sig}$	2.280 ± 0.115	2.465 ± 0.120	2.393 ± 0.132	2.488 ± 0.128	2.089 ± 0.113
$\delta_{\rm tail,sig}$	-0.819 ± 0.102	-0.963 ± 0.115	-0.963 ± 0.131	-1.204 ± 0.139	-0.813 ± 0.117
$f_{\rm tail,sig}$	0.124 ± 0.018	0.111 ± 0.013	0.100 ± 0.015	0.093 ± 0.012	0.127 ± 0.023
$f_{\rm outlier,sig}$	0.009 ± 0.001	0.009 ± 0.001	0.007 ± 0.001	0.008 ± 0.001	0.009 ± 0.001
$\Delta t_{\rm true}$ interval (ps)	$(0, 0.34]$	$(0.34, 0.79]$	$(0.79, 1.41]$	$(1.41, 2.48]$	$(2.48, \infty)$
$\mathcal{S}_{\rm core,sig}$	1.023 ± 0.018	1.081 ± 0.013	1.068 ± 0.013	1.058 ± 0.015	1.075 ± 0.015
$\delta_{\rm core,sig,Lepton}$	-0.096 ± 0.028	-0.062 ± 0.026	-0.058 ± 0.026	-0.098 ± 0.026	-0.137 ± 0.026
$\delta_{\rm core,sig,Kaon}$	-0.207 ± 0.019	-0.219 ± 0.017	-0.236 ± 0.017	-0.212 ± 0.018	-0.227 ± 0.018
$\delta_{\rm core,sig,NT1}$	-0.112 ± 0.034	-0.163 ± 0.032	-0.128 ± 0.031	-0.137 ± 0.033	-0.171 ± 0.031
$\delta_{\rm core,sig,NT2}$	-0.160 ± 0.027	-0.187 ± 0.025	-0.157 ± 0.025	-0.184 ± 0.025	-0.183 ± 0.025
$\mathcal{S}_{\rm tail,sig}$	2.055 ± 0.101	2.371 ± 0.128	2.357 ± 0.107	2.244 ± 0.105	2.284 ± 0.128
$\delta_{\rm tail,sig}$	-0.873 ± 0.107	-1.165 ± 0.157	-1.158 ± 0.138	-1.117 ± 0.131	-1.269 ± 0.164
$f_{\rm tail,sig}$	0.146 ± 0.024	0.085 ± 0.013	0.097 ± 0.013	0.117 ± 0.016	0.093 ± 0.015
$f_{\rm outlier,sig}$	0.009 ± 0.001	0.007 ± 0.001	0.007 ± 0.001	0.009 ± 0.001	0.009 ± 0.001

6.11.2 Charm Lifetime Studies

The signal Monte Carlo cocktail is divided into subsamples containing different upper bounds on the true flight distances for the charm daughters of the tag B to check whether the measured value of Δm_d has any dependence on the charm meson (D^0, D^+, D_s^+) flight distance. The results of this check are shown in Tables 6.14 through 6.18, and are illustrated graphically in Figures 6-7 through 6-9.

The measured value of Δm_d is unchanged when varying the bound on the true flight distance of the tag-side D in the event. See Section 7.1.2 for a discussion of systematics associated with D lifetimes.

The sample is also categorized according to which species of charm is generated on the tag side. For this study, events are selected for a category by the minimal requirement that *at least* one of the species be present on the tag side, and therefore always include double-charm decays. The "No charm" category includes decays to charmed baryons and charmonium final states, as well as true cases of $b \to u$ and $b \to s$ transitions. The results of fits to these categories are in Table 6.19 and Figure 6-10.

Table 6.14: Results from the likelihood fits to the Δt distributions of the hadronic B decays in 2.8 million simulated signal cocktail events (no $B \to J/\psi K^*$) for different values of upper bound on true 3-dimensional charm flight distance, l_c, for events with at least one true D^+ on the tag side (includes double charm decays).

Parameter	$l_c < 100$ μm	$l_c < 200$ μm	$l_c < 300$ μm	$l_c < 400$ μm	$l_c < 500$ μm
$\mathcal{S}_{\mathrm{core,sig}}$	0.282 ± 0.000	1.102 ± 0.053	0.894 ± 0.262	1.146 ± 0.037	1.161 ± 0.043
$\delta_{\mathrm{core,sig,Lepton}}$	−0.010 ± 0.263	−0.018 ± 0.047	−0.118 ± 0.101	−0.078 ± 0.039	−0.091 ± 0.038
$\delta_{\mathrm{core,sig,Kaon}}$	−0.230 ± 0.139	−0.134 ± 0.032	−0.333 ± 0.160	−0.247 ± 0.026	−0.284 ± 0.027
$\delta_{\mathrm{core,sig,NT1}}$	0.189 ± 0.002	0.034 ± 0.068	0.004 ± 0.138	−0.022 ± 0.055	−0.042 ± 0.054
$\delta_{\mathrm{core,sig,NT2}}$	−0.142 ± 0.196	−0.162 ± 0.048	−0.384 ± 0.199	−0.278 ± 0.040	−0.301 ± 0.039
$\mathcal{S}_{\mathrm{tail,sig}}$	1.430 ± 0.106	4.223 ± 1.146	1.603 ± 0.439	4.662 ± 1.346	3.925 ± 1.107
$\delta_{\mathrm{tail,sig}}$	−0.028 ± 0.062	−1.410 ± 1.154	0.003 ± 0.208	−1.272 ± 0.968	−1.400 ± 1.074
$f_{\mathrm{tail,sig}}$	0.725 ± 0.080	0.026 ± 0.020	0.368 ± 0.364	0.019 ± 0.012	0.022 ± 0.018
$f_{\mathrm{outlier,sig}}$	0.006 ± 0.002	0.004 ± 0.002	0.007 ± 0.001	0.004 ± 0.002	0.004 ± 0.001
$\mathcal{D}_{\mathrm{Lepton}}$	0.809 ± 0.017	0.796 ± 0.014	0.798 ± 0.012	0.793 ± 0.011	0.794 ± 0.011
$\mathcal{D}_{\mathrm{Kaon}}$	0.566 ± 0.016	0.568 ± 0.012	0.571 ± 0.011	0.573 ± 0.010	0.566 ± 0.010
$\mathcal{D}_{\mathrm{NT1}}$	0.448 ± 0.032	0.467 ± 0.024	0.475 ± 0.021	0.475 ± 0.020	0.485 ± 0.019
$\mathcal{D}_{\mathrm{NT2}}$	0.122 ± 0.025	0.110 ± 0.019	0.111 ± 0.017	0.108 ± 0.016	0.110 ± 0.015
$\Delta\mathcal{D}_{\mathrm{Lepton}}$	0.034 ± 0.028	0.010 ± 0.022	0.012 ± 0.020	0.007 ± 0.018	0.014 ± 0.018
$\Delta\mathcal{D}_{\mathrm{Kaon}}$	0.033 ± 0.024	0.039 ± 0.019	0.033 ± 0.017	0.028 ± 0.016	0.027 ± 0.015
$\Delta\mathcal{D}_{\mathrm{NT1}}$	0.087 ± 0.049	0.073 ± 0.038	0.046 ± 0.033	0.046 ± 0.031	0.044 ± 0.029
$\Delta\mathcal{D}_{\mathrm{NT2}}$	0.142 ± 0.038	0.114 ± 0.030	0.130 ± 0.027	0.132 ± 0.025	0.129 ± 0.024
Δm_d (ps^{-1})	0.4801 ± 0.0113	0.4766 ± 0.0090	0.4754 ± 0.0079	0.4753 ± 0.0074	0.4736 ± 0.0072
Events	12337	20089	25543	29176	31777

Parameter	$l_c < 600$ μm	$l_c < 700$ μm	$l_c < 800$ μm	$l_c < 900$ μm	$l_c < 1000$ μm
$\mathcal{S}_{\mathrm{core,sig}}$	1.170 ± 0.042	1.197 ± 0.040	1.207 ± 0.035	1.212 ± 0.038	1.198 ± 0.040
$\delta_{\mathrm{core,sig,Lepton}}$	−0.091 ± 0.038	−0.079 ± 0.037	−0.086 ± 0.036	−0.078 ± 0.036	−0.073 ± 0.037
$\delta_{\mathrm{core,sig,Kaon}}$	−0.301 ± 0.026	−0.316 ± 0.027	−0.323 ± 0.026	−0.332 ± 0.026	−0.331 ± 0.027
$\delta_{\mathrm{core,sig,NT1}}$	−0.053 ± 0.053	−0.062 ± 0.052	−0.074 ± 0.050	−0.085 ± 0.051	−0.088 ± 0.051
$\delta_{\mathrm{core,sig,NT2}}$	−0.314 ± 0.039	−0.324 ± 0.038	−0.321 ± 0.037	−0.333 ± 0.038	−0.327 ± 0.038
$\mathcal{S}_{\mathrm{tail,sig}}$	3.897 ± 0.901	3.804 ± 0.757	4.008 ± 0.634	3.777 ± 0.554	3.608 ± 0.450
$\delta_{\mathrm{tail,sig}}$	−1.385 ± 0.874	−1.685 ± 0.985	−2.059 ± 1.040	−1.910 ± 0.902	−1.708 ± 0.669
$f_{\mathrm{tail,sig}}$	0.027 ± 0.018	0.027 ± 0.017	0.025 ± 0.013	0.032 ± 0.015	0.044 ± 0.018
$f_{\mathrm{outlier,sig}}$	0.004 ± 0.001	0.004 ± 0.001	0.004 ± 0.001	0.004 ± 0.001	0.004 ± 0.001
$\mathcal{D}_{\mathrm{Lepton}}$	0.789 ± 0.011	0.791 ± 0.011	0.793 ± 0.010	0.794 ± 0.010	0.793 ± 0.010
$\mathcal{D}_{\mathrm{Kaon}}$	0.569 ± 0.010	0.568 ± 0.010	0.567 ± 0.009	0.567 ± 0.009	0.566 ± 0.009
$\mathcal{D}_{\mathrm{NT1}}$	0.483 ± 0.018	0.489 ± 0.018	0.491 ± 0.017	0.492 ± 0.017	0.495 ± 0.017
$\mathcal{D}_{\mathrm{NT2}}$	0.111 ± 0.015	0.115 ± 0.015	0.118 ± 0.014	0.121 ± 0.014	0.122 ± 0.014
$\Delta\mathcal{D}_{\mathrm{Lepton}}$	0.012 ± 0.017	0.013 ± 0.017	0.015 ± 0.016	0.016 ± 0.016	0.015 ± 0.016
$\Delta\mathcal{D}_{\mathrm{Kaon}}$	0.031 ± 0.015	0.033 ± 0.015	0.036 ± 0.014	0.037 ± 0.014	0.036 ± 0.014
$\Delta\mathcal{D}_{\mathrm{NT1}}$	0.036 ± 0.029	0.036 ± 0.028	0.039 ± 0.027	0.040 ± 0.027	0.042 ± 0.027
$\Delta\mathcal{D}_{\mathrm{NT2}}$	0.115 ± 0.023	0.112 ± 0.023	0.116 ± 0.022	0.117 ± 0.022	0.119 ± 0.022
Δm_d (ps^{-1})	0.4722 ± 0.0070	0.4717 ± 0.0069	0.4706 ± 0.0067	0.4720 ± 0.0067	0.4707 ± 0.0067
Events	33650	35123	36193	36987	37636

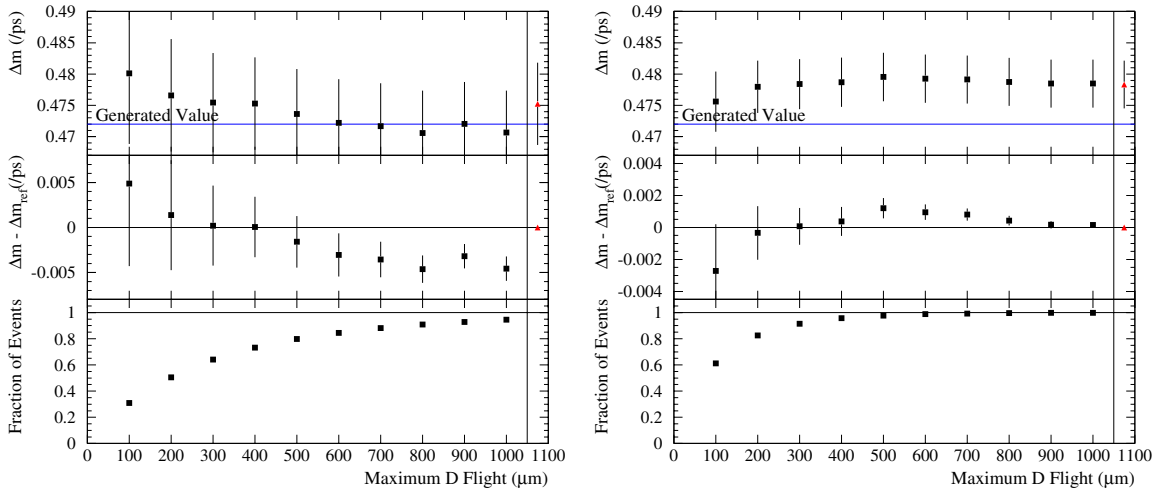

Figure 6-7: Results from the likelihood fits to the Δt distributions of the hadronic B decays in 2.8 million simulated signal cocktail events (no $B \to J/\psi K^*$) for different values of upper bound on true 3-dimensional charm flight distance, l_c, for events with at least one true D^+ on the tag side (left) and at least one D^0 on the tag side (right). (Both include double charm decays). The reference fits (triangles at right) have $l_c = \infty$. The errors shown on the plot showing the difference with the reference fit are computed as the difference in quadrature from the reference.

Table 6.15: Results from the likelihood fits to the Δt distributions of the hadronic B decays in 2.8 million simulated signal cocktail events (no $B \to J/\psi K^*$) for different values of upper bound on true 3-dimensional charm flight distance, l_c, for events with at least one true D^0 on the tag side (includes double charm decays).

Parameter	$l_c < 100$ μm	$l_c < 200$ μm	$l_c < 300$ μm	$l_c < 400$ μm	$l_c < 500$ μm
$\mathcal{S}_{\mathrm{core,sig}}$	0.884 ± 0.186	0.969 ± 0.083	0.938 ± 0.106	0.973 ± 0.092	0.978 ± 0.085
$\delta_{\mathrm{core,sig,Lepton}}$	0.196 ± 0.267	0.050 ± 0.081	0.091 ± 0.108	0.057 ± 0.094	0.050 ± 0.086
$\delta_{\mathrm{core,sig,Kaon}}$	0.081 ± 0.209	−0.053 ± 0.066	−0.039 ± 0.084	−0.080 ± 0.075	−0.088 ± 0.069
$\delta_{\mathrm{core,sig,NT1}}$	0.004 ± 0.184	−0.106 ± 0.073	−0.095 ± 0.085	−0.126 ± 0.078	−0.120 ± 0.074
$\delta_{\mathrm{core,sig,NT2}}$	0.170 ± 0.254	0.004 ± 0.076	0.034 ± 0.100	−0.020 ± 0.087	−0.039 ± 0.079
$\mathcal{S}_{\mathrm{tail,sig}}$	1.341 ± 0.387	1.797 ± 0.478	1.626 ± 0.322	1.797 ± 0.457	1.853 ± 0.459
$\delta_{\mathrm{tail,sig}}$	−0.933 ± 1.490	−1.102 ± 0.972	−0.822 ± 0.561	−1.000 ± 0.690	−1.068 ± 0.700
$f_{\mathrm{tail,sig}}$	0.202 ± 0.599	0.099 ± 0.113	0.180 ± 0.170	0.125 ± 0.132	0.115 ± 0.116
$f_{\mathrm{outlier,sig}}$	0.006 ± 0.001	0.005 ± 0.001	0.005 ± 0.001	0.005 ± 0.001	0.004 ± 0.001
$\mathcal{D}_{\mathrm{Lepton}}$	0.940 ± 0.008	0.939 ± 0.007	0.939 ± 0.006	0.936 ± 0.006	0.936 ± 0.006
$\mathcal{D}_{\mathrm{Kaon}}$	0.807 ± 0.007	0.809 ± 0.006	0.806 ± 0.006	0.808 ± 0.006	0.808 ± 0.006
$\mathcal{D}_{\mathrm{NT1}}$	0.819 ± 0.013	0.808 ± 0.011	0.811 ± 0.011	0.812 ± 0.010	0.813 ± 0.010
$\mathcal{D}_{\mathrm{NT2}}$	0.503 ± 0.014	0.514 ± 0.012	0.517 ± 0.011	0.517 ± 0.011	0.518 ± 0.011
$\Delta\mathcal{D}_{\mathrm{Lepton}}$	−0.008 ± 0.013	−0.005 ± 0.012	−0.005 ± 0.011	−0.003 ± 0.011	−0.004 ± 0.011
$\Delta\mathcal{D}_{\mathrm{Kaon}}$	0.042 ± 0.011	0.040 ± 0.010	0.040 ± 0.009	0.040 ± 0.009	0.040 ± 0.009
$\Delta\mathcal{D}_{\mathrm{NT1}}$	−0.080 ± 0.022	−0.083 ± 0.019	−0.059 ± 0.018	−0.057 ± 0.017	−0.061 ± 0.017
$\Delta\mathcal{D}_{\mathrm{NT2}}$	0.032 ± 0.022	0.026 ± 0.019	0.031 ± 0.018	0.033 ± 0.017	0.034 ± 0.017
Δm_d (ps^{-1})	0.4756 ± 0.0048	0.4780 ± 0.0042	0.4784 ± 0.0040	0.4787 ± 0.0039	0.4795 ± 0.0039
Events	36826	49624	55039	57538	58725

Parameter	$l_c < 600$ μm	$l_c < 700$ μm	$l_c < 800$ μm	$l_c < 900$ μm	$l_c < 1000$ μm
$\mathcal{S}_{\mathrm{core,sig}}$	0.988 ± 0.075	0.997 ± 0.066	0.995 ± 0.068	0.998 ± 0.069	1.001 ± 0.066
$\delta_{\mathrm{core,sig,Lepton}}$	0.034 ± 0.074	0.021 ± 0.065	0.021 ± 0.066	0.019 ± 0.067	0.015 ± 0.064
$\delta_{\mathrm{core,sig,Kaon}}$	−0.106 ± 0.060	−0.113 ± 0.053	−0.112 ± 0.053	−0.114 ± 0.055	−0.117 ± 0.052
$\delta_{\mathrm{core,sig,NT1}}$	−0.139 ± 0.066	−0.143 ± 0.060	−0.146 ± 0.060	−0.149 ± 0.061	−0.151 ± 0.059
$\delta_{\mathrm{core,sig,NT2}}$	−0.063 ± 0.068	−0.073 ± 0.060	−0.075 ± 0.060	−0.077 ± 0.062	−0.081 ± 0.059
$\mathcal{S}_{\mathrm{tail,sig}}$	1.997 ± 0.527	2.102 ± 0.534	2.093 ± 0.530	2.109 ± 0.563	2.149 ± 0.571
$\delta_{\mathrm{tail,sig}}$	−1.134 ± 0.654	−1.202 ± 0.623	−1.188 ± 0.622	−1.209 ± 0.648	−1.233 ± 0.640
$f_{\mathrm{tail,sig}}$	0.097 ± 0.091	0.087 ± 0.073	0.089 ± 0.076	0.086 ± 0.077	0.083 ± 0.072
$f_{\mathrm{outlier,sig}}$	0.005 ± 0.001	0.004 ± 0.001	0.005 ± 0.001	0.005 ± 0.001	0.004 ± 0.001
$\mathcal{D}_{\mathrm{Lepton}}$	0.938 ± 0.006	0.938 ± 0.006	0.938 ± 0.006	0.938 ± 0.006	0.938 ± 0.006
$\mathcal{D}_{\mathrm{Kaon}}$	0.809 ± 0.006	0.809 ± 0.006	0.809 ± 0.006	0.809 ± 0.006	0.809 ± 0.006
$\mathcal{D}_{\mathrm{NT1}}$	0.813 ± 0.010	0.813 ± 0.010	0.813 ± 0.010	0.814 ± 0.010	0.814 ± 0.010
$\mathcal{D}_{\mathrm{NT2}}$	0.517 ± 0.011	0.518 ± 0.011	0.518 ± 0.011	0.518 ± 0.011	0.518 ± 0.011
$\Delta\mathcal{D}_{\mathrm{Lepton}}$	−0.004 ± 0.011	−0.003 ± 0.011	−0.003 ± 0.011	−0.003 ± 0.011	−0.004 ± 0.011
$\Delta\mathcal{D}_{\mathrm{Kaon}}$	0.041 ± 0.009	0.041 ± 0.009	0.041 ± 0.009	0.041 ± 0.009	0.041 ± 0.009
$\Delta\mathcal{D}_{\mathrm{NT1}}$	−0.060 ± 0.017	−0.064 ± 0.017	−0.064 ± 0.017	−0.063 ± 0.017	−0.063 ± 0.017
$\Delta\mathcal{D}_{\mathrm{NT2}}$	0.038 ± 0.017	0.039 ± 0.017	0.040 ± 0.017	0.041 ± 0.017	0.041 ± 0.017
Δm_d (ps^{-1})	0.4793 ± 0.0039	0.4791 ± 0.0038	0.4787 ± 0.0038	0.4785 ± 0.0038	0.4785 ± 0.0038
Events	59399	59735	59910	60002	60067

Table 6.16: Results from the likelihood fits to the Δt distributions of the hadronic B decays in 2.8 million simulated signal cocktail events (no $B \to J/\psi K^*$) for different values of upper bound on true 3-dimensional charm flight distance, l_c, for events with at least one true D_s on the tag side.

Parameter	$l_c < 200$ μm	$l_c < 300$ μm	$l_c < 400$ μm	$l_c < 500$ μm	$l_c < 600$ μm
$\mathcal{S}_{\mathrm{core,sig}}$	1.113 ± 0.148	1.099 ± 0.140	1.270 ± 9.212	1.141 ± 0.150	1.117 ± 0.187
$\delta_{\mathrm{core,sig,Lepton}}$	−0.003 ± 0.300	−0.126 ± 0.293	−1.442 ± 15.256	−0.368 ± 0.286	−0.358 ± 0.304
$\delta_{\mathrm{core,sig,Kaon}}$	−0.317 ± 0.143	−0.289 ± 0.152	−1.235 ± 15.107	−0.357 ± 0.144	−0.352 ± 0.155
$\delta_{\mathrm{core,sig,NT1}}$	−0.189 ± 0.185	−0.226 ± 0.185	−1.243 ± 15.112	−0.336 ± 0.179	−0.360 ± 0.185
$\delta_{\mathrm{core,sig,NT2}}$	−0.166 ± 0.169	−0.168 ± 0.165	−1.185 ± 15.070	−0.265 ± 0.159	−0.278 ± 0.167
$\mathcal{S}_{\mathrm{tail,sig}}$	2.398 ± 1.172	2.148 ± 0.962	0.657 ± 0.062	2.585 ± 1.324	2.594 ± 1.337
$\delta_{\mathrm{tail,sig}}$	−1.987 ± 1.743	−2.157 ± 1.708	−0.408 ± 0.024	−1.670 ± 1.026	−1.477 ± 0.829
$f_{\mathrm{tail,sig}}$	0.094 ± 0.121	0.101 ± 0.125	1.000 ± 0.000	0.095 ± 0.127	0.114 ± 0.163
$f_{\mathrm{outlier,sig}}$	0.001 ± 0.002	0.001 ± 0.002	0.800 ± 0.000	0.000 ± 0.004	0.001 ± 0.002
$\mathcal{D}_{\mathrm{Lepton}}$	0.174 ± 0.089	0.161 ± 0.082	0.157 ± 0.046	0.142 ± 0.080	0.136 ± 0.080
$\mathcal{D}_{\mathrm{Kaon}}$	0.724 ± 0.018	0.721 ± 0.016	0.757 ± 0.019	0.731 ± 0.016	0.730 ± 0.016
$\mathcal{D}_{\mathrm{NT1}}$	0.537 ± 0.052	0.529 ± 0.048	0.544 ± 0.044	0.534 ± 0.046	0.527 ± 0.046
$\mathcal{D}_{\mathrm{NT2}}$	0.213 ± 0.034	0.226 ± 0.032	0.221 ± 0.019	0.225 ± 0.030	0.226 ± 0.030
$\Delta\mathcal{D}_{\mathrm{Lepton}}$	0.044 ± 0.136	0.104 ± 0.128	0.136 ± 0.076	0.110 ± 0.122	0.125 ± 0.121
$\Delta\mathcal{D}_{\mathrm{Kaon}}$	0.032 ± 0.025	0.042 ± 0.024	0.034 ± 0.020	0.038 ± 0.023	0.038 ± 0.023
$\Delta\mathcal{D}_{\mathrm{NT1}}$	−0.261 ± 0.082	−0.259 ± 0.077	−0.257 ± 0.063	−0.272 ± 0.073	−0.262 ± 0.073
$\Delta\mathcal{D}_{\mathrm{NT2}}$	0.059 ± 0.050	0.041 ± 0.048	0.027 ± 0.029	0.037 ± 0.046	0.036 ± 0.046
Δm_d (ps^{-1})	0.5043 ± 0.0164	0.4972 ± 0.0152	0.5649 ± 0.0169	0.5030 ± 0.0146	0.5008 ± 0.0147
Events	6555	7315	7688	7878	7968

Parameter	$l_c < 800$ μm	$l_c < 900$ μm	$l_c < 1000$ μm	$l_c < 50.0$
$\mathcal{S}_{\mathrm{core,sig}}$	1.135 ± 0.102	1.141 ± 0.100	1.143 ± 0.099	1.144 ± 0.099
$\delta_{\mathrm{core,sig,Lepton}}$	−0.362 ± 0.243	−0.397 ± 0.240	−0.399 ± 0.239	−0.399 ± 0.239
$\delta_{\mathrm{core,sig,Kaon}}$	−0.378 ± 0.073	−0.382 ± 0.071	−0.383 ± 0.070	−0.385 ± 0.070
$\delta_{\mathrm{core,sig,NT1}}$	−0.380 ± 0.139	−0.382 ± 0.138	−0.391 ± 0.138	−0.392 ± 0.137
$\delta_{\mathrm{core,sig,NT2}}$	−0.290 ± 0.098	−0.298 ± 0.096	−0.301 ± 0.096	−0.297 ± 0.096
$\mathcal{S}_{\mathrm{tail,sig}}$	2.768 ± 0.649	2.790 ± 0.638	2.803 ± 0.638	2.805 ± 0.636
$\delta_{\mathrm{tail,sig}}$	−1.553 ± 0.751	−1.548 ± 0.753	−1.545 ± 0.753	−1.547 ± 0.754
$f_{\mathrm{tail,sig}}$	0.098 ± 0.070	0.096 ± 0.068	0.094 ± 0.067	0.094 ± 0.067
$f_{\mathrm{outlier,sig}}$	0.001 ± 0.002	0.001 ± 0.002	0.001 ± 0.002	0.001 ± 0.002
$\mathcal{D}_{\mathrm{Lepton}}$	0.115 ± 0.079	0.119 ± 0.079	0.119 ± 0.079	0.117 ± 0.079
$\mathcal{D}_{\mathrm{Kaon}}$	0.728 ± 0.016	0.727 ± 0.016	0.727 ± 0.016	0.727 ± 0.016
$\mathcal{D}_{\mathrm{NT1}}$	0.528 ± 0.046	0.528 ± 0.046	0.530 ± 0.046	0.531 ± 0.046
$\mathcal{D}_{\mathrm{NT2}}$	0.226 ± 0.030	0.227 ± 0.030	0.226 ± 0.030	0.226 ± 0.030
$\Delta\mathcal{D}_{\mathrm{Lepton}}$	0.107 ± 0.121	0.113 ± 0.121	0.113 ± 0.121	0.127 ± 0.120
$\Delta\mathcal{D}_{\mathrm{Kaon}}$	0.034 ± 0.023	0.035 ± 0.022	0.035 ± 0.022	0.035 ± 0.022
$\Delta\mathcal{D}_{\mathrm{NT1}}$	−0.265 ± 0.073	−0.265 ± 0.073	−0.262 ± 0.073	−0.260 ± 0.072
$\Delta\mathcal{D}_{\mathrm{NT2}}$	0.040 ± 0.045	0.041 ± 0.045	0.043 ± 0.045	0.043 ± 0.045
Δm_d (ps^{-1})	0.4983 ± 0.0146	0.4982 ± 0.0146	0.4979 ± 0.0146	0.4982 ± 0.0146
Events	8053	8069	8072	8079

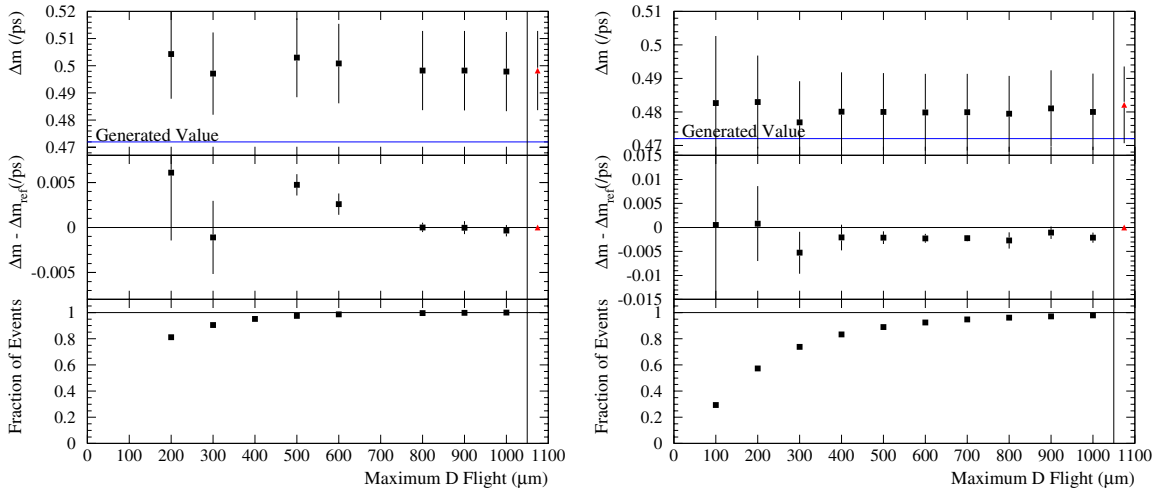

Figure 6-8: Results from the likelihood fits to the Δt distributions of the hadronic B decays in 2.8 million simulated signal cocktail events (no $B \to J/\psi K^*$) for different values of upper bound on true 3-dimensional charm flight distance, l_c, for events with at least one true D_s on the tag side (includes double charm decays) (left), and for events with two true D mesons on the tag side (right). The reference fit (triangle at right) has $l_c = \infty$. The errors shown on the plot showing the difference with the reference fit are computed as the difference in quadrature from the reference.

Table 6.17: Results from the likelihood fits to the Δt distributions of the hadronic B decays in 2.8 million simulated signal cocktail events (no $B \to J/\psi K^*$) for different values of upper bound on true 3-dimensional charm flight distance, l_c, for events with two true D mesons on the tag side.

Parameter	$l_c < 100$ μm	$l_c < 200$ μm	$l_c < 300$ μm	$l_c < 400$ μm	$l_c < 500$ μm
$\mathcal{S}_{\mathrm{core,sig}}$	1.017 ± 0.097	1.016 ± 0.051	1.050 ± 0.049	1.070 ± 0.044	1.101 ± 0.046
$\delta_{\mathrm{core,sig,Lepton}}$	0.058 ± 0.330	−0.186 ± 0.204	−0.215 ± 0.177	−0.292 ± 0.165	−0.378 ± 0.161
$\delta_{\mathrm{core,sig,Kaon}}$	−0.150 ± 0.057	−0.231 ± 0.034	−0.311 ± 0.034	−0.355 ± 0.031	−0.376 ± 0.034
$\delta_{\mathrm{core,sig,NT1}}$	−0.054 ± 0.158	−0.222 ± 0.107	−0.353 ± 0.098	−0.415 ± 0.091	−0.472 ± 0.090
$\delta_{\mathrm{core,sig,NT2}}$	−0.078 ± 0.094	−0.224 ± 0.061	−0.338 ± 0.057	−0.411 ± 0.052	−0.438 ± 0.054
$\mathcal{S}_{\mathrm{tail,sig}}$	3.336 ± 1.106	3.795 ± 0.716	3.478 ± 0.879	3.813 ± 0.922	3.401 ± 0.963
$\delta_{\mathrm{tail,sig}}$	−0.637 ± 0.695	−1.920 ± 1.099	−2.129 ± 1.341	−1.823 ± 0.950	−2.151 ± 1.439
$f_{\mathrm{tail,sig}}$	0.066 ± 0.055	0.036 ± 0.017	0.032 ± 0.020	0.032 ± 0.016	0.031 ± 0.020
$f_{\mathrm{outlier,sig}}$	0.004 ± 0.003	0.004 ± 0.002	0.005 ± 0.002	0.004 ± 0.002	0.004 ± 0.002
$\mathcal{D}_{\mathtt{Lepton}}$	0.385 ± 0.112	0.199 ± 0.076	0.205 ± 0.066	0.165 ± 0.062	0.155 ± 0.060
$\mathcal{D}_{\mathtt{Kaon}}$	0.553 ± 0.018	0.565 ± 0.013	0.561 ± 0.012	0.560 ± 0.011	0.557 ± 0.011
$\mathcal{D}_{\mathtt{NT1}}$	0.491 ± 0.059	0.500 ± 0.041	0.482 ± 0.036	0.479 ± 0.034	0.468 ± 0.033
$\mathcal{D}_{\mathtt{NT2}}$	0.216 ± 0.036	0.231 ± 0.025	0.229 ± 0.022	0.235 ± 0.021	0.230 ± 0.020
$\Delta\mathcal{D}_{\mathtt{Lepton}}$	0.099 ± 0.180	0.008 ± 0.119	0.083 ± 0.104	0.141 ± 0.096	0.113 ± 0.093
$\Delta\mathcal{D}_{\mathtt{Kaon}}$	0.085 ± 0.027	0.070 ± 0.019	0.068 ± 0.017	0.064 ± 0.016	0.061 ± 0.016
$\Delta\mathcal{D}_{\mathtt{NT1}}$	−0.253 ± 0.094	−0.309 ± 0.066	−0.348 ± 0.057	−0.345 ± 0.054	−0.358 ± 0.052
$\Delta\mathcal{D}_{\mathtt{NT2}}$	0.014 ± 0.055	0.034 ± 0.039	0.046 ± 0.035	0.029 ± 0.032	0.047 ± 0.031
Δm_d (ps^{-1})	0.4827 ± 0.0200	0.4829 ± 0.0139	0.4769 ± 0.0123	0.4801 ± 0.0118	0.4800 ± 0.0115
Events	6237	12174	15640	17655	18872

Parameter	$l_c < 600$ μm	$l_c < 700$ μm	$l_c < 800$ μm	$l_c < 900$ μm	$l_c < 1000$ μm
$\mathcal{S}_{\mathrm{core,sig}}$	1.092 ± 0.055	1.088 ± 0.065	1.082 ± 0.096	1.093 ± 0.069	1.098 ± 0.071
$\delta_{\mathrm{core,sig,Lepton}}$	−0.366 ± 0.161	−0.332 ± 0.165	−0.354 ± 0.181	−0.417 ± 0.164	−0.426 ± 0.164
$\delta_{\mathrm{core,sig,Kaon}}$	−0.365 ± 0.041	−0.363 ± 0.049	−0.358 ± 0.076	−0.370 ± 0.050	−0.374 ± 0.054
$\delta_{\mathrm{core,sig,NT1}}$	−0.469 ± 0.093	−0.453 ± 0.096	−0.436 ± 0.113	−0.453 ± 0.097	−0.479 ± 0.098
$\delta_{\mathrm{core,sig,NT2}}$	−0.457 ± 0.058	−0.443 ± 0.064	−0.441 ± 0.084	−0.459 ± 0.064	−0.464 ± 0.066
$\mathcal{S}_{\mathrm{tail,sig}}$	2.980 ± 0.794	2.746 ± 0.677	2.633 ± 0.940	2.808 ± 0.642	2.795 ± 0.694
$\delta_{\mathrm{tail,sig}}$	−2.033 ± 1.122	−1.893 ± 0.896	−1.807 ± 0.877	−1.931 ± 0.778	−1.912 ± 0.781
$f_{\mathrm{tail,sig}}$	0.047 ± 0.031	0.067 ± 0.045	0.079 ± 0.078	0.073 ± 0.047	0.073 ± 0.050
$f_{\mathrm{outlier,sig}}$	0.004 ± 0.002	0.004 ± 0.002	0.004 ± 0.002	0.004 ± 0.002	0.005 ± 0.002
$\mathcal{D}_{\mathtt{Lepton}}$	0.165 ± 0.058	0.150 ± 0.057	0.159 ± 0.057	0.150 ± 0.056	0.149 ± 0.056
$\mathcal{D}_{\mathtt{Kaon}}$	0.555 ± 0.011	0.555 ± 0.011	0.555 ± 0.010	0.553 ± 0.010	0.553 ± 0.010
$\mathcal{D}_{\mathtt{NT1}}$	0.453 ± 0.032	0.456 ± 0.032	0.457 ± 0.032	0.458 ± 0.032	0.459 ± 0.031
$\mathcal{D}_{\mathtt{NT2}}$	0.225 ± 0.020	0.226 ± 0.020	0.227 ± 0.020	0.226 ± 0.019	0.224 ± 0.019
$\Delta\mathcal{D}_{\mathtt{Lepton}}$	0.112 ± 0.090	0.114 ± 0.089	0.135 ± 0.088	0.137 ± 0.087	0.132 ± 0.086
$\Delta\mathcal{D}_{\mathtt{Kaon}}$	0.062 ± 0.015	0.062 ± 0.015	0.062 ± 0.015	0.064 ± 0.015	0.064 ± 0.015
$\Delta\mathcal{D}_{\mathtt{NT1}}$	−0.333 ± 0.051	−0.332 ± 0.051	−0.329 ± 0.050	−0.334 ± 0.050	−0.328 ± 0.050
$\Delta\mathcal{D}_{\mathtt{NT2}}$	0.040 ± 0.031	0.045 ± 0.030	0.043 ± 0.030	0.043 ± 0.030	0.044 ± 0.030
Δm_d (ps^{-1})	0.4799 ± 0.0115	0.4799 ± 0.0114	0.4795 ± 0.0113	0.4811 ± 0.0114	0.4800 ± 0.0114
Events	19603	20091	20383	20611	20756

Table 6.18: Results from the likelihood fits to the Δt distributions of the hadronic B decays in 2.8 million simulated signal cocktail events (no $B \to J/\psi K^*$) for different values of upper bound on true 3-dimensional charm flight distance, l_c, for all events.

Parameter	$l_c < 100$ μm	$l_c < 200$ μm	$l_c < 300$ μm	$l_c < 400$ μm	$l_c < 500$ μm
$\mathcal{S}_{\mathrm{core,sig}}$	1.096 ± 0.020	1.073 ± 0.081	1.095 ± 0.021	1.106 ± 0.041	1.114 ± 0.020
$\delta_{\mathrm{core,sig,Lepton}}$	−0.015 ± 0.028	−0.031 ± 0.038	−0.049 ± 0.024	−0.058 ± 0.027	−0.064 ± 0.023
$\delta_{\mathrm{core,sig,Kaon}}$	−0.072 ± 0.016	−0.118 ± 0.032	−0.165 ± 0.014	−0.188 ± 0.019	−0.206 ± 0.014
$\delta_{\mathrm{core,sig,NT1}}$	−0.080 ± 0.036	−0.097 ± 0.045	−0.126 ± 0.029	−0.142 ± 0.032	−0.147 ± 0.028
$\delta_{\mathrm{core,sig,NT2}}$	−0.029 ± 0.026	−0.080 ± 0.037	−0.128 ± 0.022	−0.161 ± 0.025	−0.178 ± 0.021
$\mathcal{S}_{\mathrm{tail,sig}}$	10.000 ± 6.206	4.343 ± 6.907	4.287 ± 0.945	4.269 ± 2.352	3.865 ± 0.612
$\delta_{\mathrm{tail,sig}}$	−0.697 ± 1.074	−1.340 ± 1.149	−1.283 ± 0.602	−1.419 ± 0.751	−1.538 ± 0.596
$f_{\mathrm{tail,sig}}$	0.006 ± 0.002	0.017 ± 0.039	0.016 ± 0.007	0.016 ± 0.020	0.019 ± 0.007
$f_{\mathrm{outlier,sig}}$	0.003 ± 0.001	0.004 ± 0.002	0.004 ± 0.001	0.004 ± 0.001	0.004 ± 0.001
$\mathcal{D}_{\mathtt{Lepton}}$	0.878 ± 0.008	0.871 ± 0.007	0.869 ± 0.006	0.862 ± 0.006	0.861 ± 0.006
$\mathcal{D}_{\mathtt{Kaon}}$	0.738 ± 0.006	0.731 ± 0.006	0.724 ± 0.005	0.720 ± 0.005	0.716 ± 0.005
$\mathcal{D}_{\mathtt{NT1}}$	0.593 ± 0.013	0.616 ± 0.011	0.624 ± 0.010	0.624 ± 0.010	0.625 ± 0.009
$\mathcal{D}_{\mathtt{NT2}}$	0.310 ± 0.011	0.322 ± 0.009	0.320 ± 0.009	0.316 ± 0.008	0.313 ± 0.008
$\Delta\mathcal{D}_{\mathtt{Lepton}}$	−0.003 ± 0.013	−0.005 ± 0.011	−0.004 ± 0.010	−0.003 ± 0.010	0.000 ± 0.010
$\Delta\mathcal{D}_{\mathtt{Kaon}}$	0.040 ± 0.010	0.038 ± 0.008	0.037 ± 0.008	0.037 ± 0.007	0.035 ± 0.007
$\Delta\mathcal{D}_{\mathtt{NT1}}$	−0.047 ± 0.021	−0.057 ± 0.017	−0.051 ± 0.016	−0.049 ± 0.015	−0.052 ± 0.015
$\Delta\mathcal{D}_{\mathtt{NT2}}$	0.054 ± 0.017	0.051 ± 0.015	0.062 ± 0.014	0.065 ± 0.013	0.066 ± 0.013
Δm_d (ps^{-1})	0.4775 ± 0.0044	0.4786 ± 0.0055	0.4785 ± 0.0035	0.4785 ± 0.0039	0.4788 ± 0.0034
Events	56965	80737	93723	101185	105720

Parameter	$l_c < 600$ μm	$l_c < 700$ μm	$l_c < 800$ μm	$l_c < 900$ μm	$l_c < 1000$ μm
$\mathcal{S}_{\mathrm{core,sig}}$	1.113 ± 0.030	1.119 ± 0.022	1.123 ± 0.030	1.125 ± 0.030	1.121 ± 0.028
$\delta_{\mathrm{core,sig,Lepton}}$	−0.062 ± 0.025	−0.058 ± 0.023	−0.063 ± 0.025	−0.059 ± 0.025	−0.058 ± 0.025
$\delta_{\mathrm{core,sig,Kaon}}$	−0.212 ± 0.017	−0.217 ± 0.015	−0.221 ± 0.017	−0.223 ± 0.017	−0.224 ± 0.017
$\delta_{\mathrm{core,sig,NT1}}$	−0.148 ± 0.029	−0.146 ± 0.028	−0.150 ± 0.029	−0.153 ± 0.030	−0.154 ± 0.029
$\delta_{\mathrm{core,sig,NT2}}$	−0.189 ± 0.023	−0.193 ± 0.021	−0.196 ± 0.023	−0.200 ± 0.023	−0.200 ± 0.023
$\mathcal{S}_{\mathrm{tail,sig}}$	3.597 ± 0.876	3.446 ± 0.432	3.510 ± 0.717	3.433 ± 0.646	3.373 ± 0.525
$\delta_{\mathrm{tail,sig}}$	−1.471 ± 0.578	−1.496 ± 0.477	−1.591 ± 0.553	−1.614 ± 0.526	−1.582 ± 0.453
$f_{\mathrm{tail,sig}}$	0.025 ± 0.016	0.029 ± 0.010	0.029 ± 0.016	0.032 ± 0.017	0.036 ± 0.016
$f_{\mathrm{outlier,sig}}$	0.004 ± 0.001	0.004 ± 0.001	0.004 ± 0.001	0.004 ± 0.001	0.004 ± 0.001
$\mathcal{D}_{\mathtt{Lepton}}$	0.858 ± 0.006	0.857 ± 0.006	0.857 ± 0.006	0.857 ± 0.006	0.856 ± 0.006
$\mathcal{D}_{\mathtt{Kaon}}$	0.715 ± 0.005	0.714 ± 0.005	0.712 ± 0.005	0.711 ± 0.005	0.710 ± 0.005
$\mathcal{D}_{\mathtt{NT1}}$	0.621 ± 0.009	0.622 ± 0.009	0.622 ± 0.009	0.622 ± 0.009	0.623 ± 0.009
$\mathcal{D}_{\mathtt{NT2}}$	0.310 ± 0.008	0.310 ± 0.008	0.309 ± 0.008	0.309 ± 0.008	0.308 ± 0.008
$\Delta\mathcal{D}_{\mathtt{Lepton}}$	−0.000 ± 0.010	0.000 ± 0.010	0.002 ± 0.010	0.003 ± 0.009	0.001 ± 0.009
$\Delta\mathcal{D}_{\mathtt{Kaon}}$	0.037 ± 0.007	0.038 ± 0.007	0.039 ± 0.007	0.039 ± 0.007	0.039 ± 0.007
$\Delta\mathcal{D}_{\mathtt{NT1}}$	−0.052 ± 0.015	−0.053 ± 0.015	−0.051 ± 0.014	−0.050 ± 0.014	−0.049 ± 0.014
$\Delta\mathcal{D}_{\mathtt{NT2}}$	0.064 ± 0.013	0.064 ± 0.013	0.066 ± 0.012	0.068 ± 0.012	0.070 ± 0.012
Δm_d (ps^{-1})	0.4781 ± 0.0034	0.4778 ± 0.0033	0.4773 ± 0.0034	0.4776 ± 0.0034	0.4771 ± 0.0034
Events	108716	110789	112226	113250	114048

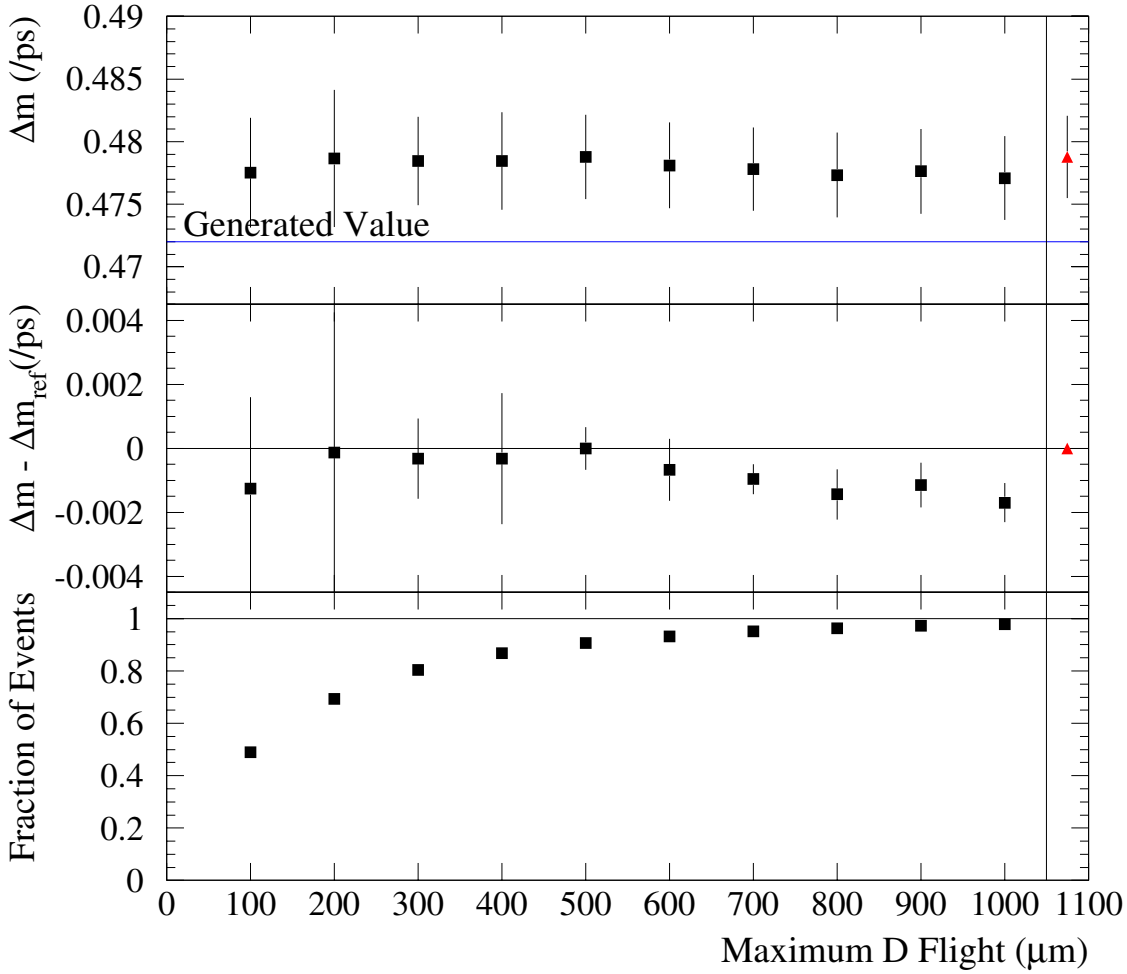

Figure 6-9: Results from the likelihood fits to the Δt distributions of the hadronic B decays in 2.8 million simulated signal cocktail events (no $B \to J/\psi K^*$) for different values of upper bound on true 3-dimensional charm flight distance, l_c, for all events. The reference fit (triangle at right) has $l_c = \infty$. The errors shown on the plot showing the difference with the reference fit are computed as the difference in quadrature from the reference.

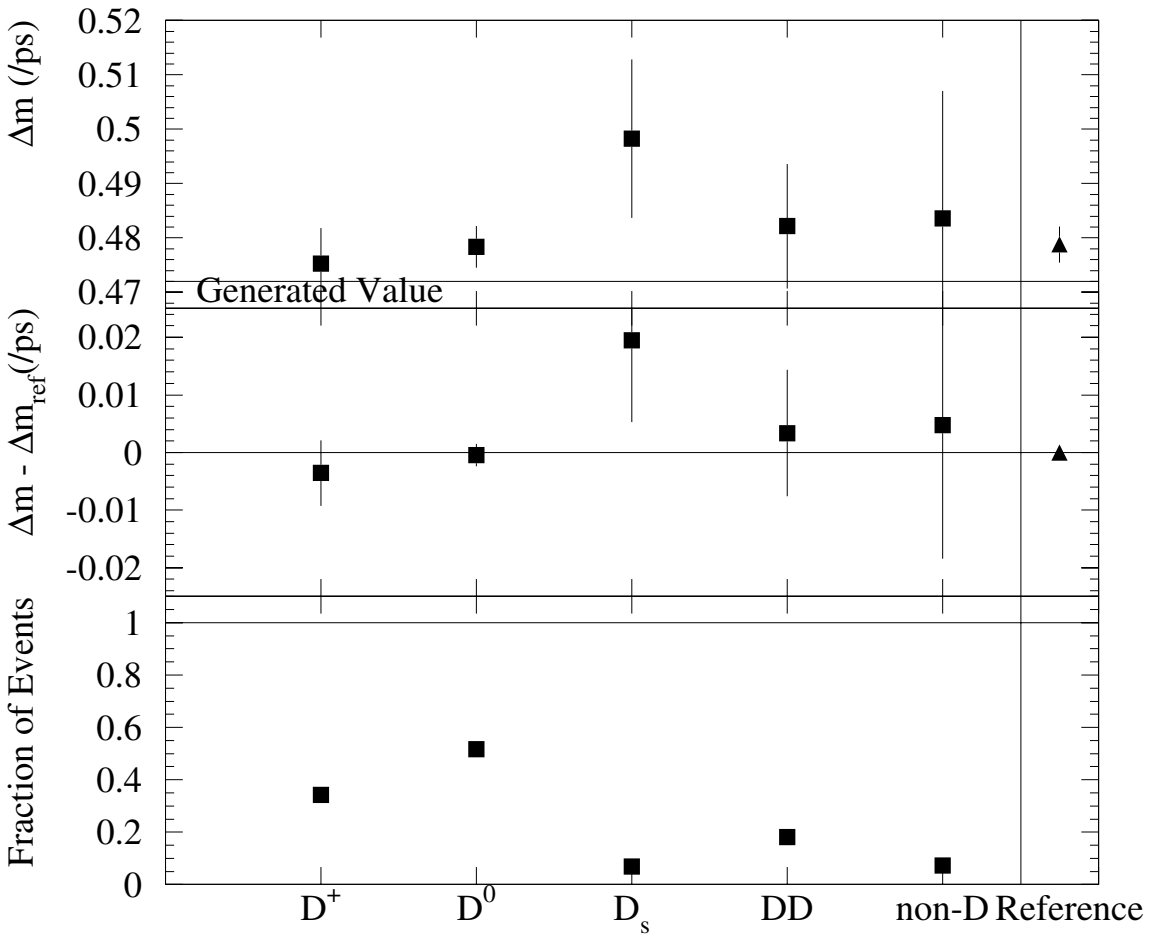

Figure 6-10: Results from the likelihood fits to the Δt distributions of the hadronic B decays in various subsets of 2.8 million simulated signal cocktail events (no $B \to J/\psi K^*$) which have different true species of charm on the tag side. (The D^+, D^0 and D_s categories include double charm decays). The reference is a fit to the nominal 2.8 million events. The errors shown on the plot showing the difference with the reference fit are computed as the difference in quadrature from the reference.

Table 6.19: Results from the likelihood fits to the Δt distributions of the hadronic B decays in 2.8 million simulated signal cocktail events(including $B \to J/\psi K^*$) for different true species of charm on the tag side. (The D^+, D^0 and D_s categories require at least one of the D species under study to be in the event on the tag side, and therefore include double charm decays).

Parameter	D^+	D^0	D_s^+	DD	Non D
$\mathcal{S}_{\mathrm{core,sig}}$	1.206 ± 0.034	1.001 ± 0.063	1.144 ± 0.099	1.095 ± 0.055	1.117 ± 0.138
$\delta_{\mathrm{core,sig,Lepton}}$	−0.071 ± 0.036	0.016 ± 0.061	−0.399 ± 0.239	−0.436 ± 0.155	−0.115 ± 0.250
$\delta_{\mathrm{core,sig,Kaon}}$	−0.328 ± 0.026	−0.119 ± 0.050	−0.385 ± 0.070	−0.380 ± 0.036	−0.126 ± 0.179
$\delta_{\mathrm{core,sig,NT1}}$	−0.097 ± 0.049	−0.151 ± 0.057	−0.392 ± 0.137	−0.494 ± 0.090	−0.077 ± 0.212
$\delta_{\mathrm{core,sig,NT2}}$	−0.309 ± 0.037	−0.082 ± 0.057	−0.297 ± 0.096	−0.449 ± 0.055	−0.181 ± 0.183
$\mathcal{S}_{\mathrm{tail,sig}}$	4.037 ± 0.341	2.158 ± 0.542	2.805 ± 0.636	3.010 ± 0.382	0.643 ± 0.962
$\delta_{\mathrm{tail,sig}}$	−2.475 ± 0.579	−1.243 ± 0.626	−1.547 ± 0.754	−2.118 ± 0.666	2.481 ± 1.583
$f_{\mathrm{tail,sig}}$	0.052 ± 0.012	0.083 ± 0.067	0.094 ± 0.067	0.080 ± 0.030	0.041 ± 0.085
$f_{\mathrm{outlier,sig}}$	0.004 ± 0.001	0.004 ± 0.001	0.001 ± 0.002	0.005 ± 0.002	0.012 ± 0.003
$\mathcal{D}_{\mathrm{Lepton}}$	0.792 ± 0.010	0.937 ± 0.006	0.117 ± 0.079	0.144 ± 0.055	0.373 ± 0.054
$\mathcal{D}_{\mathrm{Kaon}}$	0.570 ± 0.009	0.809 ± 0.006	0.727 ± 0.016	0.554 ± 0.010	0.534 ± 0.020
$\mathcal{D}_{\mathrm{NT1}}$	0.505 ± 0.016	0.813 ± 0.010	0.531 ± 0.046	0.455 ± 0.031	−0.128 ± 0.037
$\mathcal{D}_{\mathrm{NT2}}$	0.131 ± 0.014	0.518 ± 0.011	0.226 ± 0.030	0.223 ± 0.019	0.004 ± 0.025
$\Delta\mathcal{D}_{\mathrm{Lepton}}$	0.015 ± 0.016	−0.003 ± 0.011	0.127 ± 0.120	0.129 ± 0.085	−0.048 ± 0.084
$\Delta\mathcal{D}_{\mathrm{Kaon}}$	0.038 ± 0.014	0.040 ± 0.009	0.035 ± 0.022	0.064 ± 0.015	0.044 ± 0.029
$\Delta\mathcal{D}_{\mathrm{NT1}}$	0.034 ± 0.026	−0.063 ± 0.017	−0.260 ± 0.072	−0.312 ± 0.049	−0.064 ± 0.057
$\Delta\mathcal{D}_{\mathrm{NT2}}$	0.115 ± 0.021	0.041 ± 0.017	0.043 ± 0.045	0.044 ± 0.029	0.049 ± 0.038
Δm_d (ps^{-1})	0.4752 ± 0.0066	0.4783 ± 0.0038	0.4982 ± 0.0146	0.4821 ± 0.0115	0.4835 ± 0.0235
Events	39825	60153	8079	21210	8482

6.11.3 Dilution vs. $\sigma_{\Delta t}$ and Other Variables

A correlation between the mistag rate and the per-event Δt error is observed. See Figure 6-11. If a linear dependence of the dilution on the mistag rate is included in the likelihood fit, parameterized as $\mathcal{D} = \beta\sigma_{\Delta t}$, where the slope β is allowed to float, the value of Δm_d for data is 0.0054 ± 0.0030 ps^{-1} lower than when this dependence is ignored (the error is the difference in quadrature between the two fits). The value of Δm_d when including this dependence for the Monte Carlo sample is 0.0032 ± 0.0004 ps^{-1} lower. As a result, after performing the correction from the Monte Carlo, the value of Δm_d which would be measured on data is 0.0022 ± 0.0030 ps^{-1} lower than when the correlation is ignored, as in the nominal fit. The fitted dilutions and their dependence on the per-event error are listed in Table 6.20.

As the correlation seems to be well described by the Monte Carlo, and causes for possible disagreement of the size of this effect between data and Monte Carlo (such as charm meson fractions, lifetimes, and wrong sign kaon decays) are explicitly included

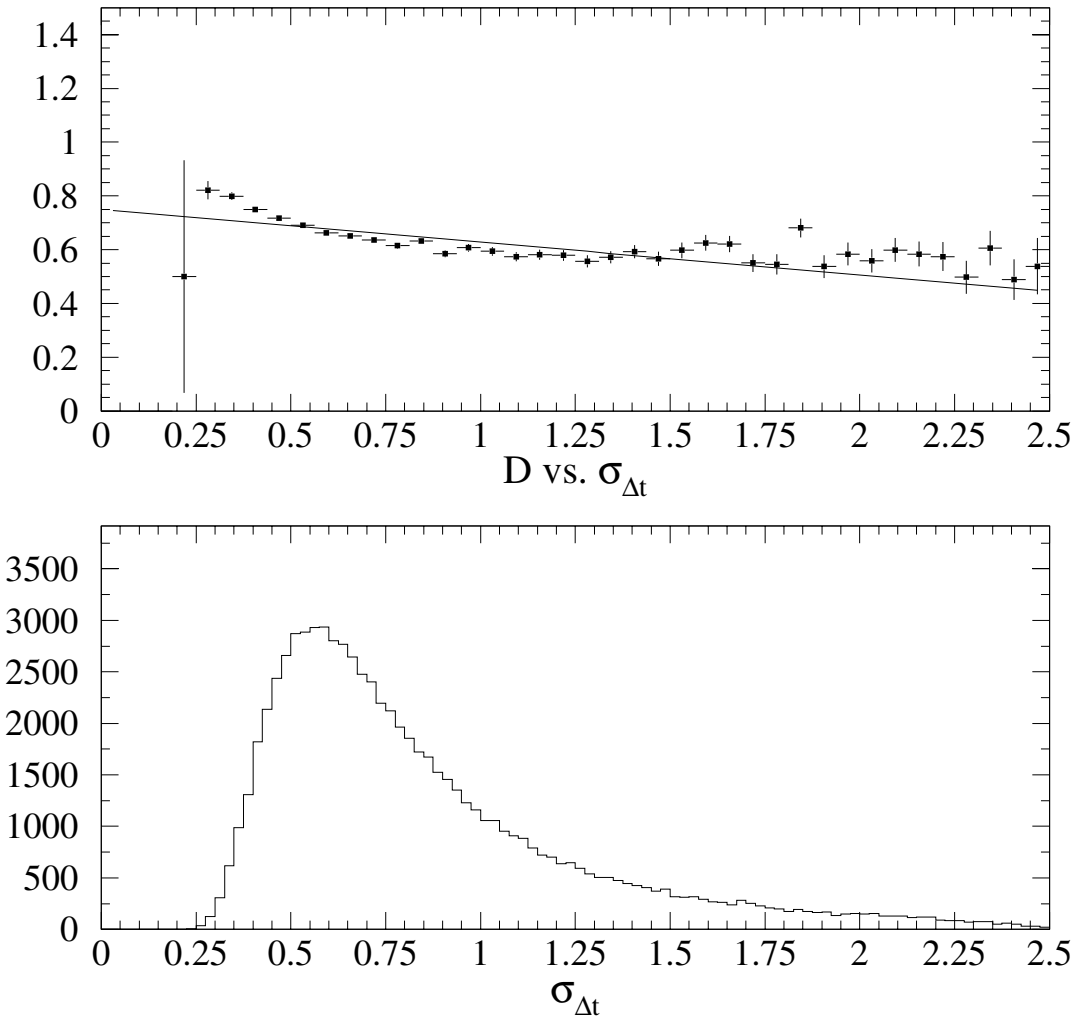

Figure 6-11: Correlation between the Dilution and per-event error (top) for the `Kaon` tagging category in a sub-sample of the cocktail signal Monte Carlo. The dilution is obtained by counting, within sample defined by the bin in Δt, the fraction of wrong-tags (defined as those events where the reconstructed flavor tag does not match the Monte Carlo truth). To illustrate the dependence, a linear fit to the points is also shown. For comparison, the distribution of per-event errors for the same sample is also shown (bottom).

Table 6.20: Results from likelihood fits (both data and Monte Carlo) which include the correlation between the mistag rate and the per-event error. For data, the difference between the values of Δm_d obtained from this fit and the nominal fit without the correlation is reported.

	Data	Monte Carlo
$\mathcal{D}_{\texttt{Lepton}}$ $(\sigma_{\Delta t} = 0)$	0.834 ± 0.079	0.847 ± 0.018
$\mathcal{D}_{\texttt{Kaon}}$ $(\sigma_{\Delta t} = 0)$	0.840 ± 0.068	0.854 ± 0.013
$\mathcal{D}_{\texttt{NT1}}$ $(\sigma_{\Delta t} = 0)$	0.723 ± 0.132	0.672 ± 0.025
$\mathcal{D}_{\texttt{NT2}}$ $(\sigma_{\Delta t} = 0)$	0.308 ± 0.121	0.363 ± 0.023
$\beta_{\mathcal{D}_{\texttt{Lepton}}}$	0.011 ± 0.133	0.009 ± 0.029
$\beta_{\mathcal{D}_{\texttt{Kaon}}}$	-0.252 ± 0.095	-0.207 ± 0.019
$\beta_{\mathcal{D}_{\texttt{NT1}}}$	-0.289 ± 0.221	-0.083 ± 0.041
$\beta_{\mathcal{D}_{\texttt{NT2}}}$	0.004 ± 0.172	-0.079 ± 0.032
$\Delta\mathcal{D}_{\texttt{Lepton}}$	-0.006 ± 0.045	0.005 ± 0.009
$\Delta\mathcal{D}_{\texttt{Kaon}}$	0.023 ± 0.033	0.036 ± 0.007
$\Delta\mathcal{D}_{\texttt{NT1}}$	-0.087 ± 0.068	-0.050 ± 0.014
$\Delta\mathcal{D}_{\texttt{NT2}}$	0.101 ± 0.060	0.070 ± 0.012
$(\delta)\Delta m_d$ (ps^{-1})	-0.0054 ± 0.016	0.475 ± 0.003

in the systematics, this effect is assumed to be fully accounted for by the Monte Carlo correction, and no additional systematic error is added.

Other variables which may exhibit a similar correlation have been explored. The effect seems to come from the correlation between the wrong-sign kaon rates of a given D species and decay multiplicity, momentum spectrum, etc. In particular, for the D^+, the ratio of wrong- to right-sign kaons is more than twice that for D^0s. Just from charge-conservation and phase-space arguments, the D^+ favors higher charge-multiplicity decays than the D^0, which combined with the wrong-sign kaon differences would introduce a correlation between the per-event error (which depends on multiplicity) and the wrong-tag rate. This has been confirmed in Monte Carlo studies.

In an effort to better parameterize the effect, an observable which seems to be correlated with the per-event wrong-tag rate for the `Kaon` category has been studied.

It is defined as

$$\alpha \;=\; \left(\sum_{\mathrm{tag-side\,tracks}} p_{\perp i}^{2} \right)^{-1/2}, \tag{6.2}$$

where $p_{\perp i}$ is the transverse momentum component of the ith track. This variable also shows a correlation with dilution (see Figure 6-12). As a check, the entire Monte Carlo sample is fit, allowing for a linear dependence on α in the `Kaon` category, and again allowing a linear dependence in all tagging categories. See Table 6.21. It is clear from Figures 6-11 and 6-12 that a linear parameterization of the dilution on α yields a better description of this effect then a linear parameterization as a function of $\sigma_{\Delta t}$.

6.11.4 Data Conditions

Data was split into several key periods to check for biases due to different conditions and/or calibrations including Run period (1,2), periods during which the drift chamber was run at different high voltage (1900,1960 V), and periods for which a different SVT local alignment set (D,E) was valid. No bias was observed. The results of these checks are shown in Figure 6-13. There were no other significant changes in the detector running conditions during the period of data taking used for this analysis.

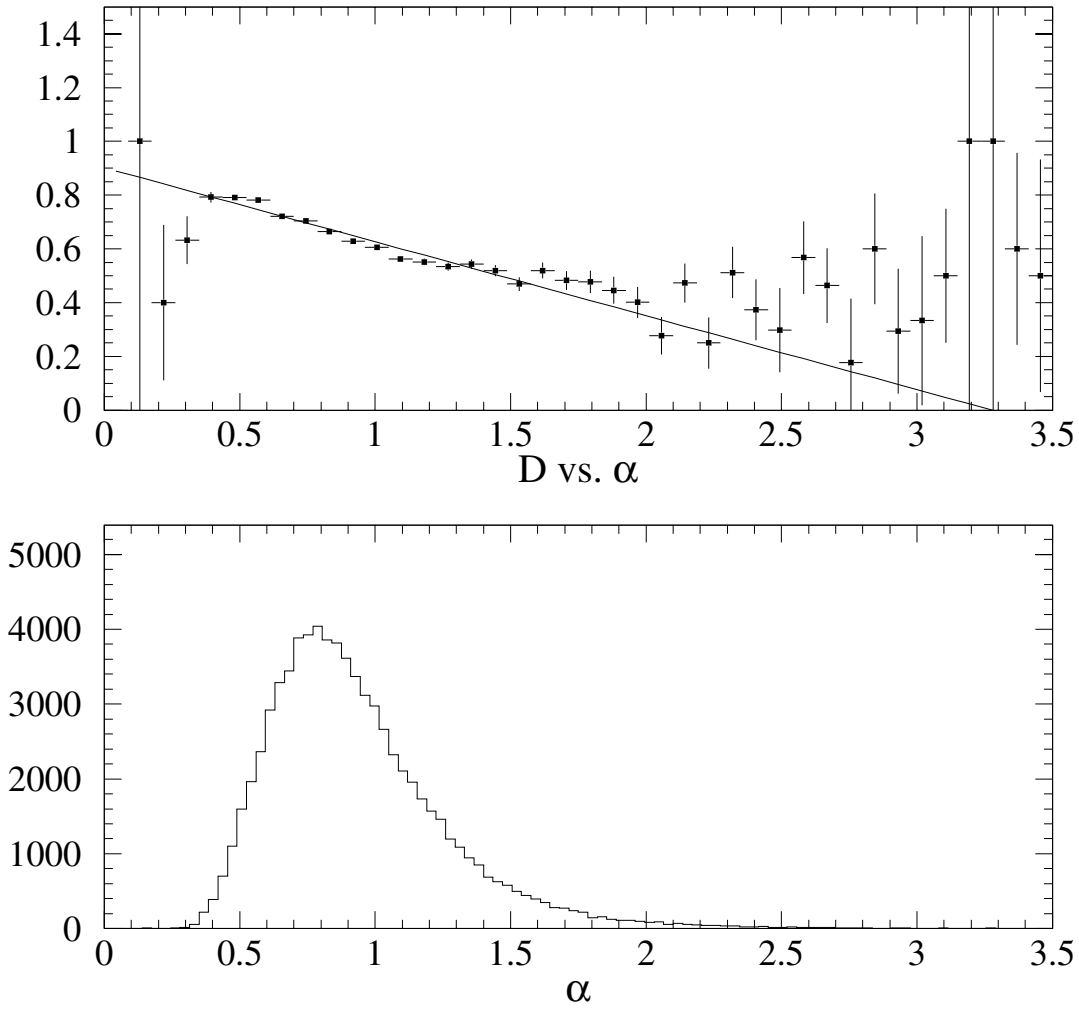

Figure 6-12: Correlation between the dilution and α (see equation 6.2 for the definition of α) (top) for the `Kaon` tagging category in a sub-sample of the cocktail signal Monte Carlo. The dilution is obtained by counting, within sample defined by the slice in Δt given by the bin, the fraction of wrong-tags (defined as those events where the reconstructed flavor tag does not match the Monte Carlo truth). To illustrate the dependence, a linear fit to the points is shown. For comparison, the distribution of α for the same sample is also shown (bottom).

Table 6.21: Results from the likelihood fits to the Δt distributions of the hadronic B decays in 2.8 million simulated signal cocktail events (no $B \to J/\psi K^*$). Here, the dilution is allowed a linear dependence on the variable α in the fit for all categories (See equation 6.2 for the definition of α). and just the `Kaon` category.

Parameter	All	`Kaon`	Nominal fit
$\mathcal{S}_{\text{core,sig}}$	1.131 ± 0.020	1.130 ± 0.020	1.129 ± 0.021
$\delta_{\text{core,sig,Lepton}}$	−0.059 ± 0.023	−0.059 ± 0.023	−0.058 ± 0.023
$\delta_{\text{core,sig,Kaon}}$	−0.228 ± 0.014	−0.228 ± 0.014	−0.227 ± 0.014
$\delta_{\text{core,sig,NT1}}$	−0.159 ± 0.027	−0.160 ± 0.027	−0.158 ± 0.028
$\delta_{\text{core,sig,NT2}}$	−0.198 ± 0.021	−0.198 ± 0.021	−0.197 ± 0.021
$\mathcal{S}_{\text{tail,sig}}$	3.722 ± 0.335	3.735 ± 0.335	3.717 ± 0.316
$\delta_{\text{tail,sig}}$	−2.243 ± 0.465	−2.208 ± 0.450	−2.060 ± 0.395
$f_{\text{tail,sig}}$	0.033 ± 0.008	0.034 ± 0.008	0.037 ± 0.008
$f_{\text{outlier,sig}}$	0.004 ± 0.001	0.004 ± 0.001	0.004 ± 0.001
$\mathcal{D}_{\texttt{Lepton}}$	0.919 ± 0.030	0.853 ± 0.006	0.854 ± 0.006
$\mathcal{D}_{\texttt{Kaon}}$	0.982 ± 0.015	0.982 ± 0.015	0.710 ± 0.005
$\mathcal{D}_{\texttt{NT1}}$	0.622 ± 0.029	0.622 ± 0.009	0.623 ± 0.009
$\mathcal{D}_{\texttt{NT2}}$	0.298 ± 0.023	0.307 ± 0.008	0.308 ± 0.008
$\Delta\mathcal{D}_{\texttt{Lepton}}$	0.002 ± 0.009	0.002 ± 0.009	0.002 ± 0.009
$\Delta\mathcal{D}_{\texttt{Kaon}}$	0.039 ± 0.007	0.039 ± 0.007	0.040 ± 0.007
$\Delta\mathcal{D}_{\texttt{NT1}}$	−0.049 ± 0.014	−0.049 ± 0.014	−0.049 ± 0.014
$\Delta\mathcal{D}_{\texttt{NT2}}$	0.068 ± 0.012	0.069 ± 0.012	0.069 ± 0.012
αD_{L}	−0.098 ± 0.044		
αD_{K}	−0.308 ± 0.017	−0.308 ± 0.017	
αD_{NT1}	−0.000 ± 0.037		
αD_{NT2}	0.010 ± 0.023		
Δm_d (ps^{-1})	0.4757 ± 0.0033	0.4760 ± 0.0033	0.4788 ± 0.0033
Events	116539	116539	116539

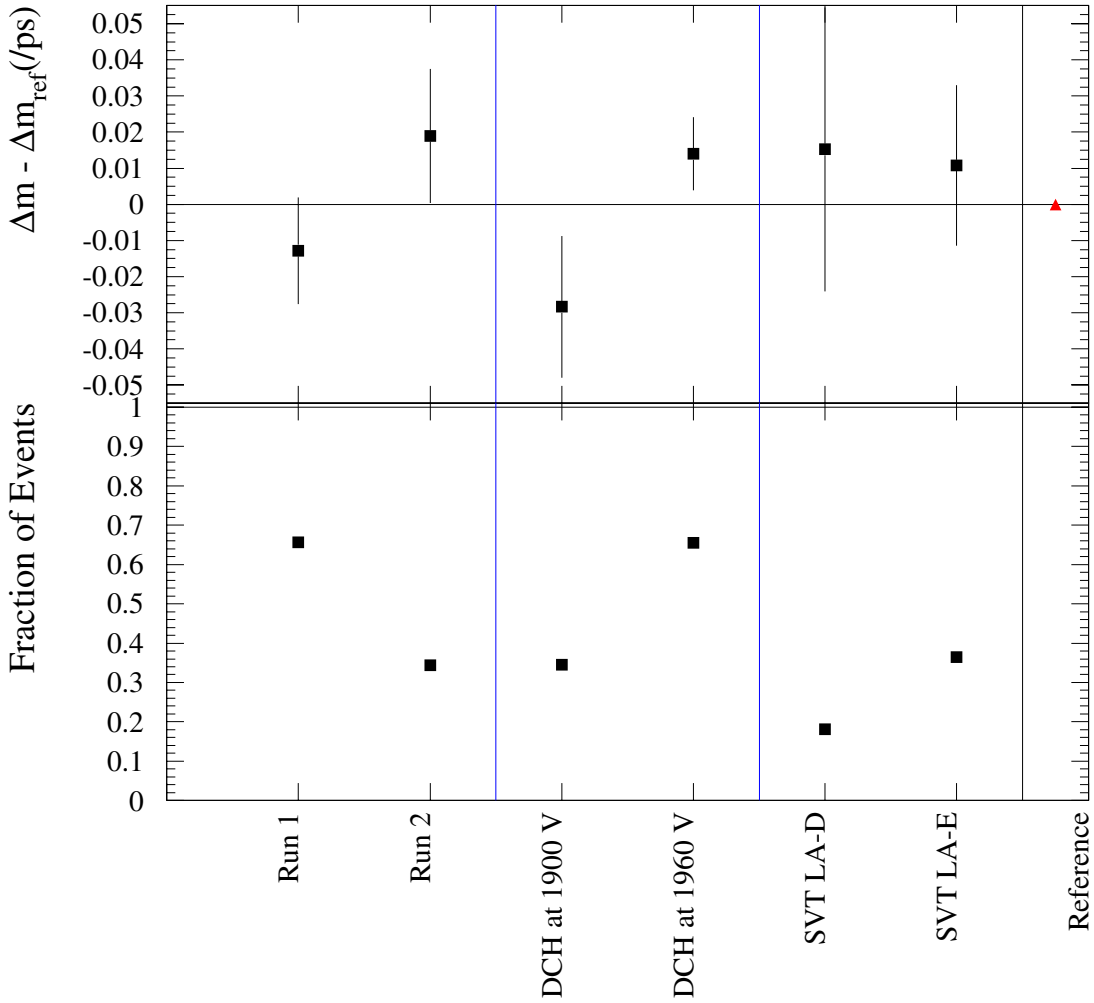

Figure 6-13: Fits to data split into key periods. The difference between the value for each period and the nominal fit is shown, and the error is reported as the difference in quadrature.

Chapter 7

Systematic Uncertainties

The methods used to estimate the systematic uncertainties in the determination of Δm_d are described here, and the systematic error is reported.

7.1 Monte Carlo Tests

A wide variety of sources of systematic uncertainty are explored using various simulation techniques. First, the fit method itself is checked with a fast parameterized Monte Carlo, generated with distributions taken from data. Next, the resolution model is checked by comparing the true Δt residual distributions to the values obtained by fitting. Finally, the complete analysis is performed on fully-simulated events to extract Δm_d. A systematic bias due to the measurement technique (event selection, Δt reconstruction and likelihood fit) is measured with fully simulated events as the difference between the value of Δm_d used to generate the sample, and the value obtained when the complete analysis is performed. This bias is corrected for and the corresponding statistical uncertainty is considered as a systematic error.

7.1.1 Toy Monte Carlo Checks

The implementation of the likelihood fit, `tFit`, is checked for systematic biases in the central values of the fit parameters and in their calculated statistical uncertainties

with a high-statistics fast parameterized (a.k.a. toy) Monte Carlo. To this end, 2000 toy Monte Carlo samples are generated with a size and parameterization identical to the data sample. The actual parameters used for the generation are therefore the ones listed in Table 5.2.

The distribution of per-event errors in data closely resembles a Landau distribution. Therefore, the Landau distribution is used as an empirical model for generating the per-event errors in the toy Monte Carlo. The parameters of the Landau distributions used are obtained from the data, separately for background (obtained from the $m_{\rm ES} < 5.27\,{\rm GeV}$ sideband) and the signal (obtained from the sideband subtracted signal region $m_{\rm ES} > 5.27\,{\rm GeV}$), and separately for each tagging category. The Landau distribution is given by

$$\Phi(x) = a\phi((x - x_0)/w) \tag{7.1}$$

$$\phi(\lambda) = \frac{1}{2\pi i}\int_{c-i\infty}^{c+i\infty} \exp(\lambda s + s\ln s)ds, \tag{7.2}$$

where a is the normalization, x_0 is the nominal peak, and w is the width. There is good agreement between the data and Monte Carlo distributions, and both are well-described by the Landau distribution (See Figs 7-1 and 7-2, and Table 7.1)

The values generated for $m_{\rm ES}$ for the combinatorial background use the Argus parameters obtained from a fit to the $m_{\rm ES}$ distribution of the combined tagged sample ($\kappa = -29$). All events use the same value of κ, the parameter in the Argus function which describes the roll-off near the kinematic limit, and only tagged events are generated.

The distributions of the results of these toy Monte Carlo studies for signal and background parameters and their pull distributions are shown in Appendix C. Although some background parameters seem to be biased, such bias is observed neither in the signal parameters nor Δm_d. Note that for the toy Monte Carlo fits the dilution of the prompt lepton background was fixed to zero, to avoid a non-negligible number of fit failures (there are O(10) events generated in this category). When fixing this parameter to zero for data, changes in neither the log-likelihood value nor Δm_d

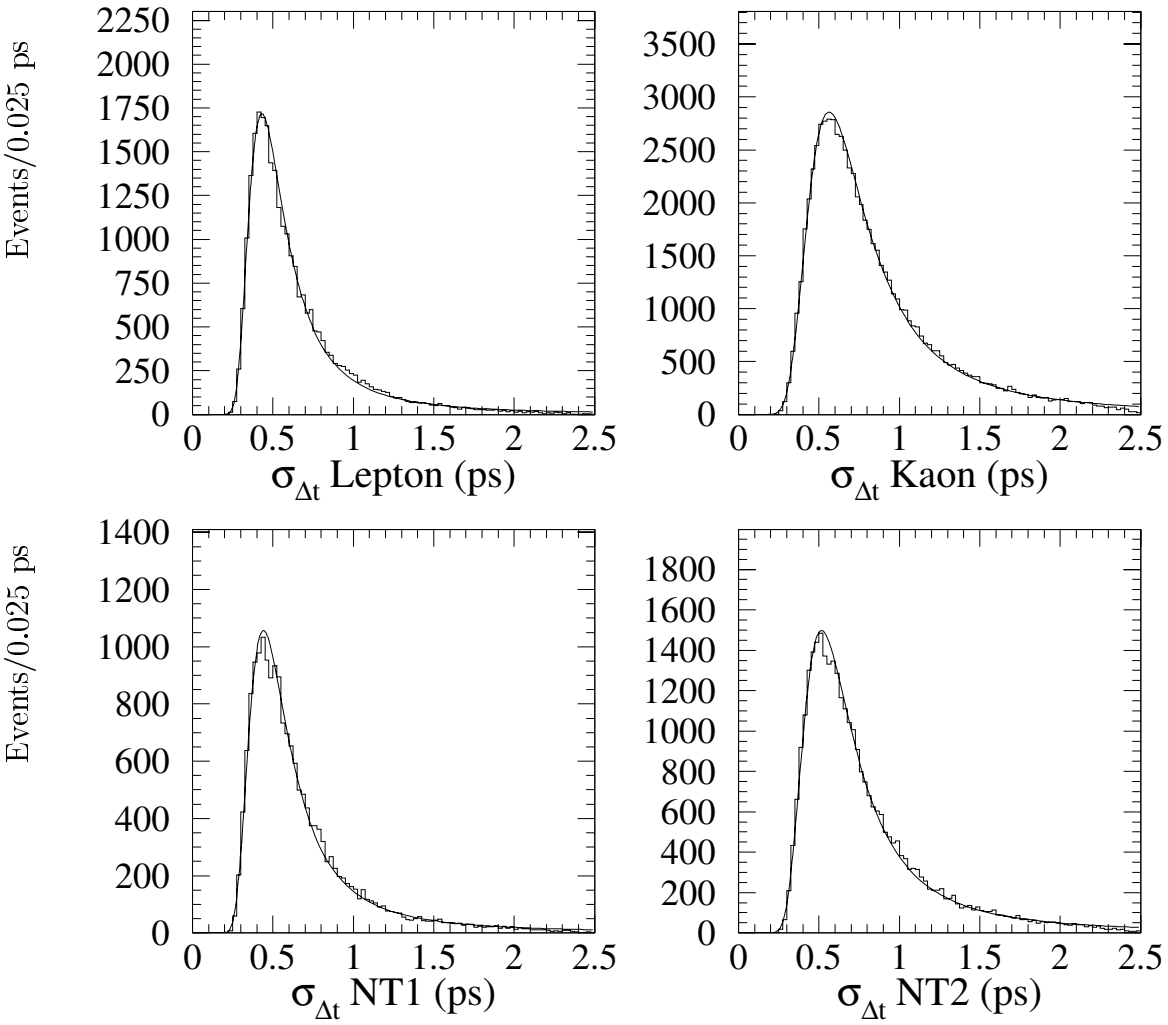

Figure 7-1: Distributions of the per-event errors in signal cocktail Monte Carlo, by tagging category

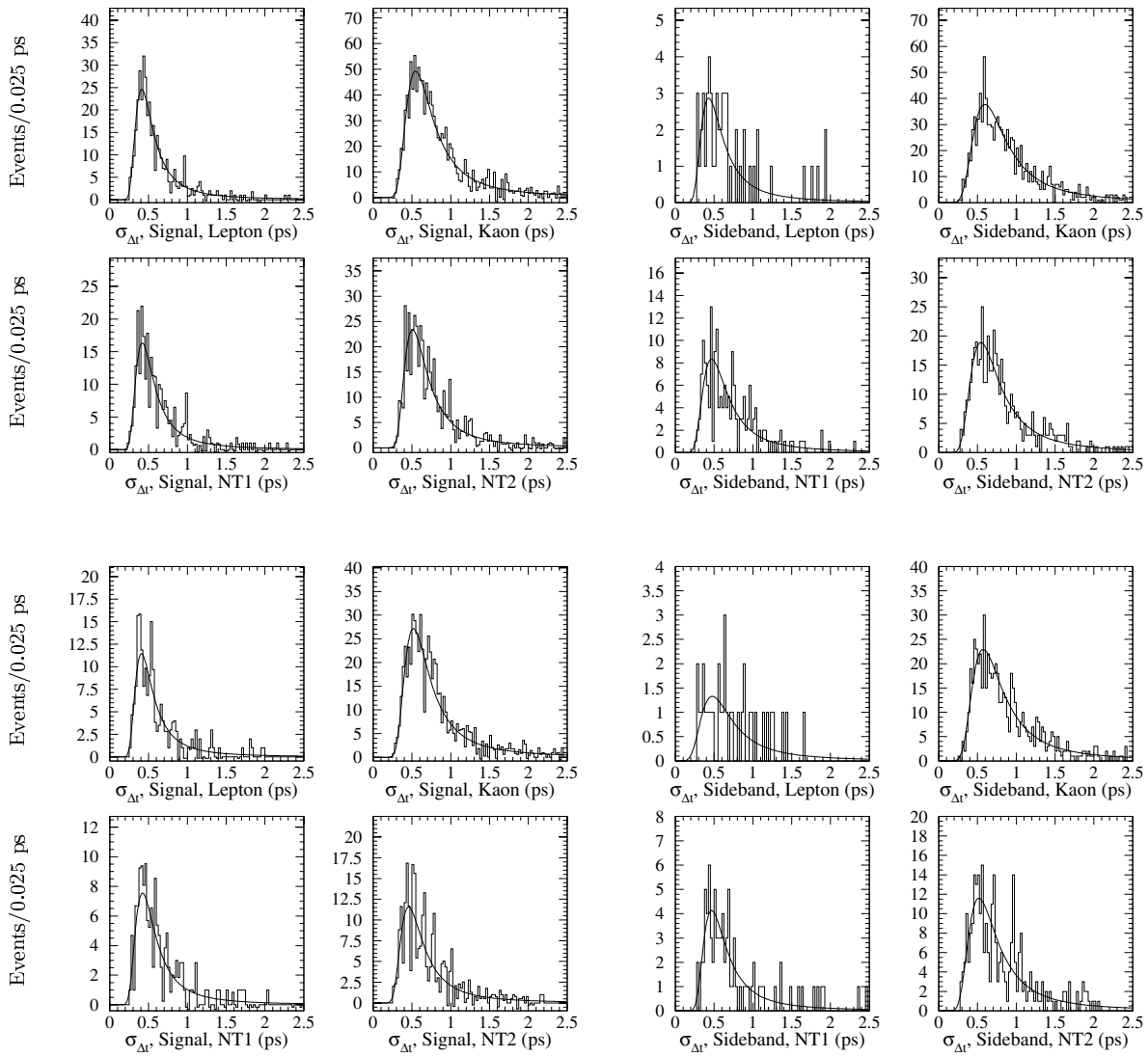

Figure 7-2: Distributions of the per-event errors in data, by tagging category, for Run 1 (top) and Run 2 (bottom).

Table 7.1: Parameters of the per-event error distributions

Category	Run 1		Run 2		Cocktail Monte Carlo	
	x_0 (ps)	w (ps)	x_0 (ps)	w (ps)	x_0 (ps)	w (ps)
`Lepton`, signal	0.43	0.073	0.42	0.070	0.45	0.740
`Kaon`, signal	0.57	0.116	0.57	0.117	0.59	0.120
`NT1`, signal	0.44	0.077	0.44	0.081	0.46	0.081
`NT2`, signal	0.53	0.102	0.51	0.099	0.54	0.102
`Lepton`, background	0.48	0.093	0.50	0.107		
`Kaon`, background	0.63	0.145	0.62	0.134		
`NT1`, background	0.49	0.103	0.51	0.117		
`NT2`, background	0.57	0.123	0.54	0.115		

are observed.

7.1.2 Signal Monte Carlo Analysis

The full analysis chain including event reconstruction, candidate selection and the likelihood fit is performed with fully simulated signal cocktail events. The resolution functions and the dilutions obtained from the fit are compared to those obtained using Monte Carlo truth information. In this section, these comparisons are described, and the likelihood fit results are presented.

Measurement of Δt

The detector resolution function for fully simulated signal B candidates is extracted by fitting the residual $\delta\Delta t = \Delta t_{\rm reco} - \Delta t_{\rm gen}$ distribution with the three-Gaussian resolution model described in Section 4.3. If the estimated per-event measurement error is a good estimate of the true error, then the normalized residual (pull) distribution of Δt should be a Gaussian with zero mean and unit width. Because of non-Gaussian measurement errors, the pull distribution will typically not be described by such a unit Gaussian.

The tail (second) Gaussian scale factor is fixed to the Monte Carlo value (3.0) in the nominal fit. As a check these parameters are floated. The value of Δm_d changes

by -0.0008 ps^{-1}, with no change in the error. Also, the value of the log likelihood changes only slightly: from -30440.8 to -30438.3.

Table 7.2: Parameters of fit of the signal resolution model to the Δt residual ($\Delta t_{\rm reco} - \Delta t_{\rm true}$) distributions for simulated hadronic B^0 cocktail events for all tags, all correct tags, all wrong tags, all unmixed events and all mixed events (where (un)mixed is defined using the reconstructed flavor tag).

	All	Correct	Incorrect	Unmixed	Mixed
$\delta_{\rm core,\ sig,Lepton}$	-0.088 ± 0.008	-0.081 ± 0.009	-0.207 ± 0.033	-0.112 ± 0.018	-0.082 ± 0.009
$\delta_{\rm core,\ sig,Kaon}$	-0.210 ± 0.006	-0.210 ± 0.006	-0.215 ± 0.015	-0.207 ± 0.011	-0.212 ± 0.006
$\delta_{\rm core,\ sig,NT1}$	-0.134 ± 0.010	-0.128 ± 0.011	-0.161 ± 0.024	-0.140 ± 0.019	-0.132 ± 0.012
$\delta_{\rm core,\ sig,NT2}$	-0.186 ± 0.008	-0.168 ± 0.010	-0.217 ± 0.014	-0.203 ± 0.013	-0.173 ± 0.010
$\delta_{\rm tail,sig}$	-1.031 ± 0.041	-0.963 ± 0.045	-1.268 ± 0.097	-1.085 ± 0.073	-1.006 ± 0.050
$f_{\rm outlier,\ sig}$	0.008 ± 0.000	0.007 ± 0.000	0.013 ± 0.001	0.011 ± 0.001	0.007 ± 0.000
$f_{\rm tail,sig}$	0.106 ± 0.005	0.104 ± 0.006	0.120 ± 0.010	0.122 ± 0.010	0.100 ± 0.006
$\mathcal{S}_{\rm core,sig}$	1.058 ± 0.005	1.054 ± 0.005	1.076 ± 0.011	1.060 ± 0.009	1.057 ± 0.005
$\mathcal{S}_{\rm tail,sig}$	2.310 ± 0.038	2.262 ± 0.042	2.462 ± 0.083	2.280 ± 0.066	2.324 ± 0.047

Restricted Δt Fit Ranges

The nominal fit is performed after requiring that events must satisfy $|\Delta t| < 20$ ps. To check that the analysis is independent of this requirement, the bound on $|\Delta t|$ is varied between 8 and 40 ps and the fit is repeated. The results of these fits (both leaving *all* parameters floating and only leaving Δm_d floating) are shown in Figure 7-3. No dependence is observed, and no systematic error due to this requirement is assigned.

Restricted $\sigma_{\Delta t}$ Fit Ranges

The nominal fit is performed after requiring that events must satisfy $\sigma_{\Delta t} < 1.4$ ps. To measure the effect of this requirement, the fit is repeated on both data and Monte Carlo, while varying the $\sigma_{\Delta t}$ requirement from 1 ps to 2 ps. The results of these fits are shown in Figure 7-4. A systematic uncertainty of $\pm\ 0.003$ ps^{-1} is assigned from the variation due to this requirement.

Resolution Dependence on Tagging

As discussed in Section 6.11.3, there is a correlation between dilutions and Δt errors. To check whether right and wrong tagged events are described by the same resolution

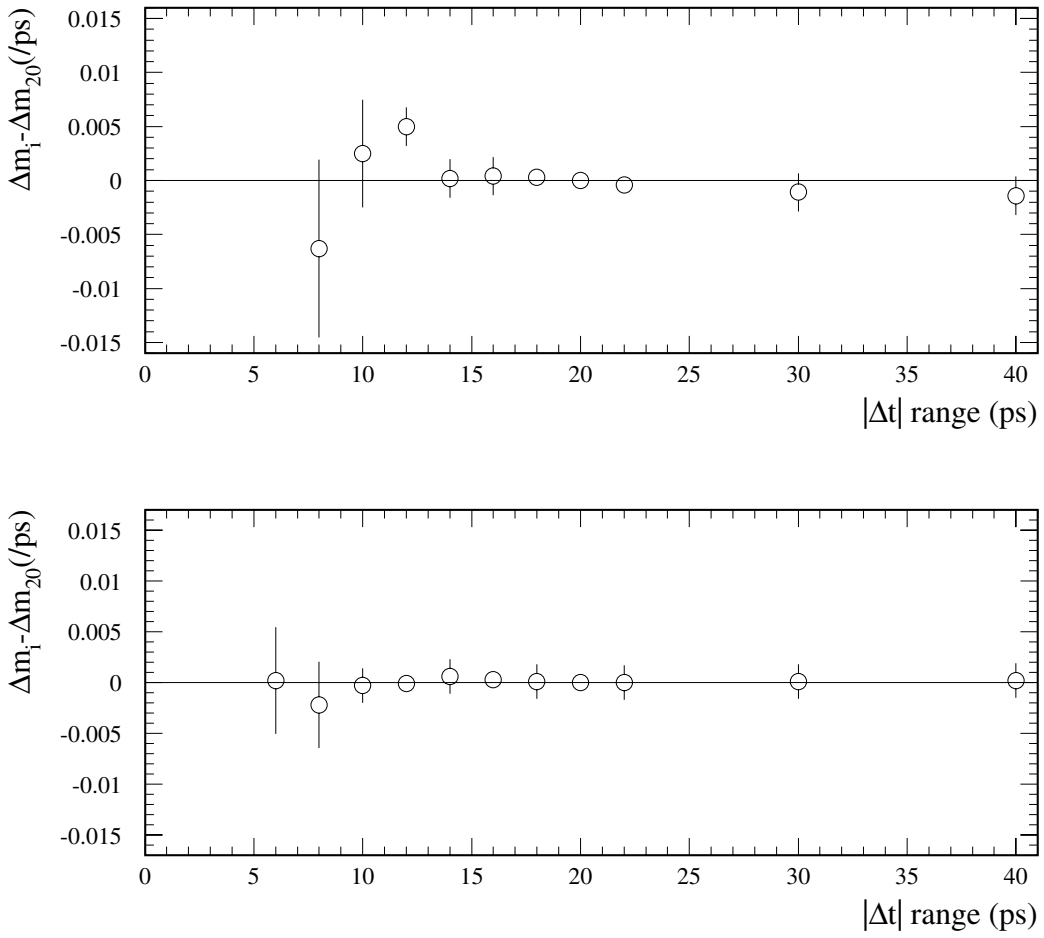

Figure 7-3: Fits with limits on the Δt intervals used. The plot shows the *difference* (and the error on the difference) as a function of the $|\Delta t|$ requirement, with respect to the fit with t_{bound} of 20 ps. In the fits shown on the top, all parameters are left free. In the fits on the bottom, only Δm_d is left free.

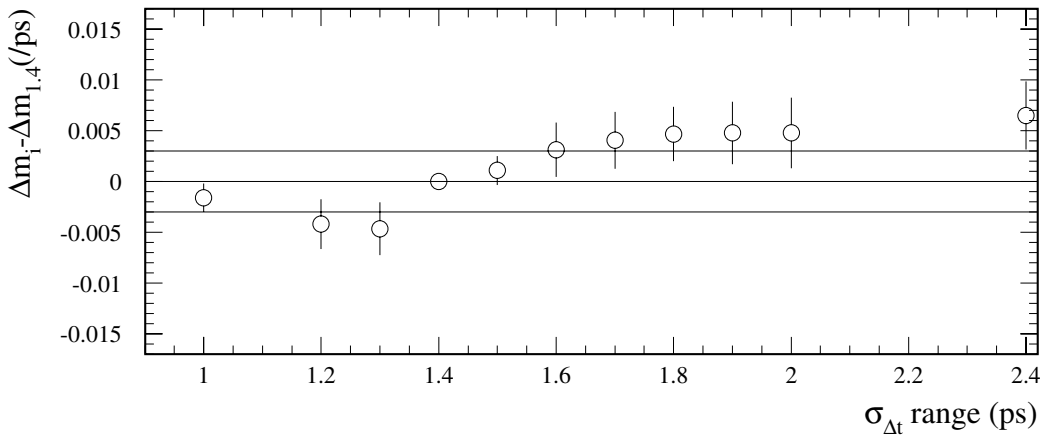

Figure 7-4: Fits on data, varying the requirement on $\sigma_{\Delta t}$. The difference between the fit results as a function of the $\sigma_{\Delta t}$ requirement and the nominal fit with a requirement that $\sigma_{\Delta t} < 1.4$ ps is shown. In each fit, all parameters are left free.

function, the Monte Carlo residual is fit separately for right and wrong tag events. Using this resolution function and Monte Carlo truth for the flavor tag, the full fit for Δm_d is performed on each of the two samples, and the values are averaged. This average is compared to the nominal fit, using Monte Carlo truth for the flavor tag. The difference (0.001 ps^{-1}) is assigned as a systematic error.

Likelihood Fit

The likelihood fit is performed on the full Monte Carlo with the same selection criteria used on data. The signal parameters floated are the same as the nominal data fit, and fixed resolution function parameters are given the same values used in the fit to data. The B^+ lifetime is fixed to the value used in event generation, $\tau_{B^0} = 1.548$ ps. In addition, a small combinatorial background in the selected events is rejected by requiring the event to be positively associated (i.e., each reconstructed stable daughter must match the generated particle). Therefore, no background parameters are floated in the fit, and the fraction of background is fixed to zero. The results of

this fit is shown in Table 5.2. The value measured in data is corrected by the difference between the result of this fit and the generated value. The statistical uncertainty on this difference is assigned as a systematic uncertainty due to limited Monte Carlo statistics.

Variation of Relative Amounts of D Species

The generic Monte Carlo generator used to model the tag-side B decays produces D mesons using the known exclusive branching fractions for B decays to specific exclusive modes, and a model based on knowledge of the inclusive rates for $B \to DX$ for the rest. Our current knowledge of the relative rates for B decays to charm is summarized in [8], page 636, and the inclusive rates for $B \to DX$ are listed in Table 7.3

Because of the uncertainty in this procedure, and the different rates for different D species to decay to particles which provide tag information, it is possible that there is a bias introduced by inaccurate modeling of the relative rates for B decays to different species of Ds. To check the bias introduced, events are first classified into one of five categories: One D^+, D^0, or D_s, two Ds, or no D mesons at all. The relative amounts of each D species are then varied up and down by an extremely conservative 30% by reweighting the Monte Carlo sample. The amount of this variation was chosen based on the current knowledge of inclusive rates given in Table 7.3, and the observation that most of the relative exclusive branching fractions for B^0 and B^+ are similar within about 30 %. The full fit is performed on each of these samples with enhanced or depleted amounts of each D species. The results of these fits are summarized in Table 7.4 and Figure 7-5. A conservative systematic error of $\pm$ 0.001 ps^{-1} is assigned due to this effect.

Variation of D Lifetimes

The event generator uses PDG [8] values for D lifetimes. The dependence of Δm_d on the D^+, D^0 and D_s lifetimes is checked by varying them up and down by 3 σ for tag-side D mesons by reweighting the signal cocktail Monte Carlo sample. The

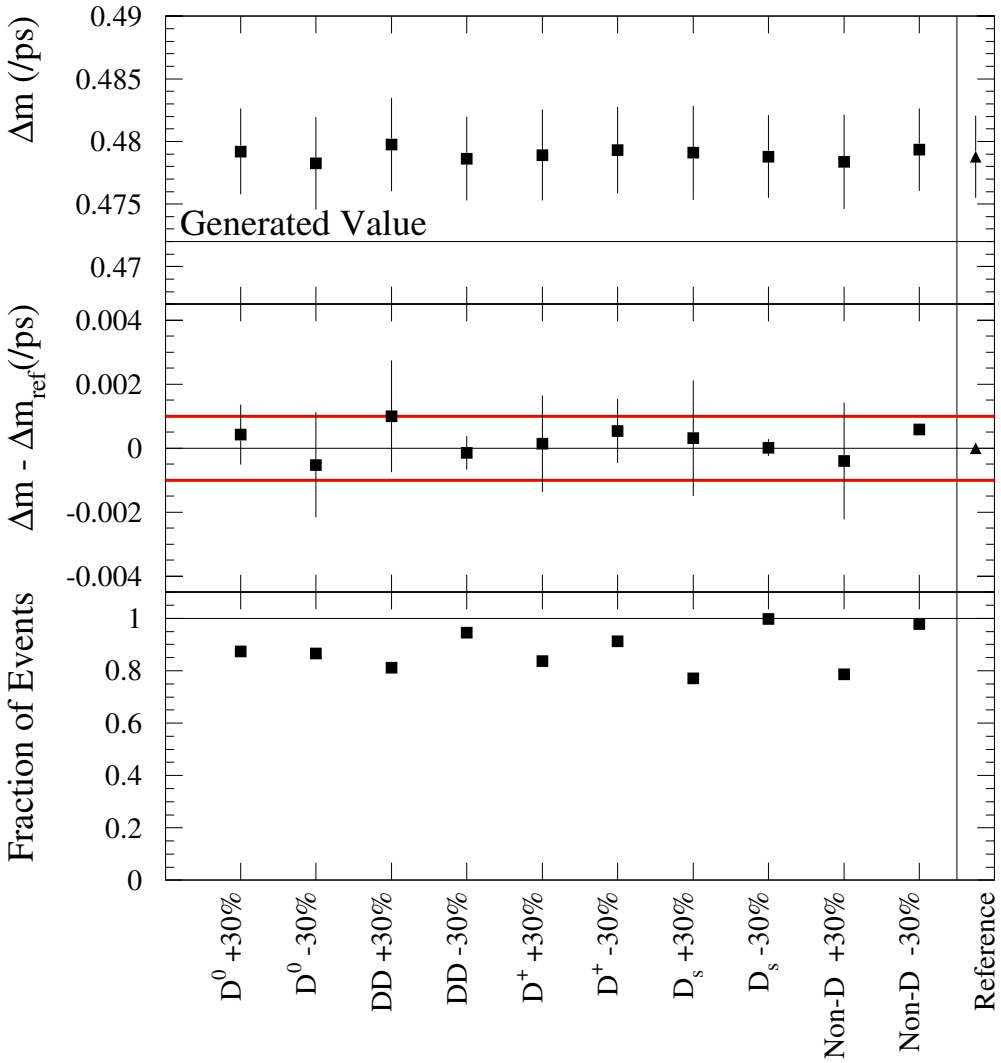

Figure 7-5: Fits to Monte Carlo samples with changes in the relative fractions of charm species on the tag side. The assigned systematic error is indicated by the thick horizontal lines. The errors shown on the middle plot are computed as the difference in quadrature from the reference.

Table 7.3: Inclusive rates for $B \to DX$ from the Particle Data Group

$\Gamma(B \to D^{\pm} X /)\Gamma(\text{total})$	0.241 ± 0.019
$\Gamma(B \to D^{0} X /)\Gamma(\text{total})$	0.635 ± 0.029
$\Gamma(B \to D_s^{\pm} X /)\Gamma(\text{total})$	0.100 ± 0.025

Table 7.4: Results from the likelihood fit to the Δt distributions of the hadronic B^0 decays in simulated signal events for different relative amounts of D species. The sample of 2.8 million (no $B \to J/\psi K^*$) was reweighted with either 30 % more or 30 % less of the species under study.

Parameter	D^0 +30 %	D^0 −30 %	DD +30 %	DD −30 %	D^++30 %
$\mathcal{S}_{\mathrm{core,sig}}$	1.142 ± 0.020	1.140 ± 0.021	1.142 ± 0.022	1.134 ± 0.020	1.149 ± 0.021
$\delta_{\mathrm{core,sig,Lepton}}$	−0.060 ± 0.023	−0.066 ± 0.024	−0.058 ± 0.025	−0.058 ± 0.022	−0.057 ± 0.024
$\delta_{\mathrm{core,sig,Kaon}}$	−0.213 ± 0.015	−0.242 ± 0.015	−0.237 ± 0.016	−0.207 ± 0.014	−0.225 ± 0.015
$\delta_{\mathrm{core,sig,NT1}}$	−0.162 ± 0.029	−0.153 ± 0.030	−0.157 ± 0.031	−0.151 ± 0.028	−0.148 ± 0.030
$\delta_{\mathrm{core,sig,NT2}}$	−0.179 ± 0.022	−0.231 ± 0.022	−0.220 ± 0.023	−0.179 ± 0.021	−0.214 ± 0.022
$\mathcal{S}_{\mathrm{tail,sig}}$	3.858 ± 0.341	3.657 ± 0.278	3.671 ± 0.325	3.840 ± 0.316	3.845 ± 0.304
$\delta_{\mathrm{tail,sig}}$	−2.288 ± 0.518	−2.164 ± 0.459	−2.195 ± 0.483	−2.169 ± 0.443	−2.395 ± 0.529
$f_{\mathrm{tail,sig}}$	0.030 ± 0.007	0.038 ± 0.008	0.037 ± 0.009	0.033 ± 0.007	0.033 ± 0.007
$f_{\mathrm{outlier,sig}}$	0.004 ± 0.001	0.005 ± 0.001	0.004 ± 0.001	0.004 ± 0.001	0.004 ± 0.001
$\mathcal{D}_{\mathtt{Lepton}}$	0.865 ± 0.006	0.837 ± 0.006	0.848 ± 0.007	0.859 ± 0.006	0.849 ± 0.006
$\mathcal{D}_{\mathtt{Kaon}}$	0.728 ± 0.005	0.685 ± 0.005	0.698 ± 0.005	0.721 ± 0.005	0.706 ± 0.005
$\mathcal{D}_{\mathtt{NT1}}$	0.649 ± 0.009	0.586 ± 0.010	0.618 ± 0.010	0.627 ± 0.009	0.616 ± 0.010
$\mathcal{D}_{\mathtt{NT2}}$	0.338 ± 0.008	0.276 ± 0.009	0.311 ± 0.009	0.310 ± 0.008	0.295 ± 0.009
$\Delta\mathcal{D}_{\mathtt{Lepton}}$	0.001 ± 0.010	0.000 ± 0.010	−0.003 ± 0.011	0.005 ± 0.009	0.002 ± 0.010
$\Delta\mathcal{D}_{\mathtt{Kaon}}$	0.040 ± 0.007	0.043 ± 0.008	0.044 ± 0.008	0.039 ± 0.007	0.043 ± 0.008
$\Delta\mathcal{D}_{\mathtt{NT1}}$	−0.046 ± 0.015	−0.044 ± 0.016	−0.055 ± 0.016	−0.039 ± 0.014	−0.040 ± 0.016
$\Delta\mathcal{D}_{\mathtt{NT2}}$	0.067 ± 0.013	0.071 ± 0.013	0.069 ± 0.014	0.068 ± 0.013	0.072 ± 0.013
Δm_d (ps^{-1})	0.4792 ± 0.0034	0.4783 ± 0.0037	0.4798 ± 0.0037	0.4786 ± 0.0033	0.4789 ± 0.0036
Events	101753	100900	94609	110230	97441

Parameter	D^+−30 %	D_s^+ +30 %	D_s^+ −30 %	Non-D +30 %	Non-D −30 %
$\mathcal{S}_{\mathrm{core,sig}}$	1.130 ± 0.022	1.154 ± 0.021	1.129 ± 0.021	1.154 ± 0.021	1.126 ± 0.020
$\delta_{\mathrm{core,sig,Lepton}}$	−0.056 ± 0.024	−0.059 ± 0.025	−0.058 ± 0.023	−0.060 ± 0.025	−0.055 ± 0.022
$\delta_{\mathrm{core,sig,Kaon}}$	−0.227 ± 0.015	−0.223 ± 0.016	−0.226 ± 0.014	−0.219 ± 0.015	−0.230 ± 0.014
$\delta_{\mathrm{core,sig,NT1}}$	−0.169 ± 0.029	−0.152 ± 0.031	−0.158 ± 0.028	−0.147 ± 0.031	−0.161 ± 0.028
$\delta_{\mathrm{core,sig,NT2}}$	−0.186 ± 0.022	−0.205 ± 0.023	−0.197 ± 0.021	−0.199 ± 0.023	−0.201 ± 0.021
$\mathcal{S}_{\mathrm{tail,sig}}$	3.679 ± 0.372	3.795 ± 0.344	3.736 ± 0.319	3.754 ± 0.336	3.751 ± 0.287
$\delta_{\mathrm{tail,sig}}$	−1.979 ± 0.425	−2.486 ± 0.615	−2.053 ± 0.394	−2.457 ± 0.628	−2.062 ± 0.385
$f_{\mathrm{tail,sig}}$	0.036 ± 0.010	0.030 ± 0.008	0.037 ± 0.008	0.030 ± 0.008	0.038 ± 0.007
$f_{\mathrm{outlier,sig}}$	0.004 ± 0.001	0.004 ± 0.001	0.004 ± 0.001	0.004 ± 0.001	0.004 ± 0.001
$\mathcal{D}_{\mathtt{Lepton}}$	0.861 ± 0.006	0.852 ± 0.007	0.854 ± 0.006	0.849 ± 0.007	0.857 ± 0.006
$\mathcal{D}_{\mathtt{Kaon}}$	0.714 ± 0.005	0.709 ± 0.005	0.710 ± 0.005	0.703 ± 0.005	0.716 ± 0.005
$\mathcal{D}_{\mathtt{NT1}}$	0.632 ± 0.009	0.622 ± 0.010	0.624 ± 0.009	0.606 ± 0.010	0.641 ± 0.009
$\mathcal{D}_{\mathtt{NT2}}$	0.328 ± 0.008	0.313 ± 0.009	0.308 ± 0.008	0.302 ± 0.009	0.319 ± 0.008
$\Delta\mathcal{D}_{\mathtt{Lepton}}$	−0.002 ± 0.010	−0.001 ± 0.011	0.002 ± 0.009	−0.002 ± 0.011	0.003 ± 0.009
$\Delta\mathcal{D}_{\mathtt{Kaon}}$	0.041 ± 0.007	0.043 ± 0.008	0.041 ± 0.007	0.043 ± 0.008	0.040 ± 0.007
$\Delta\mathcal{D}_{\mathtt{NT1}}$	−0.053 ± 0.015	−0.046 ± 0.016	−0.048 ± 0.014	−0.043 ± 0.016	−0.052 ± 0.014
$\Delta\mathcal{D}_{\mathtt{NT2}}$	0.066 ± 0.013	0.067 ± 0.014	0.069 ± 0.012	0.064 ± 0.014	0.072 ± 0.012
Δm_d (ps^{-1})	0.4793 ± 0.0034	0.4791 ± 0.0038	0.4788 ± 0.0033	0.4784 ± 0.0038	0.4794 ± 0.0033
Events	106455	89851	116327	91645	114010

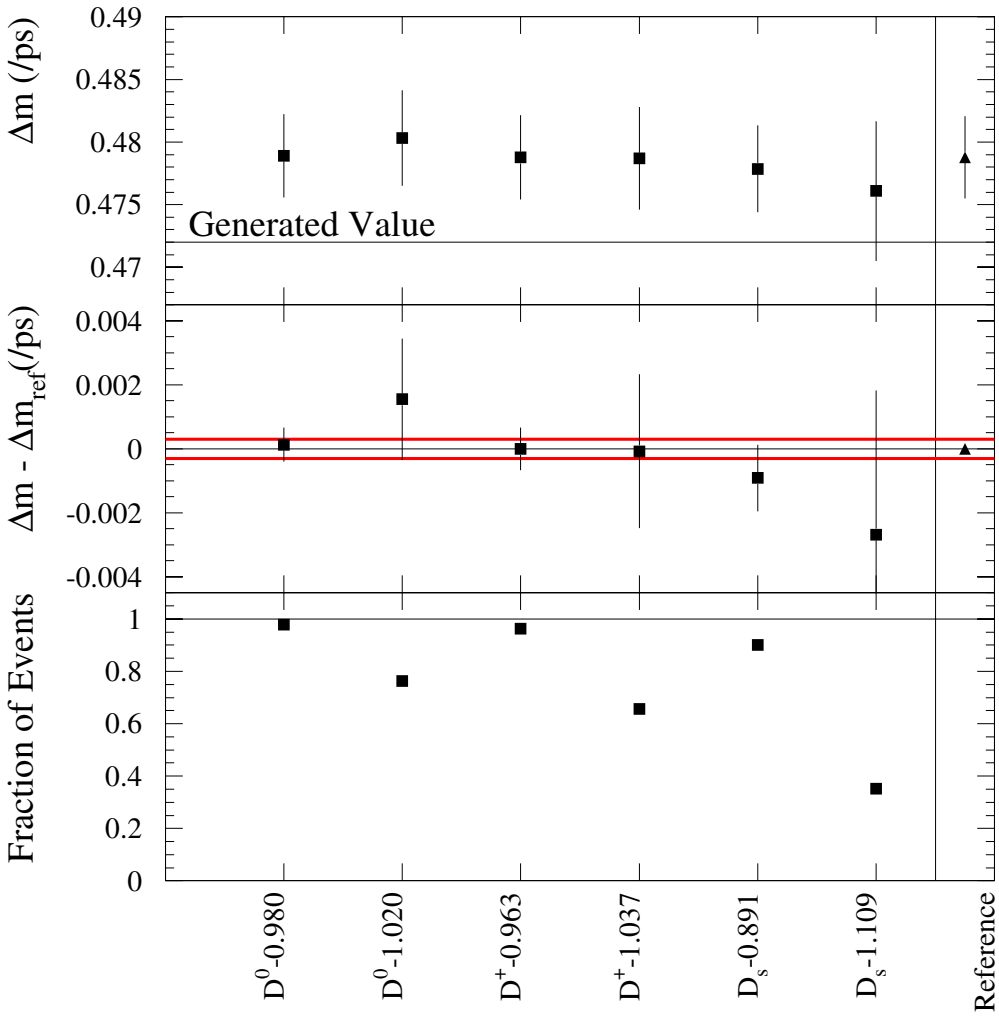

Figure 7-6: Fits to subsets of 2.8 million signal cocktail Monte Carlo events (no $B \to J/\psi K^*$) which have been reweighted with 3 σ variations in lifetimes of the tag side D mesons. The systematic error for this effect is negligible.

reweighting procedure is performed as follows: the sample is divided into events with a D_i, or without, where D_i is the D species under study. Events with a D_i are removed, using truth, in such a way that the lifetime of the D_i is modified. The algorithm maintains the relative abundances of other kinds of B decays which don't contain a D_i by removing the same fraction of those events as were removed to adjust the lifetime. The results of these fits are shown in Figure 7-6. The systematic error due to this effect is concluded to be negligible (less than 0.0005).

Variation of Wrong-sign Kaon Fraction

The event generator uses PDG [8] values for the amount of B decays that contain a final-state kaon with charge opposite to what is expected from the (most common) $b \to c \to s$ transition. The fraction of so-called wrong-sign kaons is varied up and down by up to 100 % in the Monte Carlo by removing events using Monte Carlo truth. Specifically for the removal, an event is labeled "wrong-sign" if the sum of the charges of all true kaons in the event is opposite to what is expected from the B flavor. Each subsample is then fitted to determine the effect of differing amounts of wrong-sign kaon decays on Δm_d. The fits are shown in Figure 7-7 and Table 7.5. A conservative systematic error of $\pm$ 0.001 ps^{-1} is assigned due to this effect.

7.1.3 Δt Resolution Function

To estimate the contribution to the statistical error on Δm_d due to the resolution parameters, two fits are performed: one where only Δm_d is allowed to float, and one where the signal resolution parameters are also free. The (quadratic) difference between the error on Δm_d is used as an estimate of the contribution to the statistical error on Δm_d due to the uncertainty in measuring the resolution function. (Table 7.6).

Δt Outliers

A small fraction of the selected candidates (eg. 0.8 $\pm$ 0.4 % for Run 1 and less than 0.01 % for Run 2) have very large $|\Delta t|$ values (Δt outliers). These candidates are

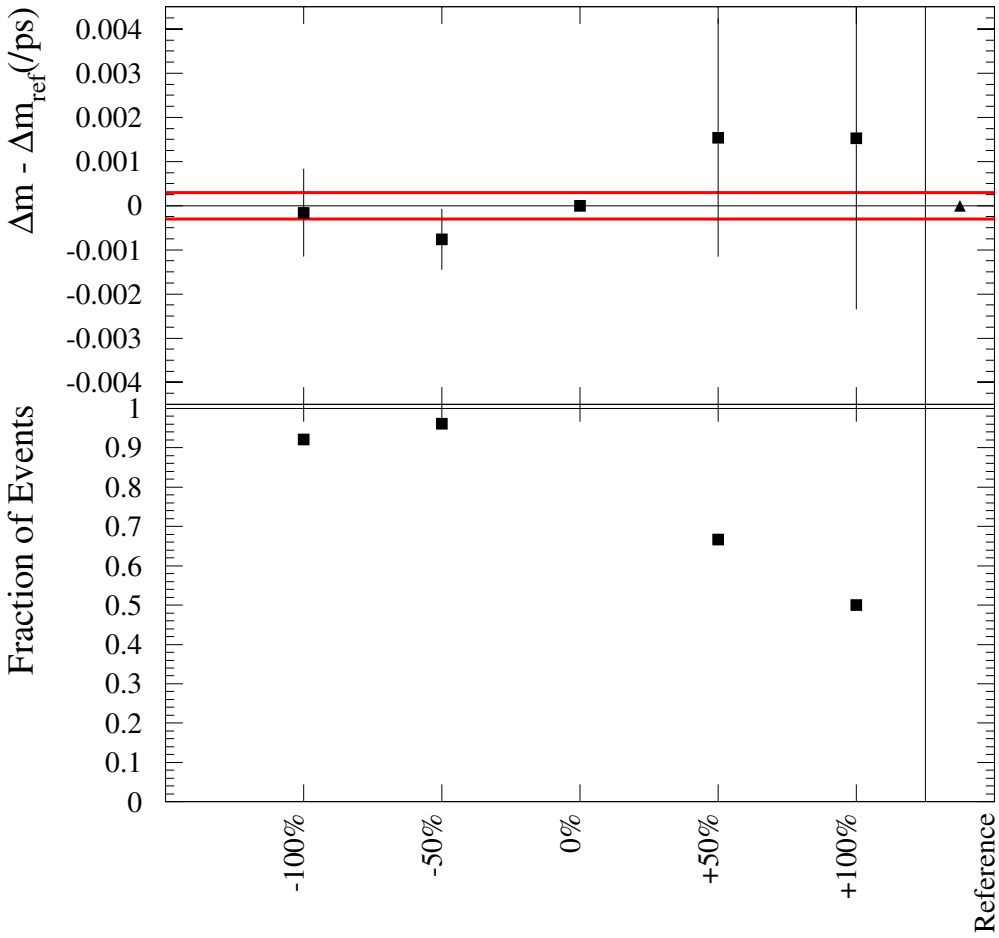

Figure 7-7: Fits to Monte Carlo samples (no $B \to J/\psi K^*$) with variations in relative amounts of B decays to wrong-sign kaons. The assigned systematic error is indicated by the thick horizontal lines.

Table 7.5: Results from the likelihood fit to the Δt distributions of the hadronic B^0 decays in simulated signal events for different amounts of wrong-sign kaon events. The sample of 2.8 million (no $B \to J/\psi K^*$) was reweighted to have up to $\pm$ 100 % wrong-sign kaon fraction.

Parameter	-100 %	-50 %	0 %	$+50$ %	$+100$ %
$\mathcal{S}_{\mathrm{core,sig}}$	1.133 $\pm$ 0.020	1.125 $\pm$ 0.020	1.129 $\pm$ 0.020	1.135 $\pm$ 0.025	1.102 $\pm$ 0.047
$\delta_{\mathrm{core,sig,Lepton}}$	-0.052 ± 0.023	-0.056 ± 0.022	-0.058 ± 0.022	-0.053 ± 0.028	-0.021 ± 0.038
$\delta_{\mathrm{core,sig,Kaon}}$	-0.238 ± 0.014	-0.232 ± 0.014	-0.227 ± 0.014	-0.208 ± 0.018	-0.208 ± 0.026
$\delta_{\mathrm{core,sig,NT1}}$	-0.162 ± 0.028	-0.160 ± 0.028	-0.158 ± 0.027	-0.157 ± 0.034	-0.115 ± 0.044
$\delta_{\mathrm{core,sig,NT2}}$	-0.210 ± 0.021	-0.204 ± 0.021	-0.197 ± 0.021	-0.176 ± 0.026	-0.166 ± 0.035
$\mathcal{S}_{\mathrm{tail,sig}}$	3.867 $\pm$ 0.352	3.753 $\pm$ 0.279	3.717 $\pm$ 0.284	3.621 $\pm$ 0.363	3.160 $\pm$ 0.509
$\delta_{\mathrm{tail,sig}}$	-1.865 ± 0.358	-1.936 ± 0.363	-2.060 ± 0.398	-2.314 ± 0.592	-1.645 ± 0.548
$f_{\mathrm{tail,sig}}$	0.035 $\pm$ 0.008	0.038 $\pm$ 0.008	0.037 $\pm$ 0.008	0.036 $\pm$ 0.010	0.059 $\pm$ 0.028
$f_{\mathrm{outlier,sig}}$	0.004 $\pm$ 0.001	0.004 $\pm$ 0.001	0.004 $\pm$ 0.001	0.004 $\pm$ 0.001	0.005 $\pm$ 0.001
$\mathcal{D}_{\mathtt{Lepton}}$	0.860 $\pm$ 0.006	0.855 $\pm$ 0.006	0.854 $\pm$ 0.006	0.853 $\pm$ 0.007	0.856 $\pm$ 0.008
$\mathcal{D}_{\mathtt{Kaon}}$	0.839 $\pm$ 0.004	0.769 $\pm$ 0.004	0.710 $\pm$ 0.005	0.643 $\pm$ 0.006	0.584 $\pm$ 0.007
$\mathcal{D}_{\mathtt{NT1}}$	0.637 $\pm$ 0.009	0.631 $\pm$ 0.009	0.623 $\pm$ 0.009	0.614 $\pm$ 0.011	0.611 $\pm$ 0.013
$\mathcal{D}_{\mathtt{NT2}}$	0.314 $\pm$ 0.008	0.312 $\pm$ 0.008	0.308 $\pm$ 0.008	0.307 $\pm$ 0.010	0.290 $\pm$ 0.011
$\Delta\mathcal{D}_{\mathtt{Lepton}}$	0.001 $\pm$ 0.010	0.001 $\pm$ 0.010	0.002 $\pm$ 0.009	0.001 $\pm$ 0.012	0.004 $\pm$ 0.013
$\Delta\mathcal{D}_{\mathtt{Kaon}}$	0.038 $\pm$ 0.006	0.041 $\pm$ 0.007	0.040 $\pm$ 0.007	0.041 $\pm$ 0.009	0.034 $\pm$ 0.011
$\Delta\mathcal{D}_{\mathtt{NT1}}$	-0.045 ± 0.015	-0.043 ± 0.014	-0.049 ± 0.014	-0.038 ± 0.017	-0.059 ± 0.020
$\Delta\mathcal{D}_{\mathtt{NT2}}$	0.064 $\pm$ 0.013	0.069 $\pm$ 0.012	0.069 $\pm$ 0.012	0.073 $\pm$ 0.015	0.090 $\pm$ 0.017
Δm_d (ps^{-1})	0.4786 $\pm$ 0.0031	0.4780 $\pm$ 0.0032	0.4788 $\pm$ 0.0033	0.4803 $\pm$ 0.0043	0.4803 $\pm$ 0.0051
Events	107300	111922	116539	77682	58327

Table 7.6: Contribution to the statistical error due to the uncertainty in the signal resolution parameters.

Floating parameters	$\sigma(\Delta m_d)$ (ps^{-1})
Δm_d	0.0139
Δm_d, signal resolution parameters	0.0148
Difference:	0.0050

accounted for in the likelihood function of the Δt distributions by an outlier Gaussian with fixed rms of 8 ps and zero bias. The fraction of outliers is a free fit parameter. Therefore, the actual fraction of outliers should not bias the fit result. To study the systematic uncertainty due to these outliers, the width of the outlier fraction is varied from 4 to 18 ps. In addition the outlier Gaussian is replaced with a flat 'box' probability density function centered around zero with a varying width. The variations are summarized in Table 7.7 and shown in Figure 7-8. The systematic uncertainty due to Δt outliers and their description is estimated to be $\pm$ 0.001 ps^{-1} for Δm_d.

Table 7.7: Systematic uncertainties in Δm_d due to fixed width of the Δt outliers estimated from data by varying the width and replacing the Gaussian outlier model with a flat probability density function model. $\delta\Delta m_d$ is the difference of the blind Δm_d for the specified fit and the reference fit with a Gaussian outlier with a width of 8 ps.

Outlier width (ps)	$\delta\Delta m_d$ (ps^{-1})	Outlier width (ps)	$\delta\Delta m_d$ (ps^{-1})
Gaussian model		Flat model	
4	0.002 ± 0.008	4	0.001 ± 0.005
6	-0.001 ± 0.003	6	0.001 ± 0.005
8	0.000 ± 0.000	8	0.001 ± 0.005
10	0.001 ± 0.002	10	0.001 ± 0.006
12	0.001 ± 0.002	14	-0.003 ± 0.005
14	0.002 ± 0.002	16	0.002 ± 0.006
16	0.002 ± 0.000	18	0.004 ± 0.005
18	0.002 ± 0.000	20	0.003 ± 0.002
20	0.002 ± 0.002	40	0.003 ± 0.002
Syst. Error	$\pm$ 0.001		

7.1.4 B^0 Lifetime

In the nominal fit configuration, the B^0 lifetime is fixed to the PDG [8] value of $\tau_{B^0} = 1.548 \pm 0.032$ ps [8], and the systematic bias due to the corresponding uncertainty is estimated by repeating the likelihood fit with τ_{B^0} varied by $\pm$ 0.032 ps. The measured values for Δm_d and the tagging dilutions are listed in Table 7.8 and shown in Figure 7-9. The break in the figure at τ_{B^0} =1.57 ps coincides with a

Figure 7-8: Systematic uncertainties in Δm_d and in the mistag fractions due to the fixed width of the Δt outliers estimated from data by varying the width and replacing the Gaussian outlier model with a flat probability density function model. $\delta\Delta m_d$ is the difference of the blind Δm_d for the specified fit and the reference fit with a Gaussian outlier with a width of 8 ps. The errors are computed as the difference in quadrature of the statistical errors of the fit under consideration and the reference fit.

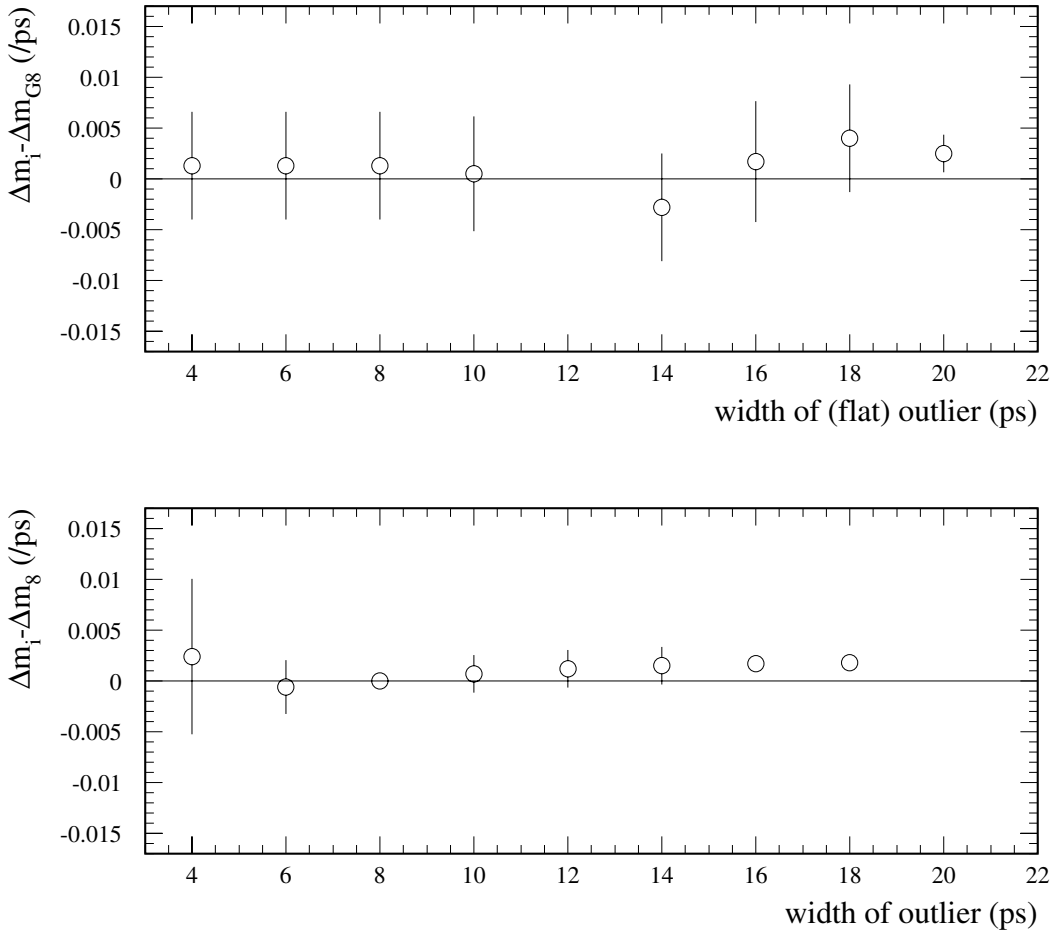

change in the resolution function parameters for Run 1. The slope of the dependence at the PDG [8] B^0 lifetime is multiplied with the PDG [8] uncertainty as a systematic uncertainty, leading to a systematic of $\pm$ 0.0056 on Δm_d.

Table 7.8: Systematic uncertainties in Δm_d due to the uncertainty in the B^0 lifetime. $\delta\Delta m_d$ is the difference in the blinded value of Δm_d for the specified fit and the reference fit where τ_{B^0} is fixed to the PDG [8] value of 1.548 ps.

τ_{B^0} (ps)	$\delta\Delta m_d$ (ps^{-1})
1.612 (+2 σ)	$-$ 0.0086 $\pm$ 0.0157
1.580 (+1 σ)	$-$ 0.0035 $\pm$ 0.0158
1.548 (PDG 2000)	$\pm$ 0.0161
1.516 ($-$1 σ)	+ 0.0056 $\pm$ 0.0163
1.484 ($-$2 σ)	+ 0.0117 $\pm$ 0.0165
$\sigma_{\rm syst}$	$\pm$ 0.006

7.1.5 z Scale

The difference between the z positions of the two B decay vertices, Δz, is used to calculate the decay-time difference in the $\Upsilon(4S)$ rest frame. A potential bias in the z scale will directly translate into a systematic bias of the B^0 lifetime and Δm_d. The uncertainty in the scale of the Δz measurement is less than $\pm$ 0.4 % [25]. Note that the measurements in [25] pertain to the beampipe, and the uncertainty has been conservatively increased by a factor of 2 to allow for scenarios where the measurements at the beampipe radius are correct, but measurements at the beamspot are not. The corresponding systematic error in Δm_d is smaller than $\pm$ 0.002 ps^{-1}.

7.1.6 $\Upsilon(4S)$ z Boost

The $\Upsilon(4S)$ boost in the z direction is used to calculate the decay-time difference using the "average τ_B" approximation [15]. A potential systematic bias in the boost translates directly into a systematic bias of Δm_d. The boost is known to a relative uncertainty of $\pm$ 0.1 % [10]. The systematic error due to the boost in Δm_d is estimated to be $\pm$ 0.0005 ps^{-1}.

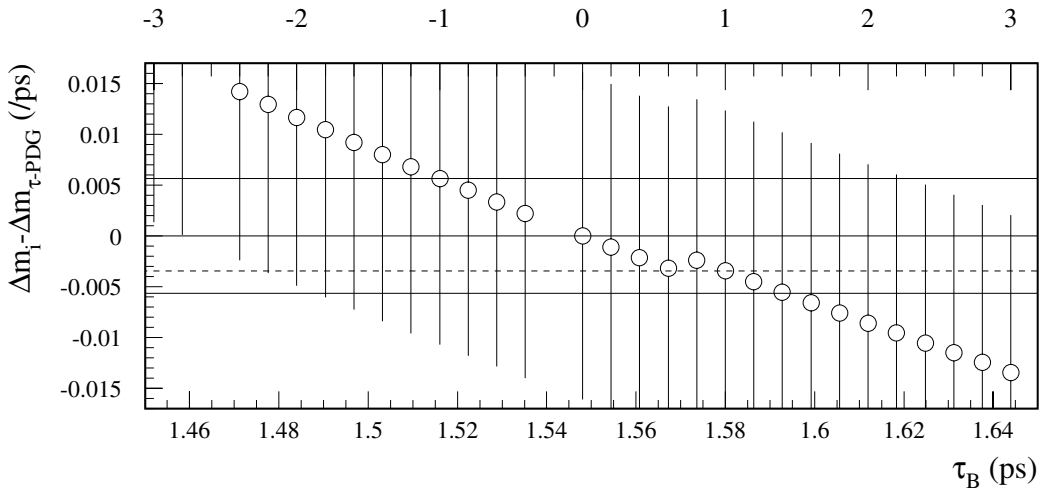

Figure 7-9: Systematic uncertainty in Δm_d due to the uncertainty in the B^0 lifetime. The 'break' at 1.57 ps coincides with a change in the Run 1 resolution function parameters.

Another source of uncertainty is the one intrinsic to the method used to convert Δz into Δt. The "average τ_B" approximation is compared with the "average boost" approximation on Monte Carlo and data in Table 7.9. The observed difference in data (after applying the corresponding Monte Carlo corrections) of 0.0014 ps is interpreted as a systematic error due to the Δz to Δt conversion method. Note that if the "average boost" approximation is used, it has been shown that the resolution depends on the value of Δz due to the non-zero boost of the B mesons in the $\Upsilon(4S)$ frame (see [24] for more details).

7.1.7 Beamspot Position

The beamspot position is used in the computation of the tag vertex [15]. Using signal cocktail Monte Carlo, the dependence of Δm_d on the assumed position of the beamspot is checked. The assumed position of the beamspot is either systematically shifted for all events or moved (event-by-event) by a random amount, drawn from a Gaussian distribution with a given spread (Table 7.10). The resolution function is refit

Table 7.9: Comparison between different boost approximations on data on Monte Carlo. The data values have been *not* been corrected by the deviation of the Monte Carlo difference.

	Monte Carlo Δm_d (ps^{-1})	Data $\delta\Delta m_d$ (ps^{-1})	Difference (ps^{-1})
Average τ_B	0.4786 ± 0.0032	± 0.016	
Average boost	0.4751 ± 0.0032	-0.0049 ± 0.016	
Difference	-0.0035	-0.0049	-0.0014

in all cases. Additionally, using data, the default beamspot determined from Bhabha and dimuon events is checked by using the position determined from multihadron events. The difference in Δm_d is -0.002 ± 0.002 ps^{-1}.

Table 7.10: Variation of Δm_d when shifting or smearing the y position of the beamspot. The reported error is the difference in quadrature between the fit under consideration and the nominal fit.

Size of Variation (μm)	$\delta\Delta m_d$ (ps^{-1})
Shift y	
5	-0.0004 ± 0.0008
10	-0.0001 ± 0.0008
20	0.0000 ± 0.0008
40	-0.0004 ± 0.0008
80	0.0002 ± 0.0012
Smear y	
10	-0.0003 ± 0.0008
20	-0.0003 ± 0.0008
40	-0.0001 ± 0.0008
80	-0.0010 ± 0.0013

7.1.8 Background Δt Distribution

The robustness of the treatment of the combinatorial background in the hadronic B^0 sample is verified as follows. A third component is added to the zero lifetime and non-zero lifetime components used in the nominal fit. The additional term describes an oscillatory Δt distribution to account for a contribution of (mis-reconstructed) $B^0\overline{B}^0$

background. The additional mixing component requires seven more fit parameters than the nominal fit. As a result of using more fit parameters, the errors on the background parameters increase; however, the signal parameters (Δm_d and the signal dilutions) remain unaffected because of the small correlation between background and signal parameters already observed in the nominal fit. The results of this study are listed in Table 7.11 and the projections of the various fits for the $m_{\rm ES}$ sideband are shown in Figure 7-10. The systematic error due to the description of the decay time structure of the combinatorial background is concluded to be less than $\pm$ 0.001 ps.

Table 7.11: Result of likelihood fit results for hadronic B^0 decays using the nominal Δt description of the combinatorial background and using an additional oscillatory term.

$\delta\Delta m_d$ (ps^{-1})	$+0.0006 \pm 0.015$
$\mathcal{S}_{\rm core,sig}$ Run 1	1.397 ± 0.072
$\mathcal{S}_{\rm core,sig}$ Run 2	1.166 ± 0.108
$\delta_{\rm core,sig,Lepton}$ Run 1	-0.035 ± 0.124
$\delta_{\rm core,sig,Lepton}$ Run 2	-0.037 ± 0.164
$\delta_{\rm core,sig,Kaon}$ Run 1	-0.245 ± 0.071
$\delta_{\rm core,sig,Kaon}$ Run 2	-0.240 ± 0.090
$\delta_{\rm core,sig,NT1}$ Run 1	-0.055 ± 0.153
$\delta_{\rm core,sig,NT1}$ Run 2	-0.502 ± 0.216
$\delta_{\rm core,sig,NT2}$ Run 1	-0.544 ± 0.121
$\delta_{\rm core,sig,NT2}$ Run 2	-0.254 ± 0.162
$\delta_{\rm tail,sig}$ Run 1	-6.885 ± 2.507
$\delta_{\rm tail,sig}$ Run 2	-7.541 ± 1.576
$f_{\rm tail,sig}$ Run 1	0.007 ± 0.005
$f_{\rm tail,sig}$ Run 2	0.016 ± 0.006
$f_{\rm outlier,sig}$ Run 1	0.009 ± 0.004
$f_{\rm outlier,sig}$ Run 2	0.000 ± 0.013
$\mathcal{D}_{\rm Lepton}$	0.829 ± 0.029
$\mathcal{D}_{\rm Kaon}$	0.665 ± 0.023
$\mathcal{D}_{\rm NT1}$	0.573 ± 0.045
$\mathcal{D}_{\rm NT2}$	0.318 ± 0.043
$\Delta\mathcal{D}_{\rm Lepton}$	-0.011 ± 0.048
$\Delta\mathcal{D}_{\rm Kaon}$	0.019 ± 0.035
$\Delta\mathcal{D}_{\rm NT1}$	-0.093 ± 0.071
$\Delta\mathcal{D}_{\rm NT2}$	0.106 ± 0.063
$\mathcal{S}_{\rm core,bgd}$ Run 1	1.333 ± 0.028
$\mathcal{S}_{\rm core,bgd}$ Run 2	1.205 ± 0.034
$\delta_{\rm core,bgd}$ Run 1	-0.123 ± 0.030
$\delta_{\rm core,bgd}$ Run 2	-0.018 ± 0.038
$f_{\rm outlier,bgd}$ Run 1	0.013 ± 0.003
$f_{\rm outlier,bgd}$ Run 2	0.024 ± 0.005
$\Delta m_{\rm mix\ bgd}$ (ps^{-1})	1.011 ± 0.062
$\tau_{\rm mix\ bgd}$ (ps)	1.160 ± 0.072
$\tau_{\tau>0}$ (ps)	1.236 ± 0.050
$\mathcal{D}'_{\tau=0,\rm Kaon}$	0.446 ± 0.024
$\mathcal{D}'_{\tau=0,\rm Lepton}$	-1.700 ± 0.221
$\mathcal{D}'_{\tau=0,\rm NT1}$	0.649 ± 0.073
$\mathcal{D}'_{\tau=0,\rm NT2}$	0.157 ± 0.041
$\mathcal{D}'_{\tau>0,\rm Kaon}$	0.222 ± 0.044
$\mathcal{D}'_{\tau>0,\rm Lepton}$	1.886 ± 0.305
$\mathcal{D}'_{\tau>0,\rm NT1}$	-0.647 ± 0.239
$\mathcal{D}'_{\tau>0,\rm NT2}$	0.104 ± 0.077
$\mathcal{D}'_{\tau>0,\rm mix,Kaon}$	0.741 ± 2.692
$\mathcal{D}'_{\tau>0,\rm mix,Lepton}$	2.000 ± 2.777
$\mathcal{D}'_{\tau>0,\rm mix,NT1}$	-1.064 ± 0.257
$\mathcal{D}'_{\tau>0,\rm mix,NT2}$	-0.084 ± 0.140
$f_{\tau=0,\rm mix,Kaon}$	0.000 ± 0.679
$f_{\tau=0,\rm mix,Lepton}$	0.713 ± 0.058
$f_{\tau=0,\rm mix,NT1}$	0.630 ± 0.037
$f_{\tau=0,\rm mix,NT2}$	1.000 ± 0.758
$f_{\tau=0,\rm Lepton}$	0.281 ± 0.022
$f_{\tau=0,\rm Kaon}$	0.656 ± 0.022
$f_{\tau=0,\rm NT1}$	0.556 ± 0.031
$f_{\tau=0,\rm NT2}$	0.504 ± 0.053

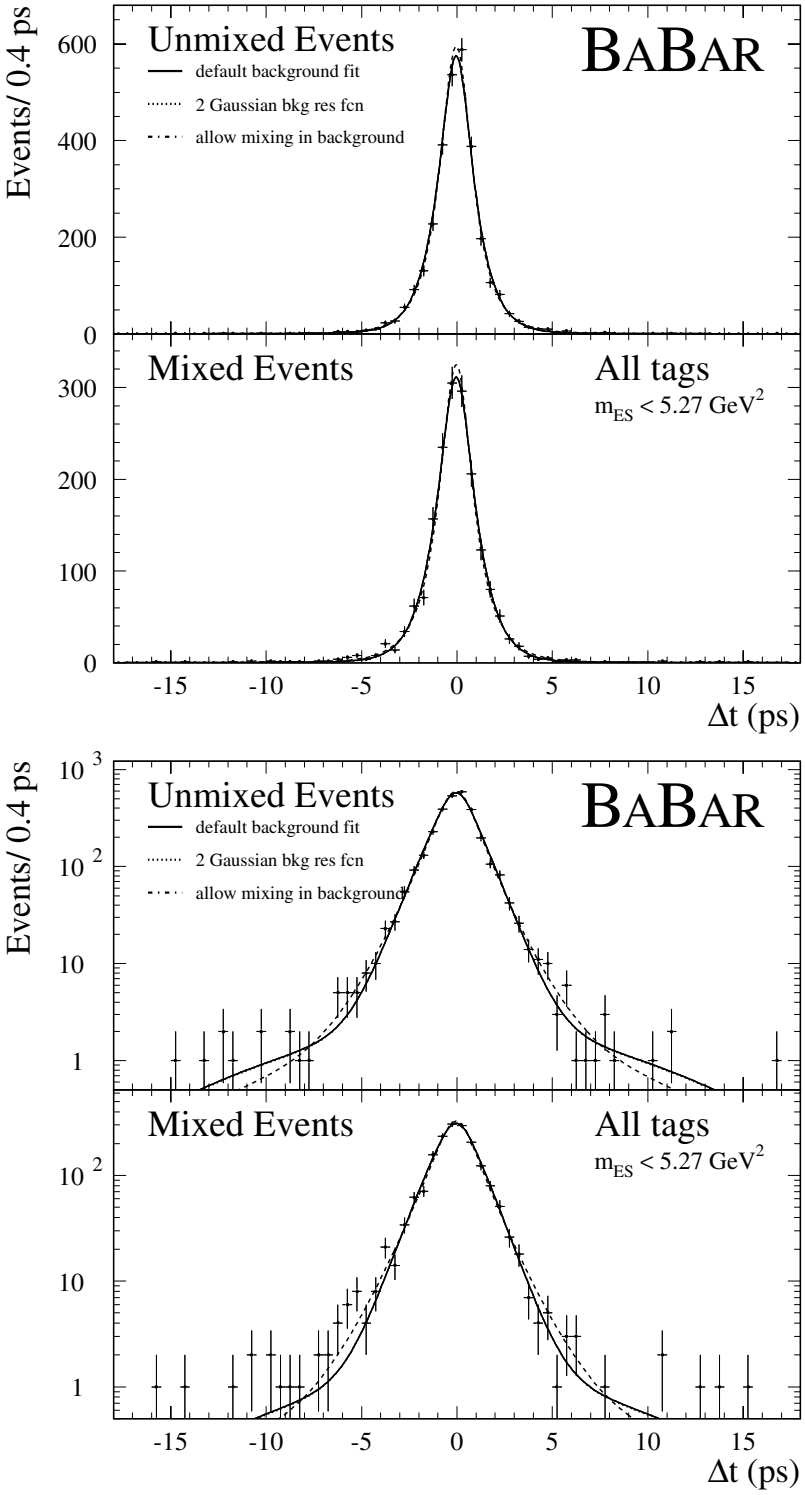

Figure 7-10: Comparison of fits with different treatment of the background description for the $m_{\rm ES}$ sideband events

7.1.9 Background Resolution Function

The error due to the unknown background Δt resolution function is estimated by varying the functional form of the Δt resolution function. Instead of a single Gaussian plus outlier Gaussian, an additional tail Gaussian in the resolution function is allowed for. The differences for Δm_d and the mistag rates are listed in Table 7.12. The observed differences are interpreted as systematic errors due to the uncertainty on the functional form of the background resolution function. The systematic uncertainty due to the background Δt resolution function is concluded to be less than xpm 0.001 ps^{-1}.

Table 7.12: Result of a likelihood fit using an additional second Gaussian (seperate for Run 1 and Run 2) for the background resolution function. Note that first the background parameters are determined from the sideband region ($m_{\text{ES}} < 5.27$ GeV), and fixed during the mixing fit.

$\delta\Delta m_d$ (ps^{-1})	-0.0006 ± 0.017	$\mathcal{S}_{\text{core,bgd}}$ Run 1	1.225 ± 0.031
$\delta_{\text{core,sig,Lepton}}$ Run 1	-0.039 ± 0.127	$\mathcal{S}_{\text{core,bgd}}$ Run 2	1.217 ± 0.037
$\delta_{\text{core,sig,Lepton}}$ Run 2	-0.047 ± 0.166	$\delta_{\text{core,bgd}}$ Run 1	-0.104 ± 0.034
$\delta_{\text{core,sig,Kaon}}$ Run 1	-0.249 ± 0.080	$\delta_{\text{core,bgd}}$ Run 2	0.023 ± 0.040
$\delta_{\text{core,sig,Kaon}}$ Run 2	-0.246 ± 0.094	$\mathcal{S}_{\text{tail,bgd}}$ Run 1	3.241 ± 0.170
$\delta_{\text{core,sig,NT1}}$ Run 1	-0.052 ± 0.155	$\mathcal{S}_{\text{tail,bgd}}$ Run 2	4.813 ± 0.335
$\delta_{\text{core,sig,NT1}}$ Run 2	-0.513 ± 0.218	$\delta_{\text{tail,bgd}}$ Run 1	-0.364 ± 0.202
$\delta_{\text{core,sig,NT2}}$ Run 1	-0.541 ± 0.124	$\delta_{\text{tail,bgd}}$ Run 2	-1.106 ± 0.418
$\delta_{\text{core,sig,NT2}}$ Run 2	-0.261 ± 0.164	$f_{\text{tail,bgd}}$ Run 1	0.164 ± 0.016
$\delta_{\text{tail,sig}}$ Run 1	-7.879 ± 0.638	$f_{\text{tail,bgd}}$ Run 2	0.117 ± 0.013
$\delta_{\text{tail,sig}}$ Run 2	-8.179 ± 2.735	$f_{\text{outlier,bgd}}$ Run 1	0.017 ± 0.004
$\Delta\mathcal{D}_{\text{Lepton}}$	-0.009 ± 0.048	$f_{\text{outlier,bgd}}$ Run 2	0.010 ± 0.004
$\Delta\mathcal{D}_{\text{Kaon}}$	0.018 ± 0.035	$\tau_{\tau>0}$ (ps)	0.552 ± 0.030
$\Delta\mathcal{D}_{\text{NT1}}$	-0.093 ± 0.071	$\mathcal{D}'_{\tau=0,\text{Lepton}}$	-0.888 ± 0.967
$\Delta\mathcal{D}_{\text{NT2}}$	0.107 ± 0.063	$\mathcal{D}'_{\tau=0,\text{Kaon}}$	0.479 ± 0.031
$f_{\text{outlier,sig}}$ Run 1	0.008 ± 0.004	$\mathcal{D}'_{\tau=0,\text{NT1}}$	1.116 ± 0.110
$f_{\text{outlier,sig}}$ Run 2	0.002 ± 0.003	$\mathcal{D}'_{\tau=0,\text{NT2}}$	-0.132 ± 0.132
$f_{\text{tail,sig}}$ Run 1	0.006 ± 0.010	$\mathcal{D}'_{\tau>0,\text{Lepton}}$	0.308 ± 0.075
$f_{\text{tail,sig}}$ Run 2	0.012 ± 0.009	$\mathcal{D}'_{\tau>0,\text{Kaon}}$	0.207 ± 0.040
$\mathcal{S}_{\text{core,sig}}$ Run 1	1.394 ± 0.092	$\mathcal{D}'_{\tau>0,\text{NT1}}$	-0.579 ± 0.076
$\mathcal{S}_{\text{core,sig}}$ Run 2	1.163 ± 0.115	$\mathcal{D}'_{\tau>0,\text{NT2}}$	0.135 ± 0.030
$\mathcal{D}_{\text{Lepton}}$	0.832 ± 0.030	$f_{\tau=0,\text{Lepton}}$	0.000 ± 0.120
$\mathcal{D}_{\text{Kaon}}$	0.667 ± 0.024	$f_{\tau=0,\text{Kaon}}$	0.561 ± 0.045
$\mathcal{D}_{\text{NT1}}$	0.576 ± 0.046	$f_{\tau=0,\text{NT1}}$	0.405 ± 0.027
$\mathcal{D}_{\text{NT2}}$	0.320 ± 0.043	$f_{\tau=0,\text{NT2}}$	0.327 ± 0.105

7.1.10 Background in the Signal Region

The backgrounds are split in two categories: peaking and combinatorial. The properties of the combinatorial background are determined from the $m_{\rm ES}$ sideband ($5.20 < m_{\rm ES} < 5.27\,{\rm GeV}$).

Combinatorial Background

Since the $m_{\rm ES}$ fit is independent of the likelihood fit to the Δt distributions, the statistical uncertainties on the signal probabilities are accounted for as systematic uncertainties in the Δt fit. The parameters of the $m_{\rm ES}$ fit are varied up and down by 1 σ, and the resulting variations in Δm_d are added in quadrature. The individual contributions are shown in Table 7.13. The total systematic error on Δm_d thus

Table 7.13: Variation in Δm_d when the parameters of the $m_{\rm ES}$ fit are varied by their statistical uncertainty.

	$\delta\Delta m_d$ (ps^{-1})	
Parameter	$+1\ \sigma$	$-1\ \sigma$
κ	-0.0014	0.0013
m_B	0.0004	-0.0001
N_{Bgd}	0.0008	-0.0009
N_{Sig}	-0.0008	0.0006
σ_{m_B}	-0.0004	0.0003
Sum in quadrature	$\pm\ 0.0016$	

obtained is 0.0016. As an alternative, the full $m_{\rm ES}$ spectrum is divided into two parts, $m_{\rm ES} < 5.27$ and $m_{\rm ES} > 5.27\,{\rm GeV}$. The events below 5.27 GeV are assigned a signal probability of zero, while the events above 5.27 GeV are assigned a signal probability corresponding to the purity of the sample listed in Table 5.1. This fit yields a change in Δm_d mof $+0.0009 \pm 0.016$ ps^{-1}. This fit is then repeated, varying the signal probabilities by $\pm$ 1 σ; the resulting variations are $\pm$ 0.0021 ps^{-1}.

An additional uncertainty originates from the assumption that the Δt structure of the sideband region is a good description of the Δt structure of the background underneath the signal. To test this assumption, the *lower edge* of the $m_{\rm ES}$ distribution

is varied from 5.20 to 5.27 GeV. The result is shown in Figure 7-11.

In addition, the sideband is split into seven equal slices each 10 MeV wide, and each of these ranges is used seperately in the mixing fit. The resulting values (relative to the nominal fit) are shown in Figure 7-12 and Table 7.14. Extrapolating the values obtained for Δm_d to the B mass, a correction of -0.024 ± 0.020 is extracted. The final value of Δm_d is corrected by this amount, the statistical error of this correction of $\pm$ 0.020 is interpreted as a systematic error.

Table 7.14: Values of Δm_d when using restricted, mutually exclusive slices of the $m_{\rm ES}$ sideband.

$m_{\rm ES}$ sideband range	$\delta\Delta m_d$ ($\rm ps^{-1}$)
5.20 – 5.21	0.0010 ± 0.0164
5.21 – 5.22	0.0012 ± 0.0162
5.22 – 5.23	-0.0017 ± 0.0161
5.23 – 5.24	0.0014 ± 0.0162
5.24 – 5.25	-0.0022 ± 0.0161
5.25 – 5.26	-0.0011 ± 0.0162
5.26 – 5.27	-0.0013 ± 0.0163
Weighted average	$-0.000379277 \pm 0.00612777$
Extrapolation to 5.28 GeV	-0.0024 ± 0.0020

Peaking Background

There is Monte Carlo evidence for a small fraction of background that peaks in $m_{\rm ES}$ and therefore is not accounted for with the phase-space motivated Argus model for extrapolating the $m_{\rm ES}$ sideband. Studies using Monte Carlo [26] indicate that this background arises from misreconstructed B mesons. In the case of misreconstructed B^0 mesons, this is irrelevant, since their time structure is identical to the signal. Only charged Bs which are reconstructed as neutral Bs require special attention, since they do not mix.

A Monte Carlo sample of charged B events generated in the modes indicated to be the main source of the peaking background by the generic Monte Carlo is

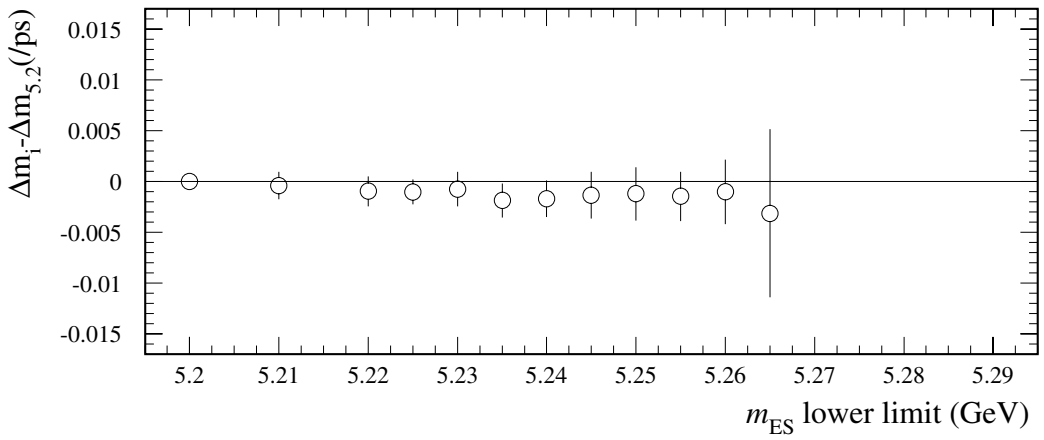

Figure 7-11: Value of Δm_d when changing the lower bound on $m_{\rm ES}$. The plot shows the variation of Δm_d relative to the reference fit with the requirement that $m_{\rm ES} > 5.2$ GeV. The errors are the difference in quadrature between the plot under consideration and the reference fit.

used to characterize these backgrounds. The time structure of those which are misreconstructed as B^0s is verified to be consistent with an exponential with the charged B lifetime (Figure 7-13). The lifetime of the peaking component of this background is fit for, using the resolution function parameters as determined from the fit to the full B^0 sample and dilutions from the charged B sample. The lifetime of the peaking background is found to be 1.42 ± 0.17 ps.

To estimate the effect on Δm_d from charged B peaking background, B^0 signal Monte Carlo is polluted with different levels of charged B Monte Carlo. The variation of Δm_d with this fraction is shown in Table 7.15. Another test is done varying the assumed fraction of charged B peaking background in the fit to data. Those results are listed in Table 7.16.

The amount of charged B peaking background is estimated by using generic and cocktail Monte Carlo events generated in the charged B modes which are indicated to be the main source of the background in the generic Monte Carlo. The B^- contamination is estimated to be $1.3 \pm 0.3^{+0.2}_{-0.5}$ %, and thus, given the dependence

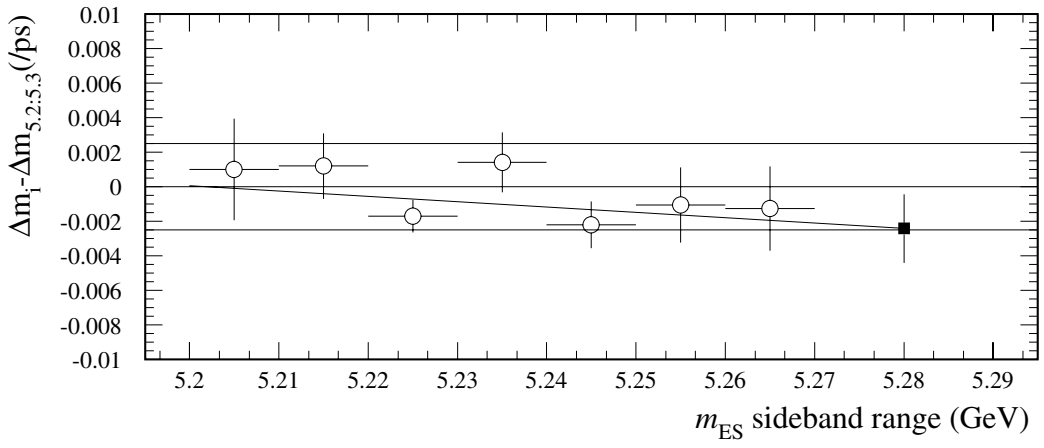

Figure 7-12: Variation of Δm_d when using restricted, mutually exclusive slices of the $m_{\rm ES}$ sideband, shown as open circles. The errors on these points is given by the difference in quadrature between the fit under consideration and the nominal fit. A fit is performed on these points, and then extrapolated to 5.28 GeV. The resulting value, -0.0024 ± 0.0020 ps^{-1}, is indicated by the solid square.

Table 7.15: Variation of Δm_d due to adding B^+ events to the B^0 signal Monte Carlo.

B^+ fraction added (%)	$\delta\Delta m_d$ (%)	slope
1.7	-0.4	-0.24
3.4	-2.0	-0.59
5.1	-4.0	-0.78
6.8	-5.2	-0.76
17	-10.6	-0.62

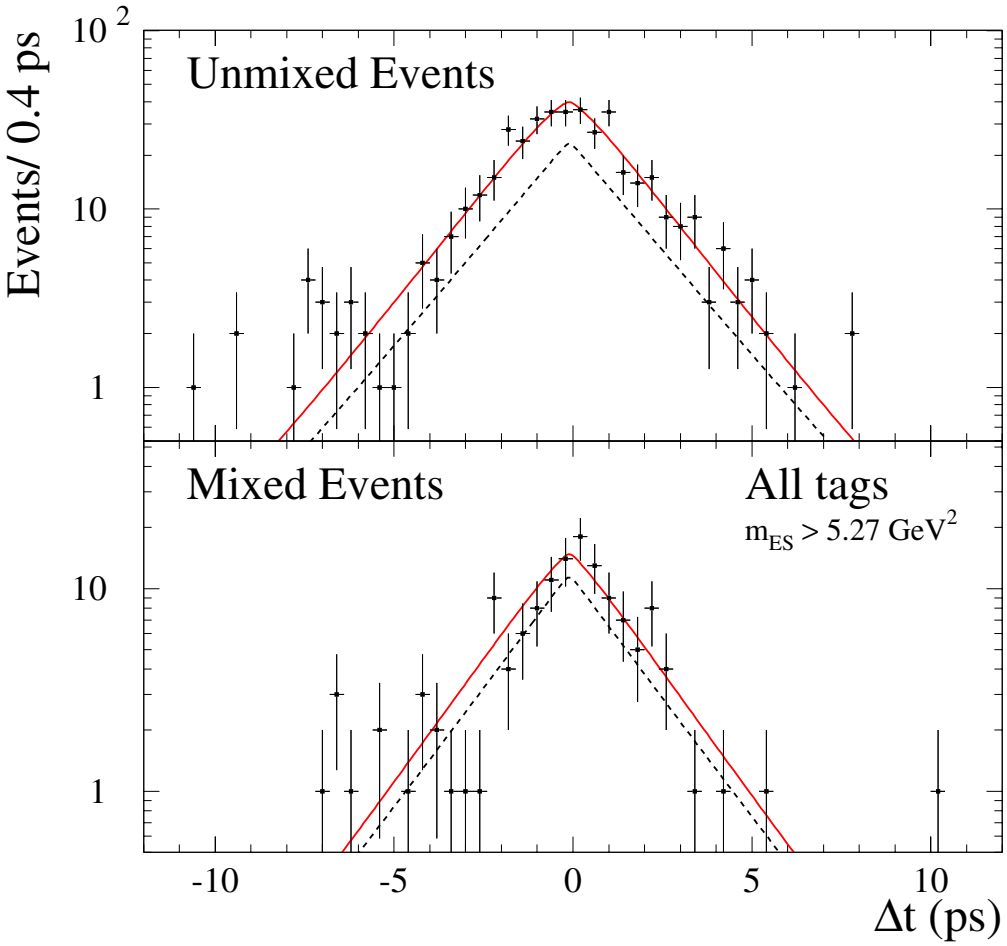

Figure 7-13: Δt distributions for Monte Carlo charged Bs reconstructed as B^0s. Projections of the lifetime fit are overlaid.

Table 7.16: Variation of Δm_d due to changing the assumed fraction of B^+ events in the fit to data (relative to the asumption of no B^+ events).

B^+ fraction assumed (%)	$\delta\Delta m_d$ (%)	Slope
0	0.0	—
3	+1.8	0.62
5	+3.1	0.62
8	+4.9	0.62
10	+6.1	0.61
15	+9.2	0.61

shown in Table 7.16, a systematic error of $\pm$ 0.002 ps^{-1} is assigned to Δm_d due to this effect.

As a cross-check, the fraction of peaking background is left as a free parameter in the likelihood fit, which yields a value of 0.8 $\pm$ 5.6 %, and a value of Δm_d which is 0.0016 ps^{-1} lower than the nominal fit, in good agreement with the above estimates. The statistical error of the fit increases from 0.016 to 0.023 ps^{-1} when floating this fraction.

7.1.11 Dilution

The signal dilutions (and the difference between B^0 and $\overline{B}^0$ dilutions) are allowed to float during the fit. In order to determine the contribution to the statistical error due to the uncertainty in the estimation of the dilutions, two fits are done: one where only Δm_d is allowed to float while all other parameters are fixed to their nominal fit values, and one where the signal dilutions and their differences are also allowed to float. The contribution to the statistical error is then computed by taking the difference in quadrature of the two errors as summarized in Table 7.17.

Table 7.17: Contribution to the statistical error due to the uncertainty in the dilutions.

Floating parameters	$\sigma(\Delta m_d)$ (ps^{-1})
Δm_d only	0.0139
Δm_d, dilutions	0.0148
Difference:	0.0051

7.1.12 SVT Alignment

In order to estimate the systematics due to possible misalignments of the SVT, the same sample of Monte Carlo events is reconstructed with a set of possible distortions. Note that because this couldn't be done in Monte Carlo production, only a very limited sample is available; more information on this sample can be found in [15].

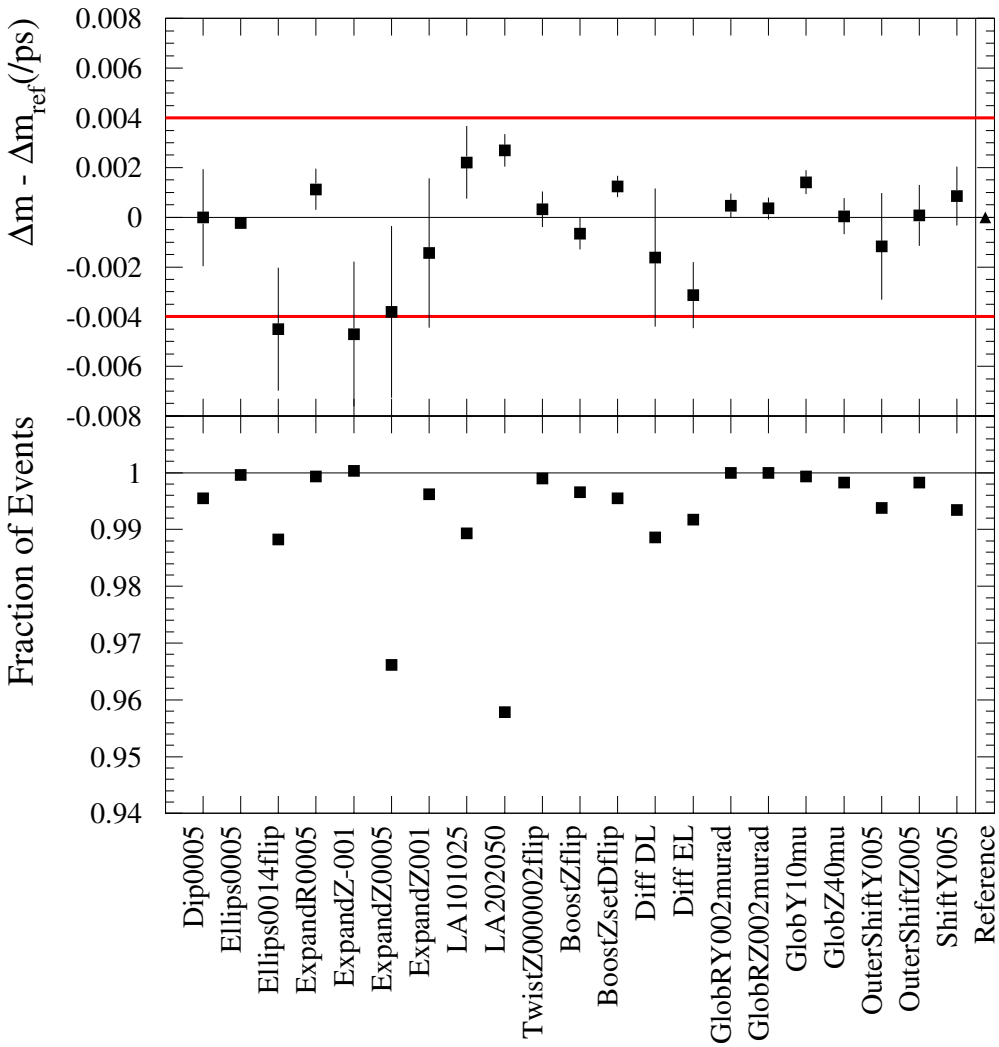

Figure 7-14: Effect of several possible SVT misalignment scenarios on Δm_d. The error quoted is the difference in quadrature between the zero misalignment set and the fit under investigation. In these fits (the results of which are shown in Table 7.18), the tag side flavor is determined from Monte Carlo truth, and the dilutions fixed accordingly. The assigned systematic error is indicated by the thick horizontal lines.

The results are shown in Table 7.18, Figure 7-14 and Table 7.19. In the first case, all parameters are floated as in the nominal Monte Carlo fit. In the second case, in order to improve the statistical power from the limited sample, the tag side flavor is taken from Monte Carlo truth and the dilutions are fixed at unity and the dilution differences at zero. The various scenarios are described in [15]. Note that some scenarios (rotateY0005, rotateZ0005, and TwistZ005) are unrealistically exaggerated. A systematic error of 0.004 ps^{-1} is assigned to Δm_d due to the uncertainty in the SVT alignment, based on the observed change from the scenarios based on the result from Table 7.19 for the `diffDL` and `diffEL` scenarios.

7.1.13 Summary of Systematic Uncertainties

The systematic uncertainties due to the individual sources are added in quadrature to calculate the total systematic uncertainty in Δm_d and the mistag rates. The results are listed in Table 7.20. The statistical errors for Δm_d and the mistag rates is the uncertainty from the nominal fit result, where the resolution function and the parameters of the combinatorial background are also fitted.

Table 7.18: Effect of several possible SVT misalignment scenarios on Δm_d. The error quoted is the difference in quadrature between the "Zero" misalignment set and the fit under investigation. The number in parenthesis is the deviation of the difference divided by the error on the difference. In these fits, all parameters are fit as part of the mixing fit.

Scenario	Δm_d fit result	Difference from Zero alignment ($n\sigma$)
Zero	0.474 ± 0.020	0.000 ± 0.000 (0.0)
Expand r 0.0005 cm	0.470 ± 0.020	-0.003 ± 0.003 (-1.2)
Expand z 0.0005 cm	0.466 ± 0.020	-0.007 ± 0.002 (-4.3)
Expand $z001$	0.475 ± 0.021	0.001 ± 0.005 (0.3)
Expand $z-001$	0.472 ± 0.020	-0.002 ± 0.004 (-0.5)
Global rz $20m$rad	0.080 ± 0.217	-0.393 ± 0.216 (-1.8)
Global ry $20m$rad	0.325 ± 0.110	-0.148 ± 0.109 (-1.4)
Global ry $002m$rad	0.476 ± 0.020	0.002 ± 0.002 (1.5)
Global rz $002m$rad	0.475 ± 0.020	0.002 ± 0.002 (0.9)
Global y 10μ	0.474 ± 0.020	0.001 ± 0.002 (0.2)
Global z 40μ	0.474 ± 0.020	0.001 ± 0.001 (0.6)
Shift y 005	0.478 ± 0.021	0.004 ± 0.006 (0.8)
Outer Shift y 005	0.469 ± 0.020	-0.005 ± 0.003 (-1.4)
Outer Shift z 005	0.474 ± 0.021	0.001 ± 0.004 (0.2)
Twist z 0005	0.452 ± 0.030	-0.022 ± 0.022 (-1.0)
Twist z 000002 flip	0.471 ± 0.020	-0.002 ± 0.003 (-0.8)
Rotate y 005	0.513 ± 0.026	0.040 ± 0.016 (2.5)
Rotate z 005	0.452 ± 0.033	-0.021 ± 0.026 (-0.8)
Ellipse 0005	0.471 ± 0.020	-0.003 ± 0.004 (-0.7)
Ellipse 0014 flip	0.473 ± 0.021	-0.000 ± 0.006 (-0.0)
Boost z flip	0.473 ± 0.020	-0.000 ± 0.001 (-0.1)
Boost z set D flip	0.477 ± 0.021	0.004 ± 0.004 (1.0)
LA101025	0.481 ± 0.021	0.008 ± 0.006 (1.4)
LA202050	0.492 ± 0.022	0.018 ± 0.009 (2.0)
diffDL	0.483 ± 0.021	0.009 ± 0.006 (1.5)
diffEL	0.480 ± 0.021	0.006 ± 0.004 (1.5)

Table 7.19: Effect of several possible SVT misalignment scenarios on Δm_d. The error quoted is the difference in quadrature between the zero misalignment set and the fit under investigation. The number in parenthesis is the deviation of the difference divided by the error on the difference. In these fits, the tag side flavor is determined from Monte Carlo truth, and the dilutions fixed accordingly in order to increase the statistical power of the samples available.

Scenario	Δm_d fit result (ps^{-1})	Difference from Zero alignment ($n\sigma$)
Zero	0.4767 ± 0.0115	0.0000 ± 0.0000 (0.0)
Expand r 0005	0.4779 ± 0.0115	0.0011 ± 0.0008 (1.4)
Expand z 0005	0.4729 ± 0.0121	-0.0038 ± 0.0035 (-1.1)
Expand z 001	0.4753 ± 0.0119	-0.0014 ± 0.0030 (-0.5)
Expand z -001	0.4720 ± 0.0112	-0.0047 ± 0.0029 (-1.6)
Global ry 20 μrad	0.5251 ± 0.0271	0.0484 ± 0.0246 (2.0)
Global rz 20 μrad	0.5133 ± 0.0356	0.0365 ± 0.0337 (1.1)
Global ry 2 μrad	0.4772 ± 0.0116	0.0005 ± 0.0005 (0.9)
Global rz 2 μrad	0.4771 ± 0.0115	0.0004 ± 0.0004 (0.8)
Global y 10μ	0.4781 ± 0.0115	0.0014 ± 0.0005 (2.9)
Global z 40μ	0.4768 ± 0.0116	0.0000 ± 0.0007 (0.1)
Shift y 005	0.4776 ± 0.0116	0.0009 ± 0.0012 (0.7)
Outer Shift y005	0.4756 ± 0.0117	-0.0012 ± 0.0021 (-0.5)
Outer Shift z005	0.4768 ± 0.0116	0.0001 ± 0.0012 (0.1)
Twist z 0005	0.4878 ± 0.0166	0.0111 ± 0.0119 (0.9)
Twist z 000002 flip	0.4771 ± 0.0116	0.0003 ± 0.0007 (0.5)
Rotate y 005	0.4861 ± 0.0143	0.0094 ± 0.0085 (1.1)
Rotate z 005	0.4716 ± 0.0227	-0.0051 ± 0.0196 (-0.3)
Ellipse 0005	0.4765 ± 0.0115	-0.0002 ± 0.0001 (-4.4)
Ellipse 0014 flip	0.4722 ± 0.0118	-0.0045 ± 0.0025 (-1.8)
Boost z flip	0.4761 ± 0.0116	-0.0007 ± 0.0006 (-1.1)
Boost z set D flip	0.4780 ± 0.0116	0.0012 ± 0.0004 (2.8)
LA101025	0.4789 ± 0.0116	0.0022 ± 0.0015 (1.5)
LA202050	0.4794 ± 0.0116	0.0027 ± 0.0007 (4.1)
Dip 0005	0.4767 ± 0.0114	-0.0000 ± 0.0020 (-0.0)
diffDL	0.4751 ± 0.0119	-0.0016 ± 0.0028 (-0.6)
diffEL	0.4736 ± 0.0115	-0.0031 ± 0.0013 (-2.4)

Table 7.20: Systematic uncertainties in Δm_d measured with hadronic B^0 decays.

Source	Δm_d (ps^{-1})
Signal Monte Carlo Statistics	0.0032
Δt Outliers	0.002
$\sigma_{\Delta t}$ requirement	0.003
SVT Alignment	0.004
Background Probability	0.0016
Sideband Extrapolation	0.0020
Background Δt structure	0.001
Background Δt resolution	0.001
Peaking B^+ Background	0.002
B^0 lifetime	0.0056
z scale	$<$0.002
z boost (param)	0.0005
z boost (method)	0.0014
Beamspot position/size	0.0010
Tag-side D composition	0.001
Resolution dependence on right/wrong tag	0.001
Total Systematic	0.0096
Statistical Error	0.0161
Total Error	0.019

Chapter 8

Conclusions

The measurement presented here uses a new technique to measure Δm_d. The value measured for Δm_d by this analysis is

$$\Delta m_d \;=\; 0.516 \;\pm\; 0.016(\text{stat.}) \;\pm 0.010(\text{syst.})\ \text{ps}^{-1} \tag{8.1}$$

The precision on this single measurement is comparable to the average of all previously published measurements. It is also subject to different systematic uncertainties than previous techniques. The sample used has little background, and contains minimal contamination from B^+ decays. Both the tagging algorithm performance and the detector resolution are extracted directly from the data themselves. Moreover, this method is not yet systematics limited. Most of the systematic uncertainties in this measurement fall into one of two general classes: those which will be reduced with more statistics (e.g., signal Monte Carlo samples), and those which will be reduced with better measurements of external parameters (e.g., τ_{B^0}). For these reasons, this analysis has the potential of being one of the most precise methods of measuring Δm_d in the foreseeable future. With 500fb^{-1}, assuming the statistical uncertainty scales as $\sqrt{N}$, that uncertainty on this measurement will be 0.004 ps^{-1}. The systematic uncertainty due to the SVT alignment will be smaller due to an improved alignment algorithm which was implemented since the data for this analysis were processed. Assuming improved measurements of the B^0 lifetime, even with the current Monte

Carlo sample the total systematic uncertainty on this analysis could be comparable to the statistical uncertainty. A comparison of other measurements with this one is shown in Figure 8-1 [27].

There are several possible ways that the precision of this measurement could be improved. The correlation between per-event-error and dilution in the `Kaon` category could be modeled directly in the fit for Δm_d. An even better analysis could use a tagging algorithm which provided a per-event "goodness-of-tag", which could be used in the fit itself to extract much more information in in the fit about correlations between variables. The tag-side vertexing algorithm could be made to attempt to recover charm secondary vertices which would reduce the bias they cause.

In the past few years, our understanding of the physics of the Cabibbo-Kobayashi-Maskawa matrix has been vastly improved. New measurements of CP violating parameters in the B system provide constraints on the angles β and α, while better limits on B_s oscillations and improved precision on measurements of Δm_d provide orthogonal constraints. Measurements which constrain the Unitarity Triangle are consistent with each other within current uncertainties [28]. Improved precision on these measurements in the years to come will allow more stringent tests of how well the triangle closes. As I stated in the introduction, the constraint on the apex of the Unitarity Triangle provided by Δm_d and Δm_s is currently limited by theoretical uncertainties.

A summary of all of the current measurements and constraints on the Unitarity triangle including a fit using the method described in [29] is shown in Figure 8-2.

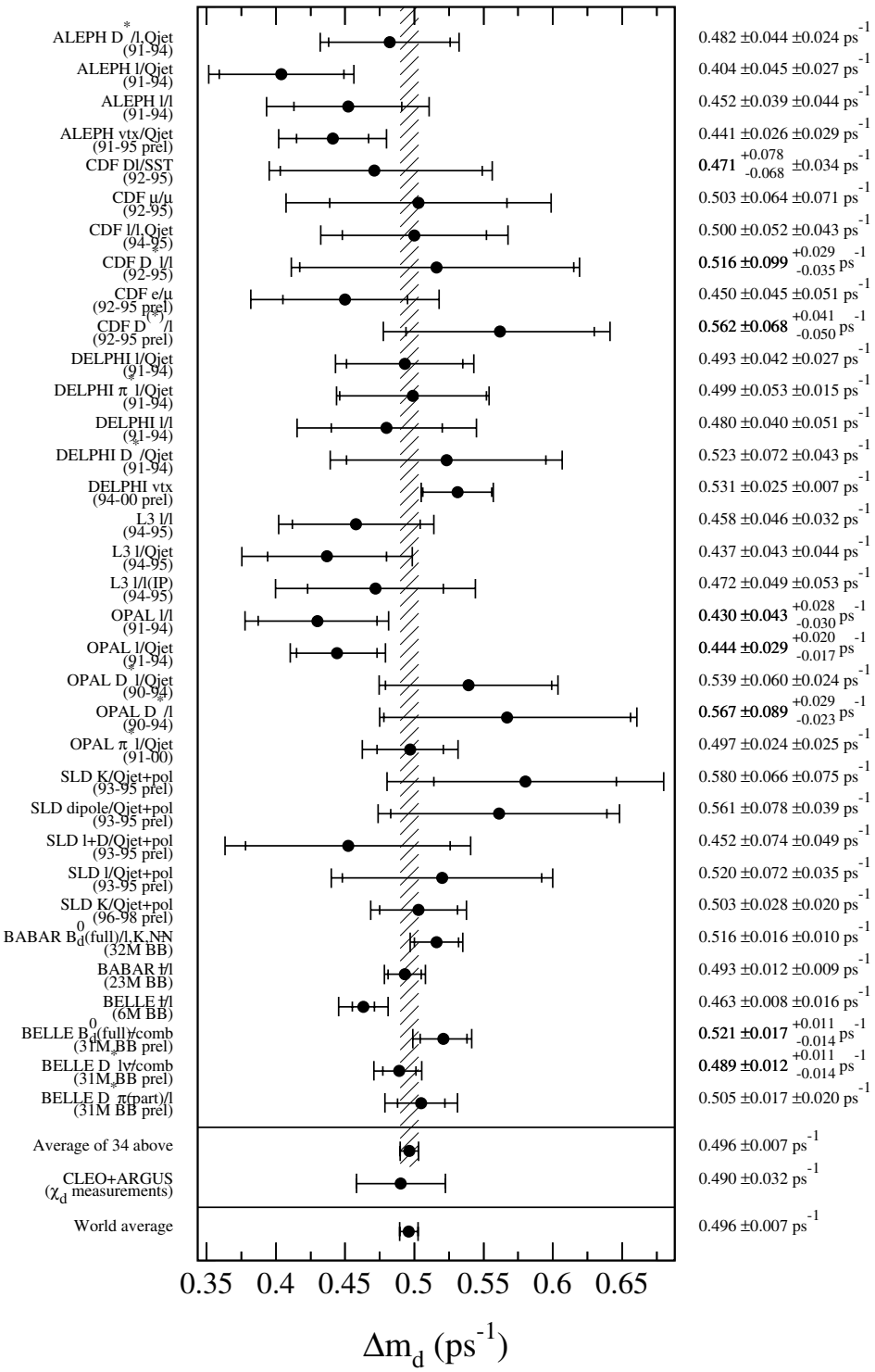

Figure 8-1: World average of Δm_d measurements as computed by the LEP B Oscillations Working Group for the Moriond 2002 conference [27]. This measurement is labeled "BABAR B^0_d (full)/l,K,NN".

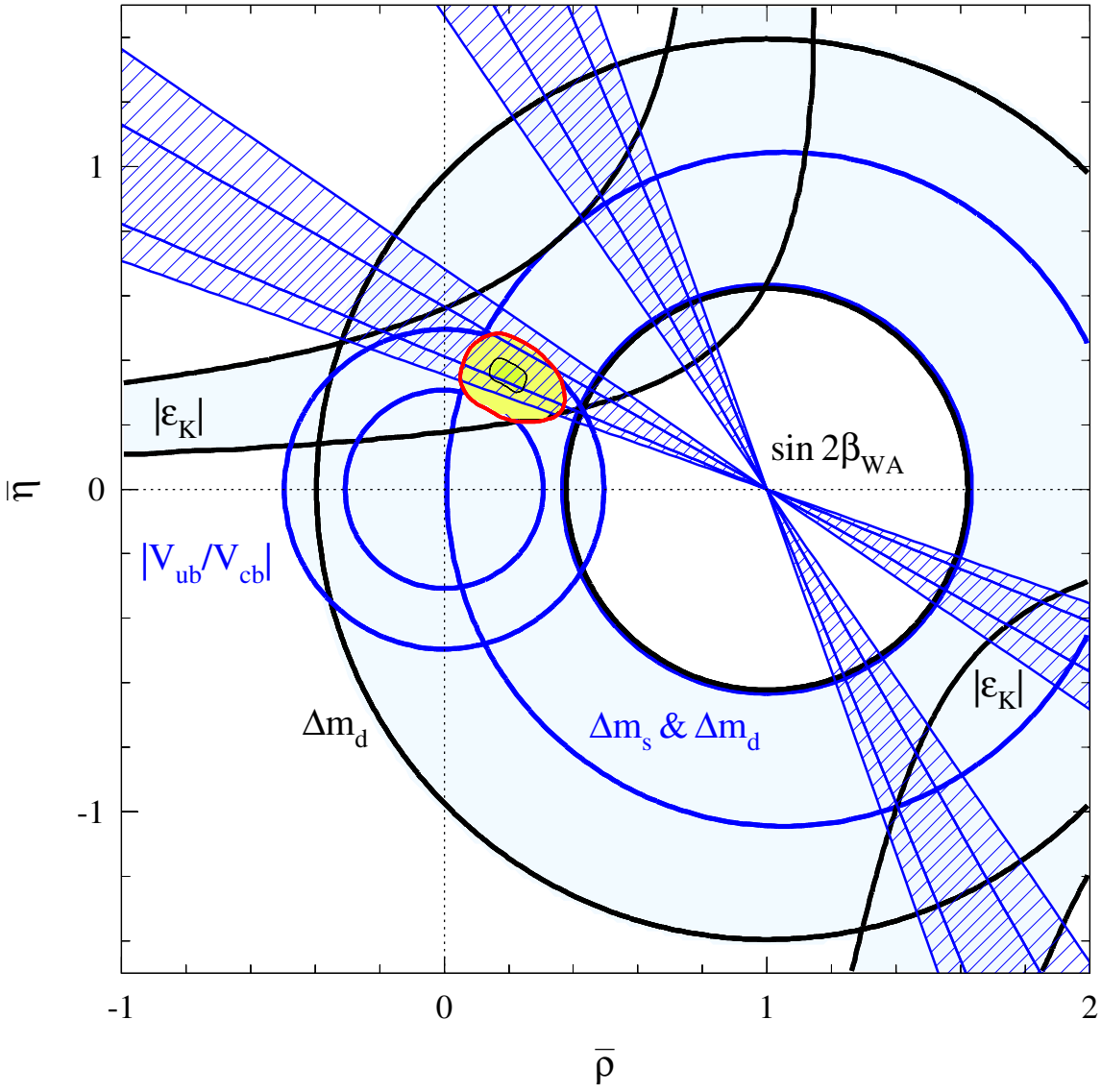

Figure 8-2: Constraints on the Unitarity Triangle. This measurement is included in the Δm_d and $\Delta m_d \& \Delta m_s$ constraints.

Appendix A

Quantum Mechanics of $B^0\overline{B}^0$ Mixing

Here the phenomenological theoretical framework describing $B^0\overline{B}^0$ flavor oscillations is presented.

A.1 Hamiltonian Mechanics

Neutral B mesons are produced in states of definite flavor. The weak interactions described above can cause the flavor to change as the state evolves. Therefore, the quantum description of neutral meson oscillations is described phenomenologically by a Hamiltonian operator describing the weak interactions, which includes both a dispersive part and an absorptive part: $\hat{H}_W = \hat{M} - \frac{i}{2}\hat{\Gamma}$. The B^0 meson is normally produced in one of two flavor states, where in terms of quark content are $|B^0\rangle = \left|\bar{b}d\right\rangle$ and $\left|\overline{B}^0\right\rangle = \left|b\bar{d}\right\rangle$. Any arbitrary state ϕ can be written as a linear combination of these basis states, $|\phi\rangle = p\,|B^0\rangle + q\left|\overline{B}^0\right\rangle$. In this section, first the energy eigenvalues are found in the flavor basis by diagonalizing the Hamiltonian, the time-dependence of these eigenstates is determined, and finally an arbitrary time-dependent state is considered.

In matrix notation, then, working in the flavor basis, the Hamiltonian for the

$B^0\overline{B}^0$ system can be written most generally

$$H_W = \begin{pmatrix} M_{11} & M_{12} \\ M_{21} & M_{22} \end{pmatrix} - \frac{i}{2} \begin{pmatrix} \Gamma_{11} & \Gamma_{12} \\ \Gamma_{21} & \Gamma_{22} \end{pmatrix} \tag{A.1}$$

CPT invariance requires $M_{11} = M_{22} \equiv M$, and $\Gamma_{11} = \Gamma_{22} \equiv \Gamma$, and hermiticity of the operators $\hat{M}$ and $\hat{\Gamma}$ enforces $M_{21} = M_{12}^*$ and $\Gamma_{21} = \Gamma_{12}^*$. The Hamiltonian is thus

$$H_W \;=\; \begin{pmatrix} M - \frac{i}{2}\Gamma & M_{12} - \frac{i}{2}\Gamma_{12} \\ M_{12}^* - \frac{i}{2}\Gamma_{12}^* & M - \frac{i}{2}\Gamma \end{pmatrix} \tag{A.2}$$

As usual, we assume separable solutions to the Schrödinger equation. The time-independent Schrödinger equation is

$$\begin{pmatrix} M - \frac{i}{2}\Gamma & M_{12} - \frac{i}{2}\Gamma_{12} \\ M_{12}^* - \frac{i}{2}\Gamma_{12}^* & M - \frac{i}{2}\Gamma \end{pmatrix} \begin{pmatrix} p \\ q \end{pmatrix} \;=\; \lambda \begin{pmatrix} p \\ q \end{pmatrix} \tag{A.3}$$

Solving for the eigenvalues of the Hamiltonian,

$$\det \begin{pmatrix} M - \frac{i}{2}\Gamma - \lambda & M_{12} - \frac{i}{2}\Gamma_{12} \\ M_{12}^* - \frac{i}{2}\Gamma_{12}^* & M - \frac{i}{2}\Gamma - \lambda \end{pmatrix} \;=\; 0 \tag{A.4}$$

yields

$$\left(M - \frac{i}{2}\Gamma - \lambda\right)^2 - \left(M_{12} - \frac{i}{2}\Gamma_{12}\right)\left(M_{12}^* - \frac{i}{2}\Gamma_{12}^*\right) \;=\; 0 \tag{A.5}$$

$$\lambda^2 - 2\lambda\left[M - \frac{i}{2}\Gamma\right] + \left[(M - \frac{i}{2}\Gamma)^2 - (M_{12} - \frac{i}{2}\Gamma_{12})(M_{12}^* - \frac{i}{2}\Gamma_{12}^*)\right] \;=\; 0 \tag{A.6}$$

The quadratic has two roots:

$$\lambda_{1,2} \;=\; \frac{2\left(M - \frac{i}{2}\Gamma\right) \pm \sqrt{4\left(M - \frac{i}{2}\Gamma\right)^2 - 4(M - \frac{i}{2}\Gamma)^2 + 4(M_{12} - \frac{i}{2}\Gamma_{12})(M_{12}^* - \frac{i}{2}\Gamma_{12}^*)}}{2}$$

$$\lambda_{1,2} = M - \frac{i}{2}\Gamma \pm \sqrt{(M_{12} - \frac{i}{2}\Gamma_{12})(M_{12}^* - \frac{i}{2}\Gamma_{12}^*)} \quad \text{(A.7)}$$

Now I will find the particular states which are eigenstates of the Hamiltonian with eigenvalues λ_1 and λ_2. In this case, the ratio p/q is constrained by two homogeneous equations. From Equation A.3,

$$(M - \frac{i}{2}\Gamma - \lambda)p + (M_{12} - \frac{i}{2}\Gamma_{12})q = 0 \quad \text{(A.8)}$$

$$(M_{12}^* - \frac{i}{2}\Gamma_{12}^*)p + (M - \frac{i}{2}\Gamma - \lambda)q = 0 \quad \text{(A.9)}$$

Substituting in for λ gives

$$\frac{q}{p} = \frac{M - \frac{i}{2}\Gamma - \lambda}{\frac{i}{2}\Gamma_{12} - M_{12}} \quad \text{(A.10)}$$

$$= \frac{M - \frac{i}{2}\Gamma - \left(M - \frac{i}{2}\Gamma + \sqrt{(M_{12} - \frac{i}{2}\Gamma_{12})(M_{12}^* - \frac{i}{2}\Gamma_{12}^*)}\right)}{\frac{i}{2}\Gamma_{12} - M_{12}} \quad \text{(A.11)}$$

$$\frac{q}{p} = \sqrt{\frac{(M_{12}^* - \frac{i}{2}\Gamma_{12}^*)}{(M_{12} - \frac{i}{2}\Gamma_{12})}} \quad \text{(A.12)}$$

The eigenvalues can be written in the more compact form in terms of p and q:

$$\lambda_{1,2} = M - \frac{i}{2}\Gamma \pm \frac{q}{p}\left(M_{12} - \frac{i}{2}\Gamma_{12}\right) \quad \text{(A.13)}$$

In terms of the flavor eigenstates, the normalized energy eigenstates are

$$|B_1\rangle = \frac{1}{\sqrt{|p|^2 + |q|^2}}\left(p\left|B^0\right\rangle + q\left|\overline{B}^0\right\rangle\right) \quad \text{(A.14)}$$

$$|B_2\rangle = \frac{1}{\sqrt{|p|^2 + |q|^2}}\left(p\left|B^0\right\rangle - q\left|\overline{B}^0\right\rangle\right) \quad \text{(A.15)}$$

The time-dependent states can be written in terms of the energy eigenstates:

$$|\psi_1(t)\rangle = a(t)\,|B_1\rangle \qquad |\psi_2(t)\rangle = b(t)\,|B_2\rangle \quad \text{(A.16)}$$

The time-evolution of the states is described by the time-dependent Schrödinger equation:

$$i\frac{d}{dt}\psi_n(t) = H_W\psi_n(t) \tag{A.17}$$

$$a(t)H_W\left|B_1\right\rangle = i\dot{a}(t)\left|B_1\right\rangle = a(t)\lambda_1\left|B_1\right\rangle \tag{A.18}$$

Solving the differential equation for a,

$$i\int_{t=0}^{t}\frac{\dot{a}(t')}{a(t')}dt' = \int_{t=0}^{t}\lambda_1 dt' \tag{A.19}$$

$$\ln(a(t)) + C = -i\lambda_1 t \tag{A.20}$$

$$a(t) = a_0 e^{-i\lambda_1 t} \tag{A.21}$$

Similarly,

$$b(t) = b_0 e^{-i\lambda_2 t} \tag{A.22}$$

where a_0 and b_0 are the normalizations.

The time-evolution of the energy eigenstates which have well-defined masses and widths

$$M_{1,2} = \mathrm{Re}(\lambda_{1,2}) \qquad \Gamma_{1,2} = -2\mathrm{Im}(\lambda_{1,2}) \tag{A.23}$$

i.e., those in Equation A.14 are evidently

$$\left|\psi_1(t)\right\rangle = \frac{e^{-i\lambda_1 t}}{\sqrt{|p|^2+|q|^2}}\left(p\left|B^0\right\rangle + q\left|\overline{B}^0\right\rangle\right) \tag{A.24}$$

$$\left|\psi_2(t)\right\rangle = \frac{e^{-i\lambda_2 t}}{\sqrt{|p|^2+|q|^2}}\left(p\left|B^0\right\rangle - q\left|\overline{B}^0\right\rangle\right)$$

Once again, any arbitrary state can be constructed from a linear combination of

these states:

$$|\phi(t)\rangle \;=\; a_0\,|\psi_1(t)\rangle + b_0\,|\psi_2(t)\rangle \tag{A.25}$$

where a_0 and b_0 are just the relative amounts of each of the two components. Substituting from Equation A.24,

$$|\phi(t)\rangle \;=\; \frac{a_0 e^{-i\lambda_1 t}}{\sqrt{|p|^2+|q|^2}}\left(p\left|B^0\right\rangle + q\left|\overline{B}^0\right\rangle\right) + \frac{b_0 e^{-i\lambda_2 t}}{\sqrt{|p|^2+|q|^2}}\left(p\left|B^0\right\rangle - q\left|\overline{B}^0\right\rangle\right)$$

$$|\phi(t)\rangle = \tag{A.26}$$
$$\frac{1}{\sqrt{|p|^2+|q|^2}}\left[\left(a_0 e^{-i\lambda_1 t} + b_0 e^{-i\lambda_2 t}\right)p\left|B^0\right\rangle + \left(a_0 e^{-i\lambda_1 t} - b_0 e^{-i\lambda_2 t}\right)q\left|\overline{B}^0\right\rangle\right]$$

The arbitrary constants a_0 and b_0 can be chosen to construct states which are flavor eigenstates at $t = a0$. At $t = 0$, Equation A.26 is just

$$|\phi(t)\rangle \;=\; \frac{1}{\sqrt{|p|^2+|q|^2}}\left[(a_0+b_0)\,p\left|B^0\right\rangle + (a_0-b_0)\,q\left|\overline{B}^0\right\rangle\right] \tag{A.27}$$

The state will be pure B^0 if $p(a_0+b_0) = \sqrt{|p|^2+|q|^2}$ and $q(a_0-b_0) = 0$. The second of these constraints means that $a_0 = b_0$. The first implies

$$a_0 \;=\; \frac{\sqrt{|p|^2+|q|^2}}{2p} \tag{A.28}$$

The state which is pure B^0 at $t = 0$ is

$$|\phi_{B^0}(t)\rangle = $$
$$\frac{1}{\sqrt{|p|^2+|q|^2}}\left[\left(a_0 e^{-i\lambda_1 t} + b_0 e^{-i\lambda_2 t}\right)p\left|B^0\right\rangle + \left(a_0 e^{-i\lambda_1 t} - b_0 e^{-i\lambda_2 t}\right)q\left|\overline{B}^0\right\rangle\right]$$

$$|\phi_{B^0}(t)\rangle \;=\; \frac{1}{2}\left(e^{-i\lambda_1 t} + e^{-i\lambda_2 t}\right)\left|B^0\right\rangle + \frac{q}{2p}\left(e^{-i\lambda_1 t} - e^{-i\lambda_2 t}\right)\left|\overline{B}^0\right\rangle \tag{A.29}$$

Similarly, the state which is pure $\overline{B}^0$ at $t = 0$ is

$$|\phi_{\overline{B}^0}(t)\rangle = \frac{p}{2q}\left(e^{-i\lambda_1 t} - e^{-i\lambda_2 t}\right)\left|B^0\right\rangle + \frac{1}{2}\left(e^{-i\lambda_1 t} + e^{-i\lambda_2 t}\right)\left|\overline{B}^0\right\rangle \quad \text{(A.30)}$$

Substituting for the eigenvalues from Equation A.23, the exponential terms are

$$e^{i\lambda_1 t} \pm e^{i\lambda_2 t} = e^{-iM_1 t}e^{\frac{-\Gamma_1 t}{2}} \pm e^{-iM_2 t}e^{\frac{-\Gamma_2 t}{2}} \quad \text{(A.31)}$$

For the B^0 system, the lifetime difference $\Gamma_1 - \Gamma_2$ is expected to be small. In the limit $\Gamma_1 - \Gamma_2 << \Gamma = (\Gamma_1 + \Gamma_2)/2$, then,

$$e^{-i\lambda_1 t} \pm e^{-i\lambda_2 t} = e^{\frac{-\Gamma t}{2}}e^{-i\frac{M_1+M_2}{2}t}\left(e^{-i\frac{M_1-M_2}{2}t} \pm e^{i\frac{M_1-M_2}{2}t}\right) \quad \text{(A.32)}$$

$$e^{-i\lambda_1 t} + e^{-i\lambda_2 t} = 2e^{\frac{-\Gamma t}{2}}e^{-iMt}\cos\left(\frac{\Delta m t}{2}\right) \quad \text{(A.33)}$$

$$e^{-i\lambda_1 t} - e^{-i\lambda_2 t} = -2ie^{\frac{-\Gamma t}{2}}e^{-iMt}\sin\left(\frac{\Delta m t}{2}\right) \quad \text{(A.34)}$$

where $M = (M_1 + M_2)/2$ and $\Delta m = M_1 - M_2$. The states which have definite flavor at $t = 0$ are now

$$|\phi_{B^0}(t)\rangle = e^{\frac{-\Gamma t}{2}}e^{-iMt}\left[\cos\left(\frac{\Delta m t}{2}\right)\left|B^0\right\rangle - \frac{q}{p}i\sin\left(\frac{\Delta m t}{2}\right)\left|\overline{B}^0\right\rangle\right] \quad \text{(A.35)}$$

$$|\phi_{\overline{B}^0}(t)\rangle = e^{\frac{-\Gamma t}{2}}e^{-iMt}\left[-\frac{p}{q}i\sin\left(\frac{\Delta m t}{2}\right)\left|B^0\right\rangle + \cos\left(\frac{\Delta m t}{2}\right)\left|\overline{B}^0\right\rangle\right] \quad \text{(A.36)}$$

A.2 Time Evolution of B^0 Mesons From $\Upsilon(4S)$ Decays

In the context of studying B^0 decays at the $\Upsilon(4S)$, it is useful to explore the time-evolution of the full two-particle final state which results from the $\Upsilon(4S)$ decay. When a $\Upsilon(4S)$ decays into two B mesons, they evolve in phase until one of them decays. The two-meson state can be thought of as though each B evolves as described above, but that at any given moment, there is exactly one B^0 and one $\overline{B}^0$ present. The

wavefunction describing the time-evolution of the pair can be written:

$$|\Psi\rangle = \frac{1}{\sqrt{2}}\left[\left|\phi_{B^0}(t_1,\vec{k}_1)\right\rangle\left|\phi_{\overline{B}^0}(t_2,\vec{k}_2)\right\rangle - \left|\phi_{\overline{B}^0}(t_1,\vec{k}_1)\right\rangle\left|\phi_{B^0}(t_2,\vec{k}_2)\right\rangle\right] \quad \text{(A.37)}$$

where $\vec{k}_i$ is the momentum of the ith B, and $\vec{k}_1 = -\vec{k}_2$. Substituting in from Equations A.35 and A.36,

$$\begin{aligned}|\Psi\rangle = {} & \frac{1}{\sqrt{2}}e^{(iM+\Gamma/2)(t_1+t_2)}\times \quad \text{(A.38)}\\ & \left\{\cos\left(\Delta m_d(t_1-t_2)/2\right)\left[\left|B^0(\vec{k}_1)\right\rangle\left|\overline{B}^0(\vec{k}_2)\right\rangle - \left|\overline{B}^0(\vec{k}_1)\right\rangle\left|B^0(\vec{k}_2)\right\rangle\right]\right.\\ & \left.-i\sin\left(\Delta m_d(t_1-t_2)/2\right)\left[\frac{p}{q}\left|B^0(\vec{k}_1)\right\rangle\left|B^0(\vec{k}_2)\right\rangle - \frac{q}{p}\left|\overline{B}^0(\vec{k}_1)\right\rangle\left|\overline{B}^0(\vec{k}_2)\right\rangle\right]\right\}\end{aligned}$$

where the subscripts denote that the first B decays at t_1 and the second at t_2.

Consider the final states $\langle f_1|$ and $\langle f_2|$ produced in decays at t_1 and t_2, respectively. The combined amplitude for this process, i.e., the amplitude describing the situation where both $\langle f_1|$ and $\langle f_2|$ are produced is

$$\begin{aligned}\mathcal{A} &= \frac{1}{\sqrt{2}}e^{-(iM+\Gamma/2)(t_1+t_2)}\left[\left(A_1\bar{A}_2 - \bar{A}_1A_2\right)\cos\frac{\Delta m_d\Delta t}{2}\right. \quad \text{(A.39)}\\ &\quad \left. + i\left(\frac{p}{q}A_1A_2 - \frac{q}{p}\bar{A}_1\bar{A}_2\right)\sin\frac{\Delta m_d\Delta t}{2}\right]\end{aligned}$$

where

$$A_i \equiv \left\langle f_i\left|H_W\right|B^0\right\rangle \quad \text{(A.40)}$$

$$\bar{A}_i \equiv \left\langle f_i\left|H_W\right|\overline{B}^0\right\rangle \quad \text{(A.41)}$$

$$\quad \text{(A.42)}$$

This is the combined amplitude for the case where the first B decays at time t_1 into the state $|f_1\rangle$, and the second B decays at time t_2 into the state $|f_2\rangle$, and

The complete decay rate is thus:

$$\mathcal{R}(1,2) = \tag{A.43}$$
$$Ne^{-\Gamma(t_1+t_2)}\Bigg\{ \left(|A_1|^2 + |\bar{A}_1|^2\right)\left(|A_2|^2 + |\bar{A}_2|^2\right) - 4\mathrm{Re}\left(\frac{q}{p}A_1^*\bar{A}_1\right)\mathrm{Re}\left(\frac{q}{p}A_2^*\bar{A}_2\right)$$
$$- \cos\left(\Delta m_d(t_1-t_2)\right)\left[\left(|A_1|^2 - |\bar{A}_1|^2\right)\left(|A_2|^2 - |\bar{A}_2|^2\right) + 4\mathrm{Im}\left(\frac{q}{p}A_1^*\bar{A}_1\right)\mathrm{Im}\left(\frac{q}{p}A_2^*\bar{A}_2\right)\right]$$
$$+ 2\sin\left(\Delta m_d(t_1-t_2)\right)\left[\mathrm{Im}\left(\frac{q}{p}A_1^*\bar{A}_1\right)\left(|A_2|^2 - |\bar{A}_2|^2\right) - \mathrm{Im}\left(\frac{q}{p}A_2^*\bar{A}_2\right)\left(|A_1|^2 - |\bar{A}_1|^2\right)\right]\Bigg\}$$

There are two cases to consider: either the two B mesons decay into opposite flavor states (unmixed) or the two B mesons decay into the same flavor state (mixed).

Case 1: unmixed In this case, the four amplitudes are either

$$A_1 = \left\langle B_1^0 \left| H_W \right| B^0 \right\rangle \qquad \bar{A}_1 = 0$$
$$A_2 = 0 \qquad \bar{A}_2 = \left\langle \overline{B}_2^0 \left| H_W \right| \overline{B}^0 \right\rangle$$

or

$$A_1 = 0 \qquad \bar{A}_1 = \left\langle \overline{B}_1^0 \left| H_W \right| \overline{B}^0 \right\rangle$$
$$A_2 = \left\langle B_2^0 \left| H_W \right| B^0 \right\rangle \qquad \bar{A}_2 = 0$$

Then defining $\Delta t = t_1 - t_2$, the rates for these cases are:

$$\mathcal{R}(1,2)_{\text{unmixed}} = Ne^{-\Gamma(t_1+t_2)}\left(|A_1|^2|\bar{A}_2|^2 + \cos\left(\Delta m_d \Delta t\right)|A_1|^2|\bar{A}_2|^2\right) \tag{A.44}$$
$$\mathcal{R}'(1,2)_{\text{unmixed}} = Ne^{-\Gamma(t_1+t_2)}\left(|\bar{A}_1|^2|A_2|^2 + \cos\left(\Delta m_d \Delta t\right)|\bar{A}_1|^2|A_2|^2\right) \tag{A.45}$$

Case 2: mixed In this case, the four amplitudes are either

$$A_1 = \left\langle B_1^0 \left| H_W \right| B^0 \right\rangle \qquad \bar{A}_1 = 0$$
$$A_2 = 0 \qquad \bar{A}_2 = \left\langle B_2^0 \left| H_W \right| \overline{B}^0 \right\rangle$$

or

$$A_1 = 0 \qquad \bar{A}_1 = \left\langle B_1^0 \left| H_W \right| \overline{B}^0 \right\rangle$$
$$A_2 = \left\langle B_1^0 \left| H_W \right| B^0 \right\rangle \qquad \bar{A}_2 = 0$$

The rates for these cases are:

$$\mathcal{R}(1,2)_{\text{mixed}} = Ne^{-\Gamma(t_1+t_2)} \left(|A_1|^2 |\bar{A}_2|^2 - \cos\left(\Delta m_d \Delta t\right) |A_1|^2 |\bar{A}_2|^2 \right) \quad \text{(A.46)}$$
$$\mathcal{R}'(1,2)_{\text{mixed}} = Ne^{-\Gamma(t_1+t_2)} \left(|\bar{A}_1|^2 |A_2|^2 - \cos\left(\Delta m_d \Delta t\right) |\bar{A}_1|^2 |A_2|^2 \right) \quad \text{(A.47)}$$

Note that the A_i in case 1 is equal to the $\bar{A}_i$ of case 2 due to the CPT theorem. In fact all remaining amplitudes are equal, so let me just call them A for simplicity. The time-dependent mixing asymmetry can then be written:

$$A_{\text{mix}} = \frac{N_{\text{unmixed}} - N_{\text{mixed}}}{N_{\text{unmixed}} + N_{\text{mixed}}} \quad \text{(A.48)}$$
$$= \frac{\mathcal{R}_{\text{unmixed}} + \mathcal{R}'_{\text{unmixed}} - \mathcal{R}_{\text{mixed}} - \mathcal{R}'_{\text{mixed}}}{\mathcal{R}_{\text{unmixed}} + \mathcal{R}'_{\text{unmixed}} + \mathcal{R}_{\text{mixed}} + \mathcal{R}'_{\text{mixed}}} \quad \text{(A.49)}$$
$$= \frac{Ne^{-\Gamma(t_1+t_2)|A|^4} \left\{ 2(1+\cos(\Delta m_d \Delta t)) - 2(1-\cos(\Delta m_d \Delta t)) \right\}}{Ne^{-\Gamma(t_1+t_2)|A|^4} \left\{ 2(1+\cos(\Delta m_d \Delta t)) + 2(1-\cos(\Delta m_d \Delta t)) \right\}} \quad \text{(A.50)}$$
$$A_{\text{mix}} = \cos(\Delta m_d \Delta t) \quad \text{(A.51)}$$

Appendix B

Event Yields

Distributions of $m_{\rm ES}$ with fits to an Argus fucntion (background) and a Gaussian (signal) are shown separately for each complete B decay chain.

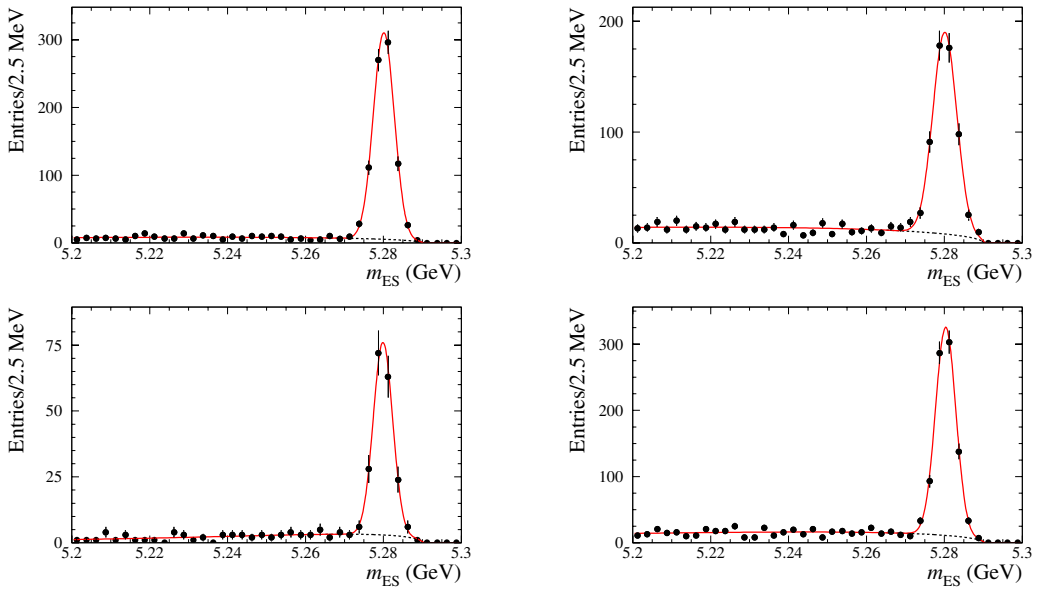

Figure B-1: $m_{\rm ES}$ distributions for $B^0 \to D^{*-}\pi^+$, $D^0 \to K^-\pi^+$ (top left) and $D^0 \to K^-\pi^+\pi^0$ (top right), $D^0 \to K^0_S\pi^+\pi^-$ (bottom left) and $D^0 \to K^-\pi^+\pi^-\pi^+$ (bottom right).

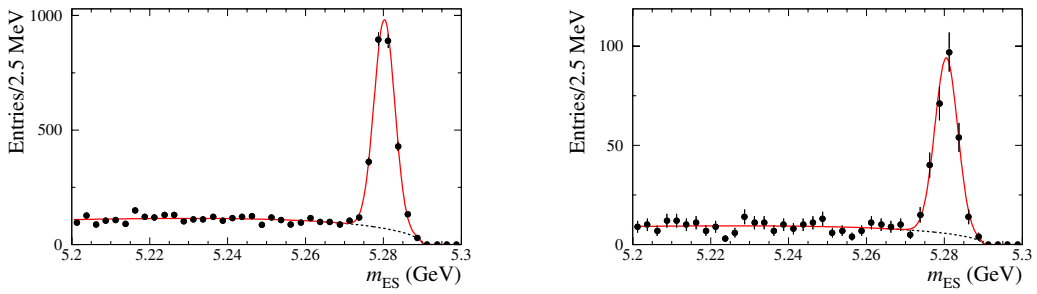

Figure B-2: $m_{\rm ES}$ distributions for $B^0 \to D^-\pi^+$, $D^- \to K^+\pi^-\pi^-$ (left) and $D^- \to K^0_S\pi^-$ (right).

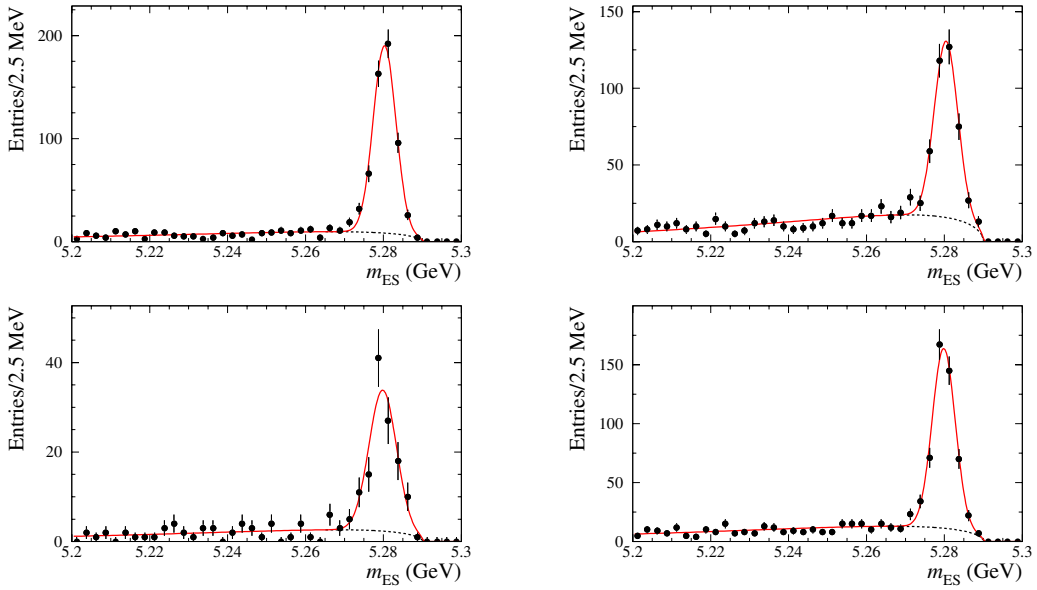

Figure B-3: $m_{\rm ES}$ distributions for $B^0 \to D^{*-}\rho^+$, $D^0 \to K^-\pi^+$ (top left) and $D^0 \to K^-\pi^+\pi^0$ (top right), , $D^0 \to K^0_S\pi^+\pi^-$ (bottom left) and $D^0 \to K^-\pi^+\pi^-\pi^+$ (bottom right).

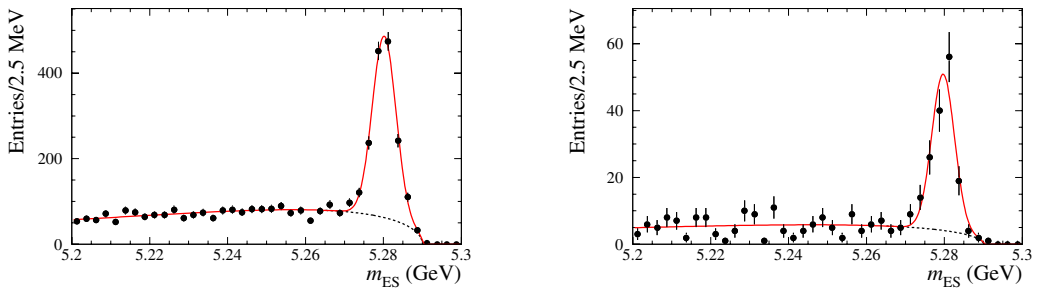

Figure B-4: $m_{\rm ES}$ distributions for $B^0 \to D^- \rho^+$, $D^- \to K^+\pi^-\pi^-$ (left) and $D^- \to K^0_S \pi^-$ (right).

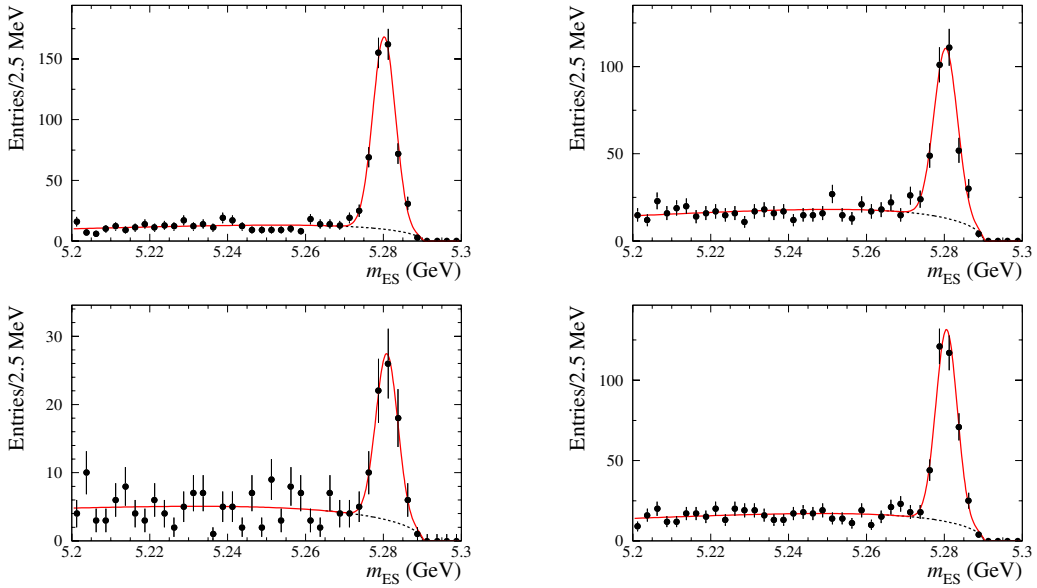

Figure B-5: $m_{\rm ES}$ distributions for $B^0 \to D^{*-} a_1^+$, $D^0 \to K^-\pi^+$ (top left) and $D^0 \to K^-\pi^+\pi^0$ (top right) , $D^0 \to K^0_S\pi^+\pi^-$ (bottom left) and $D^0 \to K^-\pi^+\pi^-\pi^+$ (bottom right).

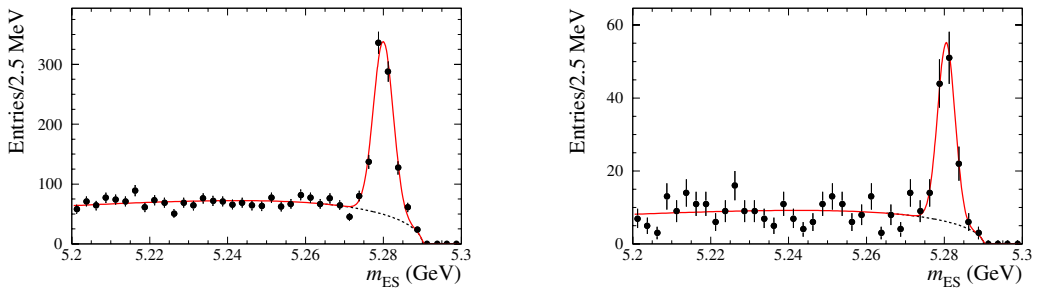

Figure B-6: $m_{\rm ES}$ distributions for $B^0 \to D^- a_1^+$, $D^- \to K^+\pi^-\pi^-$ (left) and $D^- \to K^0_S\pi^-$ (right).

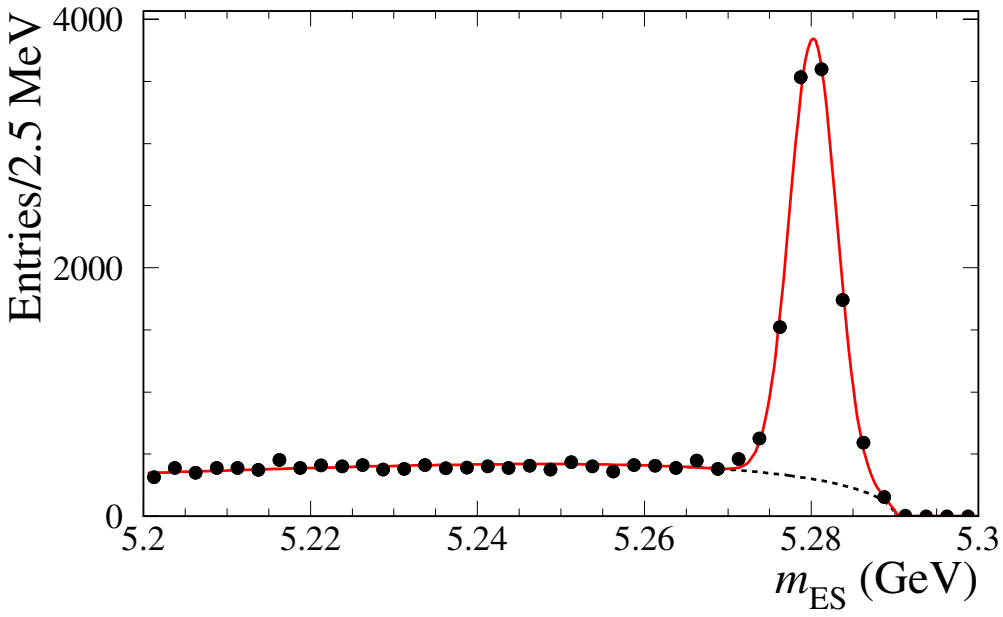

Figure B-7: $m_{\rm ES}$ distribution for all B^0 modes.

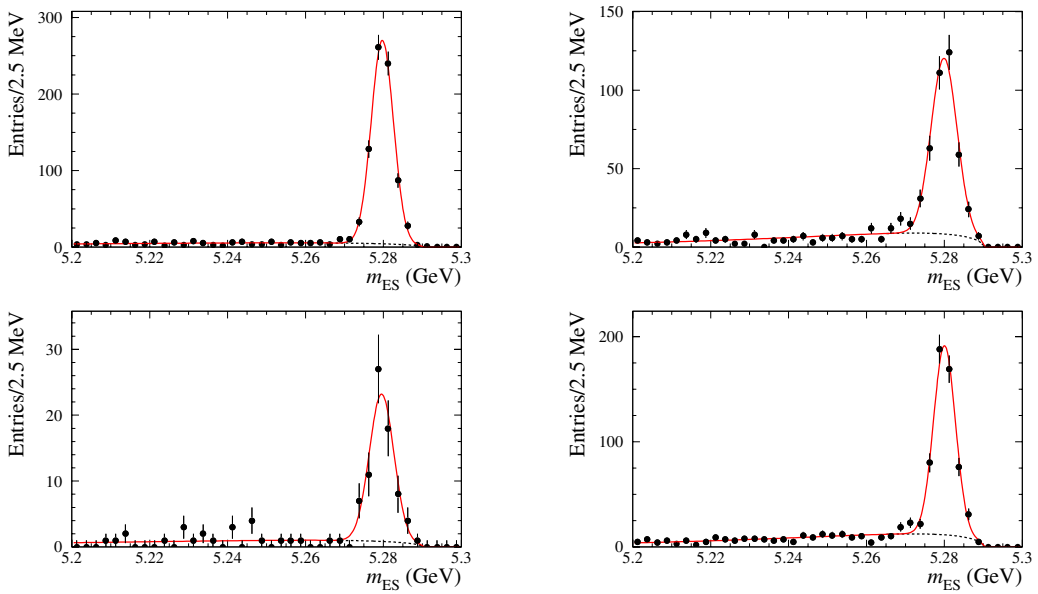

Figure B-8: $m_{\rm ES}$ distribution for $B^+ \to \overline{D}^{*0}\pi^+$, $D^0 \to K^-\pi^+$ (top left) and $D^0 \to K^-\pi^+\pi^0$ (top right), , $D^0 \to K^0_S\pi^+\pi^-$ (bottom left) and $D^0 \to K^-\pi^+\pi^-\pi^+$ (bottom right).

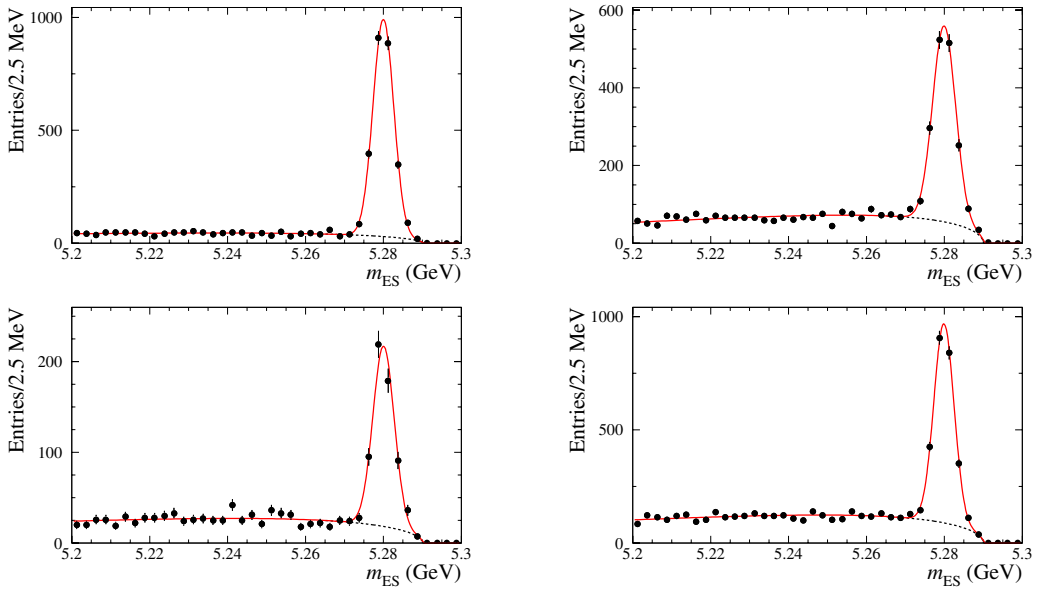

Figure B-9: $m_{\rm ES}$ distributions for $B^+ \to \overline{D}^{0}\pi^+$, $D^0 \to K^-\pi^+$ (top left) and $D^0 \to K^-\pi^+\pi^0$ (top right), , $D^0 \to K^0_S\pi^+\pi^-$ (bottom left) and $D^0 \to K^-\pi^+\pi^-\pi^+$ (bottom right).

Appendix C

Results of Fast Parameterized Monte Carlo

The results of fitting 2000 fast parameterized Monte Carlo samples, each generated with a size and parameterization identical to the one observed in data are shown here.

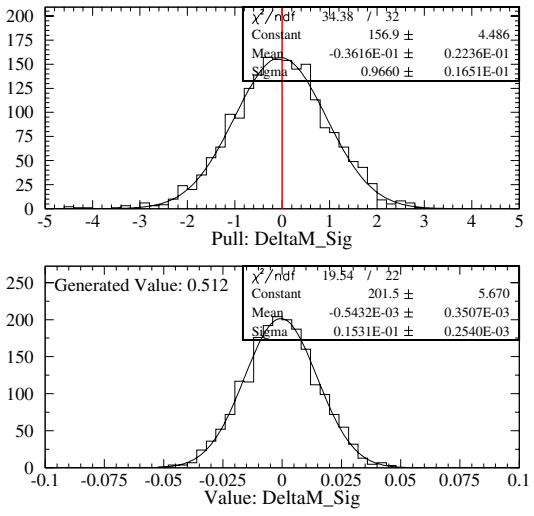

Figure C-1: Distribution of measured values of Δm_d and pull in toy MC. The vertical line corresponds to the generated value.

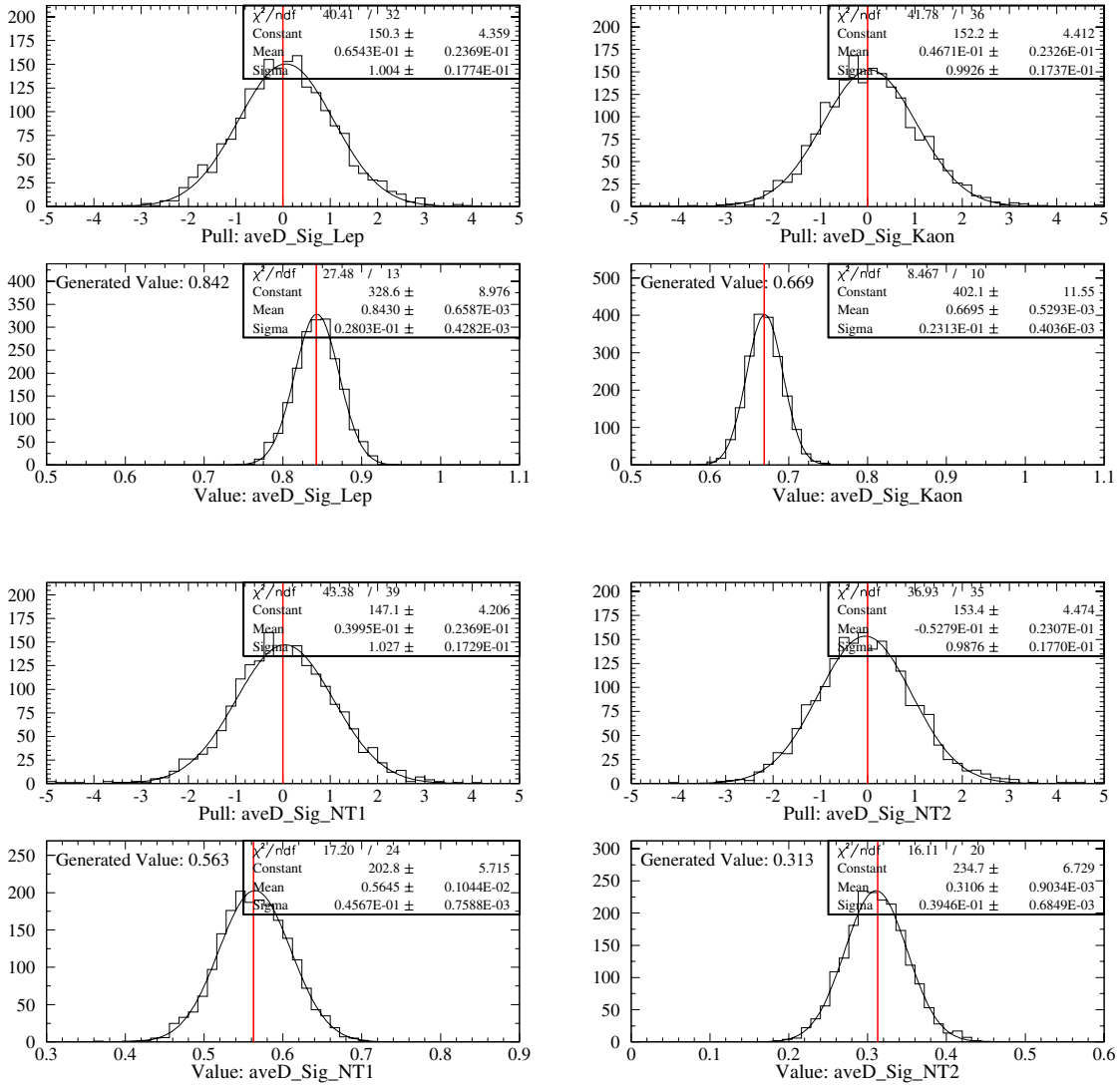

Figure C-2: Distributions of the signal dilutions and their pulls in toy MC. The vertical line corresponds to the generated value.

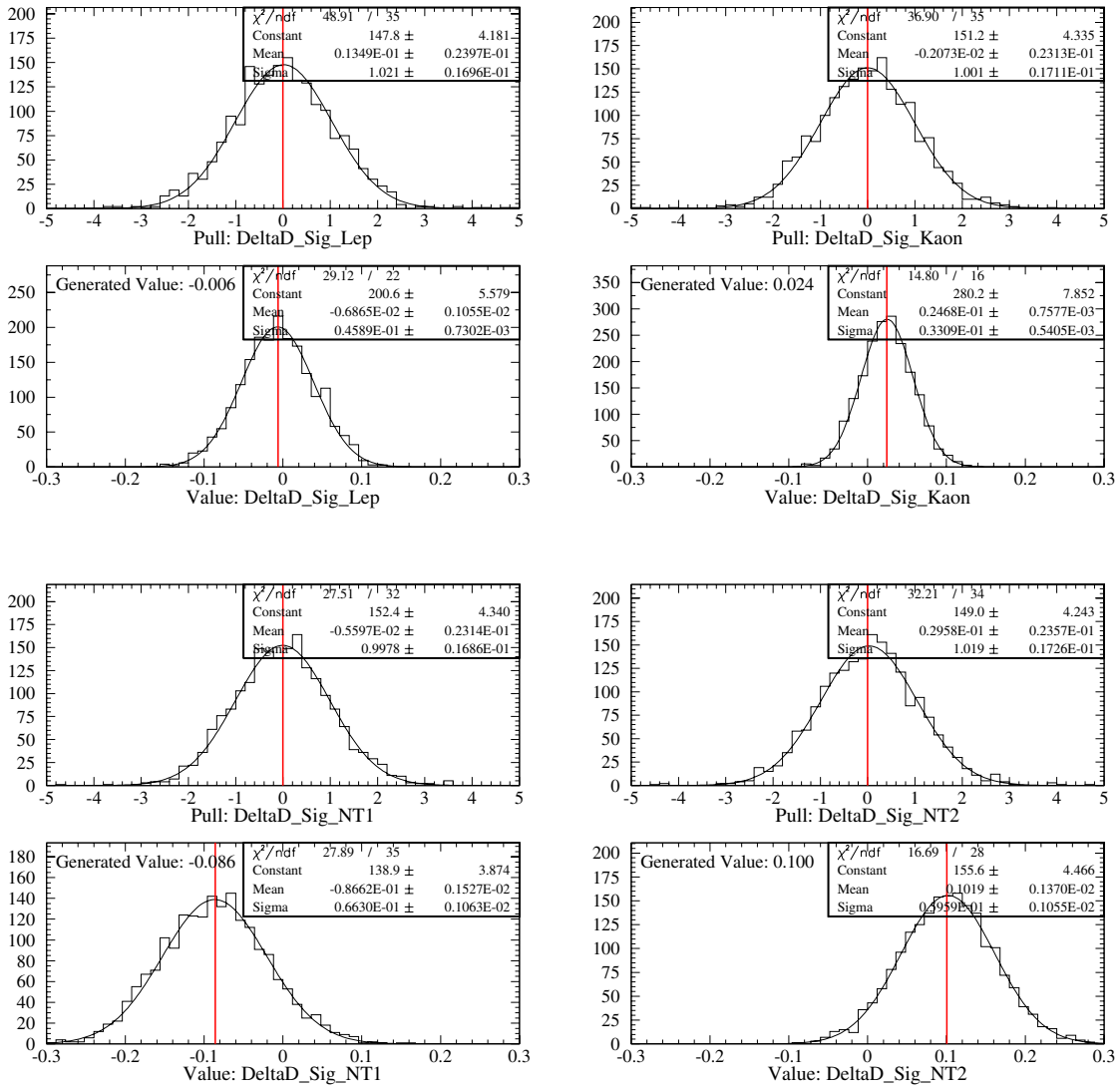

Figure C-3: Distributions of the signal ΔD values and their pulls in toy MC. The vertical line corresponds to the generated value.

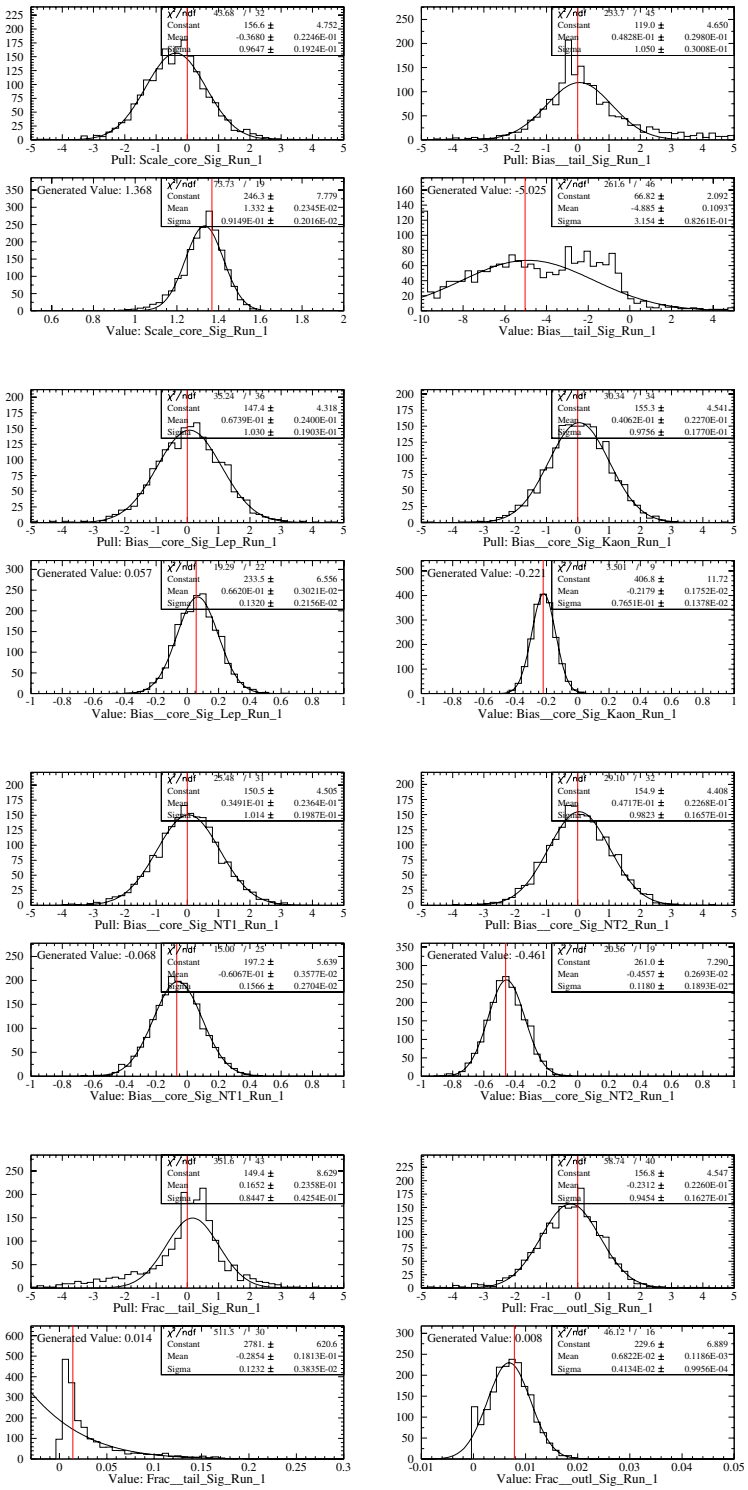

Figure C-4: Distributions of the signal resolution function fit parameters and their pull in toy MC for Run 1. The vertical line corresponds to the generated value.

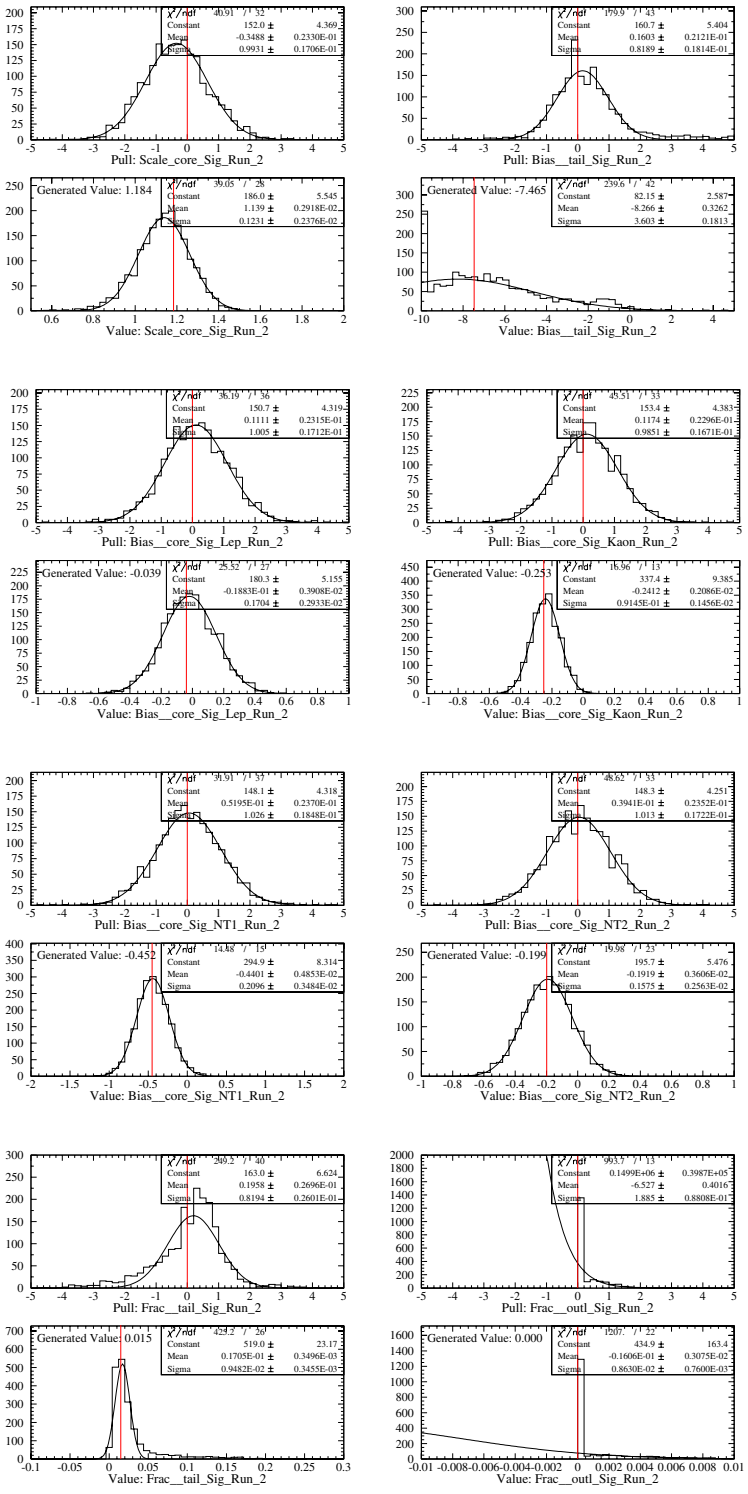

Figure C-5: Distributions of the signal resolution function fit parameters and their pull in toy MC for Run 2. The vertical line corresponds to the generated value.

Appendix D

Drift Chamber Time-to-distance ($d(t)$) Calibration

The *BABAR* drift chamber time to distance relation is extracted from data and modeled with a series of Chebyshev polynomials. The procedure used for extracting this fuction from data is described here.

The BaBar drift chamber [10] is a 2.8 meter long arrangement of 40 concentric layers containing a total of 7104 hexagonal drift cells. Each drift cell consists of a sense wire surrounded by field wires arranged in a hexagon. The layers are grouped into 4–layer superlayers which are alternatively oriented in the axial, stereo u, and stereo v directions. The stereo layers provide a z position measurement while the axial layers allow a simple pattern recognition scheme to be used.

The chamber is filled with a mixture of approximately 80 % helium, 20 % isobutane, with a nominal amount of water to retard pre-mature aging.

The sense wires are read out on one end of the chamber by custom front-end electronics assemblies (FEAs) mounted directly on the end of the chamber. These FEAs contain circuitry to measure the arrival time of the leading edge of the drift charge pulse, as well as the time structure of the pulse amplitude so the amplitude can be integrated to determine the total charge, which is used to determine dE/dx for particle identification. The other end of the sense wires is left unterminated.

The layout of the wires in the cells is shown in figure D-1. Notice that at the

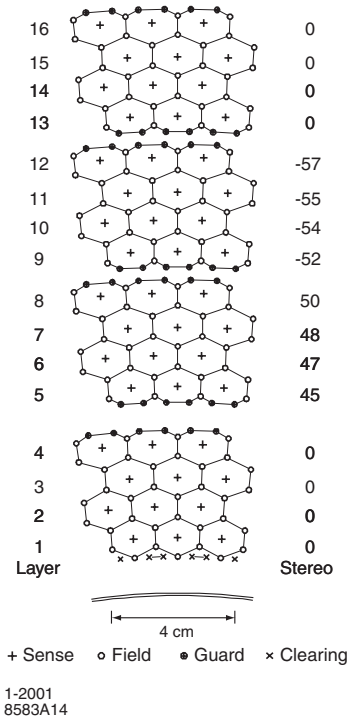

Figure D-1: Layout of Drift Chamber wires in first four superlayers, for a three-cell wide section.

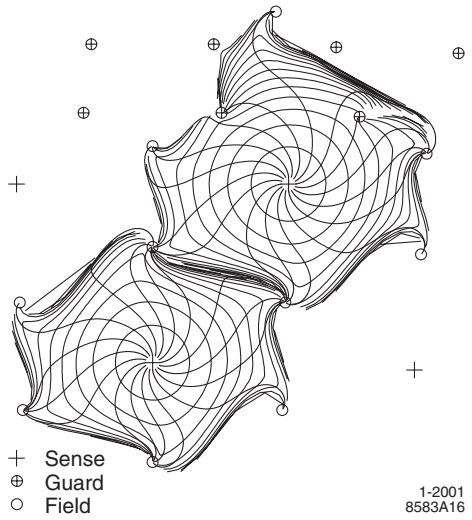

Figure D-2: Isochrones and field lines for typical cells in layers 3 (lower) and 4 (upper). Note that the isochrones are circular near the center of the cell at the sense wire, but become irregular toward the edge of the cell. The layer 4 cell also suffers a left-right asymmetry. With no magnetic field, the drift lines are radial. When the field is turned on, the drift linnes become spiral shaped. Note that the top of the cell has two guard wires instead of a single field wire. This means that the drift lines which originate from the top of the cell are different than those originating from the bottom, i.e. the left-right reflection symmetry of the cell is broken.

boundary between superlayers, there are two guard wires, where normally there would only be one field wire. These guard wires, combined with the magnetic field, conspire to create a pattern of isochrones in the cell which is left-right asymmetric. This can be seen in figure D-2. For this reason, a separate calibration function is used to describe the left and right sides of the cell.

Cosmic or di-muon events are used to calibrate the chamber as follows. First, data are reconstructed using a guess at the calibration function. For each event, in each cell, the difference in the position of the track in a cell (as measured by all of the other cells), and the position measured by the cell is recorded. After running on enough data to populate the entire chamber, each of the fourty layers' residual distributions is fit to the drift function with a minimum chi squared fit. The procedure is iterated until no appreciable difference in resolution is seen. The drift fucntion used is a 6th order Tchebyshev polynomial.

The calibration functions obtained in this way achieve a typical per-hit resolution which is typically 125 μm, averaged over the cell. The resolution as a function of signed drift distance is shown in Figure D-3.

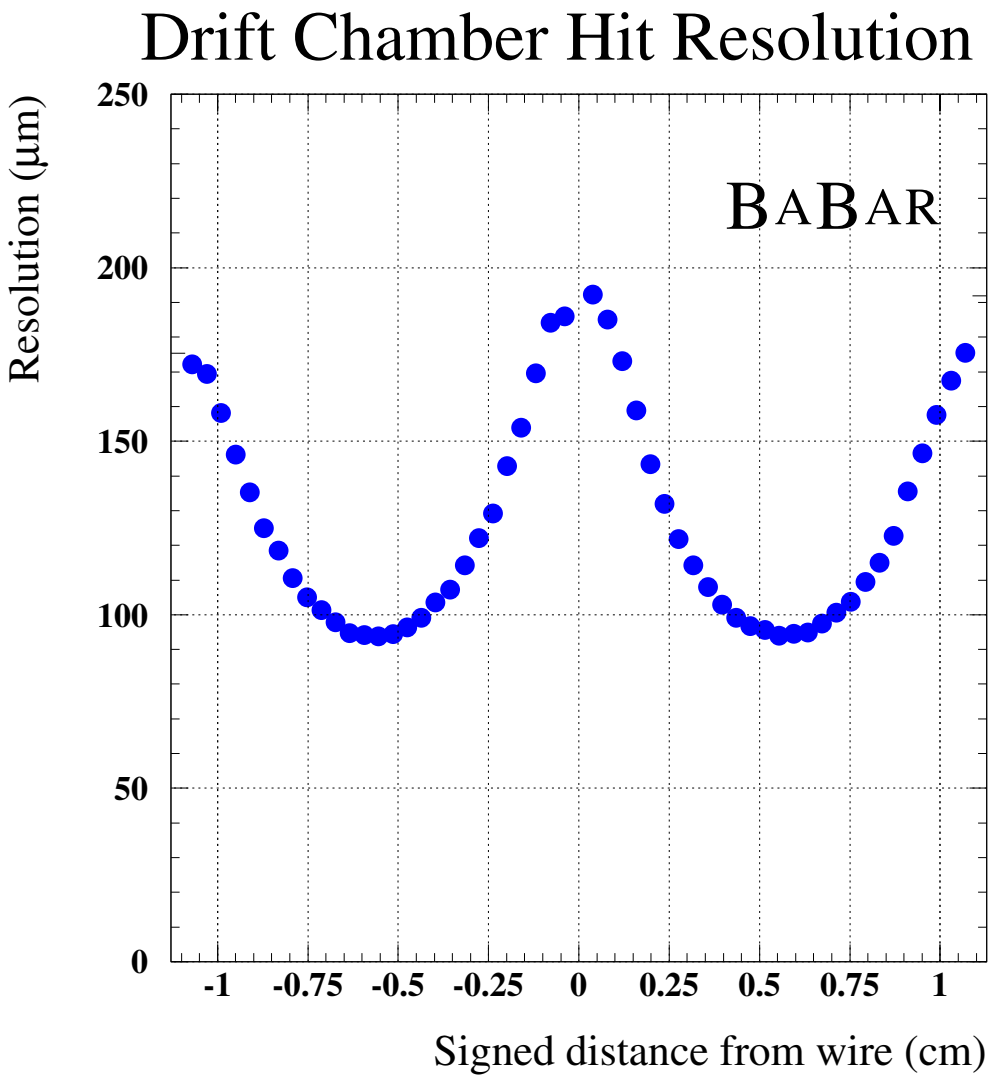

Figure D-3: Drift Chamber single hit resolution as a function of the signed distance to the sense wire.

Bibliography

[1] H. Albrecht et al. Observation of B^0-$\overline{B}^0$ mixing. *Phys. Lett. B*, 192(1,2):245–252, June 1987.

[2] C. Albajar et al. Search for B^0 $\overline{B}^0$ oscillations at the CERN proton-antiproton collider. *Phys. Lett. B*, 186(2):247–254, March 1987.

[3] L. Wolfenstein. Parameterization of the Kobayashi-Maskawa matrix. *Phys. Rev. Lett*, 51:1945, 1983.

[4] Ikaros I. Y. Bigi and F. Gabbiani. Impact of different classes of supersymmetric models on rare b decays, b0 anti-b0 mixing and cp violation. *Nucl. Phys.*, B352:309–341, 1991.

[5] Yosef Nir and Helen R. Quinn. Theory of cp violation in b decays. SLAC-PUB-5643.

[6] Colin Gay. B mixing. *Ann. Rev. Nucl. Part. Sci.*, 50:577–641, 2000.

[7] T. Inami and C. S. Lim. Effects of superheavy quarks and leptons in low-energy weak processes K(L) $\rightarrow$ mu anti-mu, K+ $\rightarrow$ pi+ neutrino anti-neutrino and K0 $\leftrightarrow$ anti-K0. *Prog. Theor. Phys.*, 65:297, 1981.

[8] D. E. Groom et al. Review of particle physics. *Eur. Phys. Jour. C*, 2000.

[9] J. Papavassiliou and A. Santamaria. Extra dimensions at the one loop level: Z $\rightarrow$ $b\,\overline{b}$ and $B\overline{B}$ mixing. *Phys. Rev.*, D63:016002, 2001.

[10] B. Aubert et al. The babar detector. *Nucl. Instrum. Meth.*, A479:1–116, 2002.

[11] G. C. Fox and S. Wolfram. A Model for parton showers in QCD. *Nucl. Phys. B*, 168:285, 1980.

[12] H. Albrecht et al. Reconstruction of B mesons. *Physics Letters B*, 185(1,2):218–222, Feb 1987.

[13] B Tagging Tools Group. B tagging in babar. Babar Analysis Document 119, 2001.

[14] H. Hu et al. The NetTagger. Babar Analysis Document 103, 2000.

[15] Babar Vertexing Analysis Working Group. Babar vertexing. Babar Analysis Documents 102, 130, 254, 2000,2001.

[16] S. Prell. `tFit` — A Program to fit decay time (difference) distributions to study B^0/B^+ lifetimes, $B\overline{B}$ oscillations and CP asymmetry parameters. Babar Analysis Document 101, 2001.

[17] F. James and M. Roos. 'minuit' a system for function minimization and analysis of the parameter errors and correlations. *Comput. Phys. Commun.*, 10:343–367, 1975.

[18] J. Stark. Measurements of the charged and neutral B meson lifetimes using fully-reconstructed B decays. Babar Analysis Document 144, 2001.

[19] J. Beringer et al. Supporting document for Summer 2001 sin2beta analysis. Babar Analysis Document 205, 2001.

[20] Bob Cahn. Determining efficiency differences from time-integrated data. `http://babar-hn.slac.stanford.edu:5090/HyperNews/get/sin2beta/183.html` `http://babar-hn.slac.stanford.edu:5090/HyperNews/get/sin2beta/159.html`, 2001.

[21] Gerhard Raven. Fitting Δm_d shapes and/or normalization. http://www.slac.stanford.edu/BFROOT/www/Physics/Analysis/AWG/BBMixingHadr/Meetings/29Mar2001/mix.ps, 2001.

[22] Vuko Brigljevic and Art Snyder. CPExtract. Babar Analysis Document 95, 2001.

[23] D. Kirkby et al. A User's Guide to the RooFitTools Package for Unbinned Maximum Likelihood Fitting. Babar Analysis Document 18, 2001.

[24] C. Cheng and G. Raven. Presentations of Chih-Hsiang Cheng and Gerhard Raven, July 5th mixing and lifetimes AWG meeting. http://www.slac.stanford.edu/BFROOT/www/Physics/Analysis/AWG/BBMixingHadr/Meetings/05Jul2001.

[25] P. Robbe, C. Hast, and W. Dunwoodie. Presentations of P. Robbe, C. Hast, and W. Dunwoodie. http://babar-hn.slac.stanford.edu:5090/HyperNews/get/recoTracking/334.html, http://www.slac.stanford.edu/~wmd/beampipe/dec00.talk, 2001.

[26] B. Brau and P. Robbe. Presentations of B. Brau and P. Robbe. http://babar-hn.slac.stanford.edu:5090/HyperNews/get/EHBDOC/241/1.html, http://babar-hn.slac.stanford.edu:5090/HyperNews/get/EHBDOC/262/4.html.

[27] LEP B Oscillations Working Group. Results for the winter 2002 conferences. http://lepbosc.web.cern.ch/LEPBOSC/combined results/lathuile 2002/, 2002.

[28] A. Hocker, H. Lacker, S. Laplace, and F. Le Diberder. CKM matrix: Status and new developments. 2001.

[29] A. Höcker, H. Lacker, S. Laplace, and F. Le Diberder. A New approach to a global fit of the CKM matrix. *Eur. Phys. Jour. C*, 21:225–259, 2001.